Loughborough University

This item was submitted to Loughborough's Research Repository by the author.
Items in Figshare are protected by copyright, with all rights reserved, unless otherwise indicated.

# Optimal predictive control of thermal storage in hollow core ventilated slab systems

PLEASE CITE THE PUBLISHED VERSION

PUBLISHER

© Mei Juan Ren

LICENCE

CC BY-NC-ND 4.0

REPOSITORY RECORD

Ren, Mei J.. 2019. “Optimal Predictive Control of Thermal Storage in Hollow Core Ventilated Slab Systems”. figshare. https://hdl.handle.net/2134/12436.

Loughborough University

This item was submitted to Loughborough University as a PhD thesis by the author and is made available in the Institutional Repository (https://dspace.lboro.ac.uk/) under the following Creative Commons Licence conditions.

creative commons

COMMONS DEED

**Attribution-NonCommercial-NoDerivs 2.5**

**You are free:**

- to copy, distribute, display, and perform the work

**Under the following conditions:**

**Attribution**. You must attribute the work in the manner specified by the author or licensor.

**Noncommercial**. You may not use this work for commercial purposes.

**No Derivative Works**. You may not alter, transform, or build upon this work.

- For any reuse or distribution, you must make clear to others the license terms of this work.
- Any of these conditions can be waived if you get permission from the copyright holder.

**Your fair use and other rights are in no way affected by the above.**

This is a human-readable summary of the Legal Code (the full license).

Disclaimer

For the full text of this licence, please go to:
http://creativecommons.org/licenses/by-nc-nd/2.5/

Loughborough University

Pilkington Library

Author/Filing Title ..... REN, M.J. .....

.....

Accession/Copy No. 0401606961

Vol. No. ..... Class Mark .....

LOAN COPY

- 8 JAN 2001

25 JUN 1999

21 JAN 2000

14 JAN 2000

27 NOV 1999

FOR REFERENCE ONLY

FEB 2000

17 DEC 1999

17 MAR 2000

12 MAY 2000

0401606961

BADMINTON PRES
UNIT 1 BROOK S
SYSTON
LEICESTER LE7 1
ENGLAND
TEL 0116 260 29
FAX 0116 269 66

# Optimal Predictive Control of Thermal Storage in Hollow Core Ventilated Slab Systems

Mei Juan Ren
Department of Civil and Building Engineering
Loughborough University

A Doctoral Thesis submitted in partial fulfilment of the requirements for the award of Doctor of Philosophy of Loughborough University

August 1997

©Mei Juan Ren 1997

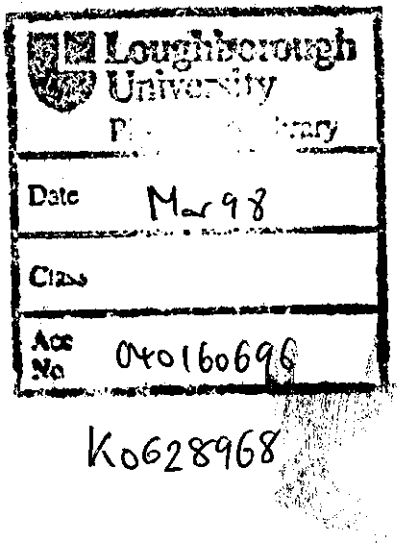
Loughborough
University
Date Mar 98
Class
Acc No 040160696
K0628968

## Abstract

The energy crisis together with greater environmental awareness, has increased interest in the construction of low energy buildings. Fabric thermal storage systems provide a promising approach for reducing building energy use and cost, and consequently, the emission of environmental pollutants. Hollow core ventilated slab systems are a form of fabric thermal storage system that, through the coupling of the ventilation air with the mass of the slab, are effective in utilizing the building fabric as a thermal store. However, the benefit of such systems can only be realized through the effective control of the thermal storage. This thesis investigates an optimum control strategy for the hollow core ventilated slab systems, that reduces the energy cost of the system without prejudicing the building occupants thermal comfort.

The controller uses the predicted ambient temperature and solar radiation, together with a model of the building, to predict the energy costs of the system and the thermal comfort conditions in the occupied space. The optimum control strategy is identified by exercising the model with a numerical optimization method, such that the energy costs are minimized without violating the building occupant's thermal comfort. The thesis describes the use of an Auto Regressive Moving Average model to predict the ambient conditions for the next 24 hours. A building dynamic lumped parameter thermal network model, is also described, together with its validation. The implementation of a Genetic Algorithm search method for optimizing the control strategy is described, and its performance in finding an optimum solution analysed.

The characteristics of the optimum schedule of control setpoints are investigated for each season, from which a simplified time-stage control strategy is derived. The effects of weather prediction errors on the optimum control strategy are investigated and the performance of the optimum controller is analysed and compared to a conventional rule-based control strategy. The on-line implementation of the optimal predictive controller would require the accurate estimation of parameters for modelling the building, which could form part of future work.



**Keywords:** building fabric thermal storage system, hollow core ventilated slab system, optimal predictive control, thermal comfort, weather prediction, Genetic Algorithm, control optimization, lumped parameter thermal network model.

## Acknowledgements

I would like to thank my supervisor Dr. J. A. Wright for his guidance, help, interest and critical discussion during the work leading to this thesis. I gratefully acknowledge the financial support from Loughborough University.

I appreciate the support and assistance from Professor V. I. Hanby and other members of the Department of Civil and Building Engineering, in particular, Dr. P. Haves, Dr. T. I. Salsbury and Dr. D. Gyi.

I would like to acknowledge the help from the UK Building Research Establishment for providing the ventilated slab system measured performance data. The acknowledgement should also be extended to Mr. D. Braham and Mr. C. C. Kendrick for their help with information about the ventilated slab building in the University of East Anglia, and Mr. M. Holmes of Ove Arup & Partners for providing some weather data.

Finally, I'm indebted to my family for the support and encouragement throughout this study.

# Contents


**1 Introduction** 1

1.1 Hollow Core Ventilated Slab Systems . . . . . 1

1.2 Optimal Supervisory Control of Building Fabric Thermal Storage Systems . . . . . 4

1.3 Objectives of the Thesis . . . . . 6

1.3.1 Research Methodology . . . . . 6

1.3.2 Strategic Objectives . . . . . 6

**2 Literature Review** 8

2.1 A Review of Hollow Core Ventilated Slab Thermal Storage Systems 9

2.1.1 Research into the Modelling of Hollow Core Ventilated Slab Systems . . . . . 12

2.2 The Control of Hollow Core Ventilated Slab Systems . . . . . 14

2.2.1 An Example of Hollow Core Ventilated Slab System Control 15

2.3 Optimal Control of Building Thermal Systems . . . . . 17

2.3.1 Optimal Control of Plant Thermal Storage Systems . . . . . 19

2.3.2 Optimal Control of Building Fabric Thermal Storage Systems 22

**3 Controller Design** 27

3.1 Control Structure and Hierarchy . . . . . 28

3.1.1 Thermal Storage Control Variables . . . . . 30

3.1.2 Plant Control Variables . . . . . 31

3.1.3 Control Process Interaction . . . . . 33

3.1.4 Definition of the Thermal Storage Optimization Problem . . 34

3.2 The Selection of an Optimization Algorithm . . . . . 36

3.2.1 Dynamic Programming . . . . . 37

3.2.2 The Complex Method . . . . . 38

3.2.3 Genetic Algorithms . . . . . 39

3.3 The Predictive Components of the Controller . . . . . 42

3.3.1 The Form of the Building and Plant Models . . . . . 42

3.3.2 The Selection of Weather Prediction Algorithms . . . . . 44

3.4 Conclusion . . . . . 45

**4 Building and Plant Model** 47
4.1 Building Thermal Simulation Methods . . . . . 48
4.1.1 Lumped Parameter Thermal Network Models . . . . . 51
4.2 The Lumped Parameter Zone and Slab Thermal Model . . . . . 54
4.2.1 The Ventilated Slab Thermal Model . . . . . 55
4.2.2 The Lumped Parameter Zone Model . . . . . 61
4.2.3 The Combined Thermal Network Model for Building Zone and Slab . . . . . 63
4.2.4 Implementation of the Combined Zone and Slab Model . . . 67
4.3 Plant Model . . . . . 71
4.3.1 Fan Model . . . . . 71
4.3.2 Heat Recovery Device . . . . . 72
4.3.3 Chiller Model and Electric Duct Heater Model . . . . . 73
4.3.4 Cooling Coil Model . . . . . 73
4.4 Model Prediction and Comparison with Measured Data . . . . . 74
4.4.1 Model Accuracy for Cyclic Operation . . . . . 76
4.4.2 Model Accuracy for Step Input Operation . . . . . 79
4.5 The Robustness of the Building Model . . . . . 82
4.5.1 Model Sensitivity Analysis . . . . . 83
4.5.2 The Capability of the Building Model . . . . . 88
4.6 Conclusion . . . . . 92

**5 The Performance of Optimization Algorithms** 94
5.1 Elements of Performance Assessment . . . . . 95
5.1.1 Factors that Control the Complex Method . . . . . 96
5.1.2 Factors that Control the Genetic Algorithm . . . . . 96
5.2 Algorithm Performance in the Scheduling of Supply Air Flow Rates 98
5.2.1 Performance of the Complex Method . . . . . 100
5.2.2 Performance of the Genetic Algorithm . . . . . 102
5.3 Algorithm Performance in the Scheduling of Supply Air Setpoints . 111
5.3.1 Performance of the Complex Method . . . . . 113
5.3.2 Performance of the Genetic Algorithm . . . . . 114
5.4 Algorithm Performance in Optimizing the Time-Stage Control . . . 115
5.4.1 Optimization Problem Formulation and Characteristics . . . 116
5.4.2 Performance of the Complex Method . . . . . 118
5.4.3 Performance of the Genetic Algorithm . . . . . 119
5.5 Conclusion . . . . . 122

**6 Characteristics of the Optimum Control Strategy and Time-Stage Control** 124
6.1 Characteristics of the Optimum Schedule of Control Variables . . . 126

6.1.1 The Influence of Mass Thermal Storage . . . . . 126
6.1.2 Summer Operation . . . . . 128
6.1.3 Transition Season Operation . . . . . 130
6.1.4 Winter Operation . . . . . 130
6.1.5 The Influence of Electricity Tariff Structure and Electricity Schedule . . . . . 132
6.1.6 The Influence of Thermal Comfort Limits . . . . . 136
6.1.7 The Influence of Plant Part Load Performance . . . . . 137
6.2 Simplified Time-Stage Control . . . . . 138
6.3 Relative Performance of the Controllers . . . . . 142
6.3.1 Summer Operation . . . . . 142
6.3.2 Transition Season Operation . . . . . 144
6.3.3 Winter Operation . . . . . 144
6.4 Conclusion . . . . . 145

**7 Weather Prediction** **147**
7.1 A Review of Weather Prediction Models . . . . . 148
7.1.1 Weather Prediction and Weather Model . . . . . 149
7.2 Temperature Prediction . . . . . 152
7.2.1 The Properties of Temperature Time Series . . . . . 152
7.2.2 ARMA Models . . . . . 155
7.2.3 Characteristics and Selection of the Order of ARMA Models 157
7.2.4 The Combined Deterministic-Stochastic Method . . . . . 160
7.2.5 The Expanded Combined Method to Include Global Radiation 162
7.2.6 Selection of Model Parameters . . . . . 165
7.2.7 Updating Temperature Prediction . . . . . 168
7.2.8 Performance Comparisons of the Temperature Prediction Models . . . . . 171
7.3 Radiation Prediction . . . . . 178
7.3.1 The Properties of Radiation Time Series . . . . . 178
7.3.2 The Radiation Prediction Model . . . . . 179
7.4 Conclusion . . . . . 182

**8 Performance Analysis of the Optimal Predictive Controller** **183**
8.1 A Comparison of the Optimal Predictive Setpoint Scheduling Control and Time-Stage Control . . . . . 184
8.2 Annual Performance Analysis for the Time-Stage Control . . . . . 185
8.2.1 Winter Operation . . . . . 186
8.2.2 Transitional Season Operation . . . . . 190
8.2.3 Summer Operation . . . . . 193

8.2.4 The Characteristics of Room Thermal Conditions and Control Performance in Annual Operation . . . . . 197
8.3 The Effect of Building Construction on Controller Performance . . . 200
8.4 On-Line Adaption of the Optimal Predictive Control Strategy . . . 207
8.5 Conclusion . . . . . 213

**9 Conclusions and Further Work** **215**
9.1 Conclusions . . . . . 215
9.2 Suggestions for Further Work . . . . . 220

**References** **225**

**A The Complex Algorithm** **234**

**B The Genetic Algorithm** **237**

**C Publications To Date** **242**

# List of Figures


1.1 A Hollow Core Ventilated Slab . . . . . 3

2.1 Duct Layout in the Ventilated Slab . . . . . 13
2.2 Supervisory Controller Software Functional Diagram . . . . . 21
2.3 Zone Air Temperature Setpoints . . . . . 24

3.1 Plant Configuration . . . . . 28
3.2 Control System Structure . . . . . 29
3.3 The Multistage Decision Problem . . . . . 38

4.1 Multi-layer Building Element . . . . . 53
4.2 Lumped Parameter Model of a Building Element . . . . . 53
4.3 Lumped Parameter Model of the Ventilated Slab . . . . . 56
4.4 Simplified Air Path and Area of Thermal Capacitance . . . . . 57
4.5 Dimensions for Slab Concrete Capacitance and Resistance Calculations . . . . . 58
4.6 Active and Inactive Capacitance During Switchflow Operation . . . 60
4.7 Lumped Parameter First-order Building Model . . . . . 62
4.8 Combined Building and Ventilated Slab Model . . . . . 64
4.9 The Operating Diagram of Regenerative Heat Recovery Device . . . 72
4.10 Test Measurements (1.18 m/s velocity) . . . . . 76
4.11 Test Measurements (3.75 m/s velocity) . . . . . 77
4.12 Measured and Simulated Performance (1.18 m/s velocity) . . . . . 78
4.13 Measured and Simulated Performance (3.75 m/s velocity) . . . . . 78
4.14 Step Test Measurements . . . . . 80
4.15 Step Test Measured and Simulated Air Temperatures . . . . . 81
4.16 Step Test Measured and Simulated Air Leaving Temperature . . . . 81
4.17 Step Test Measured and Simulated Mass Temperature . . . . . 82
4.18 The Influence of Corner Heat Transfer Coefficient on Simulated Air Leaving Temperature . . . . . 86
4.19 Comparative Performance of Ventilated Slab with Conventional Exposed Ceiling System . . . . . 89
4.20 The Influence of Ventilation on Room Thermal Conditions . . . . . 90

4.21 The Influence of Switchflow Operation on Room Thermal Conditions 92

5.1 A Surface in the Search Space for the Fan Flow Rate Scheduling Problem . . . . . 99
5.2 The Influence of Initial Point on the Complex Search . . . . . 100
5.3 An Example of the Complex Progress . . . . . 101
5.4 Exponential Penalty Function . . . . . 104
5.5 The Cost Reduction with Generations for the Two Selection Methods 105
5.6 The Influence of Crossover Rate on Cost Reduction in the Remainder Stochastic Selection . . . . . 108
5.7 The Influence of Initial Guess on the Optimum Solution in the GA Search . . . . . 109
5.8 A Surface of Supply Air Flow Rate and Temperature in the Search Space for the Setpoint Scheduling Control Problem . . . . . 111
5.9 A Surface of Two Supply Air Flow Rates in the Search Space for the Setpoint Scheduling Control Problem . . . . . 112
5.10 Solutions to Setpoint Scheduling Problem from the GA and the Complex Method . . . . . 114
5.11 A Surface of Time Switches for the Time-Stage Control Problem . . 117
5.12 A Surface of Supply Air Flow Rate and Temperature for the Time-Stage Control Problem . . . . . 118
5.13 An Example of the Search in the Time-Stage Control by the Complex Method . . . . . 119
5.14 The Cost Reduction with Generations for the Time-Stage Control Problem . . . . . 120
5.15 The Number of Feasible Solutions in Generations for the Time-Stage Control Problem . . . . . 121
5.16 An Optimal Solution to Time-Stage Problem from the GA Search . 122

6.1 The Comparison of Optimal Schedules of the Fan Operation for the Two Days . . . . . 127
6.2 Optimum Scheduling of Control Variables for One Day in the Summer 129
6.3 Optimum Scheduling of Control Variables for Seven Days in the Summer . . . . . 129
6.4 Optimum Scheduling of Control Variables for One Day in the Winter 131
6.5 Optimum Scheduling of Control Variables for Seven Days in the Winter . . . . . 132
6.6 Optimum Scheduling of Control Variables in the Summer under 1:1 and 3:1 Electricity Tariff Structures . . . . . 133
6.7 Optimum Scheduling of Control Variables in the Winter under 1:1 and 3:1 Electricity Tariff Structures . . . . . 133

6.8 Optimum Scheduling of Control Variables in the Summer under Different Schedule of On-Peak Electricity Tariff . . . . . 135
6.9 The Sensitivity of Energy Cost with Thermal Comfort . . . . . 136
6.10 The Chiller Part Load Performance . . . . . 137
6.11 Simplified Time-Stage Control . . . . . 139
6.12 Comparison of Optimal Scheduling of Control Variables from Two Controllers under Summer Operation . . . . . 140
6.13 Comparison of Optimal Scheduling of Control Variables from Two Controllers under Winter Operation . . . . . 141
6.14 Comparison of Optimal Scheduling of Control Variables from Two Controllers in the Summer Under a 1:1 Electricity Structure . . . . 141

7.1 Hourly Mean and Standard Deviation of the Ambient Temperature 153
7.2 Daily Average Ambient temperature and Total Global Radiation in CIBSE Year . . . . . 154
7.3 Updating of Temperature Profile for the $9^{th}$ May 1994 . . . . . 169
7.4 The Corrected Temperature Profile on the $22^{th}$ September 1994 . . 171
7.5 The Comparison between Sinusoidal Functions and EWMA in Modelling Deterministic Element of Temperature Profile . . . . . 172
7.6 The Predicted Ambient Temperature Profile for July of the CIBSE year . . . . . 176
7.7 The Predicted Ambient Temperature Profile from $14^{th}$ to $17^{th}$ July of the CIBSE year . . . . . 177
7.8 The Predicted Ambient Temperature Profile for September, 1994 . 177
7.9 Hourly Mean and Standard Deviation of the Global Radiation . . . 178
7.10 Modelling Stochastic Element of Global Radiation . . . . . 180
7.11 Predicted Profile of Global Radiation from $17^{th}$ to $23^{th}$ September 1994 . . . . . 181

8.1 Mean Room Temperature and Standard Deviation Profiles for February . . . . . 187
8.2 Mean Slab Mass Temperature and Standard Deviation Profiles for February . . . . . 187
8.3 Mean Room Temperature and Standard Deviation Profiles for April 191
8.4 Mean Slab Mass Temperature and Standard Deviation Profiles for April . . . . . 191
8.5 Mean Room Temperature and Standard Deviation Profiles for July 193
8.6 Mean Slab Mass Temperature and Standard Deviation Profiles for July . . . . . 194
8.7 Monthly Occupied Average Room Temperature and PMV Index, and Monthly Average Slab Temperature over 1994 . . . . . 198

8.8 The Distributions of Energy Use and Energy Cost from the Predictive Controller over 1994 . . . . . 199
8.9 Mean Room Temperature and Standard Deviation Profiles for February from the Three Buildings . . . . . 203
8.10 Mean Slab Mass Temperature and Standard Deviation Profiles for February from the Three Buildings . . . . . 204
8.11 Mean Room Temperature and Standard Deviation Profiles for July from the Three Buildings . . . . . 205
8.12 Mean Slab Mass Temperature and Standard Deviation Profiles for July from the Three Buildings . . . . . 206
8.13 Comparison of Room Temperatures in June with the Use of an Adaptive HRD Control . . . . . 210
8.14 Comparison of Room Temperatures in July with the Use of Adaptive HRD and Booster Control . . . . . 212

9.1 Proposed On-Line Tuning Building Model . . . . . 221

# List of Tables


3.1 Plant Operating Modes . . . . . 33

4.1 Model Accuracy for Cyclic Operation . . . . . 79
4.2 Model Accuracy for Step Input Operation . . . . . 81
4.3 Model Sensitivity to Corner Heat Transfer Coefficient for Step Input Operation . . . . . 85
4.4 Uncertainties of Material Properties . . . . . 87

5.1 Performance of the GA and the Complex Method in the Scheduling of Supply Air Flow Rate . . . . . 110
5.2 Performance from the GA and the Complex Method in Setpoint Scheduling Control Problem . . . . . 115
5.3 Performance of the GA in Time-Stage Control Problem . . . . . 121

6.1 Building Construction . . . . . 125
6.2 Performance Comparison for $24^{th}$ to $30^{th}$ June . . . . . 143
6.3 Performance Comparison for $9^{th}$ to $15^{th}$ July . . . . . 144
6.4 Performance Comparison for $12^{th}$ to $18^{th}$ February . . . . . 145

7.1 The Effect of $\lambda$ on the EWMA Model . . . . . 167
7.2 An Example of Parameters Fitted for Sinusoidal Functions . . . . . 167
7.3 Comparison of Sinusoidal Functions and EWMA Model . . . . . 173
7.4 Performance Comparison between the Pure Stochastic and Combined Methods . . . . . 173
7.5 Prediction Errors for the CIBSE Year and 1994 from the Combined Deterministic-Stochastic Method . . . . . 174
7.6 The Influence of Solar Radiation on the Prediction of Daily Average Temperature . . . . . 174
7.7 Performance Comparison of the Two Combined Methods . . . . . 175
7.8 Performance Comparison between EWMA Model and Sinusoidal Function Method for Modelling Solar Radiation . . . . . 180

8.1 Ambient Temperature Prediction Errors for February . . . . . 189
8.2 Room Air Temperature Errors for February . . . . . 189

8.3 Comparative Performance of the Predictive Controller in February . 190
8.4 Ambient Temperature Prediction Errors for April . . . . . 192
8.5 Room Air Temperature Prediction Errors for April . . . . . 192
8.6 Comparative Performance of the Predictive Controller in April . . . 192
8.7 Ambient Temperature Prediction Errors for July . . . . . 195
8.8 Room Air Temperature Prediction Errors for July . . . . . 195
8.9 Comparative Performance of the Predictive Controller in July . . . 196
8.10 Percentage of Time when Heating or Cooling Is Required during Annual Operation . . . . . 198
8.11 The Construction of 'low U value, low mass' Building . . . . . 201
8.12 The Construction of 'high U value, low mass' Building . . . . . 201
8.13 The Thermal Properties of the Three Types of Building . . . . . 202

# Chapter 1

# Introduction

The energy crisis of the 1970's started a move towards the design and operation of energy efficient buildings. With half of the UK's primary energy still being consumed in buildings, the need to reduce building energy consumption is now important in order to restrict the emission of environmental pollutants. One approach that reduces energy consumption is to utilize the building fabric as a thermal energy store. In buildings with low thermal loads, the use of the ambient air temperature in conjunction with the thermal store can be sufficient to regulate the room thermal environment. For high thermal loads where air conditioning is required, the integration of the building fabric with the air conditioning plant can reduce the peak demand on the plant capacity and improve operational efficiency. The application of the building fabric thermal storage system is on the increase. This thesis investigates the control of one form of active building fabric thermal storage system.

## 1.1 Hollow Core Ventilated Slab Systems

Building fabric thermal storage can be charged by the ventilation air or by a chilled water system. For instance, chilled water was driven through coils embedded into floor slabs to improve the performance of building fabric storage (Meierhans, 1993). Other fabric thermal storage systems, such as rock thermal storage (Allen *et al.*, 1984) and earth storage (Givoni, 1984), use remote massive devices to store energy

at night for relieving daytime thermal loads in buildings. The heat storage in these systems uses the sensible heat capacity of the building materials, rock and soil. A considerable effort has been made to use Phase Change Materials (PCMs) to increase the efficiency of fabric thermal storage systems. These materials can allow the thermal storage of a building to be substantially increased without an undue increase in building mass or volume (Tahat *et al.*, 1993; Hawes *et al.*, 1993).

Overnight ventilation is the simplest passive technique and utilizes the thermal capacity of the building mass to reduce cooling demand during the daytime operation. A building fabric thermal storage system that uses ventilation as cooling medium to charge and discharge the mass thermal store is investigated in this thesis. A traditional approach is to use the cool ambient night air to flush the building spaces, simply by opening windows to allow the air to enter the room. However, this natural ventilation approach is not always easily implemented, for example, security may prevent the opening of windows. In addition, a totally passive storage system may not sufficiently utilize the storage capacity of the building fabric, so that the following day's thermal loads are not met.

Mechanical ventilation at night can be used to assist the charging of the building fabric thermal store. When the building fabric is used as a heating or cooling buffer, the larger the heat capacity of fabric, the better its ability to regulate the room thermal conditions. For this reason, new buildings have a tendency to possess a 'heavier' mass than buildings of ten years ago, when conventional air conditioning techniques were more predominant, and light weight structures were adopted to allow a rapid response to the air conditioning plant. Such buildings had a false ceiling which decoupled the building mass from the occupied zones. Low energy buildings now expose as much of the ceiling as possible, so as to make the best use of the building mass in reducing energy costs and regulating the thermal comfort in the occupied space. An exposed ceiling system that utilizes the building mass as a thermal store has been the subject of some research (Ruud *et al.*, 1990; Andresen and Brandemuehl, 1992; Conniff, 1991). However, this approach to thermal storage is limited, as the building structure has a finite capacity and because of the weak coupling between the building mass and the ventilation air, the thermal capacity of the mass is under utilized.

The building mass can be further utilized by integrating mechanical ventilation within extruded hollow core concrete ceiling and floor slabs. This approach was

devised in Sweden, and has a trade name of 'Termodeck' (or 'Thermofloor' in the Netherlands). Due to its simplicity and efficiency, hollow core ventilated slab systems are receiving increasing attention in the UK (Bunn, 1994). In a hollow core ventilated slab system, the ventilation air is passed through the hollow cores of the floor and ceiling slabs, the turbulent air flow thus increasing the convective heat transfer between the air and the slab mass. The extended air supply path within the slab is created by blocking the core ends and cutting connecting holes between the cores (Figure 1.1). Having passed through the slab, the ventilation air can then enter the room directly via a diffuser, or pass through ductwork to enter the room at a low level as part of a displacement ventilation system. It was claimed from system monitoring that high energy savings had been obtained from this system (Zmeureanu and Fazio, 1988; Bunn, 1991).

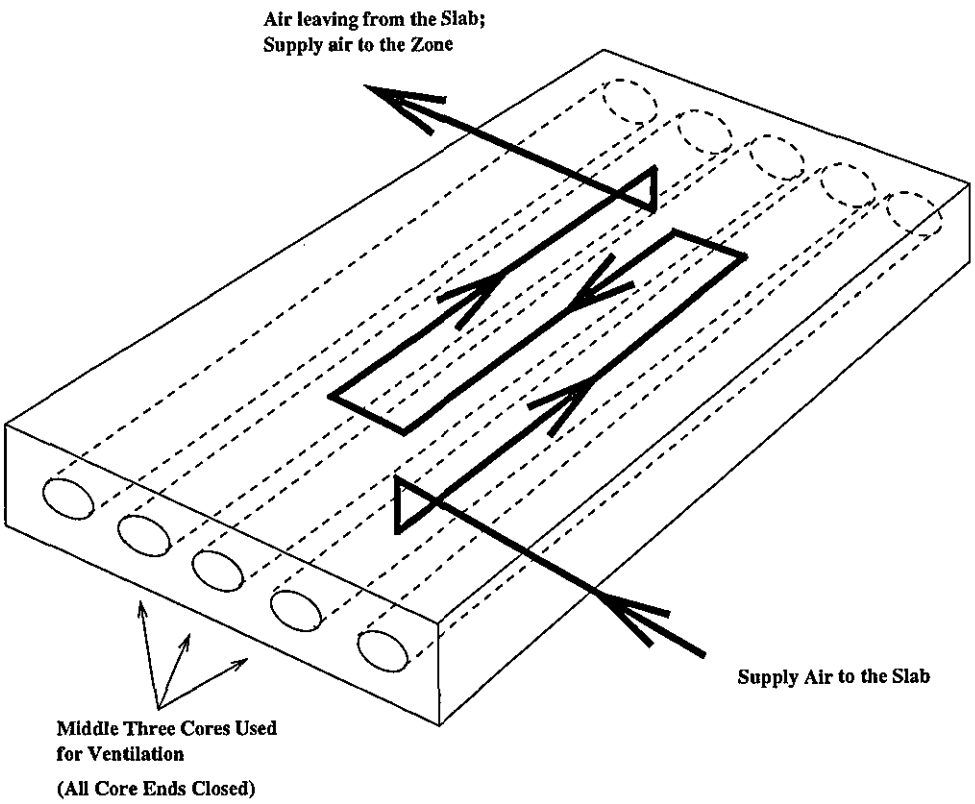


**Figure 1.1, A Hollow Core Ventilated Slab**

Due to the thermal capacity of the slab, the system is unable to provide a rapid response to the zone thermal loads, and therefore an effective control strategy is required to ensure the correct response of the system to the zone loads. Conven-

tional control strategies usually use some rules to charge and discharge the thermal store, which may fail to make full use of the storage capacity and varying ambient conditions in reducing the energy cost. In order to maximize energy savings, the optimal control of the fabric thermal storage is necessary, so that the thermal storage is scheduled according to thermal loads in the building; this is the subject of this thesis.

## 1.2 Optimal Supervisory Control of Building Fabric Thermal Storage Systems

Supervisory control monitors the total system operation and supervises the overall control of the local subsystems. The supervision given to local systems includes functions such as the selection and modification of local loop setpoints, optimizing the ON and OFF operation of the subsystems, and controlling the interaction between subsystems (Levenhagen and Spethmann, 1993). Conversely, local loop control is concerned with the individual plant component operation, such that the setpoint for the component is met, for instance, by using simple ON/OFF or PID control methods.

For a thermal storage system, where the thermal store is charged during one period so as to relieve the thermal loads during a subsequent period, the supervisory controller must decide on the operating schedule for the thermal storage system. For instance, when to begin the charge and discharge phases, and how quickly to charge and discharge the store. In comparison with plant storage systems (such as ice thermal storage), the supervisory control of building fabric thermal storage systems is more demanding, since the operation is restricted by the limited capacity of the thermal store, the close link with the occupied space in which thermal comfort must be maintained, and finally by the need to restrict condensation forming in the building structure.

Within a planning horizon (typically 24 hours), the ambient temperature, solar radiation, room temperature, occupancy schedule, etc, are all changeable. An adequate supervisory control strategy for a fabric thermal storage system would be one that determines the operational parameter setpoints in accordance with the time-varying thermal conditions. The characteristics of the supervisory control of

a building fabric thermal storage system can be attributed to:

- the dynamic response of the thermal store;
- the nature of the time-dependent energy source (such as cool night air to charge storage);
- the energy stored and lost to adjoining environment.

Since the thermal capacity of the building fabric is used as a storage medium, the dynamic response of the building must be taken into account by the controller in order to identify the proper operating schedule. The energy savings associated with a fabric thermal storage system result substantially from the free night cooling strategy, which uses the night ambient air to charge the thermal store. This energy source is highly time-dependent, which contributes to the dynamic operation of the system. The energy stored in the building fabric is not insulated from the building space, thus there is a degree of heat transfer from the thermal store to the occupied zones and then to the ambient environment. These fabric thermal storage system operating characteristics indicate a need of an optimal control strategy that maximizes the use of the thermal store in reducing energy costs.

In order to maximize energy savings from a fabric thermal storage system, the supervisory control strategy must be optimized over a planning period, in order to take account of the dynamic response of the building, to take advantage of time-dependent energy sources and the electricity tariff structure, and finally to operate the storage so that energy losses are minimized. The diurnal cycle of ambient conditions and daily occupancy patterns, dictate that 24 hours is a suitable planning period over which to optimize the system operation. Further, in order to account for the dynamic response of the building over the planning period, the controller must be able to predict the future ambient conditions and assess their impact on the building operation. Therefore, the supervisory controller provides an optimum predictive schedule of plant operation to regulate the thermal storage over the 24 hours, so that the total energy cost is minimized, and in the meantime, the occupant comfort is satisfied.

The optimal predictive controller investigated in this thesis, supervises the operation of the hollow core ventilated slab system over a 24 hour planning period. Due to its special air supply path, the control of this system differs from that of

conventional buildings. However, the approach developed in this thesis can be generalized and applied to other building fabric thermal storage systems.

## 1.3 Objectives of the Thesis

The overall objective of this research is to investigate the optimum supervisory control of hollow core concrete ventilated slab systems, such that energy costs are minimized without adversely affecting the occupant's thermal comfort.

### 1.3.1 Research Methodology

The approach to the research is to investigate the optimum control strategy by applying an optimization algorithm to a computer simulation model of a hollow core ventilated slab system and associated HVAC plant. Having analysed the characteristics of the optimum control problem, a suitable approach to simplifying the supervisory control is investigated. The implementation of the optimum controller is then conducted by incorporating a weather prediction model. The performance of the optimal predictive controller in reducing energy costs during annual operation forms the final analysis of the controller performance.

### 1.3.2 Strategic Objectives

The strategic objectives of this research are:

- to describe the fundamental concepts and review literature on the different techniques proposed for the optimum control of building thermal systems, including hollow core ventilated slab systems (Chapter 2);
- to describe the design of an optimum predictive controller for hollow core ventilated slab systems, including the definition of the control problem, development of the controller structure and the identification of pertinent controller components (Chapter 3);

- to develop a comprehensive and yet simple building and plant thermal model that is capable of predicting the building thermal response to a given plant operating schedule; examine the robustness of the model to the range of system operating conditions that will be encountered by the controller (Chapter 4);
- to apply optimization algorithms to the building and plant model, and investigate the performance of the optimization algorithms in finding an optimum solution, so that an appropriate optimization algorithm is identified for use in the optimum controller (Chapter 5);
- to investigate the control characteristics of the optimum setpoint scheduling control strategy and identify a simplified control approach that matches the control characteristics (Chapter 6);
- to develop a weather prediction model that allows the optimum controller to predict the plant operating schedules over the planning period (Chapter 7);
- to investigate the seasonal operation and annual performance of the optimum predictive control strategy in relation to the effects of weather prediction errors (Chapter 8);
- to draw conclusions and suggest possible areas where there is the potential to conduct further research (Chapter 9).

# Chapter 2

# Literature Review

## Introduction

Since the thermal capacity of the building mass is limited, and the plant operation associated with the ventilated slab is restricted and due to its close link with the occupied space, the supervisory control of ventilated slab systems is more difficult than for other thermal storage systems. The application and control of hollow core ventilated slab systems have been reviewed, significant energy savings having been reported from the system monitoring. However, the performance monitoring of hollow core ventilated slab systems indicates that a conventional control approach for hollow core ventilated slab systems is not effective, the thermal storage and free energy source being under utilized. This has led to the investigation of the optimal control of the system in this research. The methods used for the optimal control of building thermal systems are also described, the methodologies for the optimal control of building fabric thermal storage systems being highlighted.

## 2.1 A Review of Hollow Core Ventilated Slab Thermal Storage Systems

Hollow core ventilated slab systems are an active fabric thermal storage system, which were first devised in Sweden during the 1970's. The system concept is one of integrating the mechanical ventilation with structural hollow core slabs to provide air pathways. The effect is that the ventilated hollow core slabs act as regenerative heat exchangers, with enhanced heat transfer between the air and the slab resulting from turbulent air flow in slab cores. The basic operation of this system is to use cool outside air, or air cooled from plant, to reduce the slab temperature by passing it through slab cores during summer nights. During the following day, the warmer outside air is cooled when it passes through the slabs before it is supplied into the room. In the winter, before the occupants arrive, hot air (around 40~45 °C) is used to raise the slab temperature to store heat using off-peak electricity.

Since this technique was devised, interest in the use of structural hollow core slabs as thermal stores is on the increase. Birrer (1983) measured a six-storey office building in Johannesburg, South Africa, where ventilated hollow core concrete slabs were used. The results indicated a reduction in cooling load by approximately 50 $W/m^2$ due to the structural mass storage of heat. A survey conducted in Canada (Zmeureanu and Fazio, 1988) also indicated that the use of hollow core concrete slabs for ventilation could provide a reduction in cooling load by approximately 50 $W/m^2$ and energy savings between 13% and 70% could be made, depending on the particular building and prevailing weather conditions. Allen *et al.* (1984) utilized the ENERPASS program to simulate the effect of a hollow core slab in a passive solar house in Ottawa and concluded that energy savings of approximately 13% could be obtained.

Bunn (1991) reported the performance of a factory in Stockholm, which was one of the first buildings to be built in 1986 using the hollow ventilated slab principle. The performance indicated that the room thermal conditions were well controlled, and 95% of heating load was satisfied by the charge of the mass storage at night using off-peak electricity. Another building in Stockholm was also reported by Bunn (1991), where both short-term and long-term thermal storages were utilized, the short-term thermal storage being by the hollow core ventilated slab systems

and the long-term storage by the use of bedrock on a seasonal basis. The design aim of this building was to achieve total energy savings of approximately 45% compared to the energy consumption of a conventional Swedish office. Switchflow units were also designed into this building. A switchflow unit has similar size and appearance to a VAV mixing box, and can allow selective short circuiting of the air flow through the slab. The components of the unit include a changeover damper, an air flow meter and dampers for adjusting the direction of air flow. At a chosen indoor temperature, a modulating damper can increase the proportion of air flow directly from the supply air duct to the outlet diffuser, thus short circuiting the slab and providing a faster response to the demands for extra heating or cooling; the damper may also be repositioned to allow the air through a shorter run of a single slab core. It was concluded that the switchflow unit can offer better and closer control of individual offices, depending on the heating or cooling load in the space (Bunn, 1991).

In addition to the potential energy savings provided by using the slab mass storage, the perceived comfort levels are often higher during summer with this slab cooling approach due to the radiant cooling effect from the exposed ceiling slab (Kendrick, 1995). The circulation air is close to the slab temperature which is not too low, thus alleviating the uncomfortable drafts associated with conventional air conditioning methods (BSRIA, 1992).

Hollow core ventilated slab systems provide sensible cooling only, and can meet moderate sensible cooling loads. They offer a convenient means of cooling for buildings where the daily outdoor temperature fluctuations are relatively high and the ambient temperatures are lower than the internal room temperatures at night. These systems are well suited to comfort conditioning buildings in the UK climate, and as such are receiving more and more attention in the UK. A test chamber was constructed at the Building Research Establishment, Garston, UK, which incorporated hollow core ventilated slabs in the ceiling structure. Results from experimental tests indicated that the system can be used to minimize the requirement for air conditioning in commercial buildings (Willis and Wilkins, 1993). It was also found that most of the heat transfer between the ventilation air and the slab occurred at the corners of the slab cores, whereas along the straight sections of core, the heat transfer was comparatively low. This localisation has important consequences for the real thermal capacity of the slab. Therefore, in the design of such systems, the effective heat capacity of the slab mass involved in regulating

the room thermal condition, and the heat transfer between the ventilation air and the slab mass, should be evaluated.

The Building Services Research Information Association (BSRIA), UK investigated three types of fabric storage systems (Barnard, 1995): a conventional ventilation system but with an exposed ceiling slab, a false void ventilation system and a hollow core ventilated slab system. It was concluded that with an enhancement in the thermal link between the fabric and the air, the performance of the three systems could be improved. The sensitivity of the systems' performance to a number of parameters such as supply air flow rate, heat gains, ceiling surface heat transfer coefficient was also investigated. The room thermal condition resulting from a night cooling strategy was examined for each system.

Bunn (1994) described the building construction and seasonal operation of the first ventilated slab building constructed in the UK. The building is a two-storey office building located in Kent, with supplementary heating and cooling from electrical heaters and an indirect evaporative cooler. Winwood *et al.* (1997b) reported the results from monitoring the building. A steady internal temperature was maintained both from day to day and seasonally, however, the annual energy consumption was higher than expected, partly due to improperly sized heaters and uncontrolled heat losses through the ductwork. The higher energy consumption was also attributed to an inefficient control strategy for the period of active cooling and fan operation. Bunn (1995) reported the details of the building design and control strategy for a teaching building at the University of East Anglia, Norwich. It is of a heavy weight well insulated construction, typical of ventilated slab buildings. Kendrick (1995) analysed the monitored performance of this building and concluded that a storage efficiency of over 70% was obtained by the concrete slabs in storing "coolth" at night. Some suggestions on how to improve the building performance were made, such as increasing the air flow rate during the night free cooling period, and minimizing temperature gains of the night air en route to the slabs.

Operational experience of the hollow core ventilated slab buildings shows that the system provides a very effective means of thermal storage, which can reduce operating costs when properly controlled. Following the success of the first two ventilated slab buildings in the UK, there is an increasing interest in this fabric storage application (Winwood *et al.*, 1997a).

### 2.1.1 Research into the Modelling of Hollow Core Ventilated Slab Systems

The heat transfer process occurring inside the slab cores is the most critical aspect of the hollow core ventilated slab system's performance. However, many of the factors influencing the heat transfer in the slabs are still unknown, especially the heat flow around the corners of the cores. There is also a need to assess the thermal capacity of the slab that is active during the charge and discharge cycles. BSRIA (1992) suggested the following factors that influence the performance of the slabs in terms of the amount of energy that can be absorbed and stored:

- the mass and thermal properties of the slab;
- the area available for heat exchange between the air and the slab;
- the heat transfer characteristics between the air and the slab.

In order to maximize energy savings from ventilated slab systems, the ventilation and thermal storage system must be carefully designed and operated. Both the design and control of the system can be investigated using a computer simulation of the system.

To date, little research has been directed towards the modelling of hollow core thermal storage systems. A finite element method has been used to model the heat transfer process in the slab (Augenbroe and Vedder, 1985). It was concluded that the three heat transfer dimensions can be simplified to one dimension through the thickness of the slab. In general, finite element methods are computationally too intensive to allow the modelling of the major thermal disturbances on the building and to enable the investigation of different plant operation strategies. A mathematical model derived from a heat balance on the room environment and hollow core slab has been developed (Zmeureanu and Fazio, 1988), where two dimensional heat transfer was considered, through the thickness of the slab and along the airflow path, which resulted in 44 simultaneous linear equations for the heat transfer process within the hollow core slab. However, the slab cores were simplified as two parallel plates with air passing between them. A constant heat transfer coefficient along the air path was assumed so that the increase in heat transfer around the corners of the air path was not modelled.

In contrast, computational fluid dynamic modelling methods have been used to study the heat transfer within the hollow cores (Winwood *et al.*, 1994). The air path was simplified to bring the corner of the cores flush with the inlet and outlet (Figure 2.1). The overall core length along the air path was the same as for the real core. It was concluded that the majority of the heat transfer took place at the corners of the air path. The applicability of the computational fluid dynamic modelling approach is limited in that constant boundary conditions are normally assumed, so that the effect of time variant disturbances on the room and slab are not modelled.

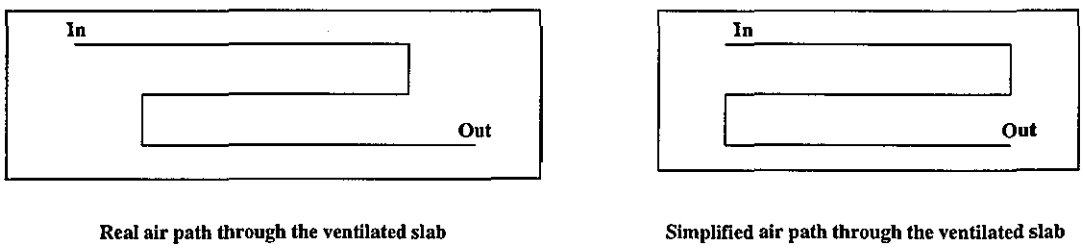


**Figure 2.1, Duct Layout in the Ventilated Slab**

General energy simulation programs, such as ESP (Clarke, 1985), and TRANSYS (Klein, *et al.*, 1994), may be of some assistance for the general design of the system, but a model for ventilated slab systems has not been developed for these programs. To summarize, the existing models are either limited in their modelling of the heat transfer along the slab air path or are unable to represent the effect of time variant disturbances on the room and ventilated slab. In order to investigate the performance of the hollow core ventilated slab system, and the effectiveness of control strategies for the system, a building model is required that can evaluate the heat transfer in the slab cores and the room thermal response to various disturbances. This model must also be able to represent various building constructions and be accurate and computationally efficient. The development of such a building model that overcomes the deficiencies in the existing simulation models is essential in this research to investigate the control of the ventilated slab system.

## 2.2 The Control of Hollow Core Ventilated Slab Systems

Ventilated slab system controllers usually use the ambient air temperature, internal space and slab mass temperature, to trigger the ventilation to charge and discharge the thermal store. During summer nights, as soon as the outside air temperature is lower than a pre-determined level, fresh air is used to flush the slabs and then the building spaces; if the outside temperature remains higher than the pre-determined level, cooling plant has to be used to reduce the fresh air temperature before delivery to the slab. This can be conducted at the lower night electricity tariff rate. During the daytime, the warmer outside air is cooled down when it passes through the precooled slab. If the room thermal load can not be entirely satisfied by the slab cooling, additional air conditioning must be used. However, the peak load demand on the plant, and hence plant size, will be reduced by the energy stored in the slab, thus making savings in both capital and running costs.

For winter operation, when the temperature of the slab drops to below the setpoint, for instance, 20 °C, the ventilated slab is recharged by recirculating the supply air through the slab cores at night, the air being heated by heater batteries with the mass temperature being raised by 2 °C to around 21 °C $\sim$ 22 °C. It was observed that this operation can create sufficient thermal storage to cover the heating requirements of the building during the occupied period (Bunn, 1991).

Switchflow operation (Section 2.1) was investigated by Willis and Wilkins (1993), with the conclusion that there was a 1.75 °C difference in the temperature of the air leaving the slab when compared to the temperature from normal three core operation (the supply air temperature was 14 °C). An example control strategy was suggested for summer operation which uses switchflow to boost the cooling supply to meet the zone loads, during the afternoon when a given internal temperature threshold is exceeded. However, the complete performance of the switchflow operation was not described.

Since the ventilated slab cooling approach involves the interaction between the plant and the building structure, it does not have the same flexibility associated with plant storage systems, such as ice or chilled water storage. The fact that the

building structure has a finite capacity means that there are inherent limits and difficulties for the system in regulating the internal temperature. In addition, as slab cooling lacks a "rapid response" to the needs of an internal space (Willis and Wilkins, 1993), the control strategy must offset the limitations. The link between the thermal mass and the air conditioning plant has an important effect on the control specifications. Simple ON/OFF or stepped control can be used instead of modulating control, as the thermal mass will tend to dampen out temperature fluctuations in the space.

In the control of the hollow core ventilated slab thermal storage, the objective is to maximize the use of free cooling from the ambient environment. As the energy source for cooling the slab is time-dependent, such as overnight free cooling, the effective operation of the system requires careful control and monitoring of the energy stored in the slabs. For instance, predictive control systems can be used to set the night operation of the system based on a prediction of the next day's thermal load. Arnold (1993; 1996) examined the characteristics for the control of ventilated slab thermal storage and suggested that only a dynamic simulation program can predict the thermal behaviour of the ventilated slab.

An example of a conventional control strategy for ventilated slab systems is described below. The rule-based control uses only a comparison of the zone, slab mass and ambient temperatures to control the thermal storage. Such a strategy is not designed for maximizing the use of thermal storage to reduce energy cost, which is however, the main incentive of using the active fabric thermal storage system. Energy monitoring in ventilated slab buildings has indicated that the effective control of the mass storage during the night precooling period is essential and can substantially improve the system performance (Kendrick, 1995). However, the conventional rule-based control can not effectively regulate the mass storage to meet the varying thermal loads in the room space.

### 2.2.1 An Example of Hollow Core Ventilated Slab System Control

In the conventional control of hollow core ventilated slab systems, it is usual to monitor the slab mass or room air temperatures and to use these to dictate the time switching of the plant operation. The ventilated slab building at the University

of East Anglia (UEA), UK, is taken as an example to illustrate the conventional control approach. The supervisory control strategy for this building is described by the following rules (Bunn, 1995):

- night operation:
  1. Summer:
     - if during the day $T_o > 15$ °C , or at 10:00 pm $T_{az} > 23$ °C and 3 °C $< T_{az} - T_o < 8$ °C, then the ventilation fans are switched ON;
     - if the fans are ON and $T_s < 21$ °C or $T_o < 8$ °C, then the fans are switched OFF.
  2. Winter:
     - if $T_{az} < 18$ °C, then the ventilation fans are switched ON to circulate supply air at 35 °C heated by a heater battery;
     - if the fans are ON and $T_{az} \geq 20$ °C, then the fans are switched OFF.
- operation during occupancy:

  the fans are ON to provide full fresh air ventilation at a constant rate in a range of $20 \sim 40$ litre/s depending on the zone type. A regenerative heat recovery device is operated in the winter to increase the fresh air supply temperature by the warm room extract air; in the summer, it may also be operated if the fresh air temperature is much higher than the room air, cooling then being available from the room extract air.

Where $T_o$ is the ambient air temperature, $T_{az}$ is the zone air temperature and $T_s$ the slab mass temperature.

These rules can not fully utilize the potential of the thermal storage and sometimes may waste energy, for instance, it may not be necessary to start free night cooling at as early as 10:00 pm to relieve the cooling load of the following day. The use of ambient and internal room temperatures in the control rules may not provide sufficient thermal storage, leading to discomfort in the occupied space.

The minimization of plant operating costs can only be achieved by the optimum control of plant operating schedule for the charging and discharging of the thermal

store. In the presence of an electricity tariff structure, optimal control is especially preferable since it can provide the optimum ventilation for both the night and day operation by taking account of the varying cost of electricity.

Research into optimal control of general building thermal systems is reviewed below, followed by a review of the optimal control of plant and fabric thermal storage systems. The optimal control of plant and fabric thermal storage systems shares some common characteristics in that the daytime cooling load is shifted to the night operation of the plant, in order to reduce energy costs and the demand on the plant. Both control problems are dynamic in nature, and are often referred to as "dynamic optimal control".

## 2.3 Optimal Control of Building Thermal Systems

Building thermal systems generally consist of the primary plant, air handling units and the building itself. Some research has been conducted to investigate the optimal control of building thermal systems. Cumali (1988) minimized energy use in a high-rise building complex by using global optimization techniques to determine the plant control and operation strategies in real-time. The optimization problem was broken into small manageable parts by parameterizing the coupling variables. Each problem was optimized using a reduced gradient method.

Cascia (1988) developed an adaptive control algorithm to optimize chiller plant control. The controller could sequence the operation of multiple chillers, as well as control the chilled and condenser water temperatures. Braun *et al.* (1988; 1989a; 1989b) investigated the optimal control of a chiller plant using detailed component models and by system-based models. The system-based method determines a "near-optimal" control strategy based on the power consumption of the system as a whole, rather than that of each component. The near optimal strategy is simpler and can provide a strategy very close to the detailed component model approach. The optimal operational parameters, such as chilled water outlet temperature or optimal cooling tower fan speed, were found by the minimization of energy cost in a quadratic form using the Lagrange multiplier optimization method. Pape *et al.* (1991) employed the methodology developed by Braun (1989a) to investigate fault

detection methods. An optimal control strategy of chiller water temperature and supply air temperature was determined first, with a minimized power consumption. A fault was then introduced to the system, the increased power consumption above that for optimal control indicating the presence of faults in the system.

Olson *et al.* (1990; 1993) developed an algorithm for the optimal sequencing of thermal plant operation in non-residential buildings. The procedure was to determine the feasible combination of equipment with the minimum steady-state operating cost by means of the integer nonlinear mathematical programming method. A modified shortest path algorithm was then used to decide the sequence of equipment selection that minimized the cost of satisfying the expected loads for the entire planning horizon (24 hours).

The optimal operational control of air-handling units has been investigated. Nizet *et al.* (1984) investigated the optimal control of air conditioning in buildings by optimizing one control variable, the Variable Air Volume (VAV) flow rate. Given a required room air temperature setpoint, the air flow rate was optimized to lead the temperature as close as possible to the setpoint while minimizing energy cost. Cooling coil setpoints were optimized to avoid reheat (Jekel *et al.*, 1992; Liu *et al.*, 1995). Global optimization strategies for high-performance controls were discussed by Hartman (1995), where optimization of VAV airflow, lighting level, space temperature setpoint, and chiller and boiler operation was considered. Although no optimization algorithm was employed, the strategies for determining setpoints, such as fan speed, heating and cooling setpoints were suggested.

Further comprehensive optimal control of air handling plant has also been investigated. A steady-state nonlinear programming optimization method was used, to find the optimal VAV parameter setpoints for a required load (Zheng and Zaheer-Uddin, 1996). At each hour, the optimal setpoints for the local loops such as, discharge air temperature, chilled water temperature, and static pressure in the ducts, were computed as a function of the predicted load using a steady state model. The optimal setpoints were then supplied to the plant local controller. Lute and Paassan (1995) investigated an optimum strategy to supply heat to the building with the use of a predictor of the indoor temperature. The heater input was optimized under the prediction of the indoor air temperature that was modelled by an ARMAX[1] model. The predictive controller was applied to a test cell,

[1]AutoRegressive Moving Average with eXogenous variables

where the results indicated that a time step of 15 minutes was sufficient to control the indoor temperature with the heater, and energy savings of 10% could be made when compared with conventional ON/OFF and PID control. Chen and Athienitis (1996) investigated an on-line adaptive generalized predictive controller with a feedforward control scheme. The recursive least squares technique was used to estimate the optimal zone setpoints and thermal comfort. The zone setpoint could be optimized through an on-line simulation at intervals of 15 to 30 minutes, based on the adaptive model of a heating process and the prediction of solar radiation and ambient temperature.

The optimal control of air handling units and plant usually provides an operation strategy to meet a required instant thermal load in the building space. This is sometimes referred to as steady-state optimization in the literature, since time is not an important factor in the control optimization, where the objective is to minimize plant energy consumption while satisfying a required instant load. This is a major difference from the optimal control of a thermal storage system.

### 2.3.1 Optimal Control of Plant Thermal Storage Systems

A large amount of research has been conducted into the optimal control of plant thermal storage systems. Plant thermal storage systems reduce energy costs over an entire planning period, and reduce the peak load on the primary chiller plant. In the control of such systems, the plant operation must be scheduled to account for the interaction between the storage and the direct cooling plant so that sufficient cooling is available to satisfy occupant comfort.

Shavit (1980) identified the key factors for operating an energy storage system, and suggested that in order to maximize system efficiency and minimize total energy cost, the output from the storage should be manageable and predictable at all times. A water storage system was taken as an example to illustrate the system's interactions in the optimum operation of energy storage systems. Spethmann (1989) investigated the energy savings from the optimal control of an ice storage system in a field test, when compared with chiller priority and storage priority control strategies. Ice thermal storage operating levels and auxiliary chillers operation were optimized for a whole day (Rupanagunta *et al.*, 1995). Based on the predicted cooling load for the next day, the optimal operating levels of ice

storage were determined for both the night and day. In addition to the ice storage operation, the auxiliary chillers were also used to relieve the daytime instant cooling load. The total energy cost over the day from the ice storage and auxiliary chillers was minimized.

The minimum-cost control of a multizone cooling system with chilled water storage was considered by Rink and Li (1995). The scheduling of the chilled water pumping rate and chiller input electrical power, as well as zone temperature, was optimized within 24 hours to minimize the energy cost and maintain the zone temperatures within comfort limits. The large dimensional problem was handled by aggregation and disaggregation of the multizone thermal model parameters. The zones were initially aggregated into two macrozones, and the three-dimensional periodic optimization problem was solved. Each macrozone was then successively disaggregated. The simulation results indicated that substantial energy cost savings could be achieved by such a near-optimal control scheme. However, this approach is difficult to extend to more complicated plant systems due to the large number of variables in the optimization procedure. In addition to the control of cold storage systems, the optimal operation of a solar heat storage system was also investigated by Rink (1994). This system consisted of two water storage tanks, a solar collector, a heat pump and water pumps. In order to take advantage of the off-peak energy price incentives, the water pumping mass flow rates and electric power input to the heat pump for 24 hours, were optimized by a state increment dynamic programming method.

Kintner-Meyer and Emery (1995a) investigated the life-cycle cost of an ice thermal storage system. The dynamic programming optimization method was used to provide an optimal operating strategy for the storage level that minimized the annual operating cost, which was then added to the total life-cycle cost function. In order to simplify the optimization problem, an optimization period of 24 hours was used and the annual optimal operating cost was then estimated from the daily optimization by the use of a multiplier. It was concluded that the cost benefit of the optimal design incorporating optimal control strategies amounted to 20% savings of the life-cycle cost compared to the none storage system. Arkin *et al.* (1997) also investigated the optimal design and optimal scheduling of a HVAC system with an ice thermal storage. The objective function for the optimal design accounted for the optimal operation of the system, while the optimal scheduling control was concerned with the charge-discharge cycle of the storage over 24 hours.

Recently Gibson (1997) presented an interesting controller for the optimal supervisory control of a building central cooling system with a plant thermal storage. The drawback of common building Energy Management and Control System (EMCS) was described as being that one or more fixed operating schedules are programmed manually at the time of EMCS start-up and then updated periodically by the building personnel. Hence, the level of sophistication necessary for operation in a dynamic building environment is not provided. In the paper (Gibson, 1997), a supervisory controller was developed that can provide scheduling decision support while adapting to the changing building conditions and utility rates. The controller structure is illustrated in Figure 2.2. The neural network model is used to predict the building and equipment operation. The input to the neural network model includes ambient conditions, cooling targets, occupancy demand, while the output is power consumption or energy use of plant components. Based on the predicted building and plant operation, the Genetic Algorithm is used as a planning module to optimize the operating schedule of the storage and direct cooling system, including the equipment operation status, such as ON or OFF or a percentage of discharge rate of the storage; temperature and flow rate setpoints are not included in the supervisory control variables.

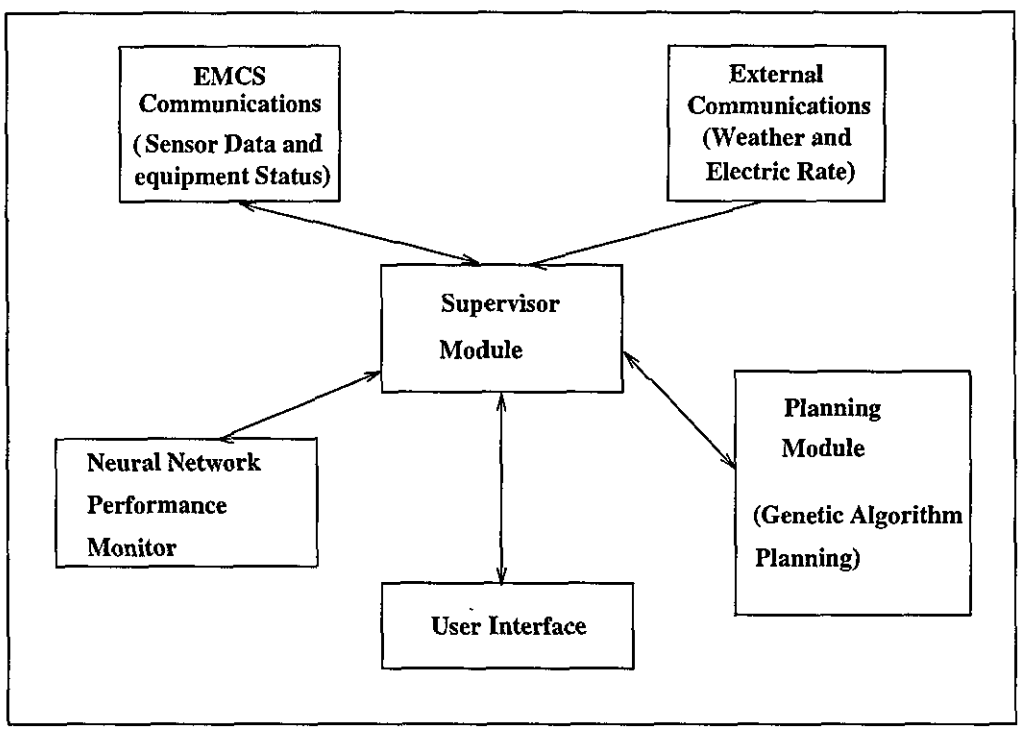


**Figure 2.2, Supervisory Controller Software Functional Diagram**

The controller developed by Gibson (1997) includes the major components essential for the optimal supervisory control of building systems, however, only the operation of the storage and the chiller for direct cooling is optimized, while an optimal zone thermal condition is not considered. This implies the key difference from the optimal control of building fabric thermal storage systems.

### 2.3.2 Optimal Control of Building Fabric Thermal Storage Systems

Since the occupant's thermal comfort can allow the zone temperature to fluctuate within a limit, a constant zone setpoint in the occupied space may waste energy. During the unoccupied period at night, the zone thermal condition can fluctuate over a much wider range. An optimal control strategy should therefore optimize the zone thermal condition so as to lead to a minimum plant operating cost. However, this is usually ignored in the optimal control of central cooling systems with plant storage, such that a prescribed cooling load curve is derived and used to optimize the plant operating schedule, while the entire system operation, including the building dynamic response, is not accounted for. This could be appropriate for plant storage systems since the plant stores the energy in a separate device and the night time operation schedule can be decoupled from the building zone thermal condition.

In contrast, since building fabric thermal storage systems use the building mass as an energy store, the building zone thermal conditions are closely coupled with the plant operating strategy. Consequently, the building dynamics must be taken into account in the optimal scheduling of the plant operation. This implies a more difficult optimal control problem for building fabric thermal storage systems in that the interaction in the entire system between the plant and the building must be accounted for simultaneously. Hence, both the plant operating setpoints and zone setpoints must be optimized over a planning period.

Since building mass exists in every building, the utilization of the building mass as an energy store by overnight cooling of the building space, is one of the simplest form of building fabric thermal storage; its potential for reducing energy costs has been proved to be significant (Ruud *et al.*, 1990; Braun, 1990). An amount of research has been conducted on the optimal control of building systems using

building thermal mass. Snyder and Newell (1990) investigated cooling cost minimization using building mass as a thermal store. Three different control stages were identified and a cooling strategy was determined for each stage. The optimization was performed by "Golden Section" search to provide the minimum cooling cost over the period of three stages.

Braun (1990) demonstrated the potential of energy cost savings from the optimal control of plant operation using building thermal mass storage. Though the study was of a conventional building, the building thermal mass capacity was utilized for relieving the daytime cooling load. Energy savings from the optimal control resulted from the optimal scheduling of night precooling and daytime operation. The approach was to formulate the zone temperature setpoints for the entire period as optimization variables and determine the optimal zone setpoints that minimized the total energy cost while still in a pre-defined comfort range. The plant optimization was decoupled from the optimal control of the building thermal storage; for a given cooling load and zone setpoint, the optimal plant supervisory control was determined, such as for the optimum operating mode and discharge air temperature. Hence, the important dynamics in the energy storage within the structure were considered in a planning period, while the plant was modelled in steady state and optimized on a hourly basis. This approach is superior to the method applied by Rink and Li (1995) in that the controller is flexible and can be easily expanded to much more complicated plant installations without affecting the formulation of the optimal control problem for thermal storage over 24 hours. The Complex search method was used for solving the optimization problem and the energy savings from the optimal control were obtained in comparison with a conventional night setback control. The approach adopted in the paper (Braun, 1990) can be generalized to be applied to the optimal control of fabric thermal storage systems.

Simmonds (1993) adopted the approach from Braun (1990) to investigate the thermal comfort in the occupied space under the optimal control strategy. It was demonstrated that energy savings could be achieved in building systems if the control was based on maintaining a Predicted Mean Vote (PMV) rather than the dry-bulb temperature within a comfort range. Preheating and precooling strategies from the optimization were also examined. Morris *et al.* (1994) evaluated the approach developed by Braun (1990), and compared it with night setback control through an experimental test facility representative of a room in a large

office building. Keeney and Braun (1996; 1997) employed this approach to investigate the characteristics of optimal control strategy for building mass storage, and identified a simplified precooling strategy (Figure 2.3). In this precooling strategy, the zone setpoints are controlled at the constant $T_{pre}$ during the precooling period, which are much lower than those of night setback control. The warm up period can vary with different buildings. The occupied setpoint $T_{occ}$ is set to a value low in the comfort region so that the building mass charge is held as long as the cooling capacity is available, and the building thermal mass is discharged to reduce the peak demand at the peak hours. Significant energy cost savings during the peak cooling season were achieved from this precooling strategy applied to an office building in Illinois, compared to the existing night setback control used in this building.

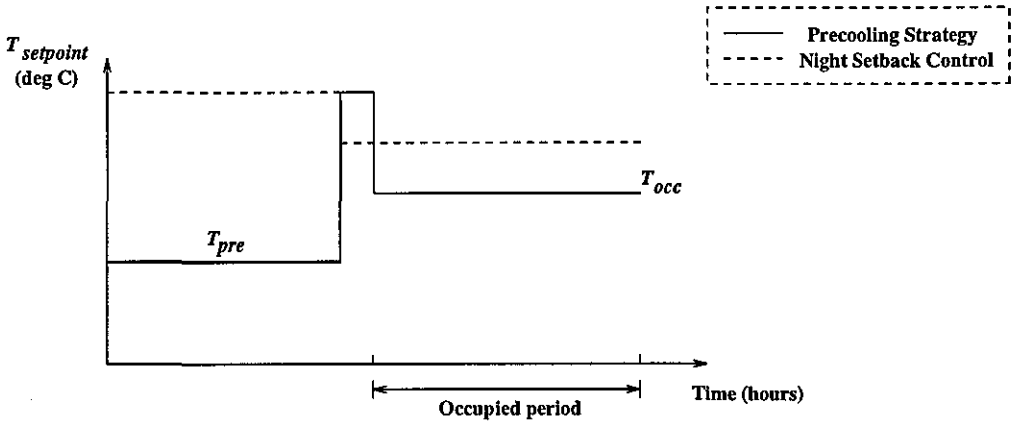


**Figure 2.3, Zone Air Temperature Setpoints**

The minimum-cost scheduling of electricity usage for buildings under real time-prices (RTP) was investigated by Daryanian and Norford (1994). The building was modelled by a discrete linear system. The control problem was to minimize the total energy cost calculated from the hourly changing unit prices and electricity usage, while without violating the permissible indoor air temperature. The optimization problem was solved by an iterative algorithm. House and Smith (1995) used a system-based approach to the optimal control of multizone building systems. The system-based approach was to schedule the plant operation for 24 hours, such that the interactive nature of the HVAC components, the building system and their associated variables was accounted for. A five-zone building system was taken as an example to illustrate the optimization of plant operating setpoints and fuel use, the problem being constrained by five PMV values for the five zones. The control variables included fuel use from the central cooling and

heating devices, and the five zone local reheat coils, as well as mass flow rate to each zone, 13 variables in total. The cost function was the integral penalized cost in a quadratic form for 24 hours, using a cost-weighting factor for each of the control variables and zone state variables. The optimal solution of the multiple control variables was searched by a sequential quadratic programming method. The results indicated energy savings of up to 24% from the system-based optimal control approach in comparison to a conventional night setback control strategy.

Two storage systems were considered in the optimal control of a HVAC system by Kintner-Meyer and Emery (1995b): cold plant storage and building thermal mass storage. The control variables were optimized for 24 hours, including the zone air temperature, humidity ratio, sensible cooling load, air supply rate, fresh air fraction, load from the direct cooling and load from discharge of the cold storage. The paper suggested a new approach which incorporates the cooling load as part of the optimization. It was claimed that this approach broadens the control options since the new set of control variables are considered, such that the building precooling and warming-up options can be optimized and used for reducing the load on a traditional cold storage system.

A prototype predictive controller was developed by Oestreicher *et al.* (1996) to assess an active floor heating and cooling system. Under the predicted solar gains and internal gains (free gains), the energy input to the building over a period of 24 hours was optimized to satisfy the comfort condition in the building space. A maximum energy saving from the optimal control of a non-residential building in Switzerland was reported to be 24% during the cold season and 31% during the hot season, compared with the conventional control.

In the optimal control of building and plant using building mass as an energy store, the formulation of the cost function is very similar among the studies in literature. Differences arise when the cost function is penalized for violated comfort conditions; the control variables also differ for each application. Since there are a large number of variables in the building systems that can affect the energy cost of the building and plant operation, the independent supervisory control variables should be identified for the optimization of plant, air handling unit and building operation. As the primary objective of the control optimization is to maintain the building zone thermal conditions within a limit while minimizing the operating cost, the primary supervisory control variable in the building is the zone

temperature setpoint; moisture content has less impact on thermal comfort and is not often controlled. In an air handling unit, the primary target is to select the operating mode, such as full or minimum fresh air, and the setpoints of the supply air to the building. The primary plant can be optimized to meet these setpoints for the chiller and boiler operation. Hence, these supervisory control setpoints for building, air handling unit and plant operation interact with each other, making the system control complicated. However, a control hierarchy exists in the building system, such that the zone setpoints govern the control of the air handling unit, and can be further used to control the primary plant operation. A proper decoupling of the control levels can substantially reduce the control complexity.

Studies in literature usually consider the energy input to the building, the plant operating setpoints and the building zone setpoints as the control variables that are optimized over a planning period. However, in many cases, it may not be necessary to optimize the energy input to the building and the plant operating setpoints over the planning period, since these can be determined from the zone setpoint control. The approach proposed by Braun (1990) provides a means of simplification by decoupling the optimization of building thermal storage and plant operation. The optimization accounts for the complicated interactive nature between the building dynamic response and plant operation. This approach is thus computationally efficient, flexible and accurate.

The objective of this research is to develop an optimal controller for building fabric thermal storage systems and as a protocol for further implementation in real buildings. The approach from Braun (1990) therefore forms the basic methodology for the development of the optimal supervisory controller in this research.

As one of the active fabric thermal storage systems, the optimal control of the hollow core ventilated slab system has not been investigated in the literature. However, the effective control of this system is even more crucial, since the structural element is used as a supply duct, leading to a closer link between the zone thermal conditions and plant operation. In addition, due to its special air supply path, the control of this system differs from that of conventional buildings. Therefore, the focus of this research is on the development of the optimal predictive controller for the hollow core ventilated slab thermal storage system. However, the optimal predictive controller can also be applied to other building fabric thermal storage systems that use ventilation as cooling medium.

# Chapter 3

# Controller Design

## Introduction

This chapter develops the optimal predictive controller by considering the pertinent components of the controller and its structure.

A building installed with a hollow core ventilated slab system is usually well insulated and heavy weight. This reduces the required thermal capacity of the associated plant. A possible plant installation is shown in Figure 3.1. It contains three components: the building with installed ventilated slabs, the primary plant and an air-handling unit (AHU). The primary plant consists only of a chiller, heat being supplied from an electric duct heater. The AHU includes a heat recovery device (HRD), a cooling coil, the electric duct heater, and supply and exhaust fans. Although a chiller may not be commonly used in ventilated slab buildings, it has been included in this research so that the need for mechanical cooling can be evaluated.

The optimum control of the building thermal system involves minimizing the total energy cost from the primary plant and AHU over a specified period of 24 hours, while maintaining the zone thermal comfort requirements. The optimum solution to this problem is a schedule of control operation throughout the 24 hours optimization period. The problem can be solved using an optimization algorithm to search for the feasible solution with the minimum total energy cost over the

planning period.

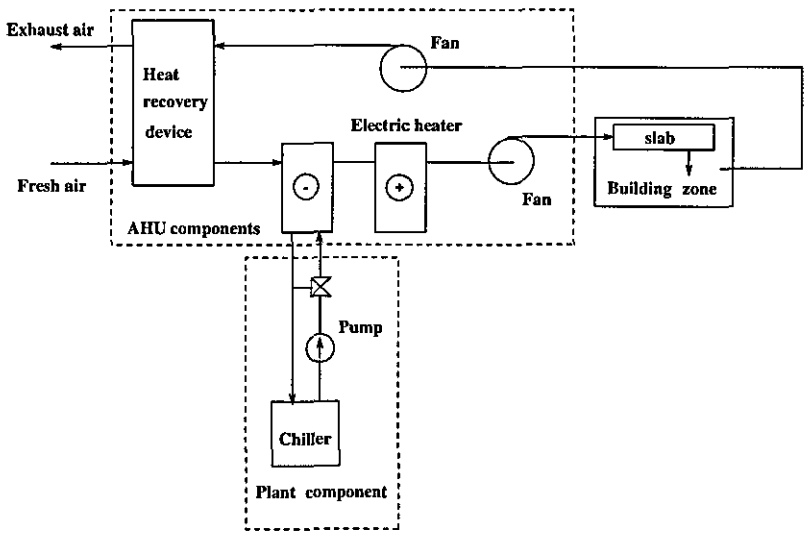


**Figure 3.1, Plant Configuration**

The optimum controller must charge the thermal store during the unoccupied period such that sufficient thermal storage exists to relieve the next day's cooling or heating loads. Hence, the controller must include algorithms to predict the next day's ambient conditions and the subsequent performance of the building.

The design of the predictive optimal controller therefore, includes the development of the predictive components, the selection of an appropriate optimization algorithm and the design of the controller structure, which includes the identification of control variables and the information flow between these components.

## 3.1 Control Structure and Hierarchy

To provide an optimal schedule of plant operation for the thermal storage system, the optimal predictive controller applies the optimization algorithm to the building and plant simulation model, to search for the best plan of controls over the planning period. In doing so, appropriate control variables need to be selected and the information flow between the components established.

The potentially large number of control variables for the operating schedule of

the thermal storage system and the large number of independent variables in the control of the plant equipment, together with discontinuities in the search space (Chapter 5) make the optimal control a difficult optimization problem to solve. However, the decoupling of the different levels of control can significantly reduce the complexity of the problem.

Figure 3.2 illustrates the control system structure. The controller can be considered at two levels. The higher level is concerned with optimizing the control variables that directly influence the thermal storage over a planning period of 24 hours. This allows the daily variation in the ambient and room thermal environments, as well as the cost of electricity, to be taken into account. In order to ensure that the energy cost is minimized, it is necessary to optimize the plant operation in each hour at the lower level; the problem being constrained by plant design capacity and the setpoints passed from the high level.

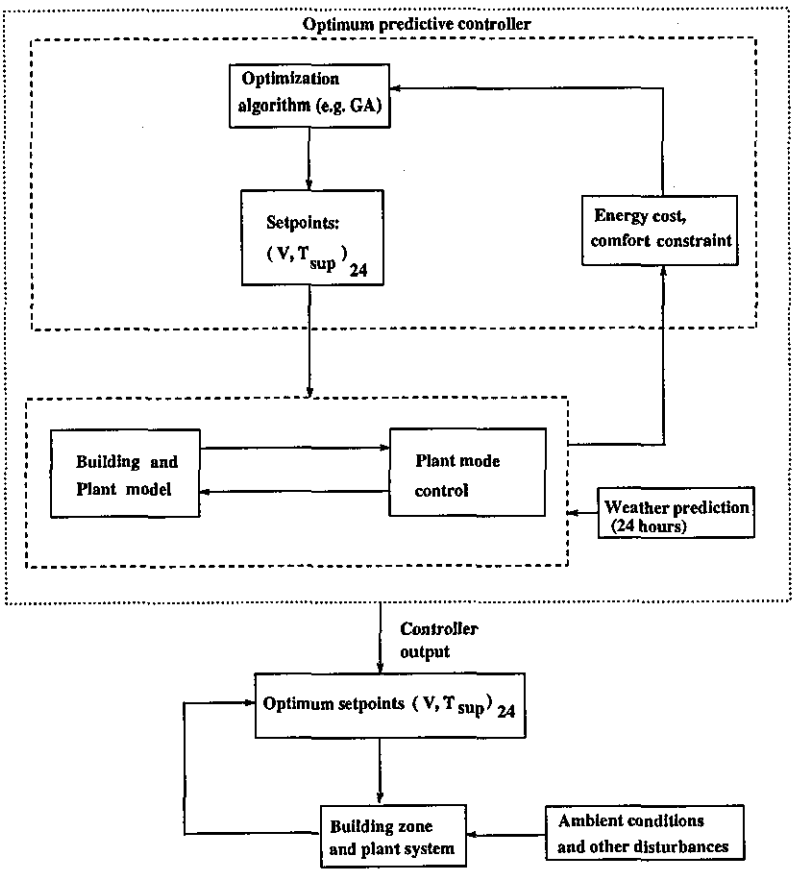


**Figure 3.2, Control System Structure**

The control hierarchy illustrated in Figure 3.2 reflects the nature of the supervisory control problem for buildings with fabric thermal storage, and forms the basis for this research. The key part of the design of such a controller is the identification of control variables, described below.

### 3.1.1 Thermal Storage Control Variables

Since the predictive controller is to supervise the control of the building system, including the thermal storage and the plant, the control variables should be those that govern the operation of the thermal storage and the plant. The control variables should also uniquely determine the cooling or heating demands on the plant and the thermal states in the building.

Previous research (Braun, 1990) identified the building zone setpoints as supervisory control variables for the control of an air conditioning system installed in a conventional building. For such a building, the thermal storage in the building fabric is controlled by the zone setpoint since it is the zone thermal condition that governs the heat flow to and from the building envelope. The use of the zone setpoints as control variables sufficiently decouples the optimum control of the thermal storage in the building fabric and the control of the plant equipment. This is not the case for a ventilated slab system where the air entering the slab has a significant influence on the thermal storage and thus the entire zone thermal conditions. Hence, the condition of the supply air to the ventilated slab forms the independent variables in the supervisory control of the ventilated slab system. The two control variables are the supply air flow rate and supply air temperature, which together with the ambient boundary conditions and room thermal disturbances, uniquely determine the thermal states of the room. The plant operation is also dictated by these variables, since they provide the control target of the supply air conditions leaving the air handling plant.

In such a fabric thermal storage system, the interaction between the thermal storage and the plant increases the complexity of the scheduling of the control operation. The feasible optimal solution that minimizes the energy cost of the plant equipment is a control strategy that maximizes the use of the thermal storage in regulating the room thermal environment. In order to maximize the effectiveness of the thermal storage and reduce energy cost, it is necessary to plan the plant

operation over 24 hour period, to take advantage of favourable ambient conditions and lower cost of electricity at night, to charge the thermal storage before occupants arrive. This gives 24 dimensions for each of the control variables on a hourly basis.

Therefore, the high level control variables are the setpoints for supply air temperature and flow rate to the ventilated slab. They are optimized in order to minimize energy costs without violating the predefined comfort levels in the occupied space. The weather predictor provides the ambient information for the next 24 hours. Under the forecast ambient conditions, energy costs and comfort levels are predicted from the building and plant model.

### 3.1.2 Plant Control Variables

The optimization of plant operation in each hour is concerned with minimizing energy consumption while meeting the supply air setpoints. The setpoint of supply air flow rate can be met directly by controlling the fan speed. However, the control of the supply air temperature can be optimized by making a choice between free or mechanical heating and cooling, and whether the heat recovery device is operated or not.

During the optimization search process, the plant is controlled to meet the supply air setpoints, even if heating is required during the summer. For a given supply air temperature setpoint, it may be necessary to heat or cool the ambient air to meet the setpoint. The operation of the heat recovery device may, or may not, benefit this process. The plant supervisory control variables to be optimized in each hour should therefore include the mode of operation of the plant. Given the required supply air temperature setpoint, the plant supervisory control searches at the lower level for the optimum operating mode in each hour.

For each mode, the operation of the plant equipment should be further optimized to ensure a minimum energy consumption. Mechanical heating is supplied by the electric duct heater. In this research, it has been assumed that the electric duct heater can meet the setpoint of supply air temperature by perfect control of its capacity, hence there is no further optimization of the mechanical heating control. Energy costs from mechanical cooling can be minimized by optimizing the chiller

operation. In terms of the chiller control variables, the water flow rates in the evaporator and condenser have less influence on the chiller performance than the chilled water leaving temperature and the condenser water leaving temperature (Braun, 1988; Braun *et al.*, 1989a). For an air-cooled chiller, the chilled water leaving temperature is the most strongly correlated with the chiller performance (Braun *et al.*, 1989a; 1989b). Hence, the mechanical cooling mode can be further optimized to ensure the minimum operating cost from the chiller operation by considering the chilled water leaving temperature as an optimization variable. However, the fabric storage and the use of the high effectiveness heat recovery device greatly reduce the required capacity of the chiller, an air-cooled package chiller usually being of sufficient capacity. It is common practice to fix the setpoint of chilled water leaving temperature in small package chillers. This together with the low mechanical cooling duty has led to the chiller control being excluded from the optimization in this study.

The controller developed in this research is structured in such a way that an expansion of the optimization of the operation of an individual plant equipment is easily realized for more complicated plant installation systems. For instance, if a large capacity chiller is installed with a variable setpoint for the chilled water leaving temperature, the chiller operation can be optimized using the chilled water leaving temperature as the control variable.

Therefore, at the plant control level, only the mode of plant operation is optimized. A single discrete problem variable can be used to represent the plant operating modes, as shown in Table 3.1. The last three modes only apply to night operation, corresponding to full recirculation of the room exhaust air. In Figure 3.1, the control of dampers in the heat recovery device allows three operating modes of the heat recovery device, full fresh air with the heat exchange, full fresh air without the heat exchange and full recirculation with the room exhaust air to be directed to the supply route.

For a given setpoint requirement passed from the high level control, many of the operating modes can be discounted through an analysis of the zone exhaust air temperature, ambient air temperature and supply air setpoint. The number of feasible modes is typically less than 3, which enables the optimum mode to be selected by an exhaustive search. The optimum plant mode is that which meets the setpoint with the minimum energy cost.

| Mode | Heat Recovery Device | Electric Heater | Chiller |
|---|---|---|---|
| 1 | ON | OFF | OFF |
| 2 | OFF | OFF | OFF |
| 3 | ON | ON | OFF |
| 4 | ON | OFF | ON |
| 5 | OFF | ON | OFF |
| 6 | OFF | OFF | ON |
| 7 | Recirculation | ON | OFF |
| 8 | Recirculation | OFF | ON |
| 9 | Recirculation | OFF | OFF |

**Table 3.1, Plant Operating Modes**

### 3.1.3 Control Process Interaction

The decoupling into the two levels of, the optimal control of the thermal storage system, and of the plant operation, has provided a flexible optimal controller structure and simplified the optimization problem to be solved, although there is still some interaction between the two levels of control.

For each trial supply air flow rate and temperature setpoint given by the thermal storage optimization, the plant mode must be optimized to provide the minimum energy cost. This requires some iterations between the building and plant model, and the plant mode optimization, since the choice of plant mode, particularly in relation to the heat recovery device, depends on the condition of the zone exhaust air. Three iterations have been found to be sufficient.

There are also some instances when the supply air temperature setpoint can not be met exactly. These occur when either the setpoint is beyond the capacity of the plant or below its minimum part load ratio. Since there are a few occasions when free cooling or heating can be used, it is often the case that the plant is operated at very low loads in order to meet the supply air setpoint temperature, which can result in inefficient plant operation. The selection of a high minimum part load ratio would reduce energy costs, but would increase the probability that the setpoint would not be met. The minimum part load ratio for the chiller and the electric heater used in this research is 0.1.

For the cases when the temperature setpoint can not be met by the plant mode control, the most appropriate mode is assigned. For instance, if the required chiller load is below the minimum part load ratio and the chiller is therefore OFF, Mode 1 or 2 is selected; the selected mode being the one that provides the temperature closest to the required setpoint. The new supply air temperature, although it is very close to the setpoint, its effect on the energy cost and thermal comfort needs to be evaluated using the building and plant model. However, the actual supply air temperature should not replace the value of the control setpoint in the high level control optimization, since this would interrupt or mislead the optimization process. The interaction between the supply air setpoint optimization and the plant mode control is addressed further in Chapter 5 and Chapter 6, in which a combined setpoint and plant mode optimization is described.

The output of the controller shown in Figure 3.2 is a schedule of supply air setpoints. The setpoints dictate the operation of the real plant over the next 24 hours, however, the plant operating mode is selected in the real operation by simple rules that employ the prevailing ambient conditions and zone temperature. Therefore, due to the inherent prediction errors in the room and ambient conditions during the control optimization, some feedback may be necessary to override the operating setpoints of the optimum schedule. The influence of prediction errors in the ambient conditions on the performance of the optimal controller and the issues regarding the on-line adaption of the optimal predictive control strategy are addressed in Chapter 8.

### 3.1.4 Definition of the Thermal Storage Optimization Problem

An optimization problem is formulated from three key parts: problem variables, an objective function and a constraint function.

The problem variables for the high level control of the thermal storage are the setpoints of the flow rate and temperature of the air supplied to the ventilated slab. Two setpoints are to be optimized over the 24 hour planning horizon, giving 48 problem variables.

The objective function is the total energy cost of the system over 24 hours, as

shown in Equation 3.1. It is a function of the electricity tariff structure and the power consumption from supply and exhaust fans, the chiller and the electric heater. The objective function can be discontinuous where a change in the supply air temperature setpoint causes a change in the operating mode of the plant, and therefore a sudden change in energy cost. The energy cost objective function $J$ is calculated by:

$$J = \sum_{k=1}^{24} P_k(X_k, U_k, F_k) \times R_k \tag{3.1}$$

where,

- $k$ is from 1 hour to 24 hours for one day;
- $R_k$ is the cost of electricity;
- $X_k$ is the vector of room thermal state variables at time $k$, assessed by the building model;
- $U_k$ are the control variables at time $k$, i.e. air flow rate and supply air temperature;
- $F_k$ are the uncontrolled driving variables, such as ambient air temperature and solar radiation;
- $P_k$ is the total energy consumption at time $k$.

The constraint upon the minimization of the energy cost is that thermal comfort in the occupied space must be maintained (Equation 3.2). The Predicted Percentage of Dissatisfied (PPD) index (Fanger, 1970), has been used to define the comfort constraint with a limit of PPD$\leq$10%, set for the occupied period. This is a generally recommended limit and corresponds to a Predicted Mean Vote in the range of -0.5 to +0.5 (ISO, 1984). No comfort constraint needs to be set for the unoccupied period. However, in the summer, in order to reduce the risk of over cooling the building and of condensation in the ventilated slab, a nominal limit of 20% PPD has been set during the unoccupied period, (a more precise test for condensation risk could be included in further research). The constraint function is:

$$PPD_i(X_i, U_i, F_i) \leq 10\%, \quad i \in \text{occupancy} \tag{3.2}$$

A robust and powerful optimization algorithm must be selected to solve such an optimization problem having a large number of control variables. The performance of the optimization algorithm being applied to the optimal controller is examined in Chapter 5, and the analysis of the characteristics of the control optimization problem is presented in Chapter 6.

## 3.2 The Selection of an Optimization Algorithm

The objective of the development of the predictive optimal controller for the hollow core ventilated slab system is to obtain an optimal control strategy for the system so that the total energy cost is minimized and the room thermal comfort conditions are satisfied. An optimization algorithm can be used as an effective engine to search for the optimal solution to the control problem. The choice of optimization algorithm is dependent upon the characteristic of the problem.

Nizet, *et al.* (1984) applied the conjugate gradient method to the optimal control of air conditioning in buildings. The room thermal comfort constraints were dealt with by a penalty function, of which the penalty coefficients had an important influence on the optimal control strategy. Improper selection of the coefficients may lead to a badly conditioned problem and cause the problem diverge from the minimum. This method was applied to one continuous control variable, Variable Air Volume (VAV) flow rate (no discrete variables). Air flow was supplied to the room during the occupancy hours and with no precooling. The gradient of the energy cost, the search direction and step length of the search, had to be computed step by step. It was concluded that the conjugate gradient method was efficient when working far from the solution, but it progressed very slowly in the neighbourhood of the minimum.

The nature of the optimal predictive controller for the ventilated slab system shown in Figure 3.1 dictates that such a control optimization problem has a diverse and wide range of discontinuous search space, which results from the discrete plant operating modes (Section 3.1). It is generally recognised that gradient based optimization methods can fail for problems having a highly discontinuous search space (Rao, 1984). Such problems are best solved by direct optimization methods which do not require the explicit gradient of the search space in order to find the

direction of the optimum solution. Three such approaches have been considered here, dynamic programming, the Complex method, and Genetic Algorithms.

### 3.2.1 Dynamic Programming

Since the optimal control strategy is a schedule of the plant operation for the next 24 hours, dynamic programming would seem to be the first choice for an optimization algorithm. Dynamic programming can deal with discrete variables, non-convex, non-continous and non-differentiable functions. Dynamic programming is a planning optimization algorithm in which an exhaustive search is applied to each stage of the plan. The solution for each stage is selected such that the objective function is minimized over the entire plan. However, as stated by Bellman (1957), dynamic programming has a major drawback "curse of dimensionality".

The control optimization problem considered in this research, can be configured as a 24-stage decision making process (Figure 3.3), since the planning period for calculating the total energy cost is divided into 24 hours, and for each hour (each stage), the control variables need to be searched. In Figure 3.3, $S_1, S_2, S_3, ..., S_{24}$ are state variables for 24 hours, representing the building thermal conditions; $X_1, X_2, X_3, ..., X_{24}$ are the control variables, and $C_1, C_2, C_3, ..., C_{24}$ are the energy cost from the plant operation. The objective of this problem is to find $X_1, X_2, X_3, ..., X_{24}$ so as to minimize the sum of $C_1, C_2, C_3, ..., C_{24}$, while the state variables meet some constraint requirements. The process is planned backwards, $S_{24}$ being the initial room thermal state including the room and mass temperatures at 1:00 am. At the first stage of this process, for all possible entries of $S_2$ within its feasible region ($S_2$ being the input to the first stage), an exhaust search is conducted to search for the $X_1$ that gives lowest $C_1$ while $S_1$ and $S_2$ are in comfort ranges. Similarly at the second stage, an optimum $X_2$ is searched for all possible $S_3$ to achieve $S_2$ of the first stage and minimize the sum of $C_1$ and $C_2$. This procedure is applied to all stages until the initial state $S_{24}$ is met and the values of $X_1, X_2, X_3, ..., X_{24}$ for 24 stages are found.

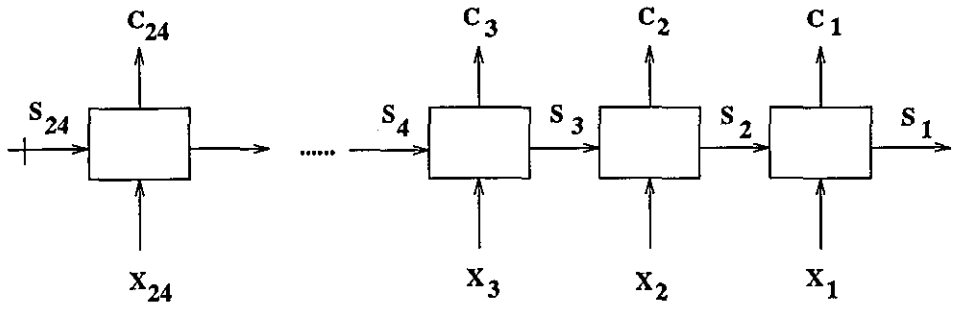


**Figure 3.3, The Multistage Decision Problem**

Dynamic programming is well suited for solving allocation problems with a few discrete points of control variables and state variables. However, if for this control problem, both the control and room state variables are discretised to have, say, 30 discrete points, then in the order of $10^{11}$ calls to the building model would be required to solve the optimization problem. Such a computational overhead is sufficient to discount dynamic programming as a viable option for solving this problem.

### 3.2.2 The Complex Method

The 'Complex', direct search method, developed by Box (1965), is a competitive choice for use in this research, since it is efficient and easily implemented. The Complex algorithm is similar to that of the 'Simplex' method (Rao, 1984) except for the inclusion of constraint handling.

An initial geometric figure (termed the 'complex') includes an initial feasible point, and $K$ ($K \geq n+1$) vertices which are constituted randomly ($n$ being the number of problem variables). Each vertex must be a feasible solution to the problem. Starting with this initial complex, a trial point is generated which is a reflection of the worst vertex (the largest objective function), about the centroid of the remaining vertices. If the trial point gives a lower objective function than the worst vertex, a new complex is formed by the worst vertex being replaced by the trial point. By this procedure, a sequence of geometric figures (complex's) are formed to find the constrained minimum point. If at any stage, a trial point falls outside of a constraint boundary, it is moved half way toward the centroid until it is feasible. In effect, the complex rolls over and over toward the optimum solution,

by reflecting and contracting itself when a constraint boundary is encountered. The details of the search procedure are described in Appendix A.

The Complex method was used by Braun (1990), for searching an optimal supervisory control strategy for an air-conditioned building. The control variable was zone setpoint. The search space was of 24 dimensions, one dimension for the control variable in each of the 24 hourly planning period. It was argued that the Complex method could deal with the discrete energy cost resulting from the discrete plant operating modes. The optimal control strategy obtained showed a significant energy saving compared with the conventional night setback control.

The Complex method has two restrictions for constrained minimization. The first is that the feasible region must be convex, which guarantees that the centroid of all feasible points is also feasible. The second is that an initial point must be feasible. In most of engineering applications, these two requirements do not impose strict limitations on the Complex method. However, this method becomes rapidly inefficient when the number of variables increases (Rao, 1984). Nevertheless, the Complex method has been selected as a possible method for solving the control optimization in this research.

### 3.2.3 Genetic Algorithms

Genetic Algorithms (GAs), as part of the evolutionary group of algorithms, are robust, global and generally more straightforward to apply to situations where there is little or no *a priori* knowledge about the problem to be addressed. They have been applied to many applications, engineering design and control, machine learning (Goldberg, 1989), financial modelling (Goonatilake and Feldman, 1994), multi-objective design (Chipperfield and Fleming, 1995a), process scheduling, and adaptive control and fault detection (Varšek, *et al.*, 1993).

A Genetic Algorithm is based on the mechanics of natural selection and natural genetics. "It combines survival of the fittest among string structures, with a structured yet randomized information exchange, to form a search algorithm with some of the innovative flair of human search" (Goldberg, 1989). The fundamental differences of a GA from other traditional search methods are:

1. GAs work with a coding of the control variables, not with the real variables themselves;

2. GAs search from a population of points, not a single point;

3. GAs use probabilistic transition rules to progress the search, not deterministic rules.

The coding of control variables, is in the form of binary string containing a sequence of 0 and 1. This is analogous to *chromosome* in biological systems. In natural systems, one or more *chromosomes* combine to form the total genetic prescription for the construction and operation of some organisms (Goldberg, 1989). In GAs, a combination of the coding represents a solution for the optimization problem. This artificial genetic algorithm emulates the adaptation methods in natural systems. Each 'individual' in the population represents one solution and is defined by a coding of the problem variables and a 'fitness' derived from the objective function and constraint violations. A population of individuals are searched in parallel. The fittest points are reproduced (copied) to the next generation. GAs use probabilistic transition rules to guide the search toward regions of the search space with likely improvement. This together with the parallel mechanism, potentially reduces the probability for the search of dropping at a local minimum.

Three basic genetic operators govern the evolution process in GAs search, reproduction, crossover and mutation. Reproduction selects individuals (solutions) that will either be copied to the next generation of solutions, or "mated" to produce new individuals. The probability that an individual will be selected for reproduction increases with the "fitness" of the individual. Mating (crossover) takes place by randomly swapping the partial binary strings (representing the variables). Mutation introduces new solutions by switching individual bit values in the binary strings.

The three operators primarily involve random number generation, copying, partial string scheme exchanges and decoding of binary strings. There is no requirement of derivative information of search points. As these operations are problem independent, the implementation of GAs is straightforward and simple to an optimization problem.

Although GAs are unconstrained search methods, they have been used with penalty

functions to solve highly constrained heating, ventilating and air conditioning sizing problems (Wright, 1996). The physical dimensions of the cooling coil, heating coil and fan were selected as optimization variables. The results showed that the GA was able to overcome the difficulties that existed in other direct search algorithms, such as sometimes a direct search being unable to traverse a constraint boundary with discrete variables.

In terms of their applications to control optimization, as GAs do not require derivative information or a formal initial estimate of the solution region, and because of the stochastic nature of the search mechanism, GAs are capable of searching an entire solution space and more likely to find the global optimum than conventional optimization methods (Chipperfield and Fleming, 1995b). Since GAs place no limitation on the number of control variables, they have been applied to water pump scheduling with 96 variables (Mackle *et al.*, 1995). Gibson (1997) used a GA to identify optimal equipment schedules to meet the load requirement for building central cooling systems. Dickinson and Bradshaw (1995) applied a GA to the building heating system design, where constant parameters, such as heat transfer coefficients of the heaters, were identified by the GA and the heater input scheduling was also optimized to provide the minimum energy cost and the required room temperature.

In general, the advantage of using a GA lies in its successful applications to highly discontinuous search space and a large number of problem variables. The drawback of GAs is that they make rapid initial progress, but are slow to reach final convergence. However, the implicit parallelism and probabilistic nature of a GA enable the search over a large section of the search space and leads towards a global or near global optimum solution.

In summary, due to its high performance in dealing with a large number of control variables and a discontinuous search space, a Genetic Algorithm is the most competitive method for solving the control optimization problem in this research. Since the Complex method is easily implemented and applied to the control problem, it has also been used to search for the optimal solution. The results from the two methods are compared in Chapter 5 so as to give the confidence in the selection of the GA as the final optimization method. The detailed algorithms of the GA operators and the search procedure are given in Appendix B.

## 3.3 The Predictive Components of the Controller

The predictive components of the controller consist of a building model, plant models and a weather predictor. The controller uses the thermal models of the building and plant as the basis for predicting the schedule of plant operation and the building response to the predicted ambient conditions for the next 24 hours (Figure 3.2).

### 3.3.1 The Form of the Building and Plant Models

The building and plant models are an integral part of the predictive controller. A dynamic building model is required, as the building's transient response to thermal disturbances and plant operation is used in evaluating a variety of trial plant control strategies.

The building model in the predictive controller could be a first principles model, a neural network model or an Auto Regressive Moving Average model (ARMA). The establishment of a neural network model requires a large quantity of building thermal performance data in order to achieve an acceptable accuracy. For buildings with the hollow core ventilated slab systems, there is a lack of sufficient real data from monitored buildings or from simulation models. In addition, the data representing the building thermal conditions for this system, should include the room and mass temperatures. This increases the number of dimensions of the output of the neural network model. For conventional buildings, an appropriate output would be the cooling load profile, as used by Gibson (1997). However, this is not applicable for this fabric thermal storage system since the plant operation will affect the ventilated slab mass temperature, thus altering the cooling load required in the room. As a result, the neural network model for predicting the thermal response of the hollow core ventilated slab building has a large number of input and output variables, each of which has 24 dimensions (one for each hour of the day). ARMA models also require building performance data with which to identify the model parameters, and are not suitable for problems of a high dimension. Hence, both the neural network and ARMA models are inappropriate techniques for modelling the building performance within this research.

The first principles model approach has been used for modelling the building thermal response in this research. By using a first principles model, the performance of the thermal storage system can be assessed under various operating conditions. Once the building model is established, there is no difficulty in producing detailed information about the building thermal conditions, for example, the comfort conditions, PMV (Predicted Mean Vote) and PPD (Predicted Percentage of Dissatisfied) values, room and mass temperatures, surface temperatures, etc. A first principles building model can also be used to evaluate the different design schemes, such as buildings of different weight, and different window design. Though the first principles building model in this research is to be used for the controller development, it could also be used as the basis for optimum design study.

Due to the special supply air path in the ventilated slab system, and the strong interaction between the supply air and the structural element, the building model should be able to assess the influence of this air supply system on the thermal storage and room thermal environment. Considering its functions in the predictive controller, the building model should meet the following requirements:

- correctly model the heat transfer process along the slab air path;
- model the effective heat capacity of the slab mass storage;
- simulate the influence of all of the major thermal disturbances on the room environment;
- be able to model the effect of different wall constructions and plant operation strategies, so that the optimum control of system operation can be investigated. Ideally, the optimum design of the system can also be investigated by this model.
- be simple and quick to conduct the building simulation, so that an optimization algorithm can be applied to the model to search for the optimum operation strategy to regulate the building within the occupant comfort limit, while with minimized plant operating cost.

There are a number of techniques used for modelling buildings, such as response factor, admittance, numerical methods and electrical analogue methods (Clarke,

1985). Since the model is to be integrated in the optimal controller, it should be simple but provide sufficient details to enable the assessment of the performance of the thermal storage system. A lumped parameter method meets these requirements and has therefore been selected for developing the building model.

Since the dynamics of the thermal plant are much faster than the response of the building, steady state plant models have been used in this research. Both the building and plant models are discussed in more details in Chapter 4.

### 3.3.2 The Selection of Weather Prediction Algorithms

Since the significant benefit of a building thermal storage system is due to its ability in shifting the daytime on-peak cooling and heating loads to the night, the knowledge of the next day's weather conditions is critical in determining how much of the on-peak load can be efficiently shifted to the night. Hence, models for predicting the next day's weather conditions are required.

Since for low energy building design, the comfort conditions in the building are only concerned with the temperature control, moisture control can be neglected. Of the climatic variables, the ambient temperature and solar radiation have the most influence on the thermal conditions of the building space. Therefore, the weather predictor can be considered in two parts: temperature prediction and radiation prediction. The temperature prediction is to forecast the ambient dry-bulb temperature profile for the next 24 hours, whereas the radiation prediction algorithm forecasts the profile of global, direct and diffuse radiation.

Weather predictors have been used previously in building design and predictive control (Holst *et al.*, 1987; Athienitis, 1988; Hartman, 1988). Weather models have also been investigated for load calculation in design (Yoshida and Terai, 1990/1991; 1992), and for the analysis of stochastic properties of heating loads (Hokoi *et al.*, 1988). Each approach varies in its detail according to the application. For the predictive controller described in this research, the weather predictor must supply the next day's climatic information for calculating the optimal schedule of the setpoints of plant operation and the plant operating modes. Hence, the characteristics of the weather predictor required in this research are:

- short-term forecast of climatic variables: ambient air temperature and global radiation, direct radiation and diffuse radiation (the latent cooling load and moisture are not modelled);
- the annual periodicity and seasonal effect need not be modelled separately, since the forecasting is conducted daily, wherein the parameters of the weather predictor are updated to include the effect of the measured weather data from the passing day; therefore, the annual periodicity and seasonal effect are embedded in every new set of parameters;
- the weather predictor is to forecast a profile of the climatic variables for the next 24 hours; the method adopted here could be similar to the load profile prediction (Forrester *et al.*, 1984; MacArthur *et al.*, 1989; Seem *et al.*, 1991).

The statistical methods, Auto Regressive Moving Average (ARMA) and Exponential Weighted Moving Average (EWMA) models have been found to meet these requirements. The development of the weather prediction model is described in more details in Chapter 7.

## 3.4 Conclusion

This chapter has described the design of the optimum predictive controller. The controller structure, control variables and pertinent components have been identified. The control variables for the supervisory control of thermal storage are the supply air temperature and air flow rate to the ventilated slab for each hour of the 24 hour planning period. These setpoints are simultaneously optimized over the entire planning period so that the setpoint schedule can account for the dynamic nature of the thermal storage. For the setpoints in each hour, the mode of plant operation must be optimized to give the minimum energy consumption while meeting the setpoints. This control structure is robust, computationally efficient, while being flexible in allowing different plant installations to be controlled without affecting the formulation of the optimization of the thermal storage.

The pertinent components of the controller include an optimization algorithm, building and plant models, and a weather prediction model. The optimization algorithm is used as an optimizer to search for an optimum control strategy under

the predicted weather conditions, building thermal response and plant operation for the next day. This information is provided by using the building and plant model, and the weather prediction model. The requirements for each component model of this controller have been defined.

The following chapters (Chapters 4, 5, 7) describe these component models, together with the control characteristics in Chapter 6 and the annual performance of the optimum predictive controller in Chapter 8.

# Chapter 4

# Building and Plant Model

## Introduction

The building and plant model is the central element of the optimum predictive controller investigated in this research, since it is used as the basis for predicting the building thermal response from which the plant operation over the next 24 hours is derived. Since the fabric thermal storage system utilizes the mass of the structure as an energy store, the response of the system to thermal disturbances in the internal space is slow. Consequently, although the model of the building and ventilated slab must include the dynamic response of the building, the plant models can be steady state since their response time is significantly faster than that of the building.

The model development presented here, includes both the background theory and model validation. The building model validation has been conducted by comparing the error of the model prediction with measured data. The robustness of the model has been assessed in relation to the model's sensitivity to errors in input data and parameters, and its capability in modelling a variety of control strategies and building systems. These are essential for the investigation of optimum control of ventilated slab systems.

In order to develop a building simulation model that meets the requirements defined in Chapter 3, the existing simulation methods have also been reviewed.

## 4.1 Building Thermal Simulation Methods

The thermal modelling of buildings has been the subject of much research. According to Clarke (1985), a building simulation model should address many aspects including:

- the transient conduction of heat through the enclosure;
- casual gains from occupancy, lighting and equipment;
- infiltration and ventilation through the zone;
- the effects of shortwave solar radiation on exposed and internal surfaces;
- longwave radiation exchange between internal surfaces;
- longwave radiation exchange between exposed external surfaces and the sky and surroundings;
- window shading effect and the shading from surrounding buildings;
- the varying convective effect;
- plant characteristics and controller strategy;
- effects of moisture.

These thermal activities contribute to a complex building thermal response. Two basic methods have been used in building simulation programs to model the thermal behaviour in the building complex, the heat balance method and the weighting factor method (Tuomaala, 1992). The heat balance method solves the transient heat balance equations for the room air and enclosure simultaneously. The weighting factor method sums the effects of various heat disturbances on the room thermal response using a separate weighting factor for each disturbance. For a particular application, the weighting factors have to be calculated in advance by a program based on the heat balance method. In fact, the heat balance method is based on the principles of Thermodynamics, while the weighting factor method is a technique to solve the equations which describe the complicated building thermal activities.

In terms of the degree of simplicity and the strategy used to solve the differential and partial differential equations describing the thermal events and relationships in a building, Clarke (1985) claimed that there are five methods: steady state, simple dynamic, response function, numerical methods and electrical analogue. Steady state methods only account for the steady state heat flow through the building fabric, and omit any dynamic response of the building. These methods have no ability to address the real relationships between the building fabric and heat disturbances (including plant operation). The simple dynamic methods are based on statistical techniques (such as regression) to address the dynamic performance in order to perform energy assessment.

Response function methods use special techniques to solve the partial differential equations. There are two branches of these methods: time-domain response function and frequency-domain response function, both based on the modelling of the transient conduction and inter-zone energy balance relationship. Time-domain methods are concerned with the response of a multi-layered construction to temperature or flux series, and can handle periodic and non-periodic flux and temperature time series. These methods preprocess the response of a system to a unit excitation applied under the same boundary conditions as under the anticipated actual operation. If the system is linear, the unit response function is determined only once, otherwise, it has to be computed again when the system properties change. For a complete zone, time-domain response function methods formulate an energy balance of the zone. The total heating or cooling load is then calculated by counting each flow path of heat loss and gain with the corresponding weighting factor (the response factor). Frequency-domain response function methods make an assumption that climatological time series can be represented by a series of periodical functions, such as a Fourier series of sine wave harmonics. The influence of any heat flux to the building space is computed by superposing the cyclic contribution from each harmonic. This method is also referred to as the "admittance method" and has been adopted by the Chartered Institution of Building Services Engineers (CIBSE) as a standard approach in design (Clarke, 1985).

Numerical methods are concerned with approximating the derivatives of the differential and partial differential equations derived from heat balance relationships. These methods start with providing approximate solutions, the approximation depending on the accuracy required. However, not only can these methods solve

problems which are insoluble by analytical techniques, but also accurate solutions can be obtained by an appropriate formulation of the simulation model. The application of these methods is increasing due to their conceptual simplicity and power in solving problems with many complex conditions, such as those having time dependent thermal properties.

Electrical analogue methods analogize a heat flow as an electrical flow. The heat flow paths affecting the room thermal conditions are represented as electrical circuits, with the heat flow sources as either current or voltage sources and a node in a heat flow path with considerable thermal capacity as a capacitance. These methods are also referred to as time constant thermal networks, since the analogous electrical circuit has a $RC$ time constant, representing the response of the capacitance to disturbances. Typically one node is assigned to a fabric component, although some models even assign one node to all fabric components with the addition of their mass capacities as one capacitance in the thermal network model (Mathews *et al.*, 1989). Such lumped parameter models can be physically interpreted, and all the main heat fluxes in a room can be represented clearly. However, as a lumped method, the temperature change along the heat flux in a fabric component (e.g. wall) can not be modelled; the node has one representative temperature, and the component is at a uniform temperature condition. According to heat transfer theory (Holman, 1986), a lumped parameter method can provide reasonable confidence of modelling a uniform infinite plate only when the Biot number is less than 0.1, where the Biot number is calculated by,

$$Bi = \frac{h * L_c}{\lambda} \tag{4.1}$$

Here $h$ is the surface heat transfer coefficient (W/m$^2$ K), $L_c$ is characteristic length (m), and $\lambda$ is thermal conductivity (W/m K). For a uniform brickwork external wall of 0.22 m thick, the Biot number would be about 0.4.

In reality, a wall construction is not infinite and usually not of a uniform property, and due to the difference in air temperature between the external and internal surfaces of the wall, the temperature difference inside the wall is inevitable. However, the ambient boundary air temperature changes in a similar way to a periodic wave, and rarely with a sudden change of large amplitude. In addition, the temperature difference between the fabric and boundary air is not substantially large. The Biot number does not impose a strong restriction on the application of the lumped parameter method for modelling building fabric components, since the

temperature distribution within the component can be approximately neglected due to the relatively mild boundary condition. The lumped parameter model is useful for building energy analysis and design purposes where the influence of major heat disturbances on the building environment can be effectively assessed, without modelling the building in great detail (such as the mass temperature of each layer of a component).

Some other methods have also been termed time constant methods, for instance, an integrated time constant of the building enclosure was evaluated from the response to a "unit excitation", which was calculated from admittance factors and energy balance equations (Raychaudhuri, 1965). Such methods do not use an electric analogy and belong to response function category. Although the concept of these methods is worth propagating, the integrated time constant can only be solved for a few ideal simple conditions, and is too complicated for design purposes.

Each modelling method has advantages and disadvantages. In this research, the time constant thermal network method has been used to simulate the building thermal response, since this method is simple and able to account for all the major heat disturbances in the building. The fact that the method can be easily interpreted is also useful for optimization studies, since the influence of the different design schemes and control strategies can be clearly represented. Several building structure elements are assigned with one capacitance, each for an assumed isothermal massive node. This method, therefore utilizes the lumped parameter approach to establish the building thermal network model.

### 4.1.1 Lumped Parameter Thermal Network Models

Previous research has been conducted to improve the time constant thermal network model approach. A Total Thermal Time Constant method for the complete Building (TTTCB) was presented by Givoni (1976), in which the area-weighted average of time constants of all the exterior building elements was calculated. This method can only be applied to buildings with similar element construction. Hoffman and Feldman (1981) improved the lumped parameter network model, known as the TTTC method, which utilizes the superposition theory to calculate the step responses to heat disturbances through the heat transfer path of each element. In order to obtain an acceptable result, the same calculation has to be performed for

a considerable number of time steps.

Crabb, *et al.* (1987) developed a model which was based on the second-order method, first presented by Laret (1980). The model has two capacitances, one for the mass node and the second for the air node. The computer implementation of this model was developed at the University of Exeter, and is referred to as Excalibur. A validation conducted upon a school building showed that the approximations made in the model were not violated. However, the algorithm is not clear in calculating the resistances of an element and the lumped mass node.

Hassid (1985) used a linear model to evaluate the performance of a passive solar house, and an algorithm for calculating the total thermal time constant of a building element was developed (Equation 4.2 and 4.3). The method uses the thermal time constants of a building element to obtain the lumped thermal resistances. The algorithm is easily interpreted and can be obtained from a transfer function derivation for a building element. Consider the multi-layer construction shown in Figure 4.1 and the lumped parameter representation given in Figure 4.2, $R_i$ and $R_o$ are the resistances of the mass node to the disturbances from the inside and outside respectively. $C$ is the total heat capacity of the construction. The time constants, $\tau_i = R_i C$ and $\tau_o = R_o C$, represent the response to a disturbance from the inside and outside, and can be calculated thus:

$$\tau_i = \sum_{k=1}^{n} C_k \left( R_{si} + \sum_{j=1}^{k-1} R_j + \frac{R_k}{2} \right) \tag{4.2}$$

$$\tau_o = \sum_{k=1}^{n} C_k \left( \frac{R_k}{2} + \sum_{j=k+1}^{n} R_j + R_{so} \right) \tag{4.3}$$

where $R_j$ and $R_k$ are the thermal resistances of layers $j$ and $k$, and $R_{si}$ and $R_{so}$ are the resistances of the inside and outside surfaces. Having calculated the time constants and the total thermal capacitance of the construction ($C = \sum_{k=1}^{n} C_k$), the lumped thermal resistances can be obtained as $R_i = \frac{\tau_i}{C}$ and $R_o = \frac{\tau_o}{C}$.

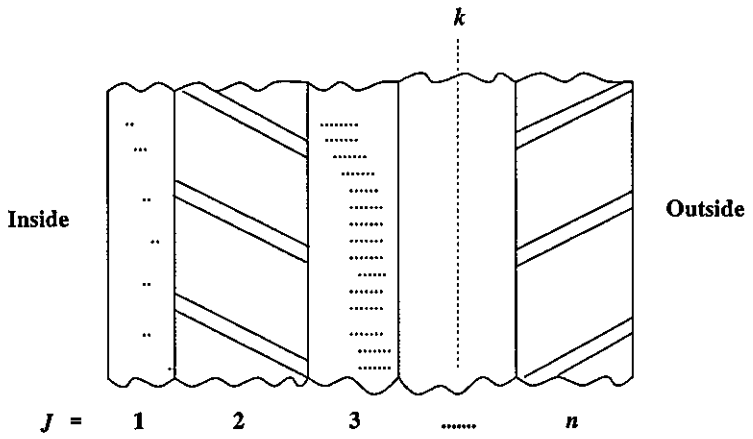


**Figure 4.1, Multi-layer Building Element**

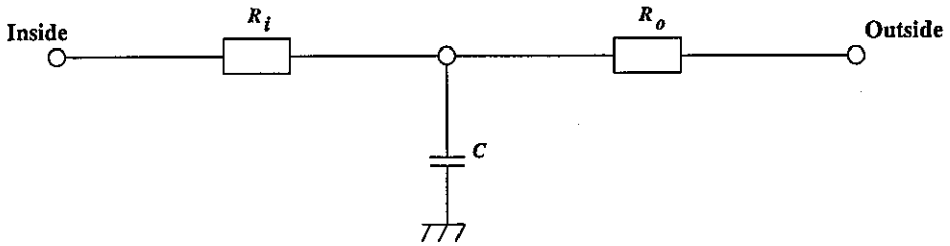


**Figure 4.2, Lumped Parameter Model of a Building Element**

Mathews *et al.* (1989) derived the same algorithm as Hassid's model and developed a first-order zone model to predict room thermal conditions at the sketch design stage. The model can take account of radiative heat gain and convective heat gain in the room. This method is simple and also easily interpreted, and can give a clear insight into the major thermal activities in a building. In order to estimate the effective heat storage capability of a building, the heat transfer through the ground floor and the internal mass, including partitions and furnitures, were also addressed by Mathews *et al.* (1991). Lombard and Mathews (1992) further improved the method by developing a technique to solve a time variant *RC* network, for instance, a variable ventilation rate leading to time dependent resistances. The technique relies on frequency domain analysis to calculate transfer functions. Mathews *et al.* (1994) reported that the model had been validated in a wide range of buildings,

with more than 80% of the indoor air temperature predictions within 2 °C of measurements in over 70 studies.

A lumped parameter thermal network approach, based on Mathews *et al.* (1989), has been chosen in this research, to model the thermal performance of the building zone and ventilated slab. The approach is attractive in that the model parameters are easily derived from the thermal properties of the building materials and that the model equations are easily solved so that optimization studies can be conducted without excessive computation. However, in the assessment of building fabric storage systems, the first-order thermal network model makes too crude an approximation, since all of the fabric components are assumed to be in an isothermal condition, and there is no facility to address the radiative exchange between the different component surfaces. Such approximations are not suitable for the modelling of hollow core ventilated slab systems.

The model developed in this research extends the first-order network approach. The model should have an ability to simulate the heat transfer between the ventilated air and the slabs so as to investigate the performance of the mass thermal storage. The model should also allow various mass temperatures for the components so that the longwave radiation between different surfaces can be addressed, as there may be a significant temperature difference, for instance, between the ceiling and the walls, when the ceiling is precooled at night to store energy. For the hollow core ventilated slab system, these functions are important if the system performance is to be evaluated to an acceptable accuracy.

## 4.2 The Lumped Parameter Zone and Slab Thermal Model

The approach adopted in the development of the building thermal model is to integrate a new model of the ventilated hollow core slab with an established zone model, based on Mathews' (1989) method. The thermal models of the ventilated slab and zone are described below, and the combined zone and slab model is illustrated in Section 4.2.3.

### 4.2.1 The Ventilated Slab Thermal Model

Previous research (Augenbroe and Vedder, 1985), into the thermal performance of ventilated slabs, suggests that there is a negligible change in the slab concrete mass temperature along the air path. However, since there can be a difference in temperature from one zone to another, the mass temperature may not be distributed symmetrically about the center of the slab. This effect can be accounted for by modelling the slab in two halves, one half coupled to the environment above the slab and the second to the environment below. Since the temperature difference that most affects the slab mass temperature is the difference between the ventilation air temperature and that of the adjacent environment, the temperature difference across the slab and thus the heat conduction through the concrete slab, has the least effect on the mass temperature, when the ventilation air is passed through the slab. However, in order to allow for a variable air ventilation rate, including no ventilation and switchflow operation (where only one core is used as an air supply path), the heat conduction across the slab from one surface to the other has been modelled. A substantial change in air temperature will exist along the air path, yet a single air temperature is required for the ventilation air node in the lumped parameter model. This has been taken as the average air temperature along the air path which can be derived from the heat exchange between the slab and the ventilation air.

The lumped parameter model of the ventilated slab is illustrated in Figure 4.3. $\bar{T}_{av}$ is the mean temperature of the ventilation air, and $T_{au}$ and $T_{al}$ are the air temperatures of the zones above and below the slab. $R_{cu}$ and $R_{cl}$ are the slab thermal resistances of the mass nodes to disturbances in the zone air temperatures. $R_{cu}$ and $R_{cl}$ are not equal due to the different floor and ceiling finishes. Similarly the thermal capacitance, $C_u$ and $C_l$, of the two halves of the slab can differ due to the surface finishes. Although the surface resistance and the resistance of the concrete between the mass node and the ventilation air are the same for both sides of the slab, the procedure for deriving the resistances from the time constants means that the finishes on the external surfaces will also result in $R_{au}$ and $R_{al}$ being different. $R_{cond}$ is the conductive resistance from one mass node to the other. When air supply through the ventilated cores is stopped, the conduction process across the mass nodes takes control and the mass temperatures float with the zone air temperatures of the environment above and below the slab.

Due to the special supply air path and geometry of the concrete slab, the calculations of heat exchange between the ventilated air and slab, the slab capacitance, the slab concrete thermal resistances and ventilation air surface resistance are discussed below. The calculation of slab resistances when the switchflow unit is operated is also described.

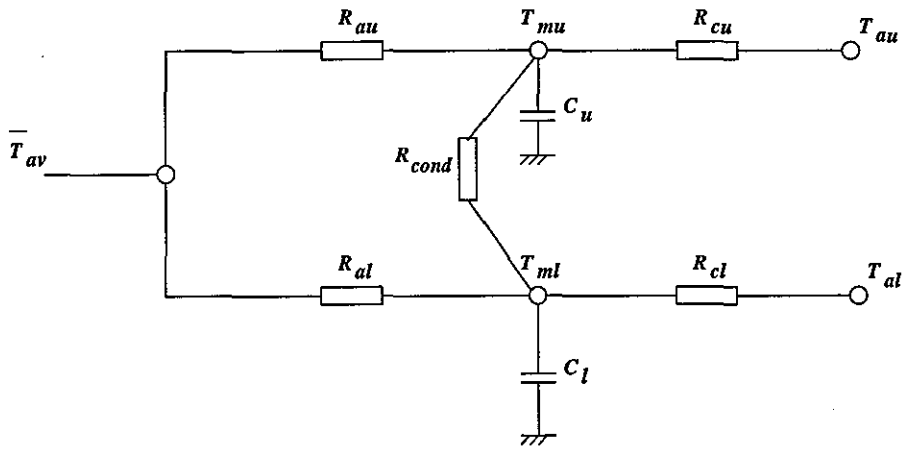


**Figure 4.3, Lumped Parameter Model of the Ventilated Slab**

### Ventilation Air to Slab Heat Exchanger Model

Since the slab mass temperature is assumed to be constant along the air path, the heat exchange between the ventilation air and the slab is analogous to that of a heat exchanger, with one fluid condensing or evaporating and therefore being of infinite thermal capacity. If the slab mass temperature is taken as the arithmetic mean, $\bar{T}_m$, of the two slab mass temperatures $T_{mu}$ and $T_{ml}$ (Figure 4.3), then the air temperature at a distance $x$ along the airpath is given by:

$$T_{ax} = \bar{T}_m + (T_{ai} - \bar{T}_m)e^{-\gamma x} \tag{4.4}$$

$\gamma x$ is the number of transfer units, $\gamma = \frac{U}{\dot{m}_a c_{pa}}$. $\dot{m}_a$ is the air mass flow rate and $c_{pa}$ the air specific heat capacity. $U$ is the transmittance per unit length of the airpath derived from the resistances $R_{au}$ and $R_{al}$ (Figure 4.3). $T_{ai}$ is the temperature of the air at the inlet to the slab. The average air temperature along the airpath $\bar{T}_{av}$ can be obtained by integrating $T_{ax}$ along the length of airpath $L$, $\bar{T}_{av} = \frac{\int_0^L T_{ax} dx}{L}$.

$$\bar{T}_{av} = \bar{T}_m + \frac{\left(T_{ai} - \bar{T}_m\right)}{\gamma L}\left(1 - e^{-\gamma L}\right) \tag{4.5}$$

### The Slab Thermal Capacitance

A typical concrete slab will have five cores but only three are generally used for ventilation (Figure 1.1, Section 1.1). This and the air path taken through the slab (Figure 2.1, Section 2.1.1), makes it difficult to determine the effective thermal capacitance of the slab. Previous research (Winwood *et al.*, 1994), suggested that a 24 hour cyclic variation of the surface temperature of a slab influences the mass to a depth of only 15.0 cm. However, using this depth to determine the thermal capacitance has proved to be ineffective when used in the model described here. The approach adopted to determining the slab thermal capacitance is first to simplify the representation of the air path (Winwood *et al.*, 1994) (Figure 4.4), and second to select a width and length of slab to provide a capacitance that gives a thermal response matching measured performance data from a commercially available system. The total length of the simplified air path is equal to that of the real system. The width of the area relating to the effective thermal capacitance $W$ has been set to equal the span of hollow core section of the slab (Figure 4.5). In order to match the measured thermal performance of a commercial ventilated slab system (Section 4.4), the length of slab beyond the core ends $\Delta$ (Figure 4.4), was found to be 30.0 cm. The remainder of the slab length and the area of slab beyond $W$ is integrated into the building zone mass node.

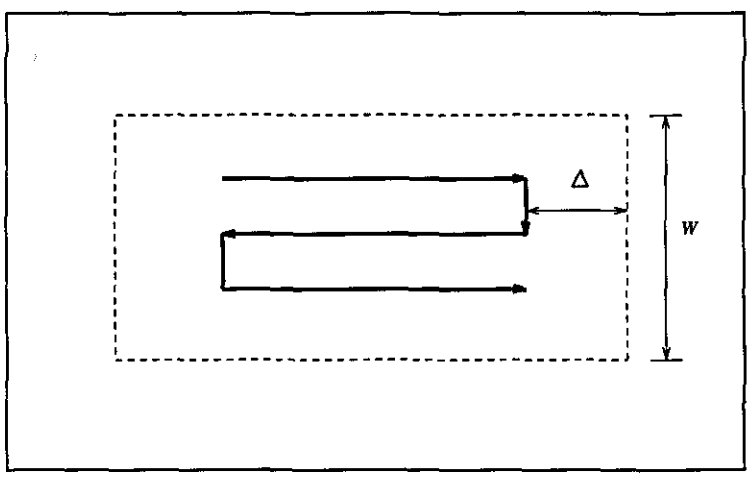


**Figure 4.4, Simplified Air Path and Area of Thermal Capacitance**

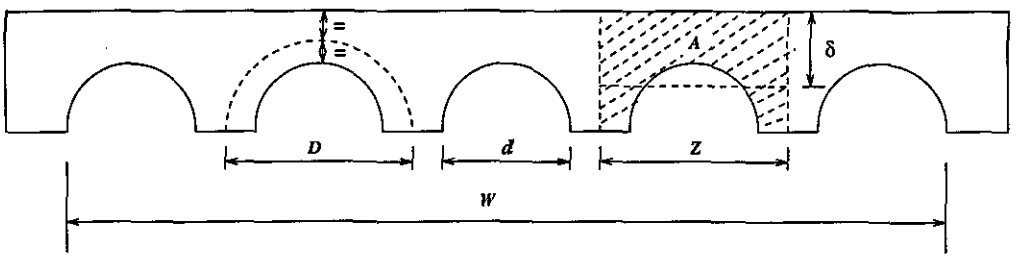


**Figure 4.5, Dimensions for Slab Concrete Capacitance and Resistance Calculations**

### The Slab Concrete Thermal Resistances

Due to the geometry of the ventilated slab, the calculation of the slab concrete resistance is considered in two parts. When calculating the resistance to a disturbance in the room air temperature, the slab is considered as a flat plate with a cross-sectional area equal to the effective storage area of the slab. The thickness of the plate used to assess the resistance is then $\delta = \frac{A}{Z}$ (Figure 4.5). However, radial heat transfer occurs between the ventilation air and the slab. Since for most commercial systems, the distance between the cores is similar to the thickness of slab above and below the cores, the mass node is assumed to be located close to the perimeter of a circle positioned half way between the edge of the core and the external surface of the slab (Figure 4.5). The circle is centered on the core and is of diameter D. Here, an isothermal cylinder has been assumed such that the resistance $R_c$ for half the core is given by:

$$R_c = \frac{ln\left(\frac{D}{d}\right)}{\pi \lambda L} \tag{4.6}$$

where $\lambda$ is the conductivity of the concrete. As for all lumped parameter resistances, the relationship may not be true for highly transient stages of heat transfer. It is also unlikely that true isothermal conditions will occur on the edge of the cylinder. However, this is unlikely to significantly affect the accuracy of the lumped parameter model.

The conductive resistance, $R_{cond}$, from the mass node above the core to the node below the core, is calculated by combining in parallel, the resistances through the

conduction paths between the cores, and the paths across the cores, within the effective capacity area $W$. It is assumed that $R_{cond}$ is invariant to the operation when the cores are ventilated or the ventilation is stopped, since the convective heat transfer between the ventilation air and the mass is accounted for by the ventilation air surface resistance, which has been integrated in the resistances of the heat exchanger model.

### Slab Resistances and Capacitance for Switchflow Operation

Switchflow operates by switching the airflow from through three cores to one core and therefore, the slab mass temperatures are more unevenly distributed than when using the middle three cores as the supply path. The horizontal heat transfer may therefore be significant between the concrete region near the ventilated core and the inactive region of unventilated cores. However, due to the large capacity of slab, the mass temperature difference between the two regions is unlikely to be large. The lumped parameter model therefore evaluates the average lumped mass temperatures of the nodes above and below cores, with the horizontal heat transfer being ignored.

The switchflow operation has been incorporated within the lumped parameter model by coupling the ventilation air flowing through the single core ($\bar{T}_{av}$), to a reduced active capacitance ($C_{ac}$) (Figure 4.6). However, the air node ($T_{az}$) is coupled to both the active ($C_{ac}$) and inactive ($C_{inac}$) regions of the slab. The time constants and hence lumped thermal resistances, for the slab model are calculated according to this coupling. The choice of the active capacitance associated with the single core operation has not been validated due to no experimental test data being available.

The fast response of the air supply system provided by the switchflow results from the reduced interaction between the ventilation air and the high capacity slab mass. The influence of the switchflow operation on the room thermal condition is investigated in Section 4.5.2.

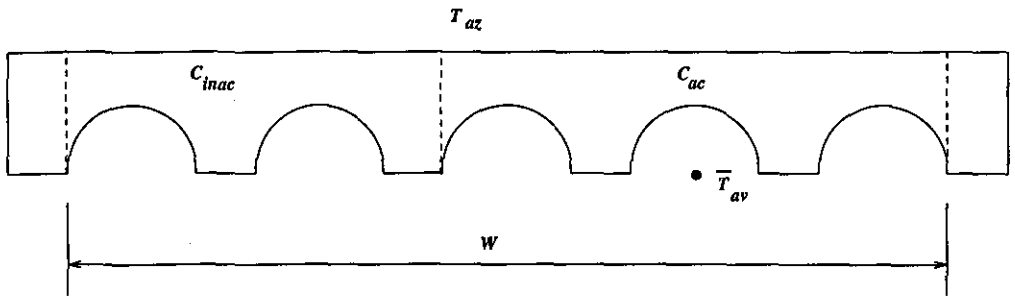


**Figure 4.6, Active and Inactive Capacitance During Switchflow Operation**

### The Ventilation Air Surface Resistance

The resistance on the inside surface of the air cores $R_{sa}$, is derived from the surface heat transfer coefficient. This is a function of the properties of both the air flow and the nature of the surface of the cores. The heat transfer is also higher around the connecting corners than along the straight sections of core (Willis and Wilkins, 1993). To further complicate the calculation of the surface resistance, the model must allow for a variable air flow rate.

Since no reliable measurements have been made of the heat transfer coefficient inside hollow core slabs, the approach adopted here is to use a standard heat transfer correlation for resistance of the straight sections of the core. To correct for the enhanced heat flow around the corners, a correction factor was calculated from the measured performance of a commercial ventilated slab system. The empirical correlation for the straight cores was taken as (Holman, 1986; CIBSE, 1986):

$$Nu = 0.023 Re^{0.8} Pr^{0.4} \tag{4.7}$$

where, $Nu$ is the Nusselt number, $Re$ the Reynolds number and $Pr$ the Prandtl number. Using the properties of air at a temperature of 20.0 °C, the heat transfer coefficient $h_{sa}$ for the straight section of duct can then be given by the approximate expression:

$$h_{sa} = 3.73 v^{0.8} d^{-0.2} \, (\mathrm{W/m^2\,K}) \tag{4.8}$$

where $v$ is the air velocity and $d$ the core diameter.

Measured air temperatures from a commercially available ventilated slab system suggest that this relationship is of the correct order (Section 4.4). The accuracy of this relationship could not be verified completely since the test data available is insufficient to enable precise measurement of heat transfer coefficients. Air temperatures measured along the air path suggest that the heat transfer coefficient for the corners is in the order of 50 times higher than that for the straight sections of core. This was determined using the measured data and the heat exchanger model. The value was further verified by comparing the lumped parameter model output to a range of measured performance data (Section 4.4). The sensitivity of this value has also been investigated and is described in Section 4.5.1. The consistency of the increase in corner heat transfer with air velocity has not been verified completely, since the measured data were only available for two core air velocities. The correction factor for a bend of a straight duct suggested by Jakob (1945) can qualitatively justify the independence of increased bend heat transfer from fluid velocity. It is unlikely therefore, that the relationship between straight section and corner heat transfer will change significantly, provided the velocity remains in the fully turbulent region.

### 4.2.2 The Lumped Parameter Zone Model

The lumped parameter zone model (Mathews *et al.*, 1989; 1994) is illustrated in Figure 4.7, where $T_{sa}$ is the sol-air temperature, $T_o$ the outside air temperature, and $T_{az}$ the zone air temperature. $T_{sb}$ and $T_{mb}$ represent the zone inside surface and mass temperatures. $Q_c$ and $Q_r$ are the convective and radiant heat gains. $R_{sb}$ is the surface resistance and $R_v$ the infiltration resistance.

$C_b$ is the effective thermal capacitance of all massive elements in the zone. $R_{ob}$ and $R_{ib}$ are obtained by combining in parallel, the external and internal resistances of all massive elements of the building fabric. Windows are considered to have no thermal capacity but their resistance is integrated in $R_{ob}$ and $R_{ib}$. The internal partitions are also lumped into $R_{ob}$, $R_{ib}$ and $C_b$. This is achieved by representing

the temperature of the adjoining zones by the environmental temperature and using this in the same manner as the sol-air temperature used for external walls.

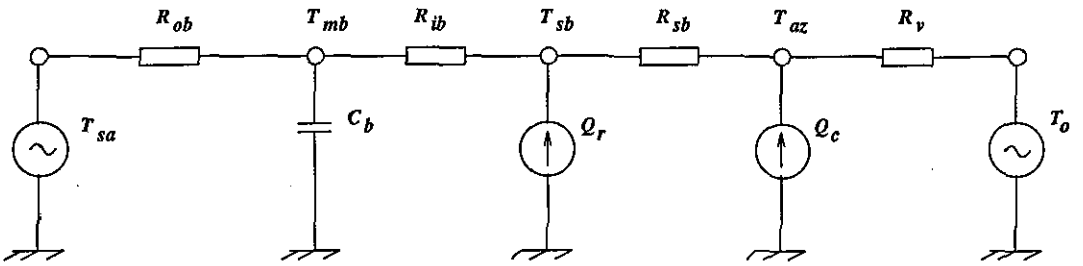


**Figure 4.7, Lumped Parameter First-order Building Model**

The solar radiation on the exposed external surfaces is modelled by the sol-air temperature $T_{sa}$. $T_{sa}$ is calculated according to the convective and radiant heat transfer occurring on the external surfaces. For a wall surface at orientation $k$, the sol-air temperature $T_{sa,k}$ is calculated by,

$$T_{sa,k} = T_o + R_{so}\,(\alpha I_{t,k} - \epsilon I_l) \tag{4.9}$$

where $R_{so}$ is the external surface resistance of the wall. $(\alpha I_{t,k} - \epsilon I_l)$ is the net amount of solar radiation received at the surface. $\alpha$ and $\epsilon$ are the absorptance and emissivity of the external surface. $I_{t,k}$ is the total intensity of solar radiation ($W/m^2$) at the surface $k$. $I_l$ is longwave radiation loss to the sky, ground or the environment. This depends on cloud cover, dry-bulb temperature, orientation of surface and the nature of the external environment. A simplified calculation for $I_l$ has been suggested by the CIBSE (1986),

$$\begin{cases} I_l = 93 - 79\,CL, \text{ for horizontal surfaces,} \\ I_l = 21 - 17\,CL, \text{ for vertical surfaces} \end{cases} \tag{4.10}$$

here $CL$ is cloudiness. While $I_{t,k}$ combines direct and diffuse radiation on the vertical surface $k$,

$$I_{t,k} = I_{D,k} + I_{dif} = I_{D,k} + 0.5\,I_d + 0.5\,g_r\,I_{TH} \tag{4.11}$$

Weather data are available for direct normal beam radiation $I_{D,N}$, diffuse horizontal radiation $I_d$ from the sky, and global horizontal radiation $I_{TH}$. Diffuse radiation $I_{dif}$ on a surface mainly includes the radiation from the sky $I_d$, and the reflected proportion from the ground (global radiation corrected by ground reflectance $g_r$). Equation 4.11 assumes that the diffuse radiation received at the vertical surface is

half that of the horizontal surface, from the sky and ground, the view factor being 0.5.

$I_{D,k}$, the direct radiation at the surface orientation $k$, can be calculated from the direct normal beam radiation, $I_{D,N}$,

$$I_{D,k} = I_{D,N} \cos i \tag{4.12}$$

$$\cos i = \cos\theta \sin\phi + \sin\theta \cos\phi \cos\gamma_s \tag{4.13}$$

where $i$ is the angle of solar incidence on the surface, which changes hour by hour. $\phi$ is solar altitude and $\gamma_s$ the wall-solar azimuth. $\theta$ is the surface tilt. For a vertical surface like a wall, $\theta = 90°$, so that $\cos i = \cos\phi \cos\gamma_s$. The solar altitude $\phi$ and wall-solar azimuth $\gamma_s$ can be calculated from the location latitude, daily solar declination, solar time and surface orientation (CIBSE, 1986).

According to Equations 4.9 to 4.13, the sol-air temperature for each wall surface can be derived. As the surfaces are at different orientations they will receive different amounts of solar radiation (or heat disturbances from the adjoining zones). $T_{sa}$ is therefore corrected for all walls based on the fact that walls are in parallel from the indoor air node to outside air node (Equation 4.14); for internal walls, $T_{sa,k}$ is the adjoining zone environmental temperature (Mathews *et al.*, 1989).

$$T_{sa} = \sum_{k=1}^{n} T_{sa,k} \frac{R_{total}}{R_k} \tag{4.14}$$

where $R_k$ is the total resistance for one element between the inside air and outside air node (or adjoining zone air node) and $R_{total}$ is the sum of $R_k$ in parallel.

### 4.2.3 The Combined Thermal Network Model for Building Zone and Slab

The lumped parameter building model has been extended to incorporate the ventilated hollow core slabs, for the ceiling and floor. Since the room surfaces may be at noticeably different temperatures when the ventilated hollow core slabs are in use, the longwave radiant heat exchange between the room surfaces have been modelled. The new model also includes the shortwave radiant heat gain distribution to the different surfaces of the room.

Figure 4.8 represents the thermal network for the integrated ventilated slab and building model. The notation is as described for Figures 4.3 and 4.7, except for the modelling of heat exchange between surfaces and in order to allow for two ventilated slabs, subscripts $c$ and $f$ have been added to denote the ceiling and floor. Unlike Figure 4.3, $R_{clc}$ and $R_{cuf}$ are the conductive resistances from the ceiling and floor slab mass nodes to the internal surfaces of the zone; the surface resistances ($R_{sc}$, $R_{sf}$), are represented separately to allow the modelling of radiant heat exchange between the surfaces.

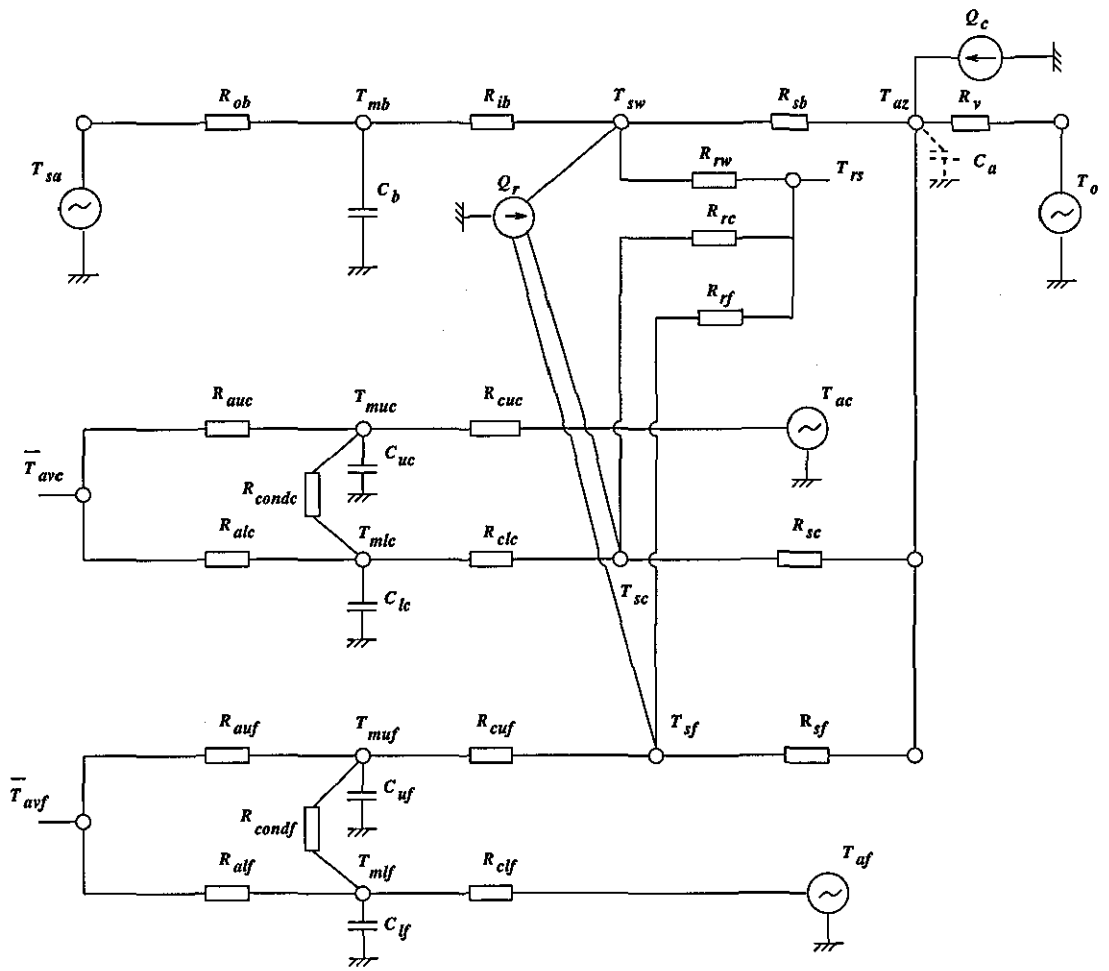


**Figure 4.8, Combined Building and Ventilated Slab Model**

The wall mass temperature is lumped to $T_{mb}$, the two ceiling mass nodes of $T_{muc}$ and $T_{mlc}$, and similarly, the floor mass nodes $T_{muf}$ and $T_{mlf}$. Whereas the internal surface temperatures for the walls, ceiling and floor are $T_{sw}$, $T_{sc}$ and $T_{sf}$ respec-

tively. $\bar{T}_{avc}$ and $\bar{T}_{avf}$ are mean ventilation air temperatures for the ceiling and floor slabs. $T_{ac}$ and $T_{af}$ are the temperatures of the zones above the ceiling and below the floor. $T_{az}$ is the air temperature of the modelled zone which is coupled to the wall, ceiling and floor surfaces by the convective surface resistances $R_{sb}$, $R_{sc}$ and $R_{sf}$.

$C_a$ represents the zone air thermal capacitance. However, the effect of the room air capacity on the building response is insignificant compared with the effect due to the structural elements. Further, the high frequency response is only a minor consideration in this study and therefore the air capacitance is not normally included in the model. The convective heat gain $Q_c$, includes the heat gain from solar, equipment, lighting and occupants, and the ventilation system supplied via the ceiling slab.

Solar gains through windows are in the form of shortwave, longwave, and convective gain, which are calculated separately.

### Solar Gain Through Windows

Solar radiation incidence on the external surfaces of the zone is taken into account by sol-air temperature. Solar gains through windows include the total radiation transmitted through windows and a part of the solar radiation absorbed by the windows.

The solar radiation transmitted through windows $I_{tr,k}$ is calculated from the shortwave irradiation on the surface, window area, transmittance, and shading coefficient (which depends on the type of glazing).

$$I_{tr,k} = (\nu_D I_{D,k} + \nu_d I_{dif})\, A_{window}\, SC \tag{4.15}$$

The solar radiation absorbed by windows $I_{ab,k}$ is partly lost to the ambient environment, and partly contributes to the heat gain in the room in the proportion of $\frac{R_{oa}}{R_{oa}+R_{ia}}$,

$$I_{ab,k} = \left[(\alpha_D I_{D,k} + \alpha_d I_{dif})\frac{R_{oa}}{R_{oa}+R_{ia}}\right] A_{window}\, SC \tag{4.16}$$

where, $I_{D,k}$ and $I_{dif}$ are the direct and diffuse radiation (Equation 4.11, Section

4.2.2). $\nu_D$ and $\nu_d$ are the transmittance, $\alpha_D$ and $\alpha_d$ the absorptance of direct and diffuse radiation respectively. $A_{window}$ is the area of window and $SC$ the shading coefficient. $R_{oa}$ and $R_{ia}$ are convective heat transfer coefficients of the external and internal surfaces of windows.

The solar radiation transmitted through windows contributes to shortwave gain to the zone. Whereas, the absorbed gain by windows is treated in this model in two parts: 65.5% contributing to the longwave heat gain and 34.5% to the convective gain to the air node directly. The calculation of longwave and shortwave heat gain in the zone is discussed below.

### Longwave Radiant Heat Exchange

The long wave radiant heat exchange between surfaces is modelled by the exchange with the radiant star index temperature $T_{rs}$. This temperature is coupled to the room surfaces by the radiant resistance $R_{rw}$ for the walls, $R_{rc}$ for the ceiling, and $R_{rf}$ for the floor (Figure 4.8). The radiant star temperature is represented by (Davies, 1993):

$$T_{rs} = \frac{S_w T_{sw} + S_c T_{sc} + S_f T_{sf} + Q_{lr}}{S_w + S_c + S_f} \tag{4.17}$$

where $Q_{lr}$ is the longwave radiant heat gain generated from solar, equipment, lighting and occupants. $T_{sw}$, $T_{sc}$ and $T_{sf}$ are the surface temperatures of the walls, ceiling and floor. $S_w$, $S_c$ and $S_f$ are radiant conductances for the walls, ceiling and floor, which depend on the surface area, emissivity, and the radiant heat transfer coefficient associated with each element. For example, for the ceiling,

$$S_c = A_c E_c h_r \tag{4.18}$$

where, $A_c$ is the ceiling surface area, $h_r$ is the radiant heat transfer coefficient of the room and $E_c$ a function of emissivity. $h_r$ is a function of $T_{rs}^3$ and so in order to avoid iteration, $T_{rs}$ is assumed to be 20 °C when calculating $h_r$ (Davies, 1993). $E_c$ can be calculated from (Davies, 1993):

$$\frac{1}{E_c} = \frac{1-\epsilon_c}{\epsilon_c} + \gamma_c \tag{4.19}$$

where, $\epsilon_c$ is the ceiling surface emissivity. $\gamma_c$ is the ceiling area weighting factor, $\gamma_c = 1 - \frac{A_c}{A_{total}}$, and $A_{total}$ is the sum of the areas of the walls, ceiling and floor.

The same algorithms are equally applicable to $S_w$ and $S_f$. Inversion of the conductances gives the radiant resistances $R_{rw}$, $R_{rc}$ and $R_{rf}$.

**Shortwave Heat Gain**

$Q_r$ is the shortwave heat gain to the zone, including gain from lighting and solar radiation. The total shortwave solar gain transmitted through windows is the sum of $I_{tr,k}$ in Equation 4.15 for the number of external windows. The proportion of incoming radiation distributed onto the wall surfaces, ceiling surface and floor surface, is calculated according to the relative surface areas; the geometry of zone surfaces is not considered in this model. The total gain absorbed by each element is the product of the shortwave radiant surface coefficient $\beta$, the proportion of radiation distributed to the surface $P$, and the total shortwave gain entering the room $Q_r$. For instance, the ceiling surface receives the shortwave gain by $Q_{r,c} = \beta_c P_c Q_r$. The same calculation is equally applied to the surfaces of the walls and floor.

### 4.2.4 Implementation of the Combined Zone and Slab Model

Based on the network model in Figure 4.8, twelve equations can be established to describe the relationships of the thermal variables, nine of which are independent.

For the network of walls,

$$\frac{T_{sa} - T_{mb}}{R_{ob}} + \frac{T_{sw} - T_{mb}}{R_{ib}} = C_b \frac{dT_{mb}}{dt} \tag{4.20}$$

For the nodes of the ceiling,

$$\frac{\bar{T}_{avc} - T_{muc}}{R_{auc}} + \frac{T_{mlc} - T_{muc}}{R_{condc}} + \frac{T_{ac} - T_{muc}}{R_{cuc}} = C_{uc} \frac{dT_{muc}}{dt} \tag{4.21}$$

$$\frac{\bar{T}_{avc} - T_{mlc}}{R_{alc}} + \frac{T_{muc} - T_{mlc}}{R_{condc}} + \frac{T_{sc} - T_{mlc}}{R_{clc}} = C_{lc}\frac{dT_{mlc}}{dt} \tag{4.22}$$

$$\bar{T}_{avc} = \frac{T_{muc} + T_{mlc}}{2} - \left(\frac{T_{muc} + T_{mlc}}{2} - T_{ai}\right)\frac{\left(1 - e^{-\gamma L}\right)}{\gamma L} \tag{4.23}$$

For the nodes of the floor,

$$\frac{\bar{T}_{avf} - T_{muf}}{R_{auf}} + \frac{T_{mlf} - T_{muf}}{R_{condf}} + \frac{T_{sf} - T_{muf}}{R_{cuf}} = C_{uf}\frac{dT_{muf}}{dt} \tag{4.24}$$

$$\frac{\bar{T}_{avf} - T_{mlf}}{R_{alf}} + \frac{T_{muf} - T_{mlf}}{R_{condf}} + \frac{T_{af} - T_{mlf}}{R_{clf}} = C_{lf}\frac{dT_{mlf}}{dt} \tag{4.25}$$

$$\bar{T}_{avf} = \frac{T_{muf} + T_{mlf}}{2} - \left(\frac{T_{muf} + T_{mlf}}{2} - T_{ai}\right)\frac{\left(1 - e^{-\gamma L}\right)}{\gamma L} \tag{4.26}$$

The heat balance in the room can be represented by the following equations:

$$\frac{T_{sw} - T_{mb}}{R_{ib}} = \frac{T_{rs} - T_{sw}}{R_{rw}} + \beta_w P_w Q_r + \frac{T_{az} - T_{sw}}{R_{sb}} \tag{4.27}$$

$$\frac{T_{sc} - T_{mlc}}{R_{clc}} = \frac{T_{rs} - T_{sc}}{R_{rc}} + \beta_c P_c Q_r + \frac{T_{az} - T_{sc}}{R_{sc}} \tag{4.28}$$

$$\frac{T_{sf} - T_{muf}}{R_{cuf}} = \frac{T_{rs} - T_{sf}}{R_{rf}} + \beta_f P_f Q_r + \frac{T_{az} - T_{sf}}{R_{sf}} \tag{4.29}$$

$$T_{rs} = \frac{\frac{1}{R_{rw}}T_{sw} + \frac{1}{R_{rc}}T_{sc} + \frac{1}{R_{rf}}T_{sf} + Q_{lr}}{\frac{1}{R_{rw}} + \frac{1}{R_{rc}} + \frac{1}{R_{rf}}} \tag{4.30}$$

$$Q_c + \frac{T_o - T_{az}}{R_v} = \frac{T_{az} - T_{sw}}{R_{sb}} + \frac{T_{az} - T_{sc}}{R_{sc}} + \frac{T_{az} - T_{sf}}{R_{sf}} \tag{4.31}$$

Equations 4.23 and 4.26 are from the heat exchanger model, Equation 4.5, derived in Section 4.2.1. Equations 4.27 to 4.31 can be rearranged to a three-dimensional linear equation set:

$$X\,T_{surface} = Y\,T_{sm} \tag{4.32}$$

where, $T_{surface}$ is the surface temperature vector,

$$T_{surface} = (T_{sw}, T_{sc}, T_{sf})^{-1}$$

$T_{sm}$ is treated as a known independent variable vector in Equation 4.32,

$$T_{sm} = (T_{mb}, T_{mlc}, T_{muf}, T_o, Q_c, Q_r, Q_{lr})^{-1}$$

$X$ is a $3 \times 3$ matrix, and $Y$ is a $3 \times 7$ matrix, consisting of the resistances and coefficients in the equations. The Gauss elimination method has been used to solve Equation 4.32.

$$T_{surface} = X^{-1} Y T_{sm} \tag{4.33}$$

A state-space equation can be used to represent Equations 4.20 to 4.26:

$$A_m \dot{T}_m = S T_m + K T_u \tag{4.34}$$

where, $\dot{T}_m$ is the differential vector of mass node temperatures,

$$\dot{T}_m = (\dot{T}_{mb}, \dot{T}_{muc}, \dot{T}_{mlc}, \dot{T}_{muf}, \dot{T}_{mlf})^{-1}$$

$T_m$ is the mass node temperature vector. $T_u$ is the heat disturbance vector in the state-space equation,

$$T_u = (T_{sa}, T_{sw}, T_{sc}, T_{sf}, T_{ai}, T_{ac}, T_{af})^{-1}$$

$A_m$ is a $5 \times 5$ diagonal matrix containing the time constants ($RC$) for each mass node. $S$ is a $5 \times 5$ matrix, and $K$ a $5 \times 7$ matrix.

If the $T_{surface}$ vector (Equation 4.33) is substituted in Equation 4.34, the state-space equation becomes:

$$\dot{T}_m = W T_m + V U \tag{4.35}$$

where, $U$ is the heat disturbance vector consisting of all the driving variables considered in the model,

$$U = (T_{sa}, T_o, Q_c, Q_r, Q_{lr}, T_{ai}, T_{ac}, T_{af})^{-1}$$

and $W$ and $V$ are $5 \times 5$ and $5 \times 8$ matrices, containing the known coefficients and resistances. Equation 4.35 is a typical state-space equation, the analytical solution for which is:

$$T_{(m),t} = e^{Wt} T_{(m),0} + \int_0^t e^{W(t-\varphi)} V U(\varphi) d\varphi \tag{4.36}$$

where, $\varphi$ is an integral time variable. $T_{(m),t}$ and $T_{(m),0}$ are the temperature vectors at time $t$ and for the initial state. The computational implementation of this

analytical solution can be difficult, particularly in the choice of the period over which the integration is performed. Therefore the purely numerical, Runge-Kutta method (Press *et al.*, 1992) has been used to solve Equation 4.35. Under this approach, both $W$ and $V$ can be time-dependent, with the solution method using the current values of $W$ and $V$, and the driving variables $U$ at each time step.

The thermal network in Figure 4.8 is for a building space in the middle of a multi-storey building, the ceiling structure being the same as that of the floor. For the modelling of a space at the top of the building or on the ground floor, the equations describing the network for the ceiling and floor are modified to be of a form similar to those for a normal structural node, such as the walls'. The model can therefore be configured to represent three different structures: the first is for a hollow core ventilated slab system located in a mid-storey of the building; the second is for a system that only uses either the floor or ceiling slab for the ventilation supply; and the third is for a conventional exposed ceiling system, with three mass nodes one for each of the wall, ceiling and floor elements.

The simulation program of the thermal network model has been written in two parts, the preprocessor and the simulator. The preprocessor reads the input files that contain data for the building structure, time invariant parameters, and weather information. The preprocessor then produces a disturbance file containing the value of the $U$ vector for the simulation period, and a file for the time invariant capacitances, resistances and other parameters. The simulator runs the simulation according to the preprocessed information and input operation strategy (which can allow for a variable ventilation rate). The simulator calculates first the variable resistances and constitutes the matrices which are then be solved by the Runge-Kutta method.

The output from the model includes the temperature prediction for the mass nodes, surface temperature, room temperature and slab air temperatures at each time step. The Fanger comfort model (Fanger, 1970) has also been integrated into the building simulation, so that the comfort level can be evaluated from the temperature conditions in the room.

### Model Initialization

Generally, if a uniform temperature is taken as the initial condition for all the mass elements of the zone, then executing the model for four days of identical

weather data has been shown to be sufficient to eliminate the effects of the initial condition, the difference in any temperature on subsequent days being less than 0.5 °C. Only a marginal improvement is gained from extending the initialization period. Similarly, any improvement in accuracy due to the numerical integration period has been shown to be insignificant for integration times shorter than 20 minutes.

## 4.3 Plant Model

For the plant investigated in this research (Figure 3.1), models are required for the fan, the heat recovery device, cooling coil, chiller and the electric duct heater. The dynamic response of the plant is not required and therefore the system components have been simulated using established steady state models. For the fan, chiller and electric heater, only a model of power consumption is required, whereas the effect on the supply air temperature must be modelled for the heat recovery device and cooling coil.

### 4.3.1 Fan Model

A variable-speed fan has been selected in this study. For variable speed control, the fan power consumption can be assumed to obey fan laws with a cube relationship between the fan power and flow rate (White, 1994):

$$P_{fan} = P_{fan,des} \left(\frac{V_{air}}{V_{air,des}}\right)^3 \tag{4.37}$$

where $P_{fan}$ and $V_{air}$ are the actual fan power and air volume flow rate. $P_{fan,des}$ and $V_{air,des}$ are design fan power and design air volume flow rate. At very low fan speeds and flow rates, the fan power no longer obeys this relationship as a result of a degradation in fan motor efficiency. However, the fan is assumed to be OFF for a fan part load (volume flow) ratio below 0.2. The design volume flow rate and design fan power must be matched to represent a fan that can overcome the resistance of the supply ductwork and ventilated slab, whilst providing the required volume flow rate.

In this research, a perfect control of fan flow rate and hence the cubic relationship between the fan power and flow rate is assumed. For any fan installed in a plant, the fan power coefficients can be estimated from manufacturers data.

### 4.3.2 Heat Recovery Device

A regenerative heat recovery device (HRD) is commonly used in ventilated slab systems. A typical heat recovery device (HRD) in a ventilated slab system is constructed with two cell packs and uses a damper to control air route through the cells (Figure 4.9).

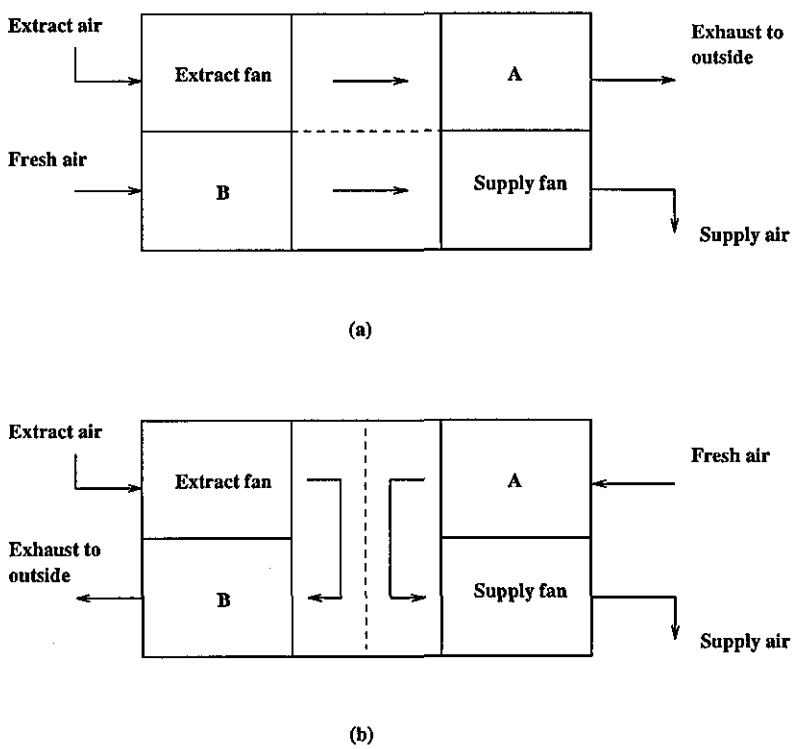


**Figure 4.9, Operating Diagram of Regenerative Recovery Device**

When the heat recovery device in operation, one cell pack (for instance, cell A in Figure 4.9a) is recharged for 30 seconds with the warm exhaust air in the winter or the cool exhaust air in the summer, during which time the fresh air is allowed to discharge the other cell pack (cell B in Figure 4.9a) to be heated or cooled. The cycle is repeated, the air route varying between Figure 4.9a and Figure 4.9b,

unless the operation strategy decides that the HRD should be OFF, where the extract air passes directly to the outside, and the fresh air passes directly to the cooling or heating components. The dampers can also be adjusted to provide full recirculation of the extract air.

The dynamic characteristics of the HRD can be neglected when compared with the dynamic response of the building. The HRD is simulated in steady state by means of its overall effectiveness. The average effectiveness of the HRD is 87.5% according to the manufacturers data. The air temperature leaving the HRD ($T_{sup}$), is given by:

$$T_{sup} = T_{fresh} - 87.5\%(T_{fresh} - T_{room,ex}) \tag{4.38}$$

### 4.3.3 Chiller Model and Electric Duct Heater Model

The performance of the chiller is closely correlated to the chilled water leaving temperature, ambient air temperature and the chiller part load ratio ($PLR$), (Braun, 1988; Braun *et al.*, 1989a). The chiller performance can therefore be modelled by a steady state curve fit of the manufacturers data, $COP = f((T_{amb} - T_{chw}), PLR)$. The chiller power consumption is then calculated from the $COP$ and the load requirement. Typical chiller performance curves are given in Section 6.1.7 together with the effect of the various part load performances on the operation of the optimum controller.

The electric duct heater has been assumed to be operated under perfect control with the limit of its capacity and 90% efficiency.

### 4.3.4 Cooling Coil Model

The output of the cooling coil has been simulated using a standard number of transfer units and effectiveness model. Since the moisture is not modelled in this research, a sensible heat exchanger model is used for the cooling coil. For a typical cooling coil with cross flow unmixed streams, the effectiveness, $\epsilon$, can be calculated by (Holman, 1986),

$$\epsilon = 1 - \exp(\frac{e^{-NTUC\eta} - 1}{C\eta}) \tag{4.39}$$

$$\eta = NTU^{-0.22} \tag{4.40}$$

where $NTU$ is the number of transfer units, $NTU = \frac{UA}{C_{min}}$. $C$ is the fluid capacity rate ratio, $C = \frac{C_{min}}{C_{max}}$. $C_{min}$ is the minimum capacity rate and $C_{max}$ is the maximum capacity rate and $UA$ is the overall heat transfer coefficient for the heat exchanger. For other types of cooling coils, such as parallel flow, counterflow, and cross flow with mixed streams, the effectiveness $\epsilon$ can also be calculated (Holman, 1986).

The heat transfer rate, $q$, across the streams can be calculated from the effectiveness $\epsilon$ and the inlet temperatures of the two streams ($T_{max}$ and $T_{min}$ are the maximum and minimum values of the two inlet temperatures),

$$q = \epsilon C_{min}(T_{max} - T_{min}) \tag{4.41}$$

The outlet temperatures of the two streams leaving the heat exchanger can then be derived from the heat transfer rate $q$, and the inlet temperatures.

Perfect control of the coil output air temperature has been assumed up to a maximum output, as dictated by the limit of the coil's effectiveness. The size of a cooling coil, $UA$, should meet the required design output air temperature, and be selected according to the design chilled water temperature and chilled water flow rate. In this research, a coil with $UA$ of 900.0 W/K has been used with a chilled water inlet temperature of 8 °C.

Since the plant model is well established, the model validation in the next section only concerns the accuracy of the building model.

## 4.4 Model Prediction and Comparison with Measured Data

In order to validate the building model's accuracy, the output from the ventilated slab and zone model have been compared with measured data obtained from an experimental test facility located at the Building Research Establishment, Garston, UK. The test room is 4.80 m × 4.00 m × 3.75 m with a door but no windows. The walls are lightweight being simply constructed and insulated with expanded

polystyrene slabs. The floor and ceiling are constructed from four commercially available hollow core concrete slabs. Only the ceiling is used as a ventilated slab system with the middle two out of the four slabs being modified to provide ventilation ducts. The ceiling also has a 35.0 mm screed covering the upper surface.

The test room is located in a large laboratory hall and therefore the test room's external environment is that of the test hall. The ventilated slab system and room is supplied with the air from a central air handling unit which maintains a preset air mass flow rate and temperature. In the tests, air from the air handling unit was supplied in equal proportions to both ceiling slabs. The air from the two slabs was then combined and delivered to the room. The lightweight construction of the test room and the absence of any windows, are advantages in evaluating the performance of the model, since the new aspects of the model are concerned with the ventilated slab system, and the effects of other structural elements and uncertain solar radiation on the room environment are reduced in these tests.

The room temperature was measured by a sensor positioned in the middle of the test room. Velocity and temperature measurements were made inside the ventilated slab cores and the slab mass temperature was measured at two depths, 70.0 mm and 210.0 mm from the upper surface (the slabs being 270.0 mm thick with 180.0 mm core diameter). The overall average mass temperature has been taken as the mean of the measurements at both depths.

The model output has been compared to two sets of test data. The first set is for normal cyclic operation, at two air velocities, 1.18 m/s and 3.75 m/s. The second set is for a step change in air flow temperature supplied to the slab at an air velocity of 1.05 m/s. These velocities correspond to Reynolds numbers which are within the range for which Equation 4.7 for duct heat transfer is valid. During comparisons of the model with measured performance data, the model was initialized using the measured data values.

In order to quantify the differences between the predicted results and the measured data, three standard error functions have been adopted, the maximum absolute error (MAXAE), the maximum percentage error (MAXPE), and the root mean square error (RMSE). The maximum absolute error between the predicted and measured data is useful in a comparison with the accuracy that could be expected from industrial standard sensors. The maximum error expressed as a percentage of the measured values indicates the relative accuracy of the model (note that

the datum for percentage calculation has been taken as 0.0 °C rather than 0.0 $K$). The root mean square error indicates the average accuracy over the whole simulation time period, although this error is sensitive to extreme errors.

### 4.4.1 Model Accuracy for Cyclic Operation

The cyclic tests emulate normal daily operation of the ventilated slab system. During these tests, the room heat gains were imitated by a convector heater of approximately 1.0 kW output. Both the heater and ventilation air supply were in operation between 8:00 am and 7:00 pm. During other time periods, there was no ventilation and no room heat gain.

Figure 4.10 shows the measured temperatures for an air velocity of 1.18 m/s in the slab cores. The *hall* temperature is the test room's external air temperature and the *supply* temperature is that of the air entering the ventilated slab. Figure 4.11 illustrates the same variables but for a supply air velocity of 3.75 m/s in the slab cores.

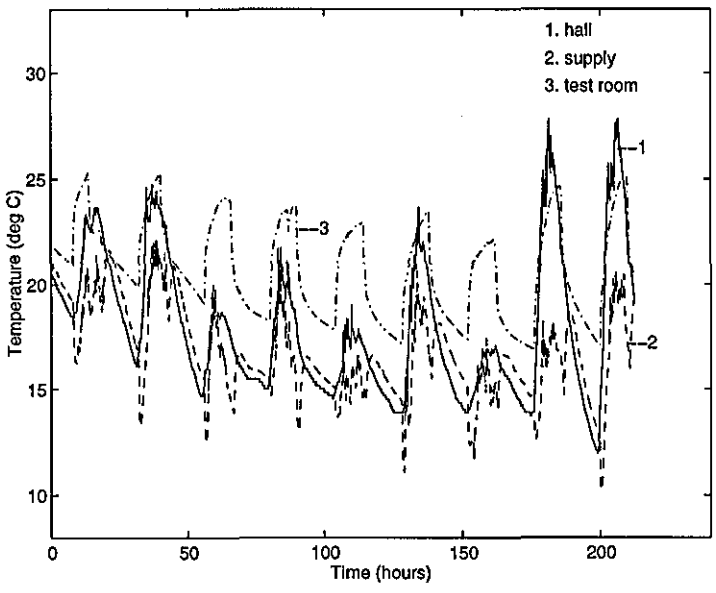


**Figure 4.10, Test Measurements (1.18 m/s velocity)**

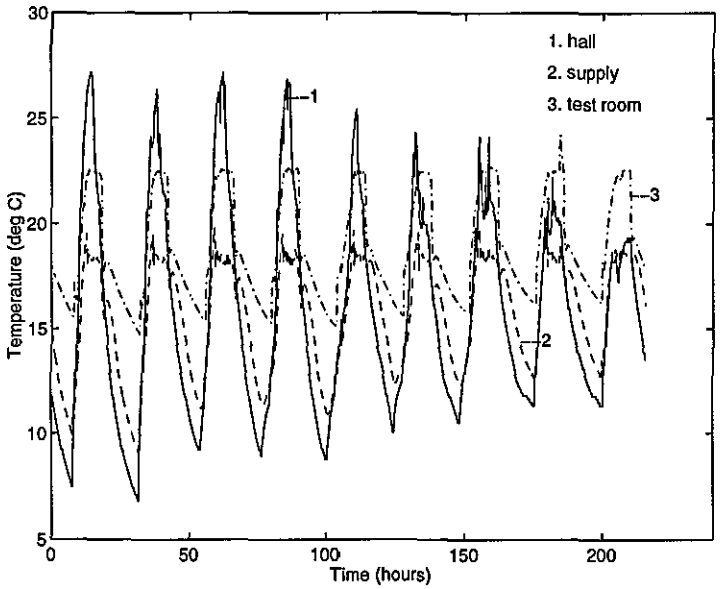


**Figure 4.11, Test Measurements (3.75 m/s velocity)**

Figure 4.12 compares the model output with the measured data for an air velocity of 1.18 m/s. Similarly, Figure 4.13 shows the simulated and measured data for an air velocity of 3.75 m/s in the air cores. The predicted and measured results are in phase but an error in peak amplitude of approximately 1.0 °C in the room air temperature is apparent during the period of heat gain and ventilation. This error can be partly attributed to the uncertainty in the output of the convector heater during this test period. For both tests, the mass temperatures of the ceiling slabs suggest that the simulated model is more responsive than the test slab. Since the specific thermal capacity and density of the concrete have been measured, the faster response of the model can be attributed to uncertainties in the calculation of the thermal resistances and the choice of effective thermal storage volume. A more accurate approach to identifying these parameters can form part of any future research.

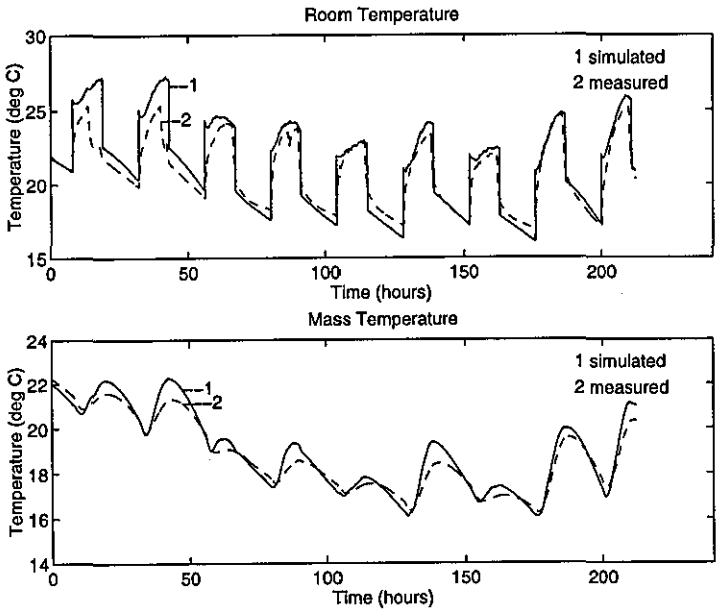


**Figure 4.12, Measured and Simulated Performance (1.18 m/s velocity)**

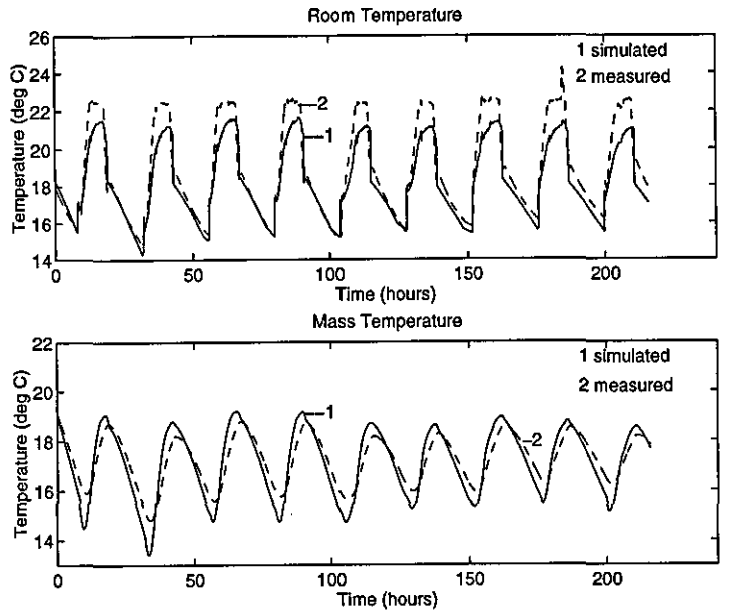


**Figure 4.13, Measured and Simulated Performance (3.75 m/s velocity)**

Table 4.1, gives the errors between the model output and measured data for the zone air temperature $T_{az}$, and the average slab mass temperature $\bar{T}_m$. The maximum errors (MAXAE, MAXPE) in zone temperature occur during the highly transient, but brief, periods at the beginning and end of plant operation. However, a maximum root mean square error RMSE, of 1.0 °C for the zone air tempera-

ture and of 0.5 °C for the slab average mass temperature can be considered to be acceptable.

| | 1.18 m/s | | 3.75 m/s | |
|---|---|---|---|---|
| Error | $T_{az}$ | $\bar{T}_m$ | $T_{az}$ | $\bar{T}_m$ |
| MAXAE | 4.2 °C | 0.7 °C | 2.3 °C | 0.9 °C |
| MAXPE | 24.0 % | 3.6 % | 12.0 % | 5.0 % |
| RMSE | 0.9 °C | 0.4 °C | 1.0 °C | 0.5 °C |

**Table 4.1, Model Accuracy for Cyclic Operation**

### 4.4.2 Model Accuracy for Step Input Operation

The step input test emulates a winter operation of the system where some time prior to the start of occupancy, a step increase is made to the air temperature supplied to the ventilated slab. In this test, the initial supply temperature was set to 12.7 °C. At 2:25 pm the supply air temperature setpoint was increased to 40.0 °C. The air velocity in the slab cores was maintained at approximately 1.05 m/s throughout the test. Figure 4.14, illustrates the measured performance data, in which *supply* is the temperature of the air entering the ventilated slab, *leaving* is the air temperature leaving the slab and entering the zone, and finally *mass* is the average mass temperature of the slab. Closer inspection of the supply air temperature, suggests that the noise of the supply air temperature is due to the operation of the heating coil control system. The effect of the slab mass on damping the oscillations is apparent from the air temperature leaving the slab.

The zone and hall temperatures were not measured in this test. Therefore the sol-air temperature for the simulation was assumed to be a constant 20.0 °C from 8:00 am to 7:00 pm (working hours), and 12.0 °C during the other periods. This assumption should not invalidate the comparison of the model output with measured data, since the dominant effects are clearly due to the high air temperature supplied to the slab.

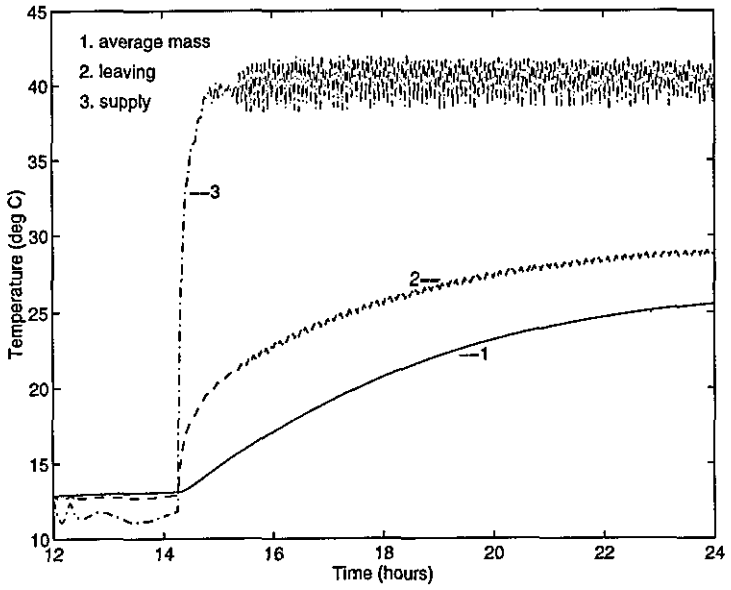


**Figure 4.14, Step Test Measurements**

In this test, the slab air temperatures were measured by six sensors located along the supply air path, the sensors being located at the beginning and end of each straight section of the core. Figure 4.15 compares the simulated and measured slab air temperatures at the end of the first straight section (*sensor2*) and at the beginning of the second straight section (which is immediately after the first corner) (*sensor3*). The close agreement between the measured and simulated temperatures for *sensor2* indicates that Equation 4.8 for heat transfer in straight ducts can be applied to the straight sections of core. Similarly, although the simulated temperature is slightly lower than the measured temperature, the results for *sensor3* (located after the first bend), suggests that the model for bend heat transfer is of acceptable accuracy.

Figure 4.16, gives a comparison between the measured and modelled air temperature leaving the slab, whereas Figure 4.17 compares the slab average mass temperatures. The maximum error in air temperature leaving the slab is 1.1 °C with a root mean square error of 0.6 °C over the test period (Table 4.2). The maximum error in average mass temperature is only 0.3 °C with a root mean square error of 0.2 °C over the test period. The model is therefore considered to be of acceptable accuracy.

| Error | $T_{al}$ | $\bar{T}_m$ |
|---|---|---|
| MAXAE | 1.1 °C | 0.3 °C |
| MAXPE | 4.8 % | 2.5 % |
| RMSE | 0.6 °C | 0.2 °C |

**Table 4.2, Model Accuracy for Step Input Operation**

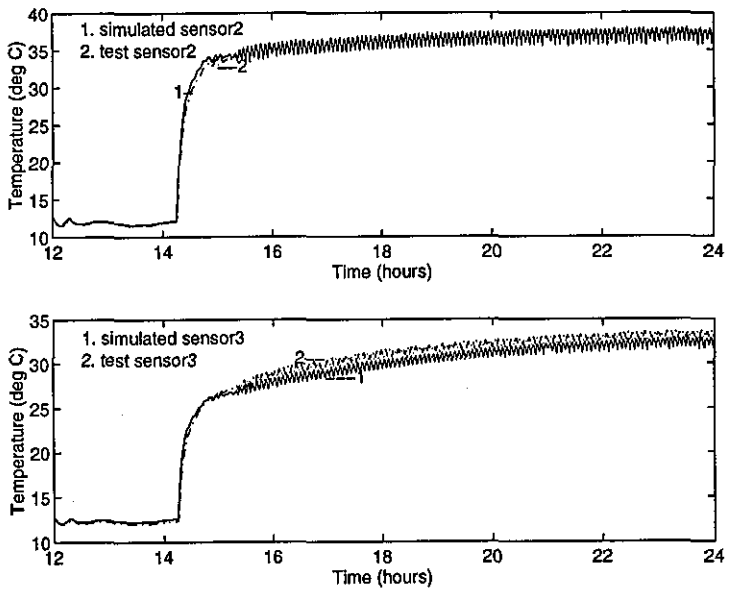


**Figure 4.15, Step Test Measured and Simulated Air Temperatures**

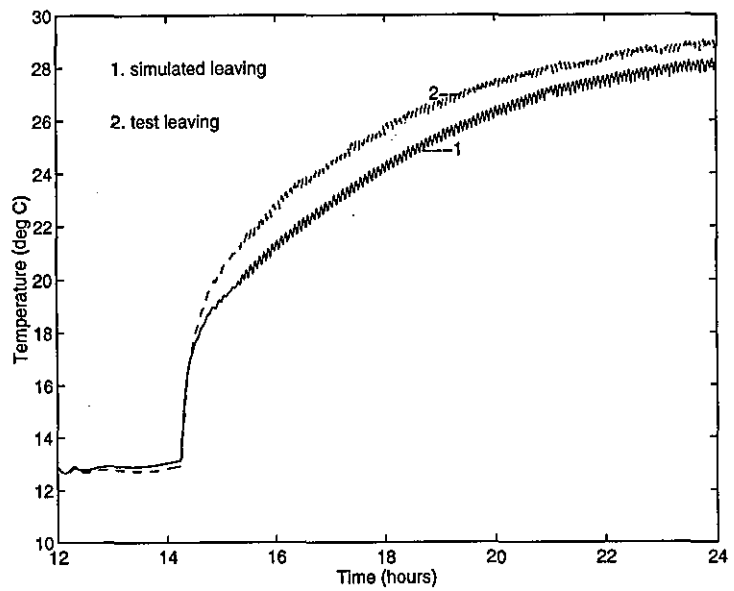


**Figure 4.16, Step Test Measured and Simulated Air Leaving Temperature**

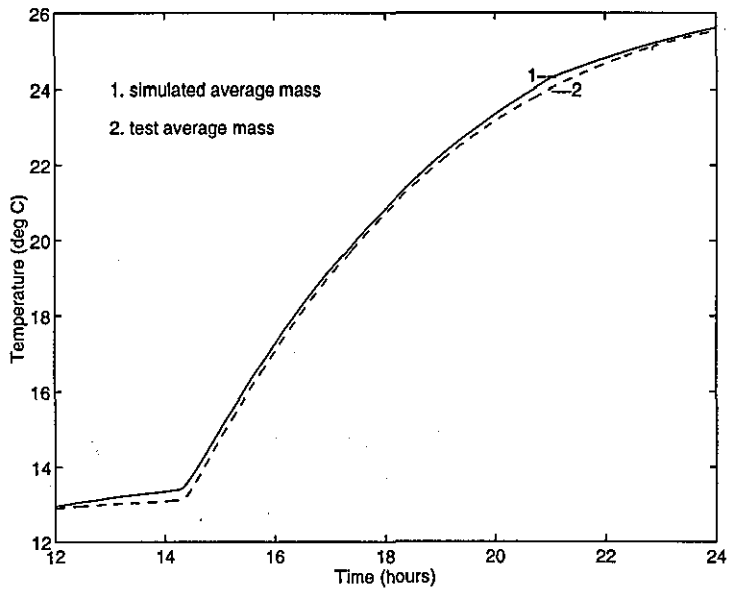


**Figure 4.17, Step Test Measured and Simulated Mass Temperature**

Section 4.4 has compared the simulated and measured performance of the ventilated slab system, by visual and statistical analysis of the errors. If the modelling errors are less than the errors in the measurement alone, then the model is deemed to pass the validation based on experimental test data (Lomas, 1991). Although the measurement errors are not available in these tests, the comparison of the simulation results with the measurements suggests that the accuracy of the model is acceptable.

## 4.5 The Robustness of the Building Model

An understanding of the robustness of the model is important if the model is to be used with confidence. The model's robustness can be assessed by the sensitivity of the model predictions to uncertainties in the input data and parameters. The robustness of the model can also be demonstrated through its consistency in producing viable results for a range of building types and control strategies.

### 4.5.1 Model Sensitivity Analysis

Lomas and Eppel (1992) suggested three sensitivity analysis techniques for validation of building thermal simulation models: Differential Sensitivity Analysis (DSA), Monte Carlo Analysis (MCA) and Stochastic Sensitivity Analysis (SSA). Since the DSA is a simple, powerful and widely used method, and can provide individual sensitivity to each uncertain input, it has been used here to investigate the building model's sensitivity. In the DSA method, each input is perturbed within its uncertainty band during each simulation, whilst keeping other inputs unchanged. The individual sensitivity of an output to the input is the difference between the perturbed and base simulation result. The total sensitivity of the output to all the uncertain inputs is estimated by the quadrature sum of the individual sensitivities. In this section, the differences in the base and perturbed results are referred to as "errors", the base case being assumed to be correct (from Section 4.4.1 and 4.4.2).

The sensitivity analysis described here has been conducted to further justify the model validation described in Section 4.4. The most uncertain measurement of input variables was for the air velocity in the cores, and hence the model's sensitivity to this has been evaluated. In terms of the parameters of the model, the sensitivity to the coefficient for increased heat transfer around the core bends has been evaluated, as has the model's sensitivity to the properties of the construction materials.

#### Sensitivity to Slab Air Flow Rate

Since ventilation air is used to charge the thermal storage in the ventilated slab system, the air flow rate is an important input variable. A significant amount of noise was apparent in the air velocity measurement during the cyclic test in supply air temperature (Section 4.4.1), and therefore these measurements have been used to assess the model sensitivity to the core air velocity.

The mean air velocity during the cyclic test was 3.75 m/s with a standard deviation of 0.61 m/s. If it is assumed that the measurement noise is normally distributed, the velocity can be assumed to be in the range of 2.18 m/s to 5.32 m/s with 99% confidence. Perturbing the air velocity from the mean of 3.75 m/s to 5.32 m/s, a 42% change, produced only a 0.1 °C mean error in the slab mass temperature,

and 0.4 °C in the zone air temperature. A similar sensitivity was apparent when the velocity was perturbed from 3.75 m/s to 2.18 m/s.

It can be concluded that the model is relatively insensitive to errors in the air velocity. It is conceivable that the model would be more sensitive to the air velocity during a step increase in input temperature (Section 4.4.2). However, the cyclic test used here to evaluate the model's sensitivity is more representative of normal operation.

**Sensitivity of the Slab Air Heat Transfer Coefficient**

Since the heat transfer inside the ventilated slab is the most critical process for the performance of the ventilated slab system, the sensitivity of the model to the heat transfer coefficient has been investigated.

The air temperature along the slab cores was measured during the step test in the supply air temperature (Section 4.4.2). The relationship between the steady state heat transfer along a straight section of duct and around a core bend, can be represented by,

$$\frac{K_c A_c}{K_s A_s} = \frac{\ln \frac{T_2 - T_m}{T_3 - T_m}}{\ln \frac{T_1 - T_m}{T_2 - T_m}} \tag{4.42}$$

where, $K_s$ and $K_c$ are the overall heat transfer coefficients for the straight duct and the corner. $A_s$ and $A_c$ are heat transfer areas for the two locations. $T_m$ is the mass temperature. $T_1$, $T_2$ and $T_3$ are the slab air temperatures at three different locations. $T_1$ is measured at the beginning (entry) of the straight duct, $T_2$ at the end of the straight duct (which is also the entry to the corner), and $T_3$ is at the end of the corner.

An analysis of the step test data indicates that the ratio of temperature differences $\Delta T_{ln} = \frac{\ln \frac{T_2 - T_m}{T_3 - T_m}}{\ln \frac{T_1 - T_m}{T_2 - T_m}}$, is within the range 1.5 to 2.0. By substituting this range into Equation 4.42, the ratio of the corner to the straight duct surface heat transfer coefficient $\xi = \frac{h_c}{h_s}$ is in the range 20 to 50 (the conductances $K$, include the conductance of the concrete slab and surface coefficient; $h_s$ is given by Equation 4.8).

Note that this calculation is derived from a step test on a commercially available ventilated slab system with an air velocity of 1.05 m/s. This relationship however,

is unlikely to change significantly with fluid velocity (Section 4.2.1). A comparison between the simulated and measured performance during the three different test conditions, indicated that the correction factor $\xi = 50$ for the corner heat transfer provides the smallest errors. The sensitivity of this correction factor has been further investigated, by perturbing the factor from 50 to 20.

During the normal cyclic tests (Section 4.4.1), it was found that the system is not sensitive to $\xi$. A lower corner heat transfer resulted in a 0.2 °C root mean square error for the slab mass temperature. This was due to less cooling being transferred from the supply ventilation air to the mass storage. Since the temperature difference between the slab air and the mass is relatively small during the cyclic tests, the rate of heat transfer is low such that the model is not sensitive to the corner heat transfer coefficient.

However, the higher air to slab temperature difference results in a greater sensitivity during the step test operation (Section 4.4.2). The lower value 20 for $\xi$ reduces the heat absorbed by the mass storage around the corners, resulting in a lower slab mass temperature $\bar{T}_m$ and higher air temperature leaving the slab $T_{al}$. The sensitivity is in the order of 1.9 °C (root mean square error) for both the average slab mass and the air leaving temperatures (Table 4.3). The mean error (ME) is introduced here to indicate the effect of the reduced heat transfer resulting from the lower corner coefficient. The negative mean error of -1.3 °C indicates the reduced slab mass temperature. The lower corner heat transfer ($\xi = 20$), results in a higher air leaving temperature during the early transient stages of the step test (Figure 4.18), since less heat is transferred from the air to the slab. However, the subsequently lower slab mass temperature leads to a higher heat transfer rate between the air and slab towards the steady state, which results in a negative mean error in the air leaving temperature of -0.4 °C.

| Error | $T_{al}$ | $\bar{T}_m$ |
|---|---|---|
| MAXAE | 1.5 °C | 2.7 °C |
| MAXPE | 5.7 % | 10.4 % |
| RMSE | 1.9 °C | 1.9 °C |
| ME | -0.4 °C | -1.3 °C |

**Table 4.3, Model Sensitivity to Corner Heat Transfer Coefficient for Step Input Operation**

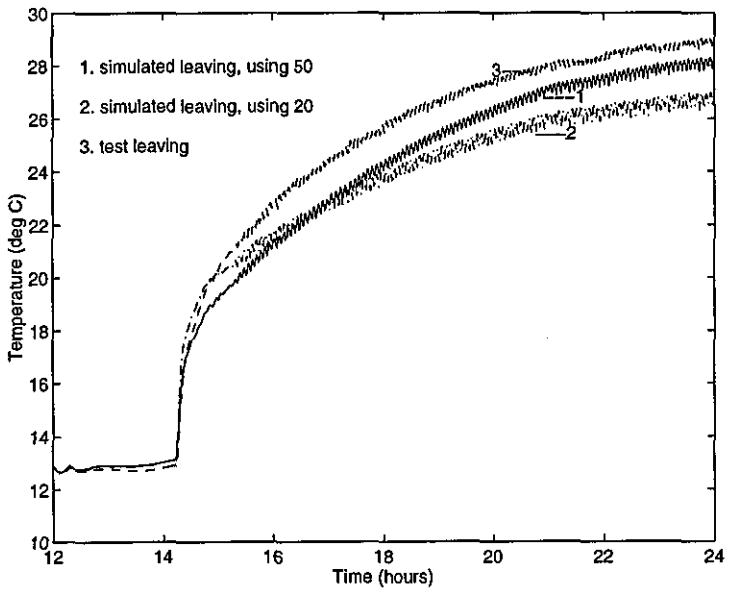


**Figure 4.18, The Influence of Corner Heat Transfer Coefficient on Simulated Air Leaving Temperature**

A comparison of the model results with the measured test data suggests that a corner heat transfer correction factor of $\xi = 50$ gives lower errors than for $\xi = 20$. Increasing $\xi$ above 50 also leads to an increase in modelling error. It can be concluded that during normal cyclic operation, the model is insensitive to the correction factor, although the higher slab air temperature and heat transfer rate during winter operation, leads to an increase in model sensitivity.

### Sensitivity of Input Parameters

The sensitivity of the model to uncertain model parameters, has been evaluated for properties of the building materials, the convective heat transfer coefficients, building dimensions, and infiltration rate. The materials used in the test cell for model validation, include polystyrene, screed and concrete for the ventilated slabs (Section 4.4). The uncertainties in these materials have been obtained from Clarke *et al.* (1990), or by estimation (Table 4.4).

The test cell has been assumed to have been constructed to a tolerance of $\pm$ 10.0 mm in all dimensions. A 50% uncertainty has been assumed for the internal and external surface heat transfer coefficients, surface emissivities, and infiltration rate.

| Material | Property | Minimum | Mean | Maximum | Uncertainty |
|---|---|---|---|---|---|
| Polystyrene | Density (kg/m$^3$) | 11 | 22.5 | 34 | 50% |
| | Capacity (J/kg K) | 1214 | 1342 | 1470 | 9.5% |
| | Conductivity (W/m K) | 0.025 | 0.0345 | 0.044 | 27.5% |
| Screed | Density (kg/m$^3$) | 900 | 1200 | 1500 | 25% |
| | Capacity (J/kg K) | 800 | 820 | 840 | 2.4% |
| | Conductivity (W/m K) | 0.34 | 0.41 | 0.48 | 17% |
| Concrete | Density (kg/m$^3$) | 2211 | 2432 | 2653 | 9% |
| | Capacity (J/kg K) | 906.3 | 985.1 | 1063.9 | 8% |
| | Conductivity (W/m K) | 1.65 | 1.9 | 2.15 | 13% |

**Table 4.4, Uncertainties of Material Properties**

The sensitivity of the model to the input parameters was evaluated by perturbing the parameters one at a time. The maximum absolute error in room temperature due to the uncertainty of the material properties was found to be less than 0.2 °C, and the maximum absolute error in mass temperature less than 0.1 °C. The mean errors in both temperatures were less than 0.1 °C. A comparison of the individual sensitivities indicates that it is the hollow core concrete properties that most affect the system response, since these are what most affect the mass thermal storage.

The model is not sensitive to the infiltration rate and heat transfer coefficients. A 50% increase in the infiltration rate from 0.5 ac/h resulted in a maximum error of 0.3 °C in room air temperature. Among the internal convective coefficients, the ceiling coefficient is the most influential parameter, with a 50% increase in the ceiling coefficient (from 4.3 W/m$^2$K) reducing the room and mass temperatures by a maximum of 0.1 °C.

The total sensitivity can be calculated either from the quadrature sum of the individual sensitivities, or from the sensitivity to a simultaneous variation in all of the uncertain parameters. A comparison of the results from the two approaches indicates a similar range of the total sensitivity, with a root mean square error of 0.2 °C in the slab mass temperature and 0.8 °C in the room air temperature. The model therefore responds almost linearly and superposably to the limited range of uncertainties in the input parameters.

Although a complete investigation of the model's sensitivity has been limited by the unavailability of detailed information about the uncertainty in all the input data and parameters (for instance, convector heat output in the room), the indi-

vidual sensitivity of the major input data and parameters has been investigated. The results indicate that the model is robust, since the model can correctly predict the trend of the system response whilst being tolerant to errors in the input data.

### 4.5.2 The Capability of the Building Model

The robustness of the building model can also be demonstrated through its consistent performance in modelling the system response for a variety of building types and control strategies, including night cooling and switchflow operation. In order to increase confidence in the building model, the typical ventilated slab building selected for the optimal control study in Chapter 6 (Table 6.1), has been used here to illustrate the ventilated slab system performance.

#### Building System

As described in Section 4.2.4, the building model can be applied to three forms of building spaces. The form of building examined here is for a typical mid-storey office space with ventilated ceiling and floor slabs. In order to illustrate the model performance, the system response of this building has been compared with that for a more conventional building having the ceiling slabs exposed, the conventional system being modelled by the established zone model.

Figure 4.19 illustrates the room thermal conditions for the ventilated slab building and the conventional exposed ceiling system for a day's operation on the $30^{th}$ June 1994 (the weather data are for Garston, UK and are described in Chapter 6). The two systems, having the same building construction, were ventilated constantly with 4.2 ac/h supplied to the room. The daily average ambient temperature was 16.6 °C with a peak temperature of 22.4 °C. The ceiling slab temperature was much reduced in the ventilated slab building, the maximum reduction being 1.4 °C just before the occupancy started (7:00 am). After 7:00 am, the mass temperature difference between the two systems became smaller due to discharge of the mass storage in the ventilated slab building. The daily mean reduction in mass temperature was 0.7 °C. The increase in zone air temperature between 8:00 am and 4:00 pm is due to the casual gains from occupancy. The room temperature was 1.5 °C lower in the ventilated slab building during the occupancy period, and the daily mean room temperature was reduced by 0.9 °C. The performance

comparison illustrated in Figure 4.19 reflects the enhanced heat transfer occurring in the slab cores, which effectively regulates the slab mass storage.

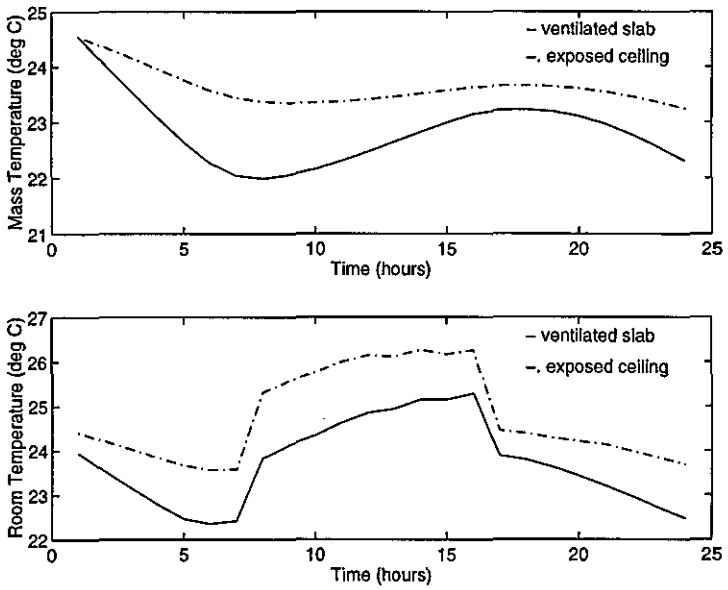


**Figure 4.19 Comparative Performance of Ventilated Slab with Conventional Exposed Ceiling System**

### Control Strategy

Since the building and plant model has been used as the basis for predicting the system performance in the optimum controller, robustness of the model is essential in its ability to predict the building performance for various control strategies.

The system performance under different control strategies is examined here by the room's thermal response to the night precooling period, ventilation rate and switchflow operation. Five test cases have been devised:

- case 1: a ventilation rate of 4.2 ac/h to the zone, supplied constantly throughout the day (all 24 hours);
- case 2: a ventilation rate of 4.2 ac/h during the occupancy period (8:00 am to 4:00 pm), and during the night precooling period (5:00 am to 7:00 am), the fan being stopped during all other hours;
- case 3: a ventilation rate of 4.2 ac/h during occupancy hours (8:00 am to

4:00 pm), increasing the ventilation to 6.8 ac/h during the night precooling period (1:00 am to 7:00 am);

- case 4: a ventilation rate of 4.2 ac/h during the occupancy and off-occupancy periods, using switchflow operation (in effect, the ventilation air only passes through one of the slab cores);
- case 5: a ventilation rate of 4.2 ac/h during occupancy (8:00 am to 4:00 pm) with the switchflow unit in operation, whilst at night (1:00 am to 7:00 am), a 4.2 ac/h ventilation rate with normal three core air supply to charge the mass storage.

The control strategies in the first three cases tend to investigate the system response to different ventilation rates and ventilation precooling periods, whereas the last two cases are concerned with the influence of the switchflow operation. The relative performance of each control strategy has been examined for a day's operation on the 30$^{th}$ June 1994. Figure 4.20 displays the daily variations of slab mass and room temperatures under the first three strategies. The reduction in the precooling period from the entire night (case 1) to three hours just before occupancy (case 2) has resulted in a maximum difference in mass temperature of 1.4 °C, the difference becoming smaller as the thermal storage is discharged during the occupancy. The daily mean room temperature has also been increased by 0.9 °C due to fewer hours of precooling.

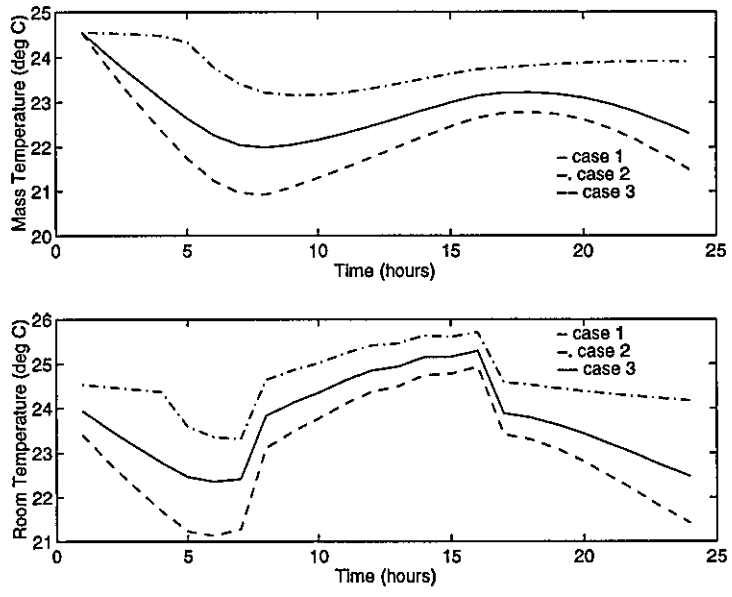


**Figure 4.20, The Influence of Ventilation on Room Thermal Conditions**

The effect of a higher ventilation rate during charging of the thermal store (case 3) is also illustrated in Figure 4.20. The mass temperature was 1.1 °C lower than for case 1 just before the occupancy, with the daily mean mass and room temperatures being lowered by 0.7 °C from the higher night precooling ventilation rate.

Figure 4.21 compares the switchflow operation (the ventilation air passing through one slab core), with normal operation (the ventilation air passing through three cores). Using one core (case 4) during night operation increases the mass temperature by a maximum of 1.2 °C just before occupancy, in comparison to using three cores at night (case 1 and 5). The room temperature is lower at night under the single core operation, due to less coupling between the cool ambient air and the mass storage and the lower temperature air supplied to the room. However, for the single core operation (case 4), the room air temperature increases rapidly as the thermal gains increase around the start of occupancy (8:00 am). This is due to the higher mass temperature providing insufficient cooling of the air supplied to the room. Switching to a single core operation after the start of occupancy (case 5) results in a subsequently higher mass temperature and slower rate of increase in room temperature. The slower increase in room air temperature was due to the ambient air temperature being lower than the mass temperature (the ambient being between 18 °C to 22 °C). The higher mass temperature was due to the lower coupling between the ventilation air and the slab. In all three modes of operation (cases 1, 4 and 5), the room air temperatures were similar during the late afternoon, when the difference in temperature between the ambient air supplied to the slab and the slab mass temperature was small, and hence the slab had little effect on the temperature of the air supplied to the room. Whereas if the ambient air temperature is much higher than the mass temperature, a much higher room temperature would result from the one core operation due to insufficient discharge of the mass storage.

The influence of the one core operation on room thermal conditions depends on the specific ambient environment. The results indicate that the model can correctly predict the system performance under the switchflow operation. Since the switchflow unit has been devised to provide a fast supply route to meet the room thermal loads, it can be used in the implementation of the optimal predictive controller (Chapter 8).

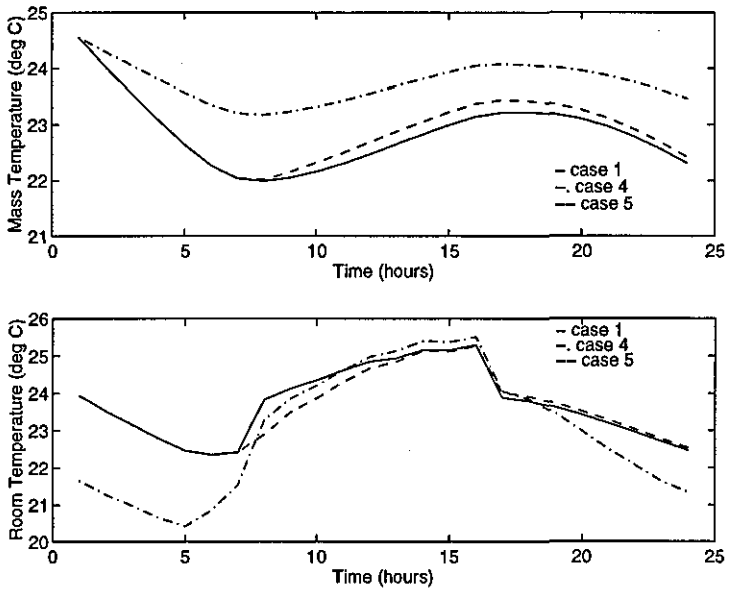


**Figure 4.21, The Influence of Switchflow Operation on Room Thermal Conditions**

The building model has demonstrated its robustness in modelling a variety of building designs and control strategies. For the optimum control of ventilated slab systems in this research, it meets the model's requirements and functionality defined in Chapter 3.

## 4.6 Conclusion

The development of building and plant models in this chapter includes both the background theory and model validation. Since the plant models are based on well established steady state models, the validation study is only for the building model.

The building model is developed by integrating a new model of the hollow core ventilated slab with a lumped parameter thermal network zone model. The slab model can simulate the heat exchange between the ventilation air and the slab mass. The zone model can allow for the assessment of the effects of all the major heat disturbances on the room thermal conditions. The integrated slab and zone model parameters can be easily derived, which enables the system control

optimization and the investigation of different design solutions.

The building model validation has been conducted by comparing the results from the model prediction with measured data for two sets of test, the first representing normal operation cycled over several days, and the second for a step input in the supply air temperature to the slab. It was concluded that the model gave an acceptable accuracy for normal operation. The errors are generally due to the amplitude rather than a phase shift in the temperature cycle. The step input test gives an insight into the accuracy of the model for the heat exchange between the ventilation air and the slab. The root mean square error in air temperature leaving the ventilated slab was 0.6 °C, whereas the maximum error for the average temperature of the slab was 0.3 °C, both of which indicate an acceptable level of accuracy.

The robustness of the model has been assessed from an analysis of the model's sensitivity to errors in input data and parameters, and its capability in modelling a variety of control strategies and building systems. The thermal response of the ventilated slab system to different control strategies also indicates the need for careful control of thermal storage, which will be accomplished in Chapter 5 by integrating an optimization algorithm with the building and plant model. During an optimization process, robustness of the model is necessary to allow the investigation of control strategies for all likely system operating conditions.

# Chapter 5

# The Performance of Optimization Algorithms

## Introduction

This chapter examines the performance of two optimization algorithms in finding optimum control schedules for the ventilated slab system: the Complex method and Genetic Algorithm. A typical ventilated slab office building and weather data for 1994, have been used in the performance assessment. The weather data exhibit distinct seasonal variations in the ambient conditions which provides a variety of control strategies against which to evaluate the algorithms.

The details of the zone construction and the weather data together with the characteristics of the optimum control strategies are discussed in Chapter 6. An analysis of the characteristics of the optimum schedules of plant operation has led to the development of a simplified time-stage control, as described in Chapter 6. The performance of the optimization algorithms in solving the time-stage control problem is also examined in this chapter.

## 5.1 Elements of Performance Assessment

The Complex method and Genetic Algorithm have been identified in this research as the possible algorithms for the optimization required by the controller (Section 3.2). The performance of an optimization algorithm can be assessed by its ability to find an optimum solution, the computational overhead, and sensitivity to an initial guess of the solution. Good performance in each of these three criteria is important if the optimum controller is to provide a feasible optimum control strategy, within an acceptable computation time.

If an algorithm can not find a feasible optimum solution, energy cost and consumption may be excessive, and the comfort conditions in the occupied zone may be unacceptable. The optimum controller would therefore have no advantage over a conventional control strategy. Similarly, if some initial guesses of the solution, cause the algorithm to fail to find the global optimum, then the controller may not have any advantage over a conventional control strategy.

The computational overhead can be estimated by the number of trial solutions. The number of trial solutions should be kept to a minimum, since the building model is executed for each trial solution, which demands the longest computation time within the whole optimization. A high computational overhead would restrain the implementation of the optimum controller as it may not be able to provide an optimum plant operating schedule within the limited time period. Since the optimization in the controller is conducted once at the end of every day to provide an optimum control strategy for the following day, one hour has been taken as an acceptable calculation period. The approximate number of trial solutions that could be executed within one hour depends on the particular computer. Using a typical micro-computer of the type currently used as a building control system supervisor (a Pentium, running at 120 Hz), approximately 36,000 trials can be computed in one hour.

Each algorithm has several factors that can influence its performance. In order to obtain the best performance from each algorithm, these factors must be investigated and be tuned to the control optimization problem.

The performance of the optimization algorithms is investigated using three examples of control optimization: the optimization of the supply air flow rate for 24

hours, the setpoint scheduling of the supply air flow rate and temperature over 24 hours and the time-stage control. The low number of control variables of the air flow rate optimization reduces the complexity of the optimization so that the behaviour of the optimization algorithms can be easily investigated. The tuned parameters obtained from this example have then been tested in solving the setpoint scheduling control and time-stage control problems.

### 5.1.1 Factors that Control the Complex Method

The Complex method is a direct search method that can be easily implemented (Appendix A). The method has relatively few control parameters that must be tuned to a particular optimization problem.

The two principal control parameters are the reflection and expansion coefficient $\alpha$, and the number of vertices $K$ in the complex. Rao (1984), suggested an $\alpha$ equal to 1.3 to start the reflection of the complex; if the trial is not successful, $\alpha$ is reduced by half each time to obtain a new trial point until $\alpha$ is less than a prescribed small quantity (equal to $10^{-6}$ in this implementation). Rao (1984), also suggested that the number of vertices in the complex should be, $K \geq 2n + 1$ ($n$ is the number of control variables); too small a $K$ may result in the complex collapsing across a constraint boundary. Hence in the Complex method implemented here, $\alpha$=1.3 and $K = 2n + 2$ have been applied. Therefore, the large number of control variables in this control optimization problem leads to a search complex with a large number of vertices.

There are no other uncertain factors that affect the search mechanism. However, the search may be sensitive to the initial guess of the solution since this is used in the formulation of the initial complex, and therefore, the sensitivity of the search to the initial guess has been examined in this research.

### 5.1.2 Factors that Control the Genetic Algorithm

As for the Complex method, the Genetic Algorithm (GA) can also be easily applied (Section 3.2.3 and Appendix B). As one of the evolutionary search methods, the GA has a number of factors that govern the evolution process leading to the

optimum solution. The factors are listed below and can be divided into two groups, those associated with the formulation of the algorithm (the first three factors), and those control the evolutionary process (the last four factors).

1. fitness representation form and scaling;
2. constraint penalty coefficient;
3. selection algorithm;
4. string length;
5. population size;
6. probability of crossover;
7. probability of mutation.

GAs maximize a fitness function, whereas the optimum control scheduling problem requires the energy cost to be minimized. GAs are also unconstrained search methods, so that constraint violations are generally handled by penalty functions. The form of conversion from objective function to fitness function and the weight of the constraint penalty can influence the behaviour of the GA and have therefore been examined. Finally, the procedure by which fit solutions are selected for propagation to the next generation can influence the performance of the algorithm. The effect of two different selection strategies on algorithm performance has been investigated here.

The continuous control variables are represented by discrete binary strings in the GA. Too short a string length can lead to the variables having a poor precision, whereas too long a string length can allow variable values that are beyond the variables' upper bound, which can result in an increase in the number of infeasible solutions in a given population.

The probabilities of crossover and mutation influence the rate at which new genetic information is generated (and consequently the degree to which the current search direction may be disrupted). The population size influences the amount of genetic information available from which new solutions might be generated, with large populations containing more information, but taking longer to converge.

These parameters have been investigated and tuned so that the GA provides a robust performance in the control optimization. The influence of the initial guess on the search performance and the computational overhead are also examined and compared with the Complex method.

Due to the probabilistic nature of the algorithm, it is difficult to define an absolute convergence criterion. A measure of 'activity' in the mean value of problem variables in successive generations may prove to be a basis for convergence (Wright, 1996). However, in this thesis, convergence has been confirmed by monitoring the rate of cost reduction, the fitness distribution in the populations (average, maximum and minimum fitness), and by inspection of the optimum schedules of control variables and comparison with the solutions derived from the Complex method.

## 5.2 Algorithm Performance in the Scheduling of Supply Air Flow Rates

The optimization of the supply air flow rate schedule has 24 variables. The relatively low number of variables reduces the complexity of the problem, which enables a clear analysis of the algorithm behaviour. Having only 24 variables to optimize for 24 hours of operation has also allowed the investigation of the effect of mass thermal storage on the optimum plant operation (which is examined by two days operation and requires 2×24 variables, Section 6.1.1).

The nature of the optimization problem with the supply air flow rate over 24 hours as control variables, dictates that there are no discrete plant operating modes and thus the search space is continuous. Figure 5.1 illustrates an example surface in the search space. The $x$-axis is the air flow rate at 5:00 am, the $y$-axis the air flow rate at 3:00 pm, while the $z$-axis represents the total energy cost of the fan operation over the 24 hours. The air flow rates for the other 22 hours have been kept at the optimum values obtained from the GA search. In this surface, the area marked by '$*$' is the feasible region where the room thermal comfort during occupancy is satisfied, with the PPD less than 10%. The optimum feasible point for this surface is marked by 'o'. The shape of the constrained surface also depends on the values of the other flow rate variables, however, the surfaces forming the search space display the same continuous characteristic. Such smooth surfaces

with large feasible regions indicate that the optimization problem is not highly constrained and should be easy to solve.

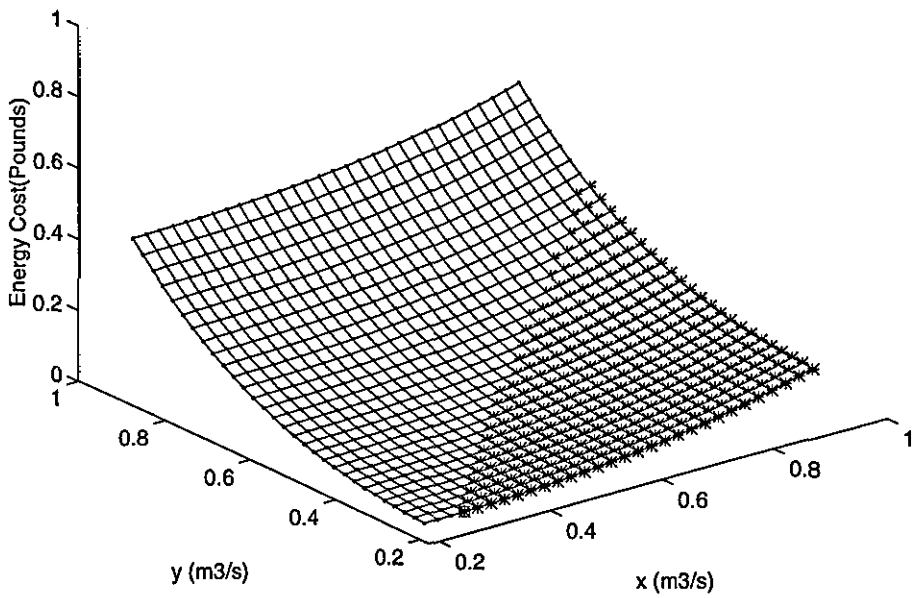


**Figure 5.1, A Surface in the Search Space for the Fan Flow Rate Scheduling Problem**

In practice, if the air flow rate is too low, the fan efficiency will be poor and therefore the fan is usually switched OFF. In this thesis, the fan is assumed to be OFF for flow rates lower than a 0.2 $PLR$ (the ratio of the fan actual flow rate to the design flow rate); the lower bound of the fan flow rate searched in the optimization algorithm is therefore 0.2×design flow rate, which is equivalent to the fan being OFF. If the fan design flow rate is 0.9 $m^3/s$, the fan flow rate ranges from 0.18 $m^3/s$ to 0.9 $m^3/s$. This eliminates the discontinuity in the fan energy cost across the flow rate of 0.2 $PLR$, thus the continuous surface illustrated in Figure 5.1.

$30^{th}$ July 1994 has been taken as an example to illustrate the performance of the Complex method and the Genetic Algorithm. On this day, the daily maximum ambient air temperature approached 29 °C (the ambient air temperature of the previous day had a maximum of 25 °C), while the night air temperature was low such that the free precooling is sufficient to relieve the daytime cooling load;

mechanical heating or cooling is not required to obtain a feasible optimum solution. The controller output is therefore an optimum schedule of fan flow rates, such that sufficient night precooling is provided to ensure occupant comfort while energy costs are minimized.

### 5.2.1 Performance of the Complex Method

The Complex method requires an initial feasible solution point about which the initial complex is generated. The result shows that a different initial point can result in a different optimum solution. For instance, if the initial air flow rate is 0.3 $m^3/s$ in all 24 hours, the minimized energy cost from the fan operation on the $30^{th}$ of July is £0.10, compared with the energy cost of £0.13 for an initial air flow rate of 0.6 $m^3/s$ in all 24 hours. However, as shown in Figure 5.2, the optimum solutions from the different initial feasible points display a similar schedule of the air flow rates over the 24 hours for the same day. The precooling ventilation is usually high, and the daytime ventilation in the region of 0.2 to 0.25 $m^3/s$ (corresponding to 2.1 to 2.64 ac/h). After the occupancy period (occupancy period 8:00 am to 4:00 pm), the fan is either OFF or operates at a low flow rate. It should be noted that the fan is assumed to be OFF when the fan part load ratio ($PLR$) is lower than 0.2 (0.18 $m^3/s$).

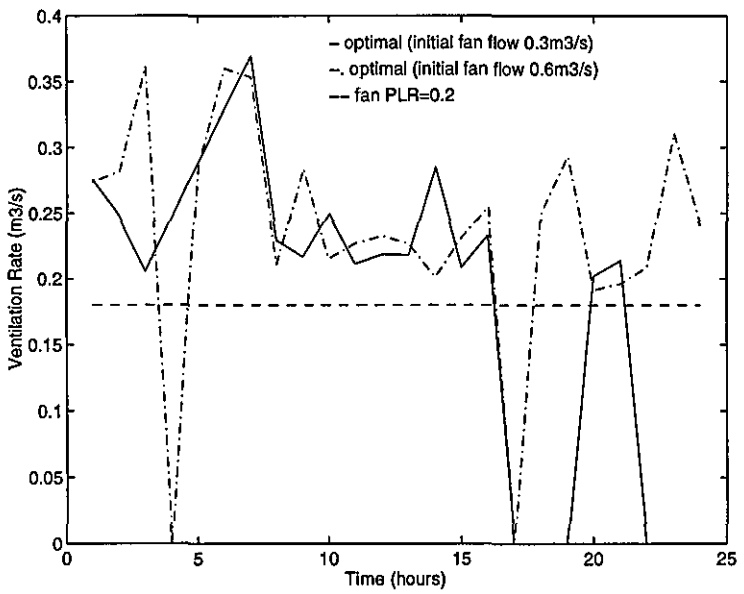


**Figure 5.2, The Influence of Initial Point on the Complex Search**

The optimum solutions show that the fan is frequently operated at a low flow rate of approximately 0.2 $m^3/s$. It can also be seen from Figure 5.2 that the fan operates in the range 0.2 to 0.3 $m^3/s$ for many hours after the occupancy period (*from 5:00 pm to 0:00 am*). It is however, expected that the fan would be OFF during this period since there is no comfort requirement, and the plant operation is not required for precooling the ventilated slab until the early hours of the next day. The optimum solutions derived from the Complex method do not therefore reflect the real character of the optimum schedule of the fan operation.

Since the gradient of the fan energy cost is so low in the region of the optimum, the Complex method has difficulty in finding the direction of the optimum, with the result that the complex collapses on a sub-optimum. The collapse of the complex is represented in Figure 5.3, in which the vertices $X_h$ are the solution points that are to be replaced with new trial points $X_r$. The trial points $X_r$ are a reflection of $X_h$ about the centroid $X_o$, of the remaining points in the complex, such that $X_r = (1 + \alpha)X_o - \alpha X_h$ (Appendix A). The objective function value associated with each point is also given in Figure 5.3.

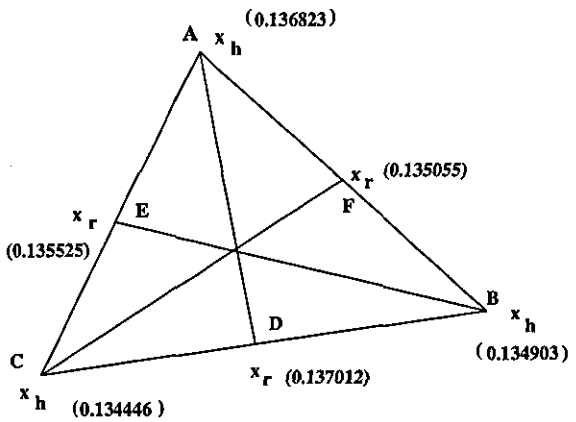


**Figure 5.3, An Example of the Complex Progress**

Suppose that the trial point to be replaced is $A$, the point with the largest objective function value in the complex. By reflection, $D$, a new search trial point $X_r$, is generated and evaluated, its objective function value being $f(X_r) = 0.137012$. Initially, $\alpha$ is set to 1.3 (Rao, 1984). Since $f(X_r) > f(X_h)$, the trial point D ($X_r$) is rejected. $\alpha$ is then halved and the reflection repeated. The reduction in $\alpha$ is repeated each time a trial point is rejected, until $\alpha \leq \epsilon$ (where $\epsilon = 10^{-6}$), whereupon a new vertex is chosen for reflection. In this instance, for vertex $A$,

$X_r$ is always such that $f(X_r) > f(X_h)$, and $A$ is therefore discarded. The same procedure is restarted with $B$ as $X_h$, the point with the second largest objective function value. The procedure continues until all the vertices have been searched. If a new favourable trial point $X_r$ can not be found, the complex can not move any further. The search is therefore, either converged if the convergence criterion is satisfied (when the complex shrinks to a sufficiently small size or the variations in objective function values associated with the vertices are sufficiently small, Appendix A), or collapses at the centroid $X_o$ with $\alpha$ reduced to a sufficiently small quantity and $X_r$ approaching $X_o$.

It can be seen from Figure 5.3, that the Complex method may lead to premature convergence if the complex can not move. As stated by Rao (1984), the Complex method is not efficient in solving problems with a large number of variables. It works very well if there is only one variable. For instance, if the air flow rate at 8:00 pm is taken as the only optimization variable, and the flow rates at the other hours are kept constant at 0.6 $m^3/s$, the 4 vertices ($K$=2n+2) quickly converge to the point with a zero flow rate, the correct solution.

In conclusion, the Complex method can find sub-optimum control schedules, but may result in premature convergence due to the high number of control variables and low objective function gradient. The search also exhibits some sensitivity to the initial guess of the solution. The number of trial solutions required to solve this problem is in the order of 2000, well within the benchmark of 36,000 trial solutions (Section 5.1).

### 5.2.2 Performance of the Genetic Algorithm

The 'Simple Genetic Algorithm' (SGA) (Goldberg, 1989), has been implemented in this research. A penalty function method (Wright, 1995) has been used to incorporate constraints into the unconstrained SGA search. The factors that influence the GA performance (Section 5.1.2) have been investigated and tuned to the control optimization problem.

### Fitness Formulation

The energy cost objective function is to be minimized, yet the SGA maximizes a fitness function. Two transformations from an objective function to a fitness function have been examined:

$$fitness = max_objective - objective_function \tag{5.1}$$

$$fitness = 1 - objective_function/worst_ever_objective \tag{5.2}$$

where the *objective_function* of each individual is penalized if the individual violates any constraint. *max_objective* is the highest objective function value (after being penalized) in the current generation, whereas *worst_ever_objective* is the highest objective function value from all generations. Equation 5.1 represents the fitness by the absolute value of the difference between an individual objective function and the worst (highest) objective function in the population. There is no fitness comparison between generations; the fitness value indicates the weight of each individual within each generation. As the evolution progresses, the highest objective function in each generation gets smaller, whereas the fitness is not necessarily lower or higher than that of the previous generation, since it is only related to the objective function values within the present generation. When the search approaches convergence, the objective function values become small and average fitness and maximum fitness of the population become close, indicating a decrease in 'activity' in the population.

Equation 5.2 uses a normalized form to calculate the fitness, which takes account of the individual objective function values throughout generations. The method in Equation 5.1 has resulted in a much better performance than Equation 5.2 for this research. Since this optimization problem has a wide solution space, the *worst_ever_objective* (found in earlier generations) can be very large. The objective function values for individuals in later generations are relatively much smaller. Equation 5.2 therefore produces high fitness values for all of the individuals in later generations and therefore the impact of 'better' solutions is lost. This results in both the average and better solutions having the same probability of being selected for reproduction, which often leads to premature convergence. Hence, Equation 5.1 has been chosen to calculate the fitness in the control optimization.

To some extent, scaling of the fitness function (Goldberg, 1989) can increase competition among the individuals of near equal fitness produced by Equation 5.2.

Scaling can also reduce the effect of extraordinary individuals dominating the search. However, scaling of the fitness function has proved to be ineffective for this problem and is therefore not used.

### Constraint Penalty Coefficient

The application of a penalty for an infeasible solution is in two parts (Wright, 1995). For each violated constraint, a normalized degree of violation is calculated first; the sum of the normalized violations is then used to penalize (increase) the objective function values. The most influential element in the process is the rate at which the penalty is applied to the objective function. The penalty is of an exponential form $y = \frac{e^{\beta x}-1}{e^{\beta}-1}$ (Figure 5.4), where $x$ is the sum of the normalized violations (1.0 indicating that all constraints are violated to their maximum degree). $y$ is the penalty, and $\beta$ the penalty coefficient that governs the rate at which the penalty is applied (Appendix B). The influence of $\beta$ on the optimization is investigated here. Figure 5.4 shows the influence of $\beta$ on the penalty function.

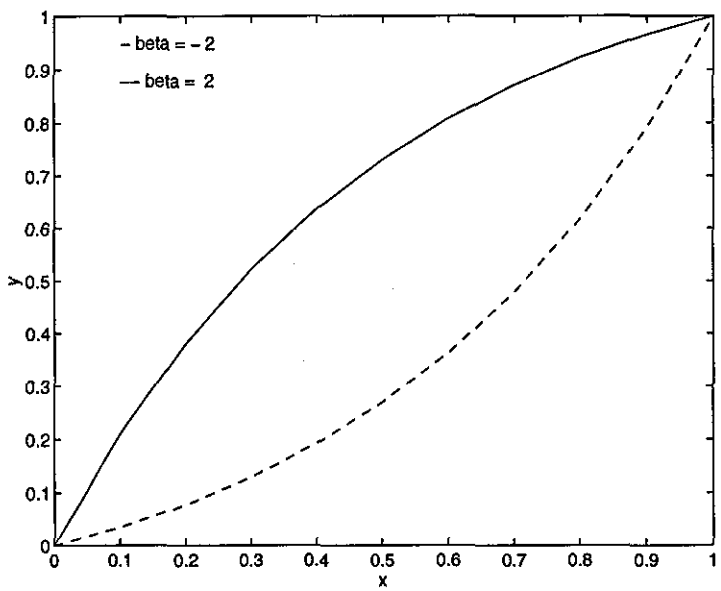


**Figure 5.4, Exponential Penalty Function**

It has been found that the less constrained the problem is, the lower the penalty should be. This is due to the fact that a lower penalty can increase the possibility of violated individuals being selected for reproduction, thus conveying their good properties in having lower objective functions to the next generation. Since the scheduling of supply air flow rate is not a highly constrained problem, the lower

weight of penalty of $\beta = 2$ (Figure 5.4) generally results in better performance with faster convergence.

### Selection for Reproduction

Two selection algorithms have been investigated, the roulette wheel strategy and the remainder stochastic sampling without replacement (Goldberg, 1989). It is expected that the chance of an individual being selected for reproduction should be proportional to its fitness relative to the rest of the population. For instance, suppose that for a population of 10 individuals, the sum of the fitness of all individuals is 20.0. If individual '$A$' has a fitness of 5.0, it is expected that the individual should be selected for reproduction, $5.0/20.0 \times 10 = 2.5$ times. The roulette wheel selection emulates this procedure, but since it is a highly probabilistic process, there is often a great disagreement between the expected and actual numbers of selections. The remainder stochastic sampling without replacement strategy attempts to redress the balance between the expected and actual values while maintaining a probabilistic element to the selection procedure. The method assigns the number of selections of an individual based on the integer of its expected value (2 for individual '$A$' in the above example), with the remainder of the individual selection assigned probabilistically according to the fraction part of the expected value (0.5 for individual '$A$' in the above example).

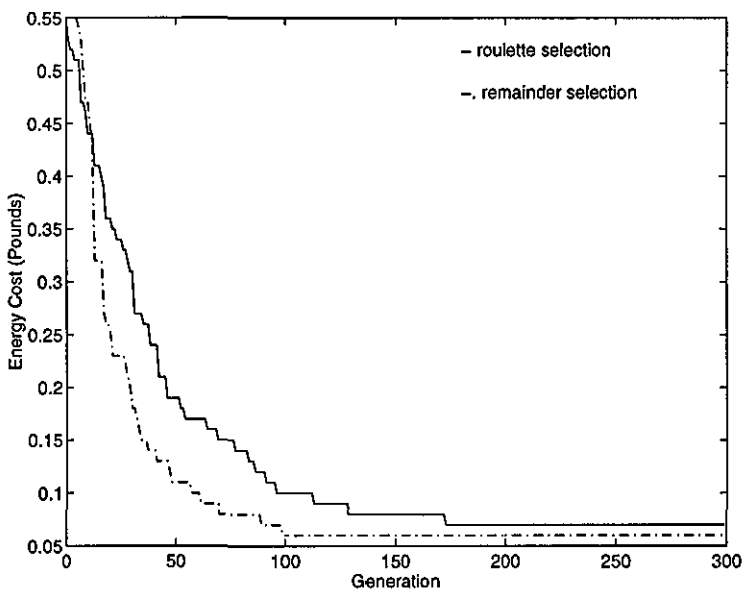


**Figure 5.5, The Cost Reduction with Generations for the Two Selection Methods**

Figure 5.5 illustrates the performance of the two selection strategies, where the most appropriate control parameters have been assigned separately for each of the two methods. It is clear that the energy cost (objective function) is reduced much quicker in the remainder sampling selection. This is due to the reduction in stochastic errors in selecting individuals for reproduction from their associated fitness values. The improvement from the remainder stochastic sampling selection strategy is significant, the optimum solutions obtained generally giving energy cost more than 10% lower than those from the roulette wheel method.

### Variable String Length

The SGA has been implemented so that discrete and continuous variables can be optimized. This is achieved by assigning a discrete interval by which the variable is incremented, the decimal value of the binary number (string) then represents the number of increments above the lower bound. The real value of a variable is calculated by:

$$variable\ value = lower\ bound + interval \times number\ of\ increments$$

An incorrect match between the discrete interval and the binary precision (string length) can therefore result in either the variable upper bound never being attainable, or there being several search points above the upper bound. For instance, if the fan flow rate varies from 0.18 to 0.9 $m^3/s$, with an increment in the flow rate of 0.024 $m^3/s$, there are 31 possible flow rates. If the string length is selected without considering the increment, say, 6 bits, then there would be 64 ($2^6$) possible flow rates. Therefore, there would be much redundancy in representing the required 31 discretised flow rates by a 6 bit binary string. As a result, there would be a large number of infeasible solutions throughout generations, which would then result in a poor distribution of individuals within a generation. This would lead to slow and possibly false convergence.

String length is therefore required to match the accuracy of discretisation of continuous control variables. An increment of 0.024 $m^3/s$ in the flow rate is accurate in terms of the building thermal response (equivalent to 0.25 air changes per hour for the zone and a velocity of 0.038 m/s in the slab core). A 5 bit string length is used, gives a total of $2^5 = 32$ increments, the string length therefore matches the variable increment size. The number of infeasible solutions is thus substantially reduced.

### Population Size, Crossover and Mutation

For off-line applications, too small a population size may lead to premature convergence as there may be insufficient variety of solutions in a generation. The larger the population, the greater the variety of solutions. However, if the population is too large, it can take too long for the search to make a significant improvement. The population sizes of 50, 80 and 100 have been examined. It was found that if the roulette wheel selection method is used, a population size of 50 can cause convergence to a false optimum, due to insufficient solutions in a generation, and being further aggravated by the stochastic errors in the selection procedure. Although a population size of 100 gives rapid cost reduction during early generations, it is followed by a very slow final convergence in the later generations. However, if the improved remainder stochastic sampling method is used, the influence of population size on the GA search is reduced, with all the three population sizes resulting in the same energy cost at their optimum solutions.

The crossover operator gives a GA much of its power, by providing the opportunity for information exchange between individuals. The mutation operator plays a secondary role in the process. Used sparingly together with reproduction and crossover, it is a safeguard against premature loss of important notions. If the mutation rate is too high, it will bring disruption to the fit solution strings and ultimately result in a purely random search.

Since a population size of 80 is sufficient to maintain a diversity of solutions within the population, a low crossover and mutation rate should be selected in order to avoid too much disruption to fit solutions. A study of the control parameters has revealed that the probability of crossover of 0.6 and mutation of 0.001 gives the best algorithm performance for the roulette wheel selection strategy. This is in accordance with the conclusion made by De Jong (Goldberg, 1989).

For the remainder stochastic sampling method, however, a higher crossover rate of 1.0, and mutation rate of 0.001 give the best performance. Therefore, the more deterministic selection of the remainder stochastic sampling method is balanced by the higher and more disruptive crossover rate, which tends to introduce new solutions into the population (as similarly argued by Mercer and Grefenstette (Goldberg, 1989)). The higher probability of crossover increases the opportunity for mating between the two fit solution strings, and thus greatly accelerates the evolution by bringing more diversity to the offsprings from fit parent strings. If

the crossover rate is lowered to 0.6, it was found that at each generation, the distance between the fit and weak individuals is generally large; therefore, there are fewer chances for mating between individuals that will bring fitter solutions to the next generations. Consequently, it may take a long time for the GA to make a substantial improvement and may lead to convergence on a false solution. Figure 5.6 shows the cost reduction with generations for a crossover rate of 0.6 and 1.0 (with the same mutation rate 0.001), indicating a crossover rate of 1.0 resulting in a faster and fitter evolutionary process.

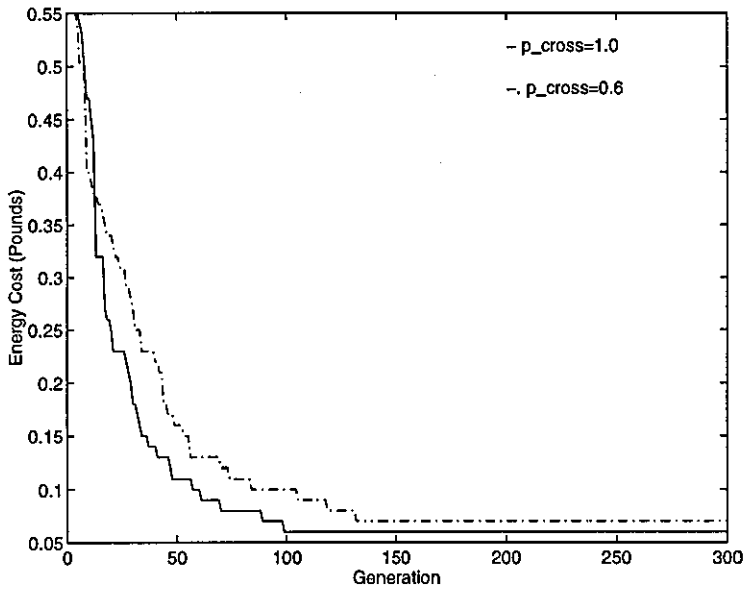


**Figure 5.6, The Influence of Crossover Rate on Cost Reduction in the Remainder Stochastic Selection**

## Conclusion

The form of fitness function and the GA control parameters influence the performance of the GA in scheduling the supply air volume flow rates. The best algorithm performance is achieved when the fitness of each individual is calculated by the absolute difference between the maximum objective function in the generation and the individual's objective function. The rate at which penalties are imposed on infeasible solutions should be low ($\beta = 2$), for the weakly constrained fan flow rate scheduling problem. The remainder stochastic selection strategy has been found to perform better than the roulette wheel selection method. Finally, the following values of control parameters have been observed to give the best performance for this control problem:

- string length: 5 bits;
- population size: 80;
- probability of crossover rate: 1.0;
- probability of mutation rate: 0.001.

### The GA Performance and Comparison with the Complex Method

The 'tuned' GA has been found to give reliable optimum solutions. Since the initial guess of the fan flow rate schedule represents only one individual of the whole population, the influence of the initial guess is not significant. For instance, the initial flow rates of 0.3 $m^3/s$ and 0.6 $m^3/s$ for all setpoints in the 24 hours (the same case as in Section 5.2.1), have resulted in the same optimum energy costs and similar schedules of flow rates over the 24 hour planning period.

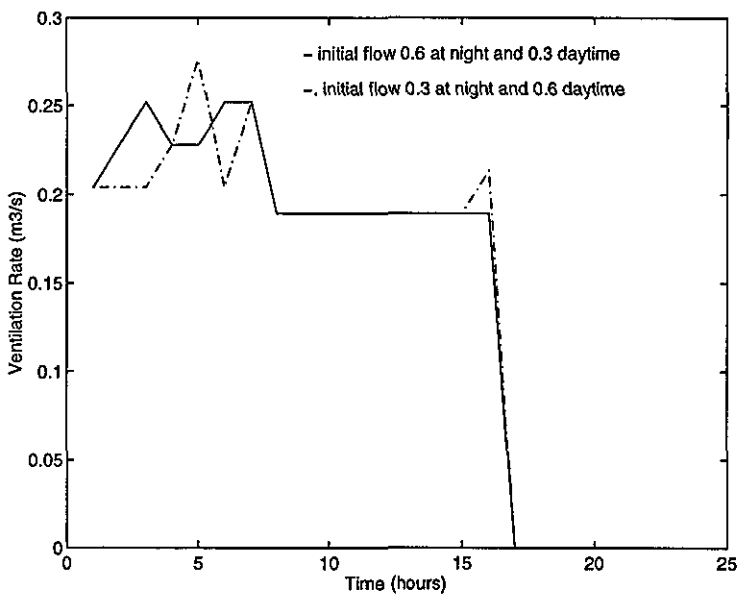


**Figure 5.7, The Influence of Initial Guess on the Optimum Solution in the GA Search**

The influence of a mixed initial guess has also been examined. For case 1, the flow rate was set to be 0.3 $m^3/s$ during the daytime and 0.6 $m^3/s$ at night. In case 2, the flow rate was set to be 0.6 $m^3/s$ during the daytime and 0.3 $m^3/s$ at night. The control parameters were kept the same for the two cases. Figure 5.7 compares the optimum solutions from the two cases for the $30^{th}$ July 1994. The same optimum energy cost has resulted from the two different initial guesses, though the schedules

of the fan flow rates slightly differ in the setpoint values. Since this control problem is not highly constrained, the low gradient of the energy cost in the neighbourhood of global optimum can lead to several feasible near optimum solutions.

The robustness of the GA search has been assessed and results have shown that the fitness representation, selection algorithm and the control parameters significantly affect the optimization performance. This is in contrast to the Complex method which has a fixed algorithm and requires little tuning of its parameters. However, the tuning of the GA to the control problem has been observed not to be difficult. It can be seen from the rate of cost reduction (Figures 5.5 and 5.6) that the GA progresses very quickly during early generations, followed by a much slower evolution during the later generations. However, the GA's implicit parallelism and probabilistic transition rules enable the search to progress towards the global optimum, or a near optimum. In addition, the GA is not sensitive to the initial guess.

The performance of the Genetic Algorithm and the Complex method is summarized in Table 5.1. It can be seen that although the GA takes longer than the Complex method to converge to an optimum, the GA solutions generally provide lower energy cost than those from the Complex method. Although the GA has taken 8000 trial points to find the optimum solution, this is small in comparison to the total search space of $6.2 \times 10^{35}$ possible points. The most significant difference between the solutions from the GA and Complex method, is that the schedule of setpoints obtained from the Complex method (Figure 5.2) is clearly sub-optimal when compared with the schedule from the GA (Figure 5.7); ventilation between the end of occupancy and the early hours of the next day is not necessary, and the daytime ventilation is at the required minimum flow rate 2 ac/h (0.19 $m^3/s$).

| Optimization algorithms | Optimum energy cost (£) | No. of trials | Sensitivity to initial guess |
|---|---|---|---|
| GA | 0.06 | 8000 | no |
| Complex | 0.10 | 2000 | yes |

**Table 5.1, Performance of the GA and the Complex Method in the Scheduling of Supply Air Flow Rate**

The performance of the Genetic Algorithm and the Complex method is further

examined for solving the setpoint scheduling problem.

## 5.3 Algorithm Performance in the Scheduling of Supply Air Setpoints

This section investigates the performance of the Complex method and GA in scheduling the supply air temperature and flow rate for 24 hours of operation (giving 48 problem variables from the 2 setpoints in each of the 24 hours).

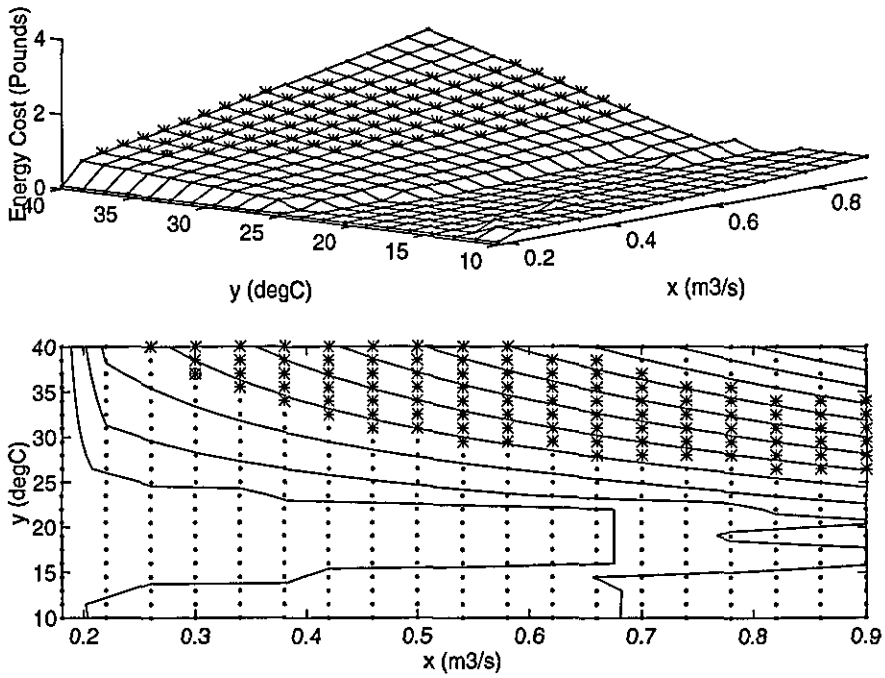


**Figure 5.8, A Surface of Supply Air Flow Rate and Temperature in the Search Space for the Setpoint Scheduling Control Problem**

Due to the discrete plant operating modes, the search surfaces are no longer continuous. Figure 5.8 and Figure 5.9 display the two surfaces of the search space for the $12^{th}$ of February 1994, an example of showing the winter mechanical heating operation. The feasible regions are marked by '$*$', and the infeasible regions by '.'. The infeasible points result from either a violation in the room comfort constraint or from a thermal load that is beyond the capacity of the plant. The optimum feasible point for this surface is indicated by 'o'. The discontinuous surfaces are

due to the discrete plant operating modes for particular supply air flow rate and temperature. The modes actively used in the winter include the preheating mode with room recirculation at night (Mode 7 in Table 3.1 of Section 3.1.2), and daytime minimum ventilation mode with the heat recovery device in operation (Mode 1).

In Figure 5.8, the $x$-axis is the supply air flow rate at 7:00 am (just before occupancy), the $y$-axis is the supply air temperature at 7:00 am, while the $z$-axis represents the total energy cost from the plant operation for the day. The other control variables have been kept at the optimum values obtained from the GA optimization. It is seen that from 10 °C to 25 °C of supply air temperature, there are several distinct regions due to the mixed modes of free cooling or heating, mechanical cooling and heating. Above 25 °C, the region becomes more continuous, since the operation is dominated by the mechanical heating mode. These modes are the optimum output from the plant mode control (Chapter 3).

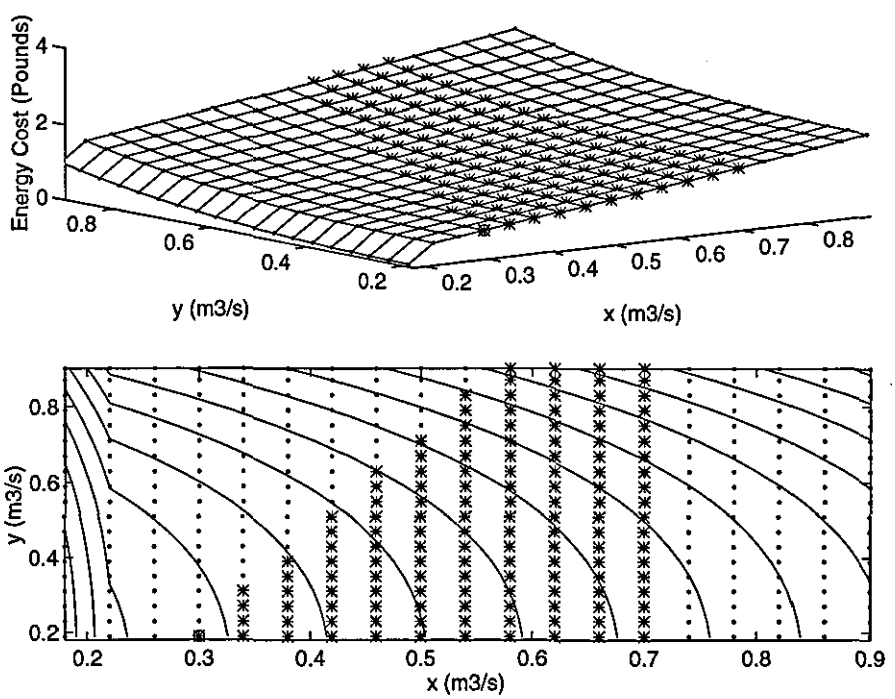


**Figure 5.9, A Surface of Two Supply Air Flow Rates in the Search Space for the Setpoint Scheduling Control Problem**

Similarly in Figure 5.9, the $x$-axis is the supply air flow rate at 7:00 am, the $y$-axis the supply air flow rate at 8:00 am, and the total energy cost illustrated by the $z$-

axis. The shape of the surface depends on the values of the other variables, which are set at the optimum values from the GA optimization. Compared with the continuous surface of the two supply air flow rates in the fan flow rate scheduling (Figure 5.1), the discontinuous surface in Figure 5.9 is due to the mode changing from free cooling or heating mode to mechanical heating.

### 5.3.1 Performance of the Complex Method

The Complex method can be used to search in a discontinuous space. In comparison to solving the 24 variable flow rate scheduling problem (Section 5.2), the Complex method is substantially slower in solving the 48 variable setpoint scheduling problem. Although the search still only takes 5000 trial points to converge, the solution is likely to be a false optimum. The solution from the Complex method is illustrated in Figure 5.10 for the 12$^{th}$ February 1994. The Complex optimization results in a higher energy cost than that from the GA, as a result of the Complex method incorrectly scheduling the plant to be in operation between midnight and 5:00 am, and after the occupancy period (5:00 pm to 0:00 am).

The performance of the Complex method is summarized in Table 5.2. This result has been obtained from an initial guess which is close to the optimum. If the initial point was selected without *a priori* knowledge of the optimum schedule, the Complex method converged to a solution with the energy cost of £1.24, which is 32% higher than £0.94 in Table 5.2. This sensitivity to the initial guess can be explained by the optimization process of rolling the complex towards the optimum, which can be very ineffective for a complex with a large number of vertices that is far away from the true minimum.

As Rao (1984) stated, the Complex method becomes rapidly inefficient in solving a problem with a large number of variables. The poor performance of the Complex method is evident in this control optimization, by the algorithm's sensitivity to the initial guess, and premature convergence on a false optimum with high energy costs.

### 5.3.2 Performance of the Genetic Algorithm

The GA provides the optimal controller with a robust and powerful tool to solve the problem having a discontinuous search space and a large number of control variables. The robustness of the GA to its fitness formulation and control parameters has been assessed in Section 5.2. Although the optimum solutions found are relatively sensitive to these factors, the evolutionary mechanism of the GA guarantees that the search will progress towards the global minimum or a near global minimum. This has been confirmed by the optimum profiles of the plant schedule found by the GA, which indicate the clear (and expected) characteristics of the control problem (Chapter 6). The algorithm formulation and the GA control parameters obtained from Section 5.2, have been tested in solving the setpoint scheduling control problem. Their reliability has been confirmed by the optimum results.

Figure 5.10 compares the optimum solutions from the GA and the Complex method for the $12^{th}$ February 1994. The correct characteristics of the setpoint scheduling problem are indicated by the GA solution, that only two hours night preheating is required to offset the heating load during occupancy. During the daytime the minimum ventilation is used (equivalent to 2 ac/h) with the heat recovery device in operation. The ventilation is OFF after the occupancy period.

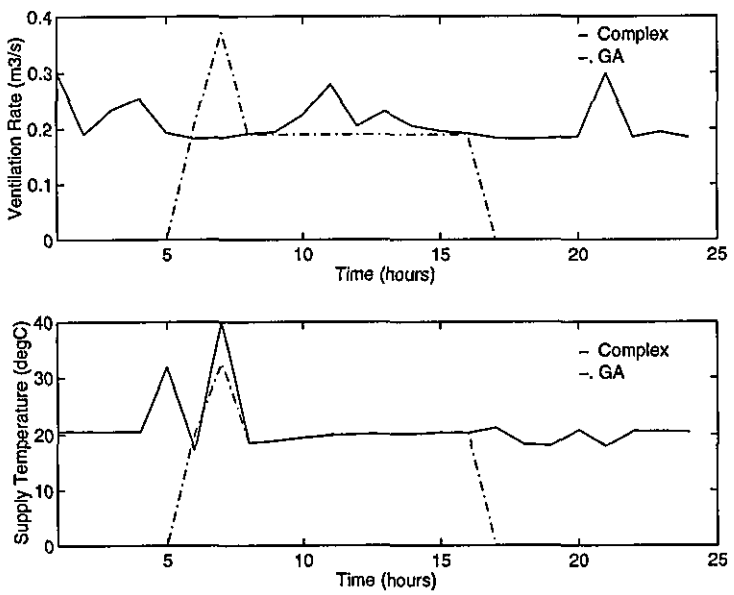


**Figure 5.10, Solutions to Setpoint Scheduling Problem from the GA and the Complex Method**

The performance of the GA is summarized in Table 5.2. Since the GA searches a whole population of individuals in parallel and the search evolves over many generations, it may require more computational overhead than a conventional direct search optimization method. In solving the setpoint scheduling problem, the GA took 24000 trial points which is within the benchmark of 36,000 trial points (Section 5.1), and is fast in relation to the total search space of $2.3 \times 10^{86}$ points. The GA implemented in this research is robust in its ability to find an optimum solution, since there is no need for *a priori* knowledge of initial guess, and it is relatively insensitive to its control parameters. It is also efficient in solving the problem with a large search space. The advantages of the GA search are apparent when compared with the Complex method, and therefore, the GA is chosen for use in the optimum setpoint scheduling control (Chapters 6 and 8).

| Optimization algorithms | Optimum energy cost (£) | No. of trials | Sensitivity to initial guess |
|---|---|---|---|
| GA | 0.69 | 24000 | no |
| Complex | 0.94 | 5000 | yes |

**Table 5.2, Performance from the GA and the Complex Method in Setpoint Scheduling Control Problem**

## 5.4 Algorithm Performance in Optimizing the Time-Stage Control

The investigation of the characteristics of the optimum solutions to the setpoint scheduling control problem has led to the development of a simplified time-stage controller. This controller encompasses the control characteristics with fewer control variables, and provides more stable operation of the plant (Chapter 6). Due to the different nature of the control variables defined in the time-stage control, the performance of the optimization algorithms in solving this problem has also been investigated.

### 5.4.1 Optimization Problem Formulation and Characteristics

The control variables in the time-stage control include integer variables for the time stages and the switching of the heat recovery device operation. The setpoints for the supply air flow rate and temperature are real continuous variables, giving 15 variables in total (Section 6.2). The mixed integer-continuous variable nature of the problem is distinct from the setpoint scheduling problem that has only real continuous variables. The constraints of the time-stage control include the limits of time switches, and comfort constraints in the occupied space. The objective function of the time-stage control optimization is however, the same as the setpoint scheduling control, being the total energy cost over the planning period.

The same notation is used here to represent the control variables as has been defined in Section 6.2. $S_1$, $S_2$, $C_1$, $C_2$, $C_3$ and $C_4$ are time switch variables. $V_1$ and $V_2$ are two air flow rate setpoints, $T_1$ and $T_2$, two supply air temperature setpoints (Figure 6.11, Section 6.2). In order to further simplify the constraint handling, the differences between the time stages are used as optimization variables. The integer problem variables then become the start time for the initial period of plant operation, $S_1$, the period of passive heating or cooling $(C_1 - S_1)$, and the period of active heating or cooling $(C_2 - C_1)$; similarly, for the second period of high plant output, the integer variables are $S_2$, $(C_3 - S_2)$ and $(C_4 - C_3)$. As well as the constraints on occupant comfort, further constraints are required here to ensure that the periods of active heating and cooling fall within the periods of plant operation ($S_1$ to 8:00 am and $S_2$ to 4:00 pm).

Figure 5.11 displays the objective function surface for the control variables $S_1$ and $(C_2 - C_1)$ for the $12^{\text{th}}$ of February 1994. The $x$-axis is $S_1$, and the $y$-axis is $(C_2 - C_1)$ (in this instance, the solution gives $C_1 = S_1$). The feasible regions are marked by '$*$', and the infeasible regions by '.'. The other control variables have been kept at the optimum values obtained from the GA search. The optimum feasible point for this surface is indicated by 'o'. In this instance, the violated points in the upper region of the surface are due to the time constraint for night plant operation being violated ($C_2$ should be no more than 8:00 am), whereas the violated points in the lower region are due to insufficient preheating resulting in the comfort constraint being violated.

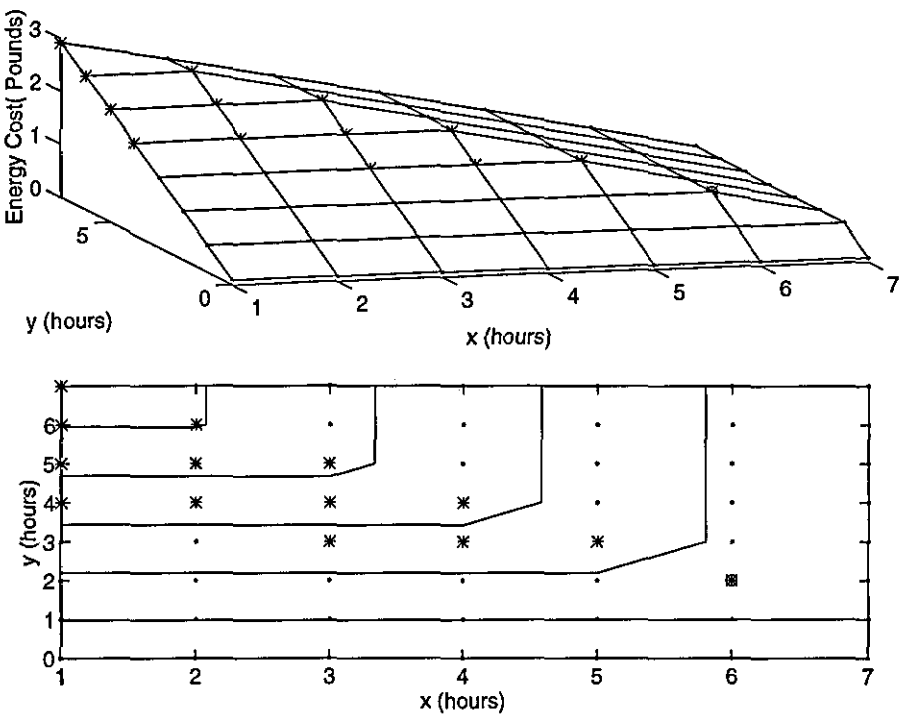


**Figure 5.11, A Surface of Time Switches for the Time-Stage Control Problem**

Figure 5.12 illustrates the objective function surface for the supply air flow rate and temperature. The $x$-axis and $y$-axis are the supply air flow rate $V_1$ and supply temperature setpoint $T_1$, respectively. It can be seen that the shape of the surface is similar to that in Figure 5.8. It is also observed that the contours are much denser (two figures have the same scale and contour 'level'). This is due to the optimum values set for the other control variables. In this case, the heater is operated for two hours at night ($C_2 - C_1 = 2$), which causes a much sharper increase in the energy cost with respect to the changes in supply air flow rate and temperature.

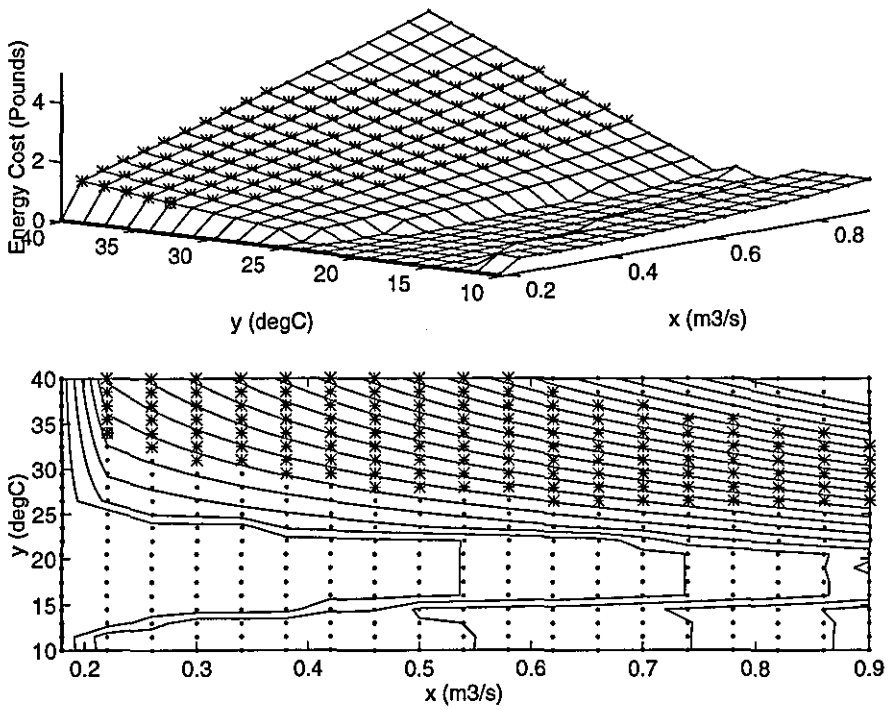


**Figure 5.12, A Surface of Supply Air Flow Rate and Temperature for the Time-Stage Control Problem**

The performance of the Complex method and the GA in solving the time-stage control has also been assessed in relation to their ability to find an optimum solution, the number of trial solutions and the sensitivity to initial guess. Since the problem is different from the setpoint scheduling control (its unique characteristic can be seen in Figure 5.11), the control parameters in the GA search have been examined and tuned for solving this problem.

## 5.4.2 Performance of the Complex Method

The investigation of the Complex method indicates that it is incapable of solving the time-stage optimization problem. This is due to the representation of the integer time-stage control variables by rounding the values of continuous control variables to the nearest integers. The discretisation of the variables means that the Complex search may not be able to progress and may collapse against a constraint boundary. This is illustrated in Figure 5.13. The curve marked by $g$ signifies a constraint boundary. Since Point 1 is outside of $g$, it is moved by the algorithm to

Point 2' which is inside of $g$. However, due to rounding, Point 2' becomes Point 2 which is again infeasible and the search is therefore unable to make progress.

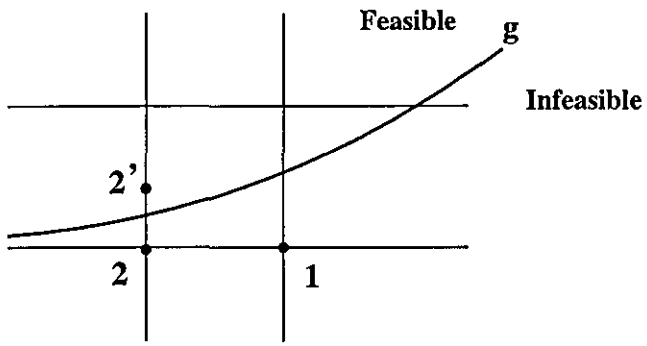


**Figure 5.13, An Example of the Search in the Time-Stage Control by the Complex Method**

The difficulty in the Complex search associated with integer variables prevents it from being a viable optimization method for solving the time-stage control problem.

### 5.4.3 Performance of the Genetic Algorithm

Since the GA handles the control variables by string codings, the integer nature of control variables does not impose a limitation on the performance of the GA search. The representation of the variables in the GA is discussed in Section 5.2.2; the string length required to represent the integer time stage control variables depends on the possible number of values for each time switch variable.

A study of the GA formulation and its control parameters has shown that most parameters used in the optimal scheduling control (Section 5.2.2) are appropriate for this problem. However, a difference in the time-stage control optimization from that of the optimal scheduling control is that the time-stage control is a more highly constrained problem. The highly constrained nature of the search space in the time-stage control means that a higher constraint violation penalty rate ($\beta = -2.0$) should be used to prevent the search converging to an infeasible solution (Section 5.2.2).

The probability of mutation has also been increased to 0.01. Figure 5.14 shows that the low mutation rate of 0.001 leads the search converging as early as the $50^{th}$ generation. Compared to the very flexible combination of plant operating schedules offered by the hourly setpoint control, the time stages limit the choices of plant schedules that can be used to meet the comfort constraints. For such a highly constrained problem, the number of similar solution strings increases substantially in the later generations with the use of the remainder stochastic sampling selection strategy. The high crossover rate of 1.0 is no longer sufficient on its own to bring new fit solutions to the population. Therefore, a higher mutation rate is required to introduce a greater variety of solutions, and prevent premature convergence.

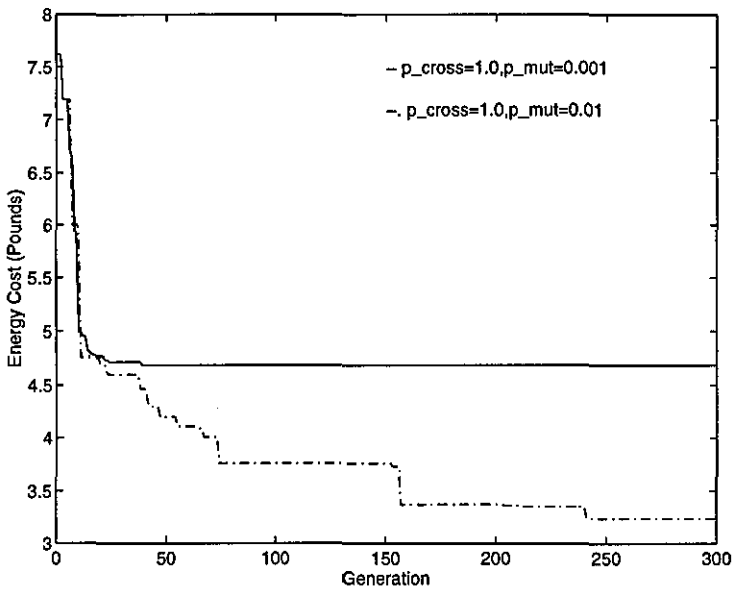


**Figure 5.14, The Cost Reduction with Generations for the Time-Stage Control Problem**

The effect of the mutation operator can also be indicated by the number of feasible solutions in generations (Figure 5.15). For a mutation rate of 0.001, the number of feasible solutions in each generation is much higher than that for a mutation rate of 0.01. This is the evidence of the disruption of the mutation operator to the solutions, which for this highly constrained problem, is useful in preventing premature convergence.

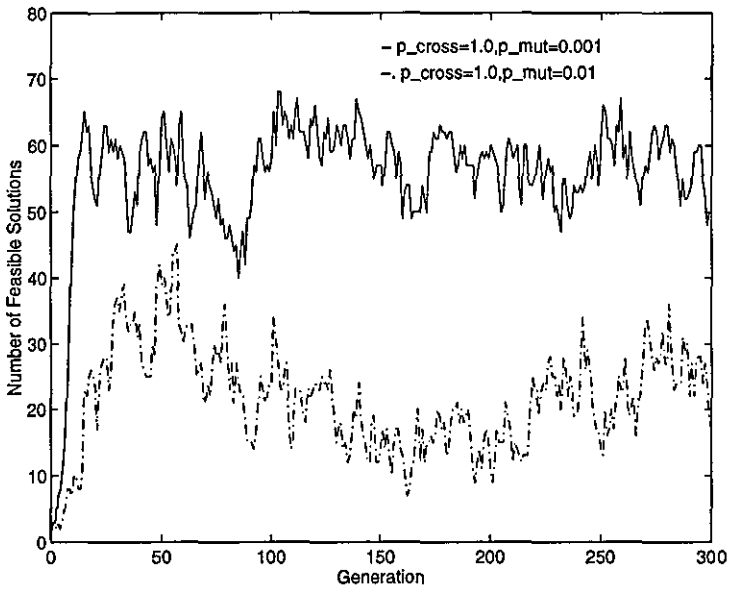


**Figure 5.15, The Number of Feasible Solutions in Generations for the Time-Stage Control Problem**

The performance of the GA in solving the time-stage control problem is indicated in Table 5.3, with the resulting supply air volume flow rates and temperatures shown in Figure 5.16. The energy cost and schedules are for the $12^{th}$ of February 1994. The optimization results from the GA justify its reliability in finding the global minimum or near global minimum. The algorithm has proved to be efficient and robust in searching through the discontinuous solution space resulting from the mixed nature of the control variables. The GA is also insensitive to the initial guess of the time switches and plant setpoints, and the search takes 12000 trial points to converge to an optimum in a search space of $5.3 \times 10^{14}$ points. Therefore, the GA is robust and can be used for the time-stage control optimization. The further investigation on the time-stage control and comparison with the optimum setpoint scheduling control is described in Chapter 6.

| Optimization algorithms | Optimum energy cost (£) | No. of trials | Sensitivity to initial guess |
|---|---|---|---|
| GA | 0.71 | 12000 | no |

**Table 5.3, Performance of the GA in Time-Stage Control Problem**

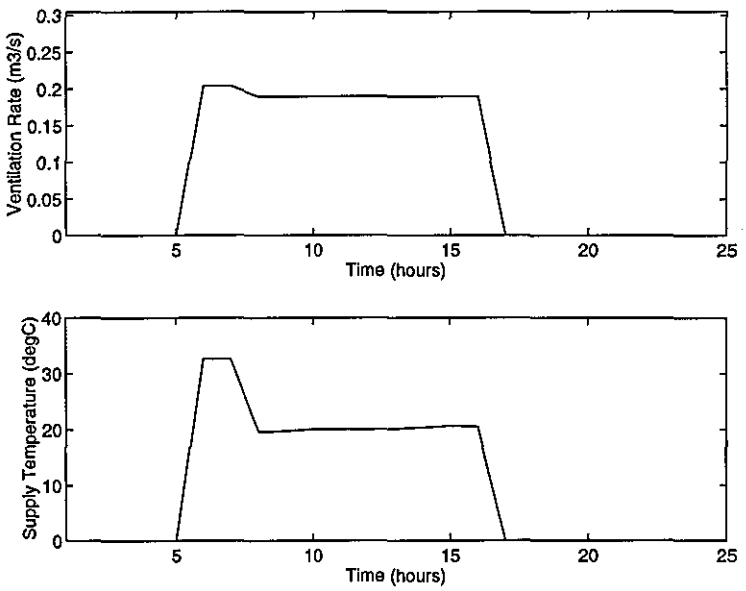


**Figure 5.16, An Optimal Solution to Time-Stage Problem from the GA Search**

## 5.5 Conclusion

The performance of the Complex method and the GA has been investigated in this chapter. The results have shown that the GA is robust and efficient in solving the three control problems: the scheduling of supply air flow rates, the scheduling of supply air setpoints and the time-stage control. However, to obtain a satisfactory performance from the GA search, some tuning of its parameters and formulation is required. The GA implemented in this research is able to find an optimum solution (inspection of the results suggests that the solutions are always close to the global minimum). The search is also insensitive to the initial guess. The GA requires between 12000 and 24000 trial solutions to solve the control problems, but these trial solutions can be evaluated and the optimum found within the one hour calculation period required for the implementation of the controller (Section 5.1).

In comparison, the Complex method can find a solution to the control problem of scheduling supply air flow rates in a shorter time than the GA. The solution is however, clearly sub-optimal and gives higher energy cost than that from the GA

search. The Complex algorithm is also sensitive to the initial guess. In solving the problem of scheduling supply air setpoints, the Complex method becomes substantially slower and even more sensitive to the initial guess. The energy cost of the solution is much higher than that provided by the GA search, the solution being sub-optimal. The Complex method can not solve the time-stage control problem since it is ineffective in handling integer control variables.

Therefore, the GA is selected to be the search algorithm used in the optimum predictive controller. The problem characteristics investigated in Chapter 6 and the analysis of the controller performance in Chapter 8, are based on the use of the GA search method.

# Chapter 6

# Characteristics of the Optimum Control Strategy and Time-Stage Control

## Introduction

This chapter investigates the characteristics of the optimum control strategy for the ventilated slab systems. The optimum control schedules have been identified using the Genetic Algorithm search method described in Appendix B and Chapter 5. A 'typical' office zone in a hollow core ventilated slab building has been selected for this study, and therefore, to some degree, the characteristics of the results can be considered as 'generic'.

A hollow core ventilated slab building is usually well-insulated. Table 6.1 describes the typical building construction adopted in this research. The construction is for a ventilated slab building located at the University of East Anglia, UK (Bunn, 1995). The conductance (U value) of external walls is only 0.2 $W/m^2K$ and that of the window is 1.3 $W/m^2K$.

| Element | Construction |
|---|---|
| External Wall | 200mm Rockwool, 25mm air gap,<br>200mm heavy weight concrete block, 10mm plasterboard |
| Internal Wall | 10mm plaster,100mm heavy weight concrete block,<br>25mm air gap, 100 heavy weight concrete block,10mm plaster |
| Floor/Ceiling | 250mm hollow core concrete slab, 100mm screed |
| Window | triple-glazed, low-emissivity coated |

**Table 6.1, Building Construction**

The floor area of the zone is 4.0 m×6.0 m with a ceiling height of 2.84 m. The ventilation air is introduced to the space by ceiling diffusers, which are connected to the ventilated slab air outlet. The ceiling has five ventilated slabs, each of which is 4.0 m long, × 1.2 m wide, × 0.25 m thick.

Five identical zones in the building have been modelled. All zones have one south facing external wall with a 4.2 $m^2$ window. Ventilation from the plant is equally divided and supplied to each zone. The design minimum ventilation during the occupancy period is 2 air changes per hour (ac/h) for each zone. Occupancy is scheduled from 8:00 am to 4:00 pm. Three electricity tariff structures have been studied, 3:1, 2:1 and 1:1 (the ratio of the cost of on-peak electricity to the cost of off-peak electricity); the schedule of on-peak electricity tariff coincides with the occupancy schedule. If it is not stated in the following sections, the 3:1 electricity tariff is applied to calculate the optimum control strategy. In addition, the influence of different schedules of the electricity tariff structure on the optimum plant operation is also investigated.

The investigation in this chapter is based on the assumption that the next day's weather conditions can be predicted perfectly. The real weather data of 1994 monitored at Garston, Watford, UK, have been used as the example year for which to conduct the study, since it encompasses weather conditions that are suitable for assessing the performance of low energy buildings. In particular, the diurnal variation in summer conditions is such that the effectiveness of using free night cooling to offset the next day's cooling loads can be assessed.

An analysis of the control characteristics suggests that, the optimization of the scheduling of the plant operation can be simplified. This has led to the devel-

opment of the 'time-stage' controller, its performance being compared with the setpoint scheduling control and conventional control strategy in Section 6.3.

## 6.1 Characteristics of the Optimum Schedule of Control Variables

The control optimization problem for the plant setpoint scheduling has been defined in Chapter 3. In some instances, the gradient of the energy cost is low, which can lead to several feasible near optimum solutions. However, the optimum solutions obtained give a clear indication of the dominant characteristics of the control problem.

The characteristics of the optimum solutions have been investigated under various operating conditions which would significantly influence the optimum strategies, including varying weather conditions for the summer and winter and the transitional seasons between the two. The effects of varying occupant thermal comfort requirements, different electricity tariff structures and plant part load performance, have also been examined. The influence of mass thermal storage in the building on the plant schedules is investigated below.

### 6.1.1 The Influence of Mass Thermal Storage

Due to the heavy weight construction of the ventilated slab building, the mass storage in the building from the previous day may affect the optimum plant operating schedule of the following day. The power of the GA search in handling a large number of optimization variables makes it possible to investigate the influence of mass storage on the optimum plant operation for two days in succession.

In this study, only the supply air flow rate is optimized, which restricts the building and plant to only passive modes of operation, with no mechanical cooling or heating. The optimization problem therefore consists of 48 fan flow rates for the 48 hours as control variables, and 48 constraints for the two days' thermal comfort requirements. The optimum solution for the two days' fan operation has

been compared with the optimum schedules obtained from separate one day optimizations. If the optimum schedules from these two procedures differ significantly, then it suggests that a one day planning period (24 hours) may not be enough to optimally plan the plant operating schedule, since the second day's thermal requirements may be effected by the previous day's optimum operation strategy.

Figure 6.1 compares the optimum schedules of fan flow rates for the two days operation from these two procedures. The results are for the $30^{th}$ and $31^{th}$ of July 1994. It can be seen that the schedules from the two procedures are virtually the same (the energy consumption being only 3% different between the two strategies). During the late evening of the first day, ventilation is stopped, since there is no need to reduce the room temperature further by night cooling for the following day. In the early morning of the second day, the free night cooling is operated for several hours so that the daytime room cooling load can be offset.

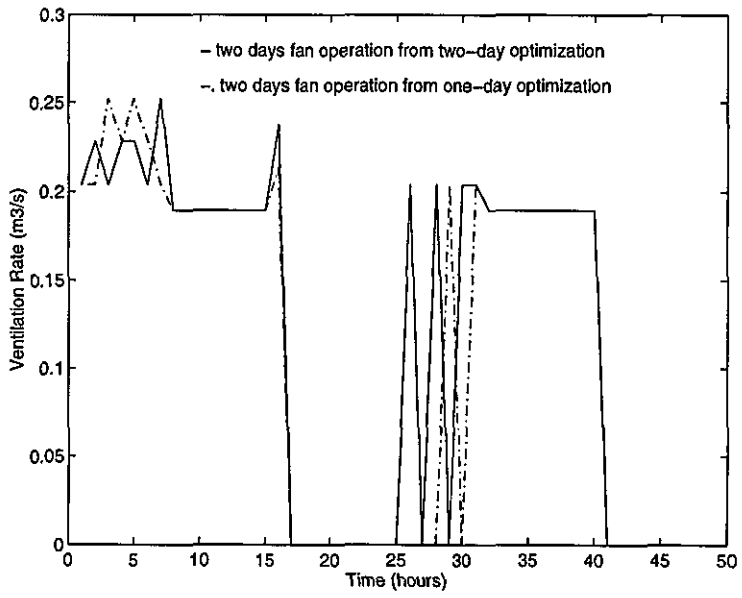


**Figure 6.1, The Comparison of Optimal Schedules of the Fan Operation for the Two Days**

The mass thermal storage from the previous day determines the initial thermal state in the room for the next day, which would largely influence the optimum plant operation. However, the results in Figure 6.1 suggest that the two days fan operation schedules can be planned separately. In addition, most of time the ambient air temperature drops to its lowest point between midnight and early morning. It is therefore sufficient to plan the night cooling after midnight without

affecting the first day's operation. This is true for similar ambient conditions in two successive days; the planning of the plant operation for the two days has equal weight and can be decoupled. Whereas if for instance, the first day is cool, but the night of the second day is too hot to meet the daytime cooling load only by free cooling, the planning of the plant operation over two days could reduce the total energy cost of the two days operation by overcooling the room (without violating comfort constraints) in the first day, using night free precooling, giving sufficient cool storage to relieve the second day's cooling load. However, an accurate weather prediction for two days ahead is almost impractical (Chapter 7), which limits the effectiveness of having a planning period of more than 24 hours. Therefore, a one-day optimization procedure is appropriate for the scheduling of the plant operation for the ventilated slab system. Figure 6.1 displays an important characteristic in that the plant operation is decoupled from one day to the next day, with the control optimization only needing to be considered over a 24 hour period.

The following sections investigate the characteristics of the optimum control of the thermal storage (Chapter 3) with supply air flow rate and temperature over 24 hours as the control variables.

### 6.1.2 Summer Operation

Figure 6.2 displays the optimum solution for a day in the summer, $13^{th}$ July 1994. Three obvious stages can be observed in the ventilation rate schedule. They result from the thermal comfort requirement during occupancy and the applied electricity tariff structure (3:1). During the night, a low ambient temperature and the cheaper cost of electricity encourages higher ventilation rates, shifting the daytime cooling load to the night. When occupancy starts in the morning and the high electricity tariff period begins, only the minimum ventilation is required. As soon as the cooling load increases near midday, higher ventilation is required to extract more 'coolth' from the slab thermal store. The ventilation is switched OFF after the occupancy period.

Figure 6.2 also illustrates the setpoint temperature for the air supplied to the ventilated slab. In the figures of plant setpoint schedules (Figures 6.2 and 6.3), where the supply air setpoint is lower than the ambient air temperature, either the heat recovery device, and or, the chiller is in operation; where the setpoint

matches the ambient air temperature, then the plant is operating in a free cooling mode. In this instance, the chiller is operated for 6 hours at night and one hour during occupancy period. The heat recovery device is always in operation to reduce the fresh air supply temperature throughout the occupied period. Note when the ventilation is OFF, the supply air temperature setpoint is set to zero.

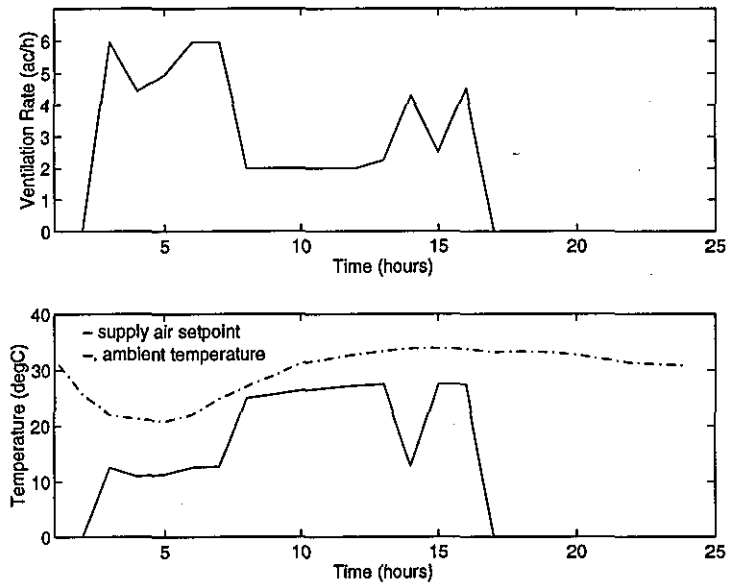


**Figure 6.2, Optimum Scheduling of Control Variables for One Day in the Summer**

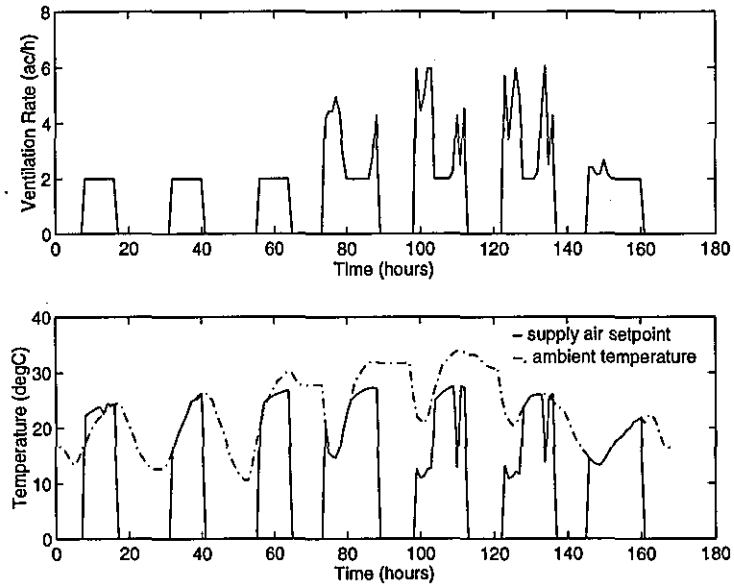


**Figure 6.3, Optimum Scheduling of Control Variables for Seven Days in the Summer**

Figure 6.3 displays the optimum schedule of the plant operating setpoints for the week from the $9^{th}$ to the $15^{th}$ of July 1994. During the first three days, the cooling loads are relatively low leading to no precooling of the ventilated slab, the residual thermal storage being sufficient to offset the cooling loads and only minimum ventilation being necessary during the occupied period. However, the thermal loads are higher during the rest of the week with precooling of the ventilated slab being evident. The 'spikes' in the temperature setpoints during occupancy are a result of the chiller being operated to offset the peak loads. In practice, such short periods of chiller operation and frequently varying fan flow rate should be avoided.

### 6.1.3 Transition Season Operation

The plant operation in the transitional seasons between summer and winter is similar to that during the first three days in Figure 6.3. Night precooling or heating is not necessary and only minimum ventilation is required during the occupancy period. On the cooler days, heat is retained in the building by the operation of the heat recovery device. On the warmer days however, an increase in zone temperature is suppressed by fresh supply air directly to the ventilated slab. Since the thermal conditions in the building space are normally well within the comfort band, the control of the plant is relatively simple during the transition seasons.

### 6.1.4 Winter Operation

During winter operation, the optimum schedules of the plant operation display a rather simple and uniform plant operating mode. Figure 6.4 illustrates the optimum solution for the $14^{th}$ of February 1994. During the night, higher ventilation rates are used to shift the daytime heating load to the night due to the cheaper cost of electricity and the use of the air recirculation mode. During the occupancy period, ventilation rates are kept at a minimum, since this coincides with the period of peak electricity tariff. In the same manner as for summer operation, the ventilation is OFF after occupancy.

The supply air setpoint temperature to the ventilated slab and the ambient air

temperature are also shown in Figure 6.4. The supply air temperature is indicated as being zero if the ventilation is OFF. During the night, the recirculated room air is preheated before being supplied to the ventilated slab. The supply temperature varies between 30 °C and 40 °C depending on the room heating load requirement for the following day. In Figure 6.4, preheating is used for 4 hours (Mode 7 in Section 3.1). During the occupancy period, the plant is operated with the minimum ventilation and with the heat recovery device in operation (Mode 1), which heats the air to approximately 19 °C before supplying it to the ventilated slab.

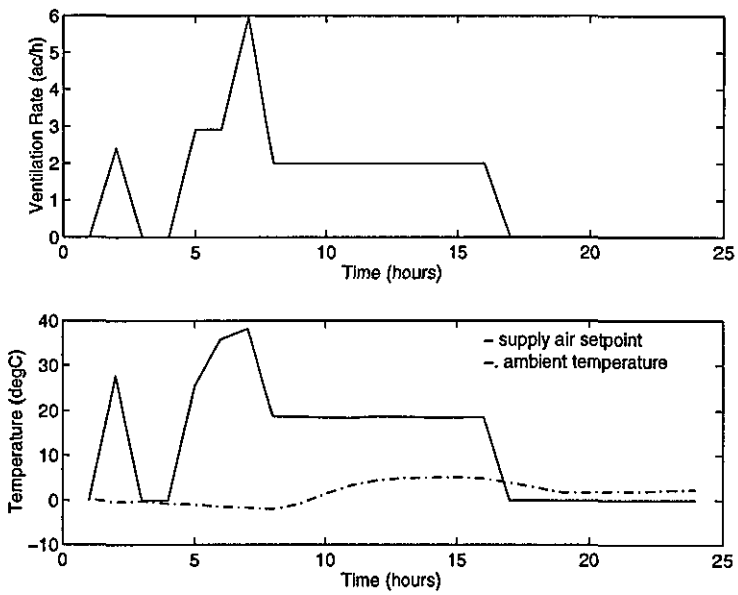


**Figure 6.4, Optimum Scheduling of Control Variables for One Day in the Winter**

Figure 6.5 displays the optimum schedule for the week from the $12^{th}$ to the $18^{th}$ of February 1994. It can be seen that the ventilation rate schedule shows a clear stage effect. The supply air temperature schedule exhibits simpler plant operating modes when compared with those used in the summer (Figure 6.2 and 6.3). Figure 6.5 also indicates some short periods of plant operation at night when the supply air temperature is close to 20 °C (on the $2^{nd}$, $4^{th}$ and $6^{th}$ days of operation). This is due to the plant being operated with full recirculation but without the electric heater. This mode of operation should be avoided since it does not contribute to the charge of the thermal storage and only leads to a small reduction in the room and mass temperatures. These operating points appear since the short period of operation has a low energy cost and such operation is not constrained in the

optimization. These short periods of operation are eliminated in the time-stage control described in Section 6.2. The daytime plant operation is rather simple and applied to all the winter periods with the minimum ventilation and the heat recovery device in operation.

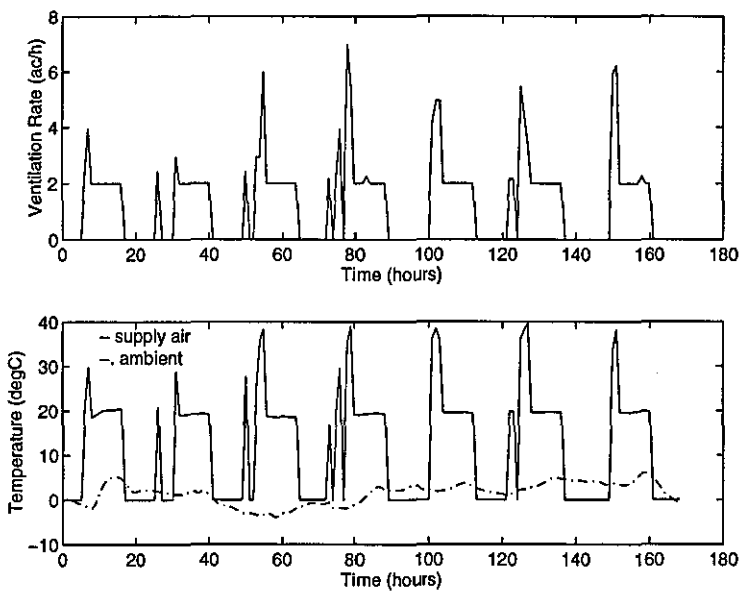


**Figure 6.5, Optimum Scheduling of Control Variables for Seven Days in the Winter**

### 6.1.5 The Influence of Electricity Tariff Structure and Electricity Schedule

The optimum solutions for 1:1 and 3:1 tariff structures for the summer operation are shown in Figure 6.6, and those for the winter operation are shown in Figure 6.7.

It can be seen from Figure 6.6 (for the $13^{th}$ of July 1994) that the weight of shifting the cooling load to the night is reduced for the 1:1 tariff, the maximum ventilation rate at night being similar to that during occupancy hours. The chiller is also operated for 4 hours during the occupancy period, but not at all at night. This is in contrast to the 5 hours night chiller operation for the 3:1 tariff. For the 1:1 tariff, there is no incentive to shift more cooling load to the night. However, free cooling using the lower night air temperature is still effective in saving energy, due

to the active utilization of the building fabric thermal storage. The total power consumption is slightly lower for the 1:1 tariff than that for the 3:1 structure. The result from a 2:1 tariff structure shows no significant difference from that of the 3:1 tariff structure.

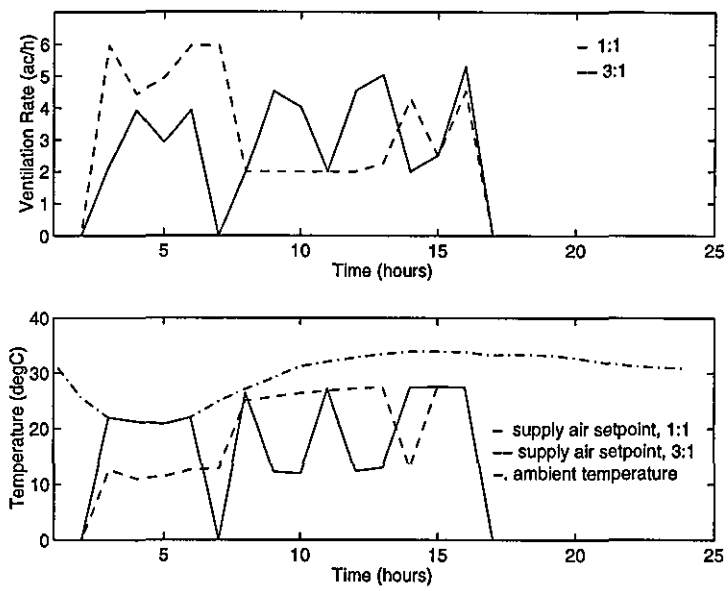


**Figure 6.6, Optimum Scheduling of Control Variables in the Summer under 1:1 and 3:1 Electricity Tariff Structures**

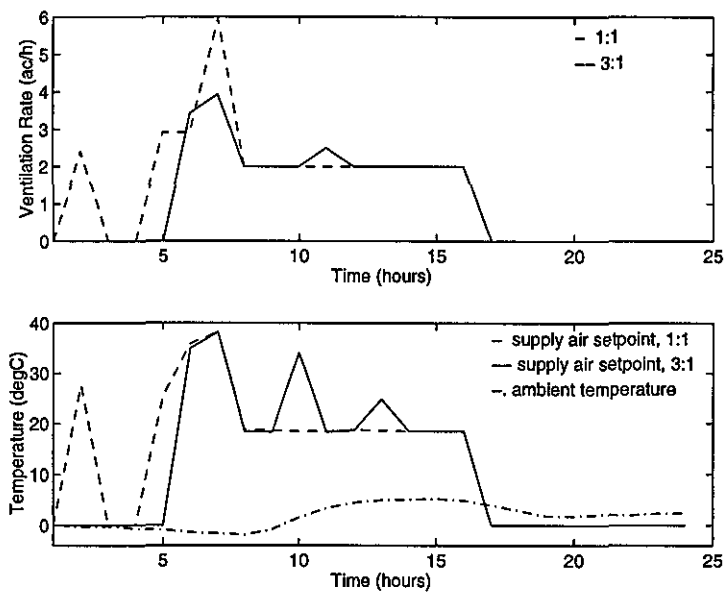


**Figure 6.7, Optimum Scheduling of Control Variables in the Winter under 1:1 and 3:1 Electricity Tariff Structures**

During winter operation, Figure 6.7 reveals that a part of the heating load totally satisfied by the off-peak electricity for the 3:1 tariff is moved to the occupancy period for the 1:1 tariff. The preheating ventilation rate is also reduced and with 2 hours fewer operation at night for the 1:1 tariff, while the heater is operated for 2 hours during occupancy.

The 3:1 and 2:1 electricity tariff structures apply to the same schedule that the start of high electricity tariff coincides with the start of occupancy at 8:00 am. If a different electricity schedule is applied, for instance, the on-peak tariff starts from 10:00 am or 12:00 pm (2 hours or 4 hours later than the occupancy start time), the end of the higher charge of the thermal storage would move from 8:00 am to 10:00 am or 12:00 pm respectively. Figure 6.8 compares the optimum setpoint schedules for the $13^{th}$ of July 1994, when the peak electricity tariff starts from 8:00 am (as for Figure 6.2), 10:00 am and 12:00 pm, while the occupancy starts at 8:00 am for the three cases and the end of peak electricity coincides with the end of occupancy. It can be seen from Figure 6.8 that in order to offset the cooling loads during peak hours at the late afternoon, the charge of the thermal store continues from the night to the early occupancy period using the low cost of electricity, until the start of high electricity (in Figure 6.8, 10:00 am or 12:00 pm). When the peak electricity period starts, the minimum ventilation is then used to save energy cost and to meet the fresh air requirement in the occupied space. During the late afternoon, when the cooling load increases, higher ventilation is used in all the three cases to discharge the mass store. The time scheduling of the plant operation corresponds to the electricity and occupancy schedules. This is illustrated in Figure 6.8 where 3 hours chiller operation at night in the case of the electricity schedule starting at 8:00 am, being moved to the early occupancy period from 8:00 am to 11:00 am prior to the start of the high electricity (12:00 pm). It is exhibited that this optimum setpoint scheduling control can provide an optimum schedule of plant operation that takes advantage of cheaper cost of electricity while the occupant comfort is still satisfied.

When the night free cooling using ambient air to charge the thermal store is sufficient to offset the daytime cooling load, the plant operating schedule depends on the occupancy schedule and may not be effected by the electricity schedule. This is due to the fact that the ambient air temperature at night before 8:00 am is generally lower so that night free cooling can provide sufficient charging of the thermal store without mechanical cooling; the ambient air temperature rises after

8:00 am and there is fewer opportunity for using free cooling to further charge the mass store during the early occupancy period prior to the start of high electricity. The plant is therefore operated to maintain the occupant comfort without shifting the cooling load to the off-peak occupancy period.

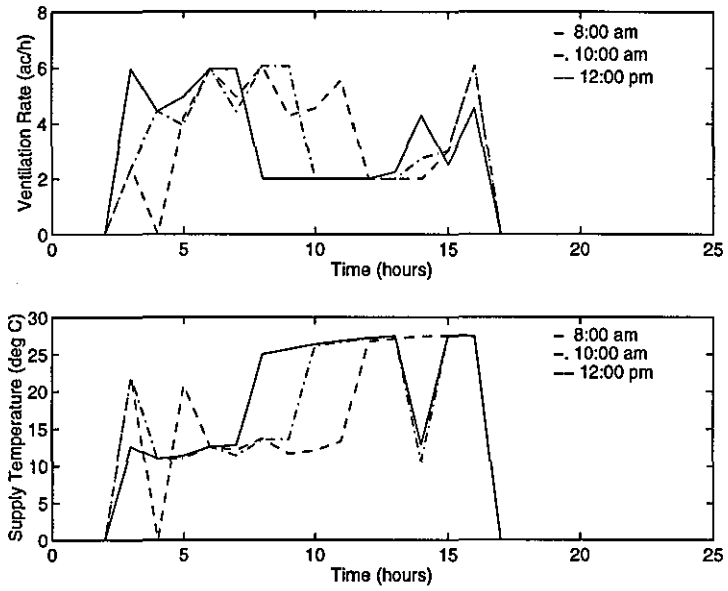


**Figure 6.8, Optimum Scheduling of Control Variables in the Summer under Different Schedule of On-Peak Electricity Tariff**

During the winter operation, the most critical period of occupant comfort is the early occupancy period. Whether the on-peak electricity starts at the same time or later than the occupancy (generally it does not start earlier than occupancy), night preheating to charge the thermal storage is used to reduce the total energy cost; there is no load shifting during the occupancy period. However, the heater may be operated during the off-peak occupancy hours to relieve the instant cooling load if the on-peak electricity starts later than the occupancy.

In summary, the electricity tariff structure and electricity schedule have great influence on the optimum schedule of the plant operation. However, it is also clear from the optimum solutions, that the night precooling and preheating operations are effective in reducing energy cost, due to the use of thermal storage in the ventilated slab.

### 6.1.6 The Influence of Thermal Comfort Limits

As described in Section 3.1.4, a Predicted Mean Vote (PMV) of $\pm$ 0.5 is recommended as a comfort limit for air-conditioned office buildings (ISO, 1984). This corresponds to a Predicted Percentage Dissatisfied (PPD) of 10%. However, in the region of 10%, the PPD is very sensitive to changes in room temperature, which can in turn result in the optimum energy cost being sensitive. The sensitivity of the optimum energy cost in terms of varying the thermal comfort requirement (PPD) for the $13^{th}$ of July 1994 is illustrated in Figure 6.9. It is clear that the energy cost is significantly reduced if the constraint is relaxed. The cost reduction from 10% to 11% PPD is due to the fewer hours chiller operation and lower night precooling ventilation required for the 11% PPD. A significant energy saving is apparent in increasing the PPD from 12% to 13% since this results in the chiller operation being eliminated during the daytime. Such sensitivity depends on the specific ambient and room thermal conditions. For this very hot summer day, the chiller operation can only be avoided when the PPD limit is relaxed to 13%.

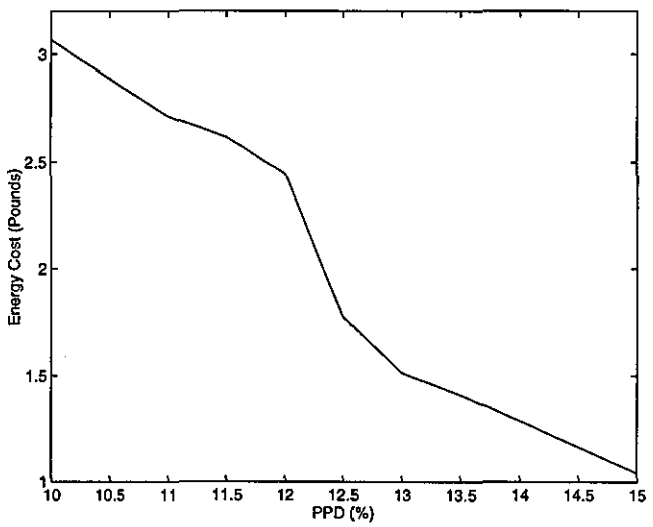


**Figure 6.9, The Sensitivity of Energy Cost with Thermal Comfort**

It is suggested that for fabric thermal storage systems, if a lower thermal comfort requirement is allowed, significant energy savings may be obtained for the operating conditions with a high cooling or heating load.

### 6.1.7 The Influence of Plant Part Load Performance

In this research, an electric heater has been used for heating, the efficiency of the heater having been assumed to be a constant at 90%. However, the chiller part load performance is an important factor that influences the optimum solutions of plant schedule during the summer operation. There are three types of chiller Part Load (PL) performance, 'good', 'poor' and 'flat' (Braun, 1990). The 'good' PL characteristic is usually with a chiller driven by variable-speed motor. A 'poor' PL performance is one which provides the highest $COP$ at the design load and a lower $COP$ at part load. 'Flat' PL performance assumes a constant plant efficiency with respect to changes in load, which is representative of a plant with multiple stages of control to respond to a load. Figure 6.10 gives an example of the 'good' and 'poor' PL characteristic. The two cases have the same $COP$ for a chiller at design conditions but with different sensitivities to the load and temperature differential. The package chiller used in this research is assumed to have a 'poor' PL performance.

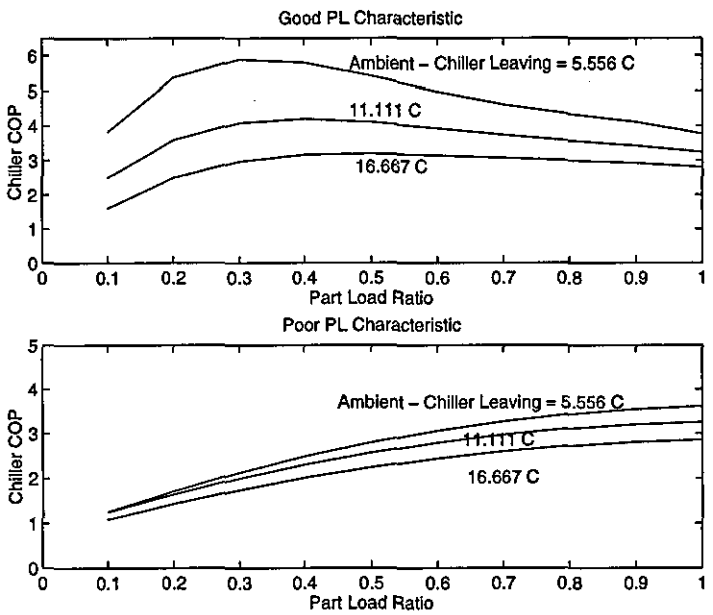


**Figure 6.10, The Chiller Part Load Performance**

If the optimum setpoints from the 'good' PL performance are compared with those from the 'poor' PL performance, it has been found that energy cost savings up to 30% result from the favourable 'good' chiller part load performance. It has also been observed from the optimum solutions that the chiller is less likely to

be operated with 'poor' part load performance, which is usually compensated for by a higher ventilation rate in order to meet a certain cooling load. For specific ambient and room thermal conditions, the optimum control strategy plans the load optimally through simultaneous control of both the fan and the chiller.

Although the ambient conditions, electricity tariff structure, thermal comfort limit and chiller part load performance have large impact on the optimum schedules of plant operation, the characteristics of the operating schedules are dictated by the fact that the night preheating and precooling operations are effective in reducing energy cost and are scheduled to offset the thermal loads during the occupancy period.

## 6.2 Simplified Time-Stage Control

The optimum schedules of plant operation produced by the optimal controller exhibit common characteristics under the summer and winter operations. The control schedules have three distinct stages. The first stage is the precooling or preheating of the thermal store prior to the start of the high electricity tariff period (and the start of occupancy). During this stage, the plant is operated to make as much use of free cooling or heating as possible. The second stage begins at the start of occupancy when ventilation rates are reduced to a minimum. The final stage offsets the room thermal load using higher discharge of the thermal store or use plant direct cooling should the thermal store not be able to offset the load. These are the intrinsic characteristics for the optimal control of the fabric thermal storage system, which have led to the development of a simplified time-stage control strategy.

Figure 6.11 illustrates the control time stages. The start of the high electricity tariff period coincides with the start of occupancy at 8:00 am. $S_1$ signifies the start of plant operation at night with a supply air flow rate of $V_1$. $C_1$-$C_2$ is a period of chiller or heater operation during which the supply air temperature has a setpoint of $T_1$. No temperature setpoint is required during the free cooling periods ($S_1$-$C_1$, $C_2$-8:00, 8:00-$S_2$, $S_2$-$C_3$, $C_4$-16:00), since the supply air temperature is dictated by the ambient temperature and whether the heat recovery device has been selected to be in operation or not. From the start of occupancy (8:00) to $S_2$ is a period of

minimum ventilation rate. $S_2$ signifies the second stage of high cooling or heating with the ventilation rate set to $V_2$, and a supply air temperature setpoint of $T_2$ during chiller or heater operating period $C_3$-$C_4$. The plant operation stops at the end of occupancy (16:00).

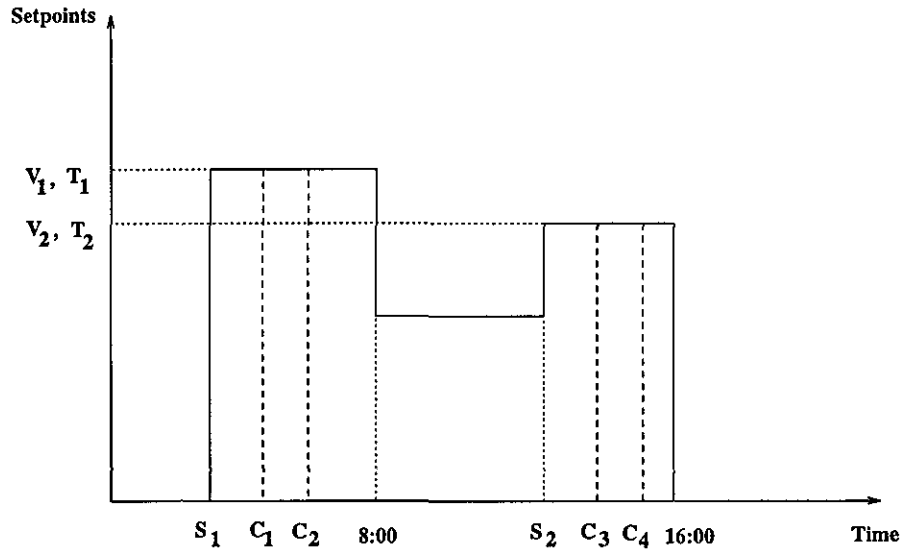


**Figure 6.11, Simplified Time-Stage Control**

If the peak electricity period starts at a different time, for instance, 10:00 am, the period between 8:00 am and 10:00 am is a distinct stage where the occupant comfort is required and the electricity is cheaper, such that the plant can be operated to shift the thermal loads from the on-peak occupancy period. This control stage is not included in the time-stage controller developed in this thesis (Figure 6.11), however, the characteristics of the operating schedules obtained from the setpoint scheduling control (Figure 6.8, Section 6.1.5), indicate that this electricity schedule can be easily modelled by adding another time stage between 8:00 am and 10:00 am to the time-stage controller.

The optimization problem of the time-stage controller is therefore reduced from 48 variables to 15 variables, consisting of 6 time stage variables ($S_1$, $C_1$, $C_2$, $S_2$, $C_3$, $C_4$), 4 setpoints ($V_1$, $T_1$, $V_2$ and $T_2$) and the ON/OFF operation of the heat recovery device in each of the 5 free cooling periods. This framework makes for robust supervisory control which tends to eliminate the short periods of chiller or heater operation and the frequently varying fan flow rate operation observed in

the optimum schedules of plant setpoints in Section 6.1. The same GA has been applied to solve the time-stage control problem as used in the setpoint scheduling control, the performance of the GA in finding the optimum solutions to this problem having been discussed in Section 5.4.

Figure 6.12 illustrates the optimal time-stage control strategy for the $13^{th}$ of July 1994. The chiller is in operation for 4 hours during the night and 2 hours during the occupancy period. The heat recovery device is in use for the free cooling periods. Figure 6.13 displays the optimum solution from the time-stage controller for the $14^{th}$ of February 1994. The electric heater is operated for 3 hours with full recirculation before the start of occupancy. The minimum ventilation is supplied with the heat recovery device in operation throughout the occupied hours.

Figure 6.12 and Figure 6.13 indicate that the time-stage control encompasses the characteristics of the optimum scheduling of the supply air flow rate and temperature, the main difference being that in the time-stage control, one hour night chiller operation is moved to the occupancy period in summer, and one hour fewer preheating is used in winter. A further comparison of the controllers' performance is discussed in Section 6.3.

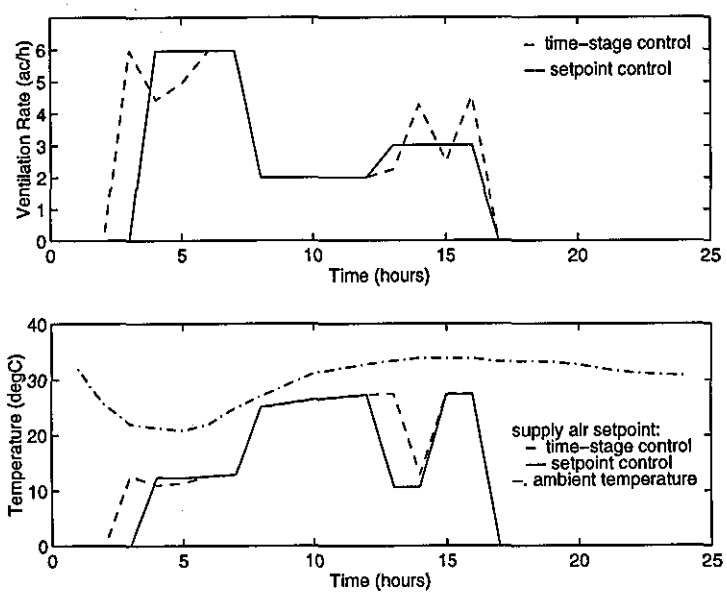


**Figure 6.12, Comparison of Optimal Scheduling of Control Variables from Two Controllers under Summer Operation**

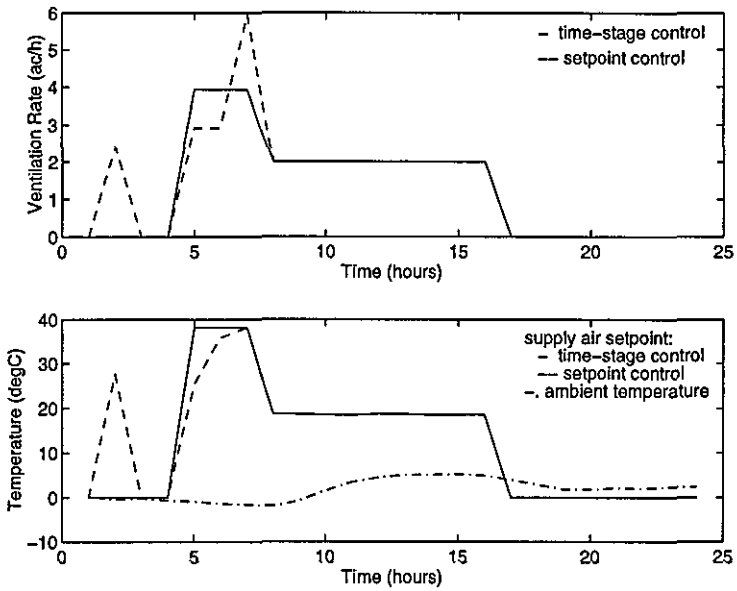


**Figure 6.13, Comparison of Optimal Scheduling of Control Variables from Two Controllers under Winter Operation**

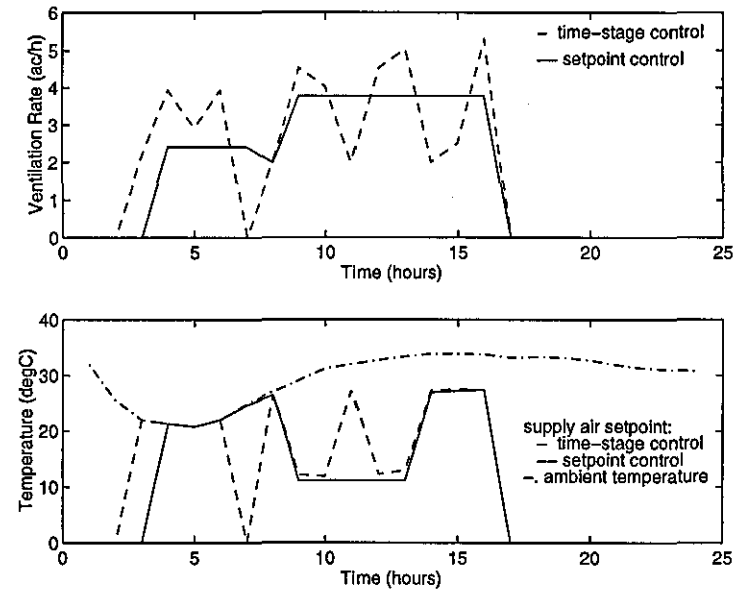


**Figure 6.14, Comparison of Optimal Scheduling of Control Variables from Two Controllers in the Summer Under a 1:1 Electricity Structure**

The optimum control strategy from the time-stage control under the 1:1 electricity tariff structure is examined in Figure 6.14 for the $13^{th}$ of July 1994. It is clear that the time-stage control appropriately simplifies the plant operation with

encompassing characteristics in comparison to the optimum setpoint control.

In summary, the time-stage controller simplifies the control problem and provides more stable plant operating conditions. It can be seen from the optimum results that the time-stage control can encompass the control characteristics indicated in the optimum setpoint scheduling control under various operating conditions, including the summer and winter operation, and electricity structures of 3:1 and 1:1.

## 6.3 Relative Performance of the Controllers

The performance of the optimum setpoint scheduling control, the time-stage control and the conventional control strategy (as described in Section 2.2.1), has been compared for two weeks in the summer and one week in the winter of 1994. During the first summer week, 24$^{th}$ to 30$^{th}$ June, the cooling load is such that the comfort constraints could be met without the use of mechanical cooling. Mechanical cooling is however necessary during the second week, 9$^{th}$ to 15$^{th}$ July. In the third week of the winter from 12$^{th}$ to 18$^{th}$ February, mechanical heating is required. The 3:1 electricity tariff is applied and a nominal cost of £0.10/kWh is used for the cost of off-peak electricity.

### 6.3.1 Summer Operation

Table 6.2 indicates the relative performance of the controllers for the week when no mechanical cooling is required in the summer (24$^{th}$ to 30$^{th}$ June). The thermal comfort in the zone is maintained under all three control strategies, with on average a slightly cool room (PMV below 0) resulting from the conventional controller and a slightly warm room resulting from the optimum controllers (PMV above 0). The energy cost from the optimum setpoint scheduling control is £0.54, with an energy consumption of 1.95 kWh, whereas the conventional control energy cost is £6.08 and consumes 28.07 kWh of energy. From these results, it is clear that the optimum setpoint scheduling control strategy leads to significant savings in both the energy use and cost. This is due to shorter periods of precooling operation, and indeed for some days, the plant is controlled with minimum ventilation throughout the

occupancy period and without precooling at night. However for the conventional control, a constant ventilation rate is applied for both the night and the day. Since under the conventional control strategy, the ventilation operation is based on if-then rules, it is impossible to take account of the hourly varying ambient and room thermal conditions. Although under the conventional control strategy, the occupant thermal comfort is satisfied during the week, the plant is operated for unnecessarily longer hours of precooling, which results in a slightly cool zone comfort condition. The optimum time-stage control has a similar performance to the optimum setpoint scheduling control, the difference being due to a slightly different strategy for the operation of the heat recovery device.

| Type of Controller | Energy Cost (£) | Energy Use (kWh) | Mean PMV | Maximum PPD (%) |
|---|---|---|---|---|
| Conventional Control | 6.08 | 28.07 | -0.2 | 9.4 |
| Setpoint Scheduling | 0.54 | 1.95 | 0.1 | 10.1 |
| Time-stage Control | 0.52 | 1.74 | 0.1 | 9.9 |

**Table 6.2. Performance Comparison for 24$^{th}$ to 30$^{th}$ June**

Table 6.3 compares the control strategies where mechanical cooling is required if the thermal comfort conditions are to be maintained throughout the occupancy period. The energy cost from the conventional control strategy is £5.98 with an energy consumption of 27.03 kWh. The energy cost under the setpoint scheduling control is £6.58 and the energy consumption 42.86 kWh. Although the mean PMV under the conventional control is relatively low, the comfort conditions in the occupied zone are frequently unacceptable with a maximum PPD of 19.8 %. This is due to the conventional control not including any chiller operation and the ambient air temperature remaining high throughout the night, which prevents effective precooling of the ventilated slab and results in the conventional controller only assigning short periods of night ventilation. This leads to a lower energy consumption than for the operation under moderate thermal gains as for the first test period (Table 6.2). The higher energy consumption and cost from the optimum control is due to the chiller operation which is necessary to maintain thermal comfort. During the period of the highest thermal load, the chiller is in operation for a few hours at night and one hour during the occupancy period. It is also evident that although the plant energy consumption is much higher than that from the conventional control, the energy cost is only marginally higher.

| Type of Controller | Energy Cost (£) | Energy Use (kWh) | Mean PMV | Maximum PPD (%) |
|---|---|---|---|---|
| Conventional Control | 5.98 | 27.03 | 0.2 | 19.8 |
| Setpoint Scheduling | 6.58 | 42.86 | 0.3 | 10.4 |
| Time-stage Control | 7.20 | 45.72 | 0.2 | 10.0 |

**Table 6.3. Performance Comparison for $9^{th}$ to $15^{th}$ July**

The optimum time-stage control results in a higher energy consumption and cost than for the setpoint scheduling, but has the same basic strategy. This slight degradation in the controller performance is due to the simplification from the setpoints' characteristics to the simple stages of plant control. The simplifications make it more difficult to account for hourly changes in thermal load but leads to a more stable plant operation.

### 6.3.2 Transition Season Operation

The controller performance in the transitional seasons is similar to that in the first week in Table 6.2. The occupant comfort is usually satisfied by the three control strategies, while the energy cost and energy use from the conventional control are significantly higher than those from the optimal control strategies.

### 6.3.3 Winter Operation

During winter operation, Table 6.4 indicates a sharp distinction between the thermal comfort under the conventional control and optimum control strategies. The mean PMV under the conventional control is lower than the acceptable -0.5 comfort requirement, with a maximum PPD of 21.0%, frequently occurring during the early occupancy hours in the latter part of the week. Further, the energy cost is higher than that from the optimum control strategies, mainly due to the constant supply air flow rate regardless the hourly varying heating load requirement. The optimal setpoint scheduling control results in a cost of £15.25 and energy use of 148.95 kWh. The lower cost and higher energy consumption of the optimum control strategies is an evidence of the efficient use of thermal storage and taking

advantage of lower cost of electricity at night. The thermal comfort is maintained throughout the occupancy periods under the optimal control strategies, the room being under the cool comfort with the mean PMV lower than 0.

| Type of Controller | Energy Cost (£) | Energy Use (kWh) | Mean PMV | Maximum PPD (%) |
|---|---|---|---|---|
| Conventional Control | 16.21 | 129.36 | -0.7 | 21.0 |
| Setpoint Scheduling | 15.25 | 148.95 | -0.4 | 10.1 |
| Time-stage Control | 13.90 | 135.56 | -0.4 | 10.0 |

**Table 6.4. Performance Comparison for $12^{th}$ to $18^{th}$ February**

Since during the winter operation, the coupling between the ambient and the room internal thermal conditions is much reduced compared with the summer operation, changes in the ambient air temperature only slightly affect the supply air temperature to the slab. The elimination of short periods of plant operation (Section 6.2) results in the lower cost from the time-stage control compared with that from the setpoint scheduling control. Generally, the time-stage control performs better than the setpoint scheduling control during the winter and transition season operation due to its robust schedules of the plant operation, with lower energy cost and energy use. However, in typical hot summer days, the performance of the time-stage controller is degraded due to the simplifications to the setpoint schedules which make it more difficult to adapt to varying ambient and room thermal conditions.

## 6.4 Conclusion

This chapter has investigated the characteristics of the optimum control strategies for the hollow core ventilated slab system under various operating conditions, including seasonal operations, varying occupant thermal comfort requirements, different electricity tariff structures and different plant part load performance. Results have shown that the optimum control strategies can indicate clear characteristics, which are dictated by the fact that the night preheating and precooling operations are effective in reducing energy cost and to offset the thermal loads

during the occupancy period. During the summer, the general characteristics are that the low ambient air temperature and off-peak electricity tariff leads to high ventilation rates at night, followed by an initial period during occupancy when the ventilation rate is set to a minimum. The ventilation rate may be increased later in the day to compensate for higher thermal loads. Similarly, where mechanical cooling is required, the chiller will be operated during the off-peak period with supplementary operation during peak periods only when necessary. During the winter, preheating is used to charge the thermal store using higher ventilation and higher supply air temperature. When the occupancy starts, only minimum ventilation is used with the heat recovery device in operation.

The investigation of the control characteristics has led to the development of a simplified time-stage controller. The performance of the two optimum controllers, the supply air setpoint scheduling and the time-stage controller, in reducing energy costs and maintaining room thermal comfort has been investigated under seasonal operation. In comparison to a conventional rule-based controller, the optimal controllers provide significant energy cost savings and improve thermal comfort in the occupied space.

The perfect knowledge of the next day's weather conditions has been assumed in this chapter to investigate the control characteristics and relative performance of the controllers. Since in practice, the next day's weather conditions are unknown at the time of scheduling the plant operation, a weather prediction model is required to supply the weather information. The weather prediction model is investigated in Chapter 7. The performance of the optimal controllers may be degraded due to prediction errors in the ambient conditions. This is discussed in Chapter 8.

# Chapter 7

# Weather Prediction

## Introduction

In the investigation of the characteristics of the optimum supervisory controller in Chapter 6, perfect prediction of the next day's weather conditions is assumed. However, the implementation of such a controller requires an appropriate weather model to predict the ambient conditions for the next 24 hours, so that the controller can estimate the optimum plant operating schedule. In this research, the weather prediction model must be able to predict ambient air temperature and solar radiation with acceptable accuracy, since these climatic variables are the most significant in influencing the room thermal environment; moisture is not modelled.

Throughout this chapter, two sets of weather data have been selected to analyse the performance of the weather prediction models: the CIBSE weather year, measured at Kew Station from October 1964 to September 1965, and the data collected at Garston, Watford, UK during 1994. The period of data used for any particular analysis has been selected to best illustrate the particular performance of the model.

## 7.1 A Review of Weather Prediction Models

External climatic conditions, such as outdoor air temperature and solar radiation, fluctuate randomly with time, leading to fluctuating heating and cooling loads in the building space. Most previous research has focused on the development of predictive algorithms for heating and cooling loads instead of the climatic variables in the control of building systems (MacArthur *et al.*, 1989; Seem and Braun, 1991). In the power utility industry, interest in electrical load prediction has also led to some research. An algorithm for load forecasting that combines knowledge based rules and statistical techniques was developed by Rahman and Hazim (1992), in which the weather-load relationship was established.

Hybrid techniques have been commonly used for short-term load profile prediction, in which the load is divided into several parts, including base load (deterministic), weather-sensitive (or dependent) and random load (El-keib *et al.*, 1995; Fan *et al.*, 1993). In this method, the weather-sensitive load is related to the weather conditions and is modelled by a cubic polynomial function of the average equivalent temperature, which is calculated from the ambient temperature and humidity or wind-speed. The random part is modelled by an ARMA[1] model, where the on-line Weighted Recursive Least Square (WRLS) algorithm is used to estimate and update the model parameters for forecasting the load.

For the prediction of heating and cooling loads, Forrester and Wepfer (1984) used a simple linear regressor to predict the load up to four hours ahead for a large commercial all-electric building. MacArthur *et al.* (1989) developed an on-line recursive estimation algorithm for load profile prediction, in which the present load was predicted by the preceding load and ambient temperature and the present temperature. In order to predict the load profile, a clockwise recursive regression algorithm was developed. The input to the load forecast was a profile of ambient temperatures. The temperature profile was predicted using a shape factor method that used the maximum and minimum ambient temperatures. The profile was updated with each new measured maximum and minimum temperatures.

Seem and Braun (1991) developed adaptive methods for real-time forecasting of building electrical demand, which were also applicable to cooling/heating load forecasting. In this method, the load is divided into deterministic and stochastic

[1]Auto Regressive Moving Average

parts. The deterministic part is calculated by a CMAC[2] model, the stochastic part by an ARMA model. It was also suggested that the accuracy of load prediction could be greatly improved by an adequate ambient temperature forecast model.

Rupanagunta *et al.* (1995) investigated the optimal scheduling of ice thermal storage under the predicted load profile. The ambient temperature was forecast by an EWMA[3] model, which was then input to the load forecast module to predict the load profile. The load forecast module was modelled by a centered moving average method.

Ferrano and Wong (1990) developed an artificial neural network (ANN) model to predict the next day's storage load for an ice thermal storage system. Kawashima *et al.* (1995) presented a comparison of the ARIMA[4], EWMA, LR[5] and ANN models in predicting the thermal load for the next 24 hours, the results showing that the ANN model gave the lowest prediction errors. The ambient temperature profile was the input to the ANN model and was predicted using empirical shape factors and assumed daily highest and lowest temperatures.

### 7.1.1 Weather Prediction and Weather Model

Since the fluctuation in building loads is dampened by the building mass, the prediction of ambient conditions for predicting the load profile is less critical than it is for the predictive control of the building thermal plant, where an accurate weather prediction algorithm is required to obtain an acceptable control response. According to Hartman (1988), the purposes of a weather predictor in a building dynamic control are: to switch the basic operating modes of the plant such that the building space thermal requirement is satisfied and the energy use is reduced by maximizing the use of thermal storage in buildings; and to supply the next day's temperature for use in setpoint calculations.

Holst *et al.* (1987) proposed a controller that incorporated the predicted hourly

[2]Cerebellar Model Articulation Controller. A CMAC controller uses a look-up table to determine the relationships between the inputs and outputs of a system.

[3]Exponential Weighted Moving Average

[4]AutoRegressive Integrated Moving Average

[5]Linear Regressive models

ambient temperature for minimizing energy use, by optimizing the linear feedback controller gain. The weather prediction was calculated by a stochastic dynamic model, established by a combination of physical facts and empirical information, which was obtained by an analysis of several years of weather data. It was claimed that the use of the predicted climatic variables in the controller design achieved an improvement in the room thermal comfort and more stable heating supply. Athientis (1988) developed a predictive control algorithm which could identify an optimum profile of thermostat setpoints under the predicted weather conditions, so that the value of the room air temperature was kept below a maximum allowable limit while reducing energy consumption. The climatic variables, ambient temperature and solar radiation, were modelled by sinusoidal functions. Chen and Athienitis (1996) investigated an on-line adaptive generalized predictive controller with a feedforward control scheme. The zone setpoint was optimized through an on-line simulation based on the adaptive model of a heating process and prediction of solar radiation and ambient temperature. The ambient temperature prediction included identification of the next day's temperature wave pattern and prediction of the temperature profile. These two steps involved predicting daily maximum and minimum temperatures of the next day, and calculating the shape factors for temperature-up and temperature-down periods. Solar radiation was predicted by means of local weather profile forecast, such as cloudy sky, and then being corrected based on the measured solar intensity.

Weather prediction is generally used for on-line supervisory control of the building thermal plant, where the ambient conditions are usually forecast in short-term. A number of research studies have also investigated weather simulation models for the analysis of design load and annual energy uses (Hokoi and Matsumoto, 1988; Yoshida and Terai, 1990/1991). Such weather models are usually comprehensive in modelling the behaviour of annual, seasonal and diurnal weather variations. A weather model was developed for load calculation (Yoshida and Terai, 1990/1991; 1992), in which an ARMA model was applied with a system identification technique to weather data. The weather model took account of the deterministic annual and diurnal periodicity and the stochastic variations in the climatic variables, including the ambient air temperature, solar radiation and absolute humidity. The stochastic properties of the heating load of an intermittently air conditioned building were analysed (Hokoi and Matsumoto, 1988; Matsumoto *et al.*, 1990/1991), so that the maximum load and load distribution for the optimum design of the building system could be derived. The load was derived from the modelling of

the ambient air temperature which was calculated by a sinusoidal time series and an ARMA model. Jiang and Hong (1993) investigated the stochastic properties of the building thermal processes by a stochastic weather model, where the daily climatic variables were modelled by deterministic and stochastic parts. The hourly data were obtained by interpolation using shape factors that transformed the daily estimation to the hourly data. Such shape factors were considered to be constant within a month. The random thermal behaviour of the building spaces caused by stochastic weather conditions was then studied by the state-space method. Schibuola and Romagnoni (1996) also developed a weather model for long term energy analysis, using shape factors to generate hourly ambient temperature and hourly radiation data from the monthly averaged daily maximum and minimum temperatures and daily total radiation.

It is clear that modelling techniques for the climatic variables vary in detail with different applications. The requirement of the weather prediction model in this research has been discussed in Section 3.3.2. It is distinctly different from those of other applications, in that the profile of the weather conditions for the next 24 hours is required and should be updated with available ambient information at the end of every day. The method used for weather prediction in this research could be similar to that previously used for load profile prediction (MacArthur *et al.*, 1989). Since the model parameters are updated at the end of every day, it is not necessary to model the macro behaviour of the weather annual periodic and random changes. This differs from the weather model developed by Yoshida and Terai (1990/1991; 1992), where from the previously measured weather data, the properties of the data were analysed and the weather model developed to fit these data. The model had two components, the deterministic periodic component and stochastic component, each of which was divided into low, medium and high frequency (these frequency bounds corresponding to annual average, annual periodicity and diurnal periodicity in the deterministic term). In essence, their weather model is a simulation model, whereas the weather prediction model required for this research must be a forecaster that is updated every day to adapt to the new weather conditions.

Of the methods available, ARMA, EWMA, sinusoidal functions and neural network models can be used to develop a weather predictor for this research. A neural network model requires a large quantity of training data which limits the applicability of this method. Furthermore, the network would require a high number of

output variables (24 dimensions for each variable). There are also difficulties in determining the input variables, since the next day's weather profile is not only dependent on the previous day's, but may also on the preceding days. In addition, there are also correlations between the different climatic variables. Therefore, the neural network models have not been used for weather prediction in this research. EWMA and sinusoidal functions are deterministic models. Due to the randomness of the weather data, a stochastic model is also required. In this thesis, a variety of methods have been investigated and compared in Section 7.2.8. The most competent and thus adopted method in this research, is to divide the climatic variables into deterministic and stochastic parts. The deterministic part is calculated by an EWMA model, the stochastic part modelled by the ARMA time series technique.

The weather predictor has two main functions: temperature prediction and solar radiation prediction. The control and therefore modelling of humidity is not investigated in this research.

## 7.2 Temperature Prediction

The ambient dry bulb temperature is a main source of uncertain disturbances upon building thermal processes. The predictive controller requires information about the ambient temperature to calculate the optimum schedule of plant operating setpoints. The temperature prediction models are investigated from an analysis of the stochastic properties of the ambient temperature.

### 7.2.1 The Properties of Temperature Time Series

Two sets of weather data have been used to investigate the stochastic properties of the ambient temperature time series: the CIBSE year weather data and data collected at Garston, Watford, UK in 1994. Figure 7.1 shows the profiles of the hourly mean and standard deviation of the ambient temperature for the CIBSE year and 1994. It is observed that the properties of the temperature data are time-dependent and thus a nonstationary stochastic time series.

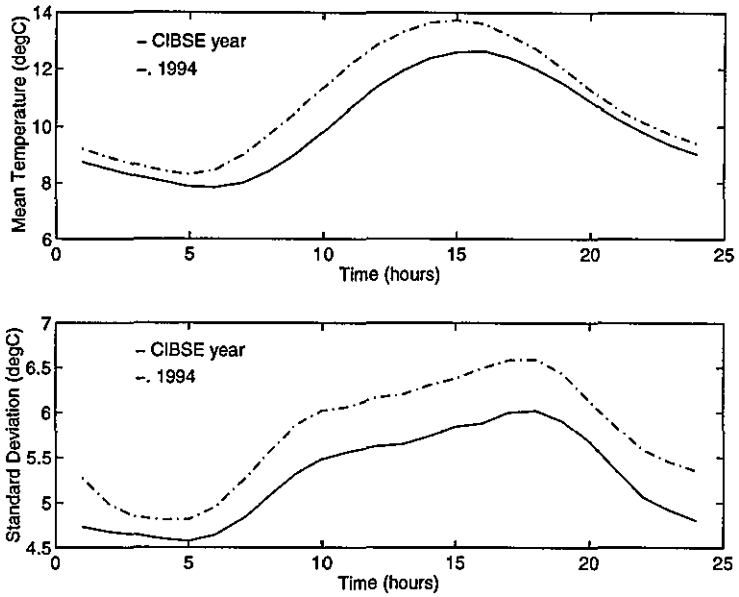


**Figure 7.1, Hourly Mean and Standard Deviation of the Ambient Temperature**

The development of a weather model is complicated by the fact that the climatic variables are correlated to each other. Yoshida and Terai (1990/1991) suggested that the following assumptions can be made to simplify the problem:

- solar radiation is not correlated to any other variable;
- temperature is only correlated to the solar radiation;
- humidity is correlated to both solar radiation and temperature.

Further, it was found from an analysis of annual weather data (Yoshida and Terai, 1990/1991), that it is the daily variation of climatic variables that has the most significant role in standard deviations for all the variables among monthly, daily and hourly sampled data. Thus the daily climatic variables can be modelled according to the above assumption, while the hourly sampled data can be modelled independently without considering the correlation between the solar radiation, temperature and humidity. To further justify this assumption, the daily average temperature and daily total global radiation have been computed from the hourly sampled data. It was found that over the entire year, there is a strong correlation between the two variables, with a correlation $\rho_{xy}$[6] $= 0.5 \sim 0.6$ from the two sets

[6] $\rho_{xy}$, correlation coefficient between $x$ and $y$, 0=no correlation, 1=complete correlation

of weather data. Such correlation can be seen in Figure 7.2, which indicates that in the summer higher radiation leads to higher temperature; and in the winter, lower radiation has a corresponding lower ambient temperature. However, there is no such strong coupling between the two variables from the monthly calculated correlations, which vary between $\rho_{xy} < 0.1$ to $\rho_{xy}$=0.6 depending on the month. The monthly correlations are also inconsistent. For instance, in July from the CIBSE year data, $\rho_{xy} = -0.14$, suggesting that the daily total solar radiation has a negative effect on the daily average temperature. This reflects the randomness of the two variables, especially the total solar radiation, which is strongly affected by cloudiness.

This suggests that it may not be necessary to consider the correlation between the daily average temperature and daily total solar radiation for the short-term weather prediction, when using the recent historical data, as the influence of the solar radiation on the ambient temperature may have already been reflected in the historical temperature itself. Therefore, the solar radiation and ambient temperature can be calculated independently. This will be justified in the following investigation by comparing the prediction methods for modelling the temperature data.

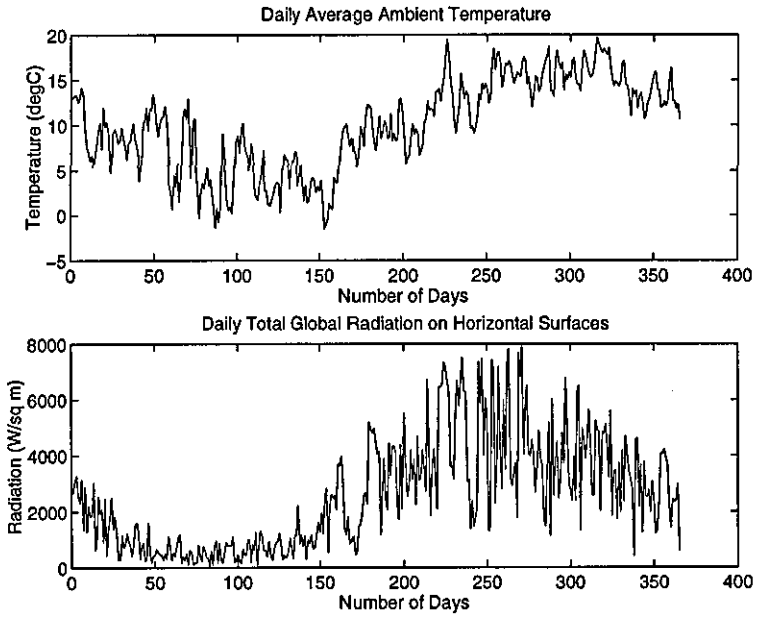


**Figure 7.2, Daily Average Ambient temperature and Total Global Radiation in CIBSE Year**

Though the temperature data are a nonstationary time series, Pandit and Wu

(1983) argued that an ARMA system could sufficiently model a nonstationary time series by a proper selection of its parameters. The trend or periodicity exhibited in the data could be reflected in the roots of the parameters. However, by making the raw temperature time series stationary, the number of parameters of the ARMA model can be substantially reduced. In this thesis, three methods of using ARMA models have been investigated. The first approach, to be referred to as a 'pure stochastic method', is to model the nonstationary temperature time series, using the raw temperature data to estimate the parameters of the ARMA model. The second method, termed the 'combined deterministic-stochastic method', models the stationary stochastic time series which is derived by subtracting the deterministic component out of the raw temperature data, so that the stochastic element can be calculated using a reduced order ARMA model. The deterministic component represents the periodicity and trend of the hourly ambient temperature. In the third method, the daily average temperature is modelled separately, with the amplitude being calculated by the same model as in the 'combined deterministic-stochastic method'. This is termed as 'expanded combined method'. The details of these three methods are presented below, followed by analysing and comparing their performance in Section 7.2.8.

The ARMA model is used in all three methods and is the basic technique used in this research to model the stochastic data series.

### 7.2.2 ARMA Models

An ARMA model is a statistical technique which uses stochastic linear difference equations to model the dependence of the data (Pandit and Wu, 1983). The model can then be used to forecast the future behaviour of the system described by the data. Since the temperature data are dependent or correlated between the observations, an ARMA model can be used to describe such dependence. The basic formula of an ARMA model is,

$$X_t = \phi_1 X_{t-1} + \phi_2 X_{t-2} + ... + \phi_n X_{t-n} + a_t - \theta_1 a_{t-1} - \theta_2 a_{t-2} - ... - \theta_m a_{t-m} \quad (7.1)$$

where,

$X_{t-i}$: observation of the temperature at $i$ time step prior to time $t$, $i = 0, 1, ..., n$,

$a_{t-j}$: sequence of uncorrelated Gaussian white noise, $j = 0, 1, ..., m$,

$\phi_i$: autoregressive parameters with an order of $n$, $i = 1, 2, ..., n$,

$\theta_j$: moving average parameters with an order of $m$, $j = 1, 2, ..., m$.

The parameters $(\phi, \theta)$ are determined so as to minimize the residual $J$ based on the least squares criterion for the number of $N$ data inputs,

$$\min \ J(\phi, \theta) = \sum_{t=1}^{N} a_t^2 \tag{7.2}$$

An off-line parameter identification technique has been used to estimate the parameters for modelling the weather data in this research. The procedure involves collecting the ambient temperature observations at present day and preceding days, and identifying the parameters at end of the day based on the criterion in Equation 7.2. The parameters are then held constant for forecasting the next day's weather condition. An on-line parameter identification approach may also be used. Slow time-varying systems can be tracked using a recursive least squares algorithm to estimate the parameters. However, the accuracy of the on-line parameter estimation may be reduced due to the linearized least squares approach used in calculating the parameter values (Ljung, 1987). At each step of the calculation, the parameters is updated with the new available observations. Updating the parameters recursively at each time step may improve the accuracy of the forecast one or two steps ahead using the new available information; however, this may not be beneficial to the profile forecasting with a long lead time, due to the random behaviour of the temperature. This will be further discussed in Section 7.2.7. Another disadvantage of the on-line approach is that the model structure must be determined before starting the recursive identification procedure. Therefore, the off-line approach has been adopted in this research.

Although an ARMA model is a linear expression of the dependence between the observations, a nonlinear regression routine is required to estimate its parameters, since an ARMA model is nonlinear in the parameters $(\phi, \theta)$ when $X_t$ (Equation 7.1) is expressed in terms of the past observations and the moving average parameters are present $(m \geq 1)$. For instance for an ARMA(2,1)[7] model, $a_{t-1}$ is recursively

[7]ARMA(2,1) indicates autoregressive parameters of order 2, and moving average of order 1

expressed by,

$$a_{t-1} = X_{t-1} - \phi_1 X_{t-2} - \phi_2 X_{t-3} + \theta_1 a_{t-2}$$

The ARMA(2,1) then becomes,

$$X_t = \phi_1 X_{t-1} + \phi_2 X_{t-2} - \theta_1 (X_{t-1} - \phi_1 X_{t-2} - \phi_2 X_{t-3} + \theta_1 a_{t-2}) + a_t$$

The estimation equation is thus nonlinear in terms of the parameters $(\phi, \theta)$. In this thesis, the Marquardt nonlinear regression method is used to estimate the ARMA model parameters (Pandit and Wu, 1983). The method is a compromise between the Gauss and steepest descent methods. Starting from an initial guess, the method iteratively minimizes $\sum_{t=1}^{N} a_t^2$ by directing the search along the smaller sum of squares of $a_t$'s.

Two weeks weather data are taken as historical observations to estimate the ARMA model parameters, since one week may be too short a period to contain a sufficient variety of patterns of the weather conditions. For instance, in one week, the ambient temperature may be extraordinarily low, in comparison to the normal temperature for the period. A longer period than two weeks can also be used, however, the results indicated no significant improvement, while the computational intensity for estimating the model parameters was increased.

### 7.2.3 Characteristics and Selection of the Order of ARMA Models

The principal difference between ARMA models from ordinary regression models is that ARMA models are dynamic, since they have 'memory' of the disturbance entering the system preceding the present time. This dynamics or memory of an ARMA model can be described by two functions. The first is Green's function $G_j$, which describes the dynamics in terms of the past disturbances $a_t$'s:

$$X_t = \sum_{j=0}^{\infty} G_j a_{t-j} \tag{7.3}$$

where $G_j$ can be calculated from the parameters $(\phi, \theta)$ in Equation 7.1. The dynamics of an ARMA system can also be represented by the inverse function, $I_j$. This indicates the influence of past $X_t$'s on the present $X_t$ by decomposing $X_t$ as a linear combination of past $X_t$'s:

$$X_t = \sum_{j=1}^{\infty} I_j X_{t-j} + a_t \tag{7.4}$$

Green's function imposes stability restrictions on the parameters of ARMA models, since $G_j$ characterizes how slow or fast the dynamic response of a system is to any particular decays in $a_t$. If the system is stable, then Green's function remains bounded. Stability implies that the memory of a distant and past $a_t$ is zero. Given sufficient time, the influence of a single $a_t$ injected in the system will eventually decay, and the system will return to its equilibrium or mean position (Pandit and Wu, 1983). The rate and type of decay will depend upon the roots $\mu_k$ of the autoregressive parameters, which can explicitly represent the stability requirement as follows:

$$| \mu_k | < 1, \quad k = 1, 2, ..., n$$

Using the backshift operator, $B^n X_n = X_{t-n}$, Equation 7.5 illustrates the autoregressive parameters of an ARMA model by their roots $\mu_k$ $(k = 1, 2, ..., n)$:

$$(1 - \phi_1 B - \phi_2 B^2 - ... - \phi_n B^n) = (1 - \mu_1 B)(1 - \mu_2 B)...(1 - \mu_n B) \qquad (7.5)$$

The boundedness of the inverse function $I_j$ imposes 'invertibility' restrictions on the parameters of an ARMA model, since the more distant the past $X_t$ is, the smaller the influence it should have on the present. The invertibility requirement can be described by the roots of the moving average parameters, $\nu_k$:

$$| \nu_k | < 1, \quad k = 1, 2, ..., m$$

If $| \nu_k | > 1$, the inverse function increases without bound. Similarly, the moving average parameters can be represented by their roots $\nu_k$ $(k = 1, 2, ..., m)$:

$$(1 - \theta_1 B - \theta_2 B^2 - ... - \theta_m B^m) = (1 - \nu_1 B)(1 - \nu_2 B)...(1 - \nu_m B) \qquad (7.6)$$

The stability and invertibility should be checked each time the parameters are estimated for an ARMA model. Generally, these requirements can be satisfied by a proper initial guess that satisfies the invertibility condition, which can be calculated using an AR model and the inverse function (Pandit and Wu, 1983).

In identifying the appropriate order of an ARMA system, a practical and proper way is to increase the order by two instead of one each time a new model is evaluated. This is due to the configuration of the characteristic of the roots $\mu_k$ of the autoregressive parameters, and also due to a system of $n$ degrees-of-freedom being governed by a $2n^{\text{th}}$ order differential equation (Pandit and Wu, 1983). For an ARMA$(n, m)$ model, only $n - 1$ moving average parameters $\theta_i$ $(i = 1, 2, ..., m)$ are independent and need to be specified. Consequently, ARMA$(2n, 2n - 1)$,

$n = 1, 2, ...$, is the sequence to be used for determining the appropriate order of the system.

The order of an ARMA model can be identified by two criteria. The first is the F-criterion, which indicates the improvement in the sum of squares of residuals $\Sigma a_t^2$, in going from the lower order ARMA$(2n, 2n-1)$ to the higher order ARMA$(2n+2, 2n+1)$. If this is insignificant, then the lower order of $2n$ is adequate in characterizing the data series. The F-criterion is only applied when one or both of these models are themselves acceptable. The second test is necessary for checking the adequacy of an ARMA model, the autocorrelations of the residuals $a_t$'s being sufficiently small, within $\pm\frac{2}{\sqrt{N}}$ band. Under this condition, there is 95% confidence level that the expected value of the residual autocorrelations is zero, which ensures that $a_t$'s are independent on each other.

If the ARMA$(2n, 2n-1)$ model is acceptable, its order may be further reduced by an examination of the parameters obtained. For instance, if the values of the highest order parameters, $\phi_{2n}$, $\theta_{2n-1}$ are small compared to the largest absolute value of other orders, and if their values fall within an interval (confidence interval) which includes zero, the order may be reduced to ARMA$(2n-1, 2n-2)$. If the F-criterion test of the new order proves to be insignificant, then the Moving Average (MA) order of parameters can be further dropped, until the adequate model with the smallest number of parameters is reached (even down to AR$(2n-1)$). Through this procedure, if the MA parameters are sufficiently small, they can be completely ignored (Pandit and Wu, 1983).

The off-line approach adopted for parameter estimation in this research enables the optimum model structure for modelling the data of different periods. Since the weather profile prediction is required and conducted at the end of every day, the optimum order of the ARMA system can be identified and changed day by day.

The pure stochastic method estimates the parameters $(\phi, \theta)$ by applying the raw data to Equation 7.1, thereby the following day's ambient temperature profile is forecast. This method is simple and only uses an ARMA model, however, as will be seen in Section 7.2.6, its model structure with a high order of parameters can be much more complicated than the combined method.

### 7.2.4 The Combined Deterministic-Stochastic Method

It is likely that the order of an ARMA model can be reduced by modelling separately the deterministic periodicity of the temperature time series. In the combined deterministic-stochastic method, the deterministic component has been modelled by either an EWMA (Exponential Weighted Moving Average) model or a sinusoidal function.

#### EWMA model

An EWMA model is a special case of the ARMA(1,1) model with $\phi_1 = 1$, $\theta_1 = 1 - \lambda$, being of the form,

$$\hat{X}_t = \lambda X_{t-1} + \lambda(1-\lambda)X_{t-2} + ... = \sum_{j=1}^{\infty} \lambda(1-\lambda)^{j-1} X_{t-j} \tag{7.7}$$

Equation 7.7 can be rearranged as,

$$\hat{X}_t = \hat{X}_{t-1} + \lambda\left(X_{t-1} - \hat{X}_{t-1}\right) \tag{7.8}$$

Equation 7.8 shows that the forecast $\hat{X}_t$ can be simply computed from $\hat{X}_{t-1}$ and the observation $X_{t-1}$ without needing to store the past observations at time $t$. For the temperature profile forecast required in this research, a 'clockwise' formula of the EWMA model is used in evaluating the periodical deterministic part of the ambient temperature,

$$\hat{D}_{t,d+1} = \hat{D}_{t,d} + \lambda(T_{t,d} - \hat{D}_{t,d}), \quad t = 1, 2, ..., 24 \tag{7.9}$$

where,

$\hat{D}_{t,d+1}$: deterministic forecast for the next day $d+1$ at time $t$,

$\hat{D}_{t,d}$: deterministic forecast for the previous 24 hours, day $d$ at time $t$,

$T_{t,d}$: temperature observations for the previous 24 hours, day $d$ at time $t$.

The only parameter to be determined in the EWMA model for calculating the deterministic element of the data series, is the exponential smoothing constant $\lambda$. The smoothing constant $\lambda$ is used to give weight to the past data. As $\lambda$ increases, greater influence from the more recent observation is given to the model. A large

$\lambda$ can result in a rapid response to the weather changes, but, also to the irregular movements in the time series. Due to highly stochastic nature of the ambient temperature, too large a $\lambda$ can cause substantial prediction errors when there is a sudden change in temperature. For instance, if the ambient temperature drops dramatically during the previous day and increases to a high level in the current day, a large $\lambda$ could give a large negative error in predicting the present day's temperature. However, too small a $\lambda$ may fail to follow the trend of the temperature variations and result in a slow response to changes in the ambient temperature (Abraham and Ledolter, 1983). For instance, if the ambient temperature remained high for a few days before dropping back to the average level, a small $\lambda$ would give a poor prediction for all the high temperature days, as a result of the low weight given to the recent temperature changes. Therefore, it is not appropriate to determine the best value for $\lambda$ from one day's forecast. A test for a suitable $\lambda$ has been conducted for a period of temperature forecasting which includes a variety of changes in the ambient temperature. The results are examined in Section 7.2.6.

### Deterministic Modelling by Sinusoidal Functions

The use of sinusoidal functions has also been investigated in this research for modelling the deterministic component of the weather data. Pandit and Wu (1983) suggested that the sinusoidal functions can be used to model the trend and periodicity of a data series:

$$y = \sum_{j=1}^{l} R_j e^{r_j t} + \sum_{j=1}^{n} B_j e^{b_j t} \left[ C_j \sin(j\omega t) + \sqrt{1 - C_j^2} \cos(j\omega t) \right] \tag{7.10}$$

where $B_j$, $b_j$, $C_j$ and $r_j$, $R_j$ are parameters to be estimated, for the temperature data with $\omega = \frac{2\pi}{24}$. The second part of Equation 7.10 is in fact, the reparameterized form of the function $y = \sum_{j=1}^{n} B_j e^{b_j t} \sin(j\omega t + \psi_j)$, in order to avoid the estimation of the parameter $\psi_j$. The Marquardt nonlinear estimation routine has been used to calculate $R_j$ and $r_j$ $(j = 1, 2, ..., l)$, and $B_j$, $b_j$, $C_j$, $(j = 1, 2, ..., n)$. The results are described in Section 7.2.6. These parameters can be updated every day.

### The Combined Deterministic-Stochastic Method

The procedure of establishing the combined model is in two steps: the deterministic part $\hat{D}_{t,d+1}$ is calculated first using Equation 7.9 (for EWMA model) or Equation 7.10 (for sinusoidal function method) for $t$=1 to 24 hours; the stochastic part $X_t$ is then derived from errors in the deterministic predictions for the previous

$n$ days, $X_t = T_t - \hat{D}_t$, $t = 1, 2, ..., n \times 24$. The data series $X_t$ is represented by the ARMA model given in Equation 7.1, the parameters being estimated by minimizing the sum of the squares of the residuals between the model predictions $\hat{X}_t$ and the stochastic component of two weeks of previously measured temperature data $X_t$ ($n$=14 days):

$$\sum_{t=1}^{n\times 24} a_t^2 = \sum_{t=1}^{n\times 24} (X_t - \hat{X}_t)^2.$$

The identification of the ARMA model parameters is discussed in Section 7.2.6. Once the model is established, the parameters are held constant and used to predict the stochastic element for the next 24 hours, $\hat{X}_{t,d+1}$. The temperature forecasts $\hat{T}_{t,d+1}$, $(t = 1, 2, ..., 24)$ are then given by combining the predictions for the deterministic (EWMA or sinusoidal functions) and stochastic (ARMA) elements:

$$\hat{T}_{t,d+1} = \hat{D}_{t,d+1} + \hat{X}_{t,d+1}, \quad (t = 1, 2, ..., 24) \tag{7.11}$$

Seem and Braun (1991) compared a trigonometric harmonic series with an EWMA in the modelling of the deterministic element of an electrical load time series. The EWMA model provided significantly better forecasts than the 25-parameter harmonic model, and the computational requirement in using the EWMA was significantly less than that for the harmonic model. This is due to the fact that the best 'set' of harmonics for a period may give a poor forecast for another period, and therefore a large effort is required in updating the harmonics. In comparison, the EWMA model provides a simple and efficient way to model the system using historical observations. The performance comparison of the EWMA model (Equation 7.9) and sinusoidal functions (Equation 7.10) in calculating the deterministic element of the temperature data is given in Section 7.2.8.

### 7.2.5 The Expanded Combined Method to Include Global Radiation

Since the daily total global radiation may have important influence on the daily average temperature variations (Yoshida and Terai, 1990/1991), the combined model can be expanded to take this into account. The expanded method consists of three parts: daily average temperature, a deterministic component and a stochastic component. In this model, the daily average temperature is subtracted

from the hourly sampled data. The remaining deterministic component is modelled by the EWMA model and the stochastic element by the ARMA model, as used for the combined method. The time series of the daily average temperature is calculated by the multivariable ARMAV[8] model:

$$\begin{aligned}\mathbf{\Phi_0 Y_t} = \mathbf{\Phi_1 Y_{t-1}} + \mathbf{\Phi_2 Y_{t-2}} + ... + \mathbf{\Phi_n Y_{t-n}} + \\ \mathbf{e_t} - \mathbf{\Theta_1 e_{t-1}} - \mathbf{\Theta_2 e_{t-2}} - ... - \mathbf{\Theta_m e_{t-m}}\end{aligned} \tag{7.12}$$

where,

$$\mathbf{Y_{t-i}} = \begin{bmatrix} \bar{T}_{d-i} \\ \bar{G}_{d-i} \end{bmatrix}, \; i = 0,1,...,n, \quad \mathbf{e_{t-j}} = \begin{bmatrix} a_{t-j} \\ b_{t-j} \end{bmatrix}, \; j = 0,1,...,m,$$

$$\mathbf{\Phi_0} = \begin{bmatrix} 1 & -\varphi_0 \\ 0 & 1 \end{bmatrix}, \quad \mathbf{\Phi_i} = \begin{bmatrix} \phi_{i1} & \varphi_{i2} \\ 0 & \varphi_{i1} \end{bmatrix}, \; i = 1,2,...,n,$$

$$\text{and } \mathbf{\Theta_j} = \begin{bmatrix} \theta_j & 0 \\ 0 & \psi_j \end{bmatrix}, \; j = 1,2,...,m.$$

$\bar{T}_d$ and $\bar{G}_d$ are the daily average temperature and the normalized daily total global radiation of day $d$. $\phi_{i1}$, $i = 1,2,...,n$ are the autoregressive parameters for the temperature $\bar{T}_d$. $\varphi_0$ and $\varphi_{i2}$, $i = 1,2,...,n$ are the parameters of the exogenous input variable $\bar{G}_d$ for modelling the temperature $\bar{T}_d$ (Equation 7.13). $\varphi_{i1}$, $i = 1,2,...,n$ are the autoregressive parameters for modelling the global radiation $\bar{G}_d$. $\theta_j$ and $\psi_j$, $j = 1,2,...,m$ are the moving average parameters for the temperature $\bar{T}_d$ and radiation $\bar{G}_d$ respectively. Equation 7.12 is formed under the assumption that global radiation is an independent time series and the temperature depends on the global radiation (Yoshida and Terai, 1990/1991). The Gaussian noises $a_t$ and $b_t$ for the two stochastic processes must also be independent, which is a common assumption for modelling multivariable control systems (Pandit and Wu, 1983).

The assumptions made in Equation 7.12 ensure the identifiability of the ARMAV model, so that the parameter estimation can be accomplished sequentially using an ARMA model for the solar radiation $\bar{G}_d$, and then an ARMAX[9] model for

[8] AutoRegressive Moving Average Vectors system

[9] AutoRegressive Moving Average with eXogenous variables

the temperature $\bar{T}_d$. The ARMAX model uses the past temperature observations, and the previous and present radiation data as exogenous variables. Equation 7.13 indicates the ARMAX model for calculating the temperature, derived from Equation 7.12:

$$\bar{T}_d = \phi_{11}\bar{T}_{d-1} + \phi_{21}\bar{T}_{d-2} + ... + \phi_{n1}\bar{T}_{d-n} + \varphi_0\bar{G}_d + \varphi_{12}\bar{G}_{d-1} + \varphi_{22}\bar{G}_{d-2} + ... + \varphi_{n2}\bar{G}_{d-n} + a_t - \theta_1 a_{t-1} - ... - \theta_m a_{t-m} \quad (7.13)$$

The daily total global radiation is normalized to $\bar{G}_d$, $\bar{G}_d = G_d/H_o$, where $G_d$ is the daily total global radiation received on the horizontal surfaces, $H_o$ is extraterrestrial daily insolation on the horizontal surfaces (Liu and Jordan, 1960), calculated by:

$$H_o = \frac{24}{\pi} r I_{sc} (\cos L \cos\delta \sin\omega_s + \omega_s \sin L \sin\delta) \quad (7.14)$$

where,

$L, \delta, \omega_s$: latitude, solar declination and sunset hour angle respectively (radians); $\delta$, and $\omega_s$ can be calculated by:

$$\delta = 23.45 \sin(360\frac{284+n}{365}) \quad (7.15)$$

$$\cos\omega_s = -\tan L \cdot \tan\delta \quad (7.16)$$

$r$: ratio of solar radiation intensity (at normal incidence to the outside of the atmosphere of the earth) to the solar constant, (dimensionless); $r$ depends on the distance between the earth and the sun:

$$r = (1 + 0.033 \cos\frac{360n}{365}) \quad (7.17)$$

$I_{sc}$: solar constant, 1353 W/m$^2$ (Duffie and Beckman, 1974).

$n$ is the number of the day in question in a year. When calculated from the solar declination and other variables, $H_o$ is fairly constant within a month (Liu and Jordan, 1960).

In modelling the daily average temperature, one month weather data of daily sampled average temperatures have been used as historical observations to estimate the model parameters (Equation 7.13), since the use of this length of period has

been observed to give an improved accuracy than the two weeks period without intensive computation of the daily sampled data.

The influence of including solar radiation to model the daily average temperature on the temperature forecast is analysed in Section 7.2.8 by comparing the prediction accuracy from the ARMAX model (Equation 7.13) with that from an ARMA model of modelling the daily average temperature from its past observations without considering its correlation to solar radiation. The performance of the expanded combined method in modelling the daily average temperature separately is then compared with the combined deterministic-stochastic method, being described in Section 7.2.8.

### 7.2.6 Selection of Model Parameters

Three methods of modelling the ambient temperature have been described, together with the parameters to be determined. ARMA models are used to account for the stochastic variations of the temperature by all the three methods. The order of ARMA models and the model parameters have been estimated according to the procedure described in Section 7.2.3. The parameters for the deterministic component in the combined deterministic-stochastic method and the expanded method have also been investigated. Four errors have been used to examine the performance of the three weather forecast models: Root Mean Square Error (RMSE), Mean Error (ME), Mean Absolute Error (MAE) and MAXimum Absolute Error (MAXAE). The model performance will be described in Section 7.2.8. These errors are also used here to identify the optimum parameters for the deterministic modelling of the temperature in the combined deterministic-stochastic method and the expanded method.

As described in Section 7.2.2, the Marquardt nonlinear regression method is used to minimize the sum of squares of residuals $\Sigma a_t^2$ for estimating the ARMA model parameters. In the pure stochastic method, the raw temperature observations are applied to Equation 7.1 and an appropriate order of the model is identified (Section 7.2.3). The model parameters are then determined and the following day's ambient temperature profile is forecast. Results have revealed that a high order of the ARMA model is required to describe the underlying system, and the periodicity in the value of $\Sigma a_t^2$ is observed in the pure stochastic model. For

instance, the ARMA(26,25) is adequate (according to F-criterion test and the sufficiently small autocorrelations of residuals $a_t$'s) and has a low $\Sigma a_t^2$ for modelling the temperature data during July of the CIBSE year. With increasing order, the value of $\Sigma a_t^2$ rises until ARMA(48,47), giving the lowest value of $\Sigma a_t^2$. Since the diurnal temperature changes by a cycle of 24 hours, the hourly sampled data may be adequately represented by an ARMA model with an order of nearly $(n \times 24)$, where $n$ is an integer. Due to the random nature of the ambient temperature, it may not be distributed by a periodicity of exactly 24 hours. Although the order estimated in this method varies with different periods of the temperature sampled, its periodicity is in the range of 24 hours. If the moving average parameters are removed and an AR model is used, a higher number of parameters of AR($2n$) may be required, in this instance, AR(36) results in the similar accuracy (with a similar value of $\Sigma a_t^2$) to ARMA(26,25).

In the combined deterministic-stochastic method, the stochastic element of the temperature data is modelled using the similar procedure to the pure stochastic method. The AR(4) has been found to be adequate, by the test of the F-criterion and autocorrelations (the moving average parameters of ARMA(4,3) are small and their confidence intervals include zero, and can thus be neglected).

The expanded combined method models the daily average temperature separately, the amplitude of the ambient temperature variations being calculated using the same models as used in the combined method. In order to model the daily average temperature including the influence of radiation, the daily total global radiation must be modelled first, and the model structure has been identified to be AR(2). The daily average temperature is then modelled using the observations of temperature and solar radiation by an ARMAX model (Equation 7.13). It has been found that the ARX(2) ($n = 2$, $m = 0$) model is adequate.

In the combined deterministic-stochastic method and the expanded method, the deterministic component can be calculated either by the clockwise EWMA model described in Section 7.2.4 or sinusoidal functions (Equation 7.10). For the EWMA model, the smoothing constant $\lambda$ should be identified. It has been found from a study on the value of the smoothing constant $\lambda$ that a value of $\lambda = 0.45$ is generally an optimum value for modelling the temperature data series, as illustrated in Table 7.1 for September, 1994.

| $\lambda$ | RMSE (°C) | MAE (°C) | ME (°C) | MAXAE (°C) |
|---|---|---|---|---|
| 0.3 | 1.91 | 1.52 | 0.19 | 5.86 |
| 0.45 | 1.90 | 1.48 | 0.11 | 6.19 |
| 0.6 | 1.92 | 1.48 | 0.07 | 6.62 |

**Table 7.1 The Effect of $\lambda$ on the EWMA Model**

The lower $\lambda$, the lower weight is given to the recent historical data. Table 7.1 shows that the prediction tends to smooth out the extreme errors, resulting in a smaller MAXAE. However, it may fail to follow the trend of the temperature variations with higher ME and MAE. Using the highest value of $\lambda = 0.6$ results in the opposite effect, giving the highest MAXAE and RMSE and the lowest ME and MAE. The value of $\lambda = 0.45$ is a good compromise of weighting the historical data, with relatively small errors (Table 7.1), and thus has been adopted in this weather prediction model. Note also that the prediction errors are not sensitive to small changes in the smoothing constant $\lambda$.

The parameters for the sinusoidal functions in Equation 7.10 have been estimated by the Marquardt nonlinear regression method. It has been found that the exponential growth trend in the temperature is very small and can be neglected, giving $l = 1$ and $r_1 = 0$. The 3-order ($n = 3$) of periodic trend is found to be sufficient for modelling the temperature data. Table 7.2 gives an example of the values for $B_j$, $b_j$, $C_j, (j = 1, 2, 3)$ and $R_1$ of the 3-order model using the temperature observations in March of the CIBSE year.

| No. order | B | b | c | R |
|---|---|---|---|---|
| 1st | -3.56 | -0.01 | 0.86 | 8.78 |
| 2nd | 8.56 | -0.34 | 0.99 | \ |
| 3rd | -4.61 | -0.33 | 1.00 | \ |

**Table 7.2 An Example of Parameters Fitted for Sinusoidal Functions**

The performance of using the EWMA model and sinusoidal functions in modelling the deterministic component of the ambient temperature will be compared in Section 7.2.8. A complete comparison of the three methods in forecasting the ambient temperature will also be presented in Section 7.2.8, using the parameters identified here.

### 7.2.7 Updating Temperature Prediction

In the three prediction methods, the ambient temperature is predicted for the next 24 hours only once at the end of every day, this information being used to calculate the optimum control strategy for the next 24 hours. It is, however, possible to improve the temperature prediction for the future hours of the day by the use of temperature observations of the past hours. The updating of the temperature prediction within a day has therefore, been investigated.

For forecasting with a longer lead time using an ARMA model, the temperature prediction error is inevitably larger later in the day than in the early morning. With the new temperature observations of the following day being available, the parameters of the ARMA model and the forecast can be updated to improve the accuracy, by re-estimating the parameters of the ARMA model or simply by the use of Green's function (Section 7.2.3).

Let $\hat{X}_t(l)$ be a forecast for a lead time $l$ at time $t$, and $X_{t+l}$ be the observation at time $t+l$. In this weather prediction model, the forecast for the lead time from $l = 1$ to 24 hours of the next day is required at the end of every day. The updating can be achieved by Green's function,

$$\hat{X}_{t+1}(l) = \hat{X}_t(l+1) + G_l \, a_{t+1} \tag{7.18}$$

where $a_{t+1} = X_{t+1} - \hat{X}_t(1)$. This equation can be easily derived from the model formula of Green's function in Equation 7.3, by stating that at time $t+1$, the updated forecast $\hat{X}_{t+1}(l)$ of the observation $X_{t+1+l}$ is obtained from the old forecast $\hat{X}_t(l+1)$ at time $t$ simply by adding $G_l$ times the new shock $a_{t+1}$ which becomes known once $X_{t+1}$ is available.

The performance of adapting to new temperature observations by re-estimating the ARMA model parameters has been compared with using Green's function. It was found that the two methods have similar performance, while the use of Green's function results in a slightly quicker response to the new temperature observations.

The updating of temperature forecasting by the use of Green's function is simple and efficient, but, only in improving the forecast accuracy for a short lead time. Due to the randomness of temperature variations, the predicted temperature profile with updating may be less accurate than that without updating for

the temperature forecast during daytime. For instance, Figure 7.3 illustrates that if updating is undertaken at 2:00 am, the forecasts for 3:00 am and 4:00 am are improved. However, since the observed temperatures at 2:00 am and 1:00 am are lower than the predictions without updating, updating the prediction at 2:00 am lowers the predicted temperatures for the rest of the day, which results in higher prediction errors during the occupancy period (Figure 7.3). Furthermore, the temperature prediction errors are small during night since the general lead time is short. It can therefore be concluded that updating the temperature prediction profile according to the new available observations during night hours is not effective in improving the forecasting of the daytime temperatures.

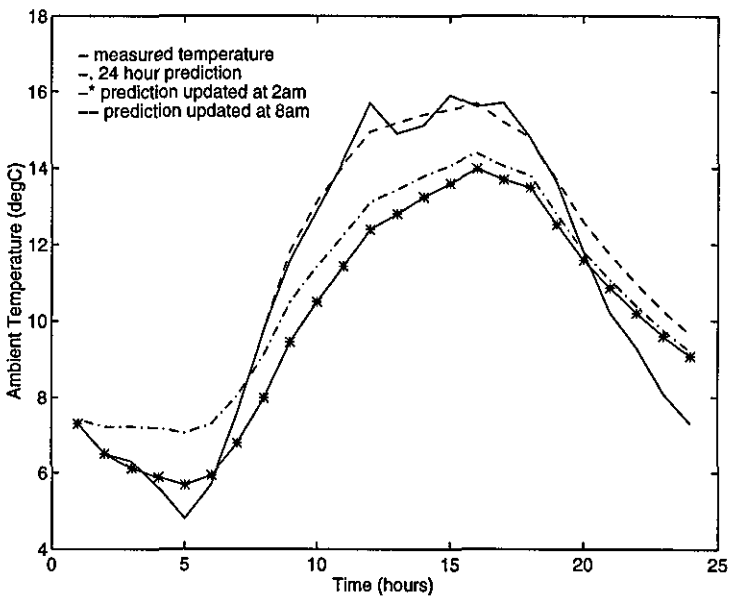


**Figure 7.3, Updating of Temperature Profile for the 9$^{th}$ May 1994**

Figure 7.3 suggests that updating the temperature prediction at the beginning of the occupancy period at 8:00 am can improve the prediction for the occupancy period. This may be useful for hourly predictive control, for instance, for a local loop controller (Holst *et al.*, 1987). However, for the purpose of the predictive control of thermal storage in this research, this procedure loses its significance, since the time for planning to utilize the potential of the plant night operation to offset the daytime thermal loads has passed. Since the optimal controller investigated in this research predicts the optimum control strategy once each day to take advantage of the night's favourable ambient conditions and the utilization of the thermal storage, the temperature prediction models are only updated at the time of the control strategy optimization. Therefore, updating weather prediction

within a day has not been used.

### Updating Using Forecast Daily Maximum and Minimum Temperatures

The temperature prediction can also be corrected by the forecast daily maximum and minimum temperatures obtained from a local weather station. Supposing that $\hat{T}_{max}$ and $\hat{T}_{min}$ and the variation $\hat{\delta}$ ($\hat{\delta} = \hat{T}_{max} - \hat{T}_{min}$) are from the predicted temperature profile, and $T_{max}$, $T_{min}$ and the variation $\delta$ ($\delta = T_{max} - T_{min}$) are provided by the forecast from the local weather station. If $\hat{\phi}_t$ is a shape factor and $\hat{\phi}_t^n$ a new shape factor at time $t$:

$$\hat{\phi}_t = \frac{\hat{T}_t - \hat{T}_{min}}{\hat{\delta}} \tag{7.19}$$

$$\hat{\phi}_t^n = \frac{\hat{T}_t^n - T_{min}}{\delta} \tag{7.20}$$

the corrected $\hat{T}_t^n$ can be derived from $\hat{\phi}_t$=$\hat{\phi}_t^n$, giving:

$$\hat{T}_t^n = \frac{\delta}{\hat{\delta}}(\hat{T}_t - \hat{T}_{min}) + T_{min} \tag{7.21}$$

As shown in Figure 7.4, the corrected profile gives a significant improvement in the temperature prediction during the daytime (assuming that the forecast of the daily maximum and minimum temperatures from the weather station is accurate), however, it is not effective in improving the predictions for night hours and may increase prediction errors. As observed in Figure 7.4, this correction procedure, in effect, enlarges or contracts the predicted temperature profile according to the input of daily maximum and minimum temperatures. Since the lead time is short, the prediction errors are usually small at night and during early morning. Correction is likely to increase the prediction errors for this period by enlarging or contracting the temperature profile. Figure 7.4 shows an example of the effect of correction leading to higher prediction errors at night and during early morning hours. Although this figure is for the case where the predicted profile is lower than the measured profile, the same effect has also been observed for other prediction profiles (such as the predicted profile being higher than or crossing the measured profile).

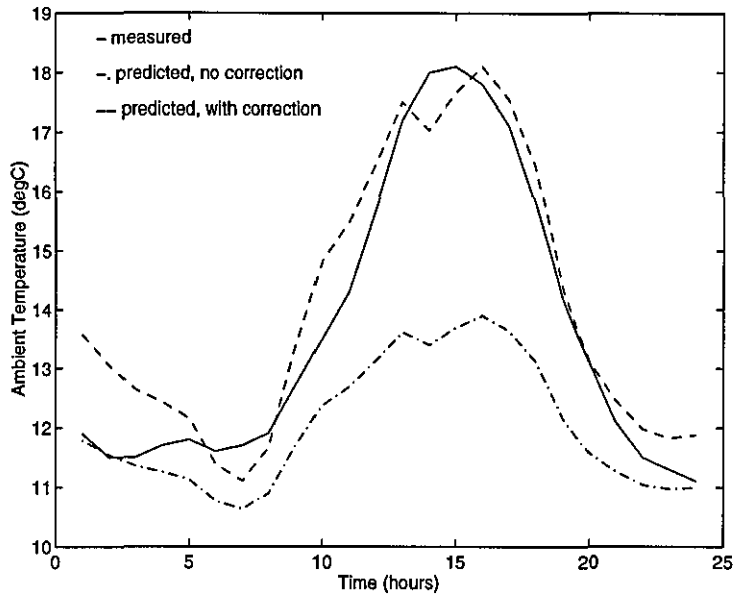


**Figure 7.4, The Corrected Temperature Profile on the $22^{th}$ September 1994**

It is thus recommended that the prediction is corrected when the ambient temperature starts to rise, such as at 7:00 am or 8:00 am if the forecast of the daily maximum and minimum temperatures from the local station is available.

This correction procedure may be used for the purpose of this predictive controller, so that at the end of every day, the profile of the predicted daytime temperature is corrected, without modifying the predicted night temperature profile (a smoothing function may be required to connect the two profiles). However, the correction of the temperature prediction is not utilized in this research, as it assumes that the local forecast of next day's maximum and minimum temperatures is not available.

### 7.2.8 Performance Comparisons of the Temperature Prediction Models

The aim of using ARMA models in this research is forecasting. The forecasting involves extrapolation to obtain the value $X_{t+l}$ $l$ steps ahead from the knowledge of the data series $X_t$ and its structure. Four errors are used to examine and compare the performance of the three prediction methods: Root Mean Square Error (RMSE), Mean Error (ME), Mean Absolute Error (MAE) and MAXimum

Absolute Error (MAXAE).

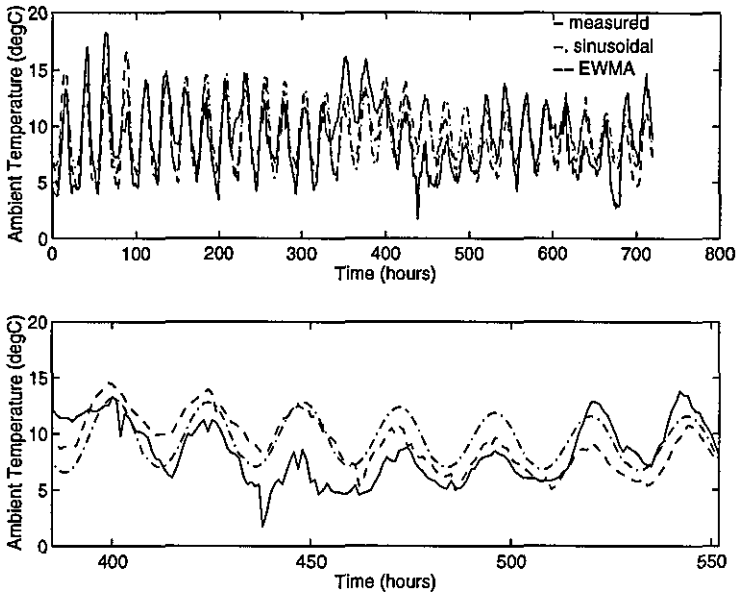


**Figure 7.5, The Comparison between Sinusoidal Functions and EWMA in Modelling Deterministic Element of Temperature Profile**

In order to compare the performance of the pure stochastic method with the combined deterministic-stochastic method, the deterministic model in the combined method needs to be selected. Table 7.3 compares the performance of the EWMA model with that of sinusoidal functions for April of the CIBSE weather year. The relative performance is also illustrated in Figure 7.5, where for the sake of a clear comparison, a second figure displays the data from the $17^{th}$ to $23^{th}$ of April. It is observed that the periodical functions can not effectively adapt to the varying trend of the temperature, even though the parameters of the functions are updated each day. This method gives higher average errors (RMSE and MAE), and slightly smaller maximum error (MAXAE). The EWMA model provides the prediction without bias and gives smaller errors except for the MAXAE, being 0.4 °C higher than the sinusoidal method. In effect, the use of sinusoidal functions results in similar performance to the EWMA model with a smaller $\lambda$, which gives smaller maximum error MAXAE but larger average errors (MAE and RMSE). It was also found that the shape of diurnal temperature variations affects the performance of the sinusoidal functions. For instance, in July when the amplitude of diurnal temperature is large and the cycle of the diurnal variation is clear, the sinusoidal functions can give more accurate prediction than for April or the winter months.

| Methods | RMSE (°C) | MAE (°C) | ME (°C) | MAXAE (°C) |
|---|---|---|---|---|
| sinusoidal | 2.35 | 1.86 | 0.31 | 6.73 |
| EWMA | 2.10 | 1.53 | 0.00 | 7.13 |

**Table 7.3 Comparison of Sinusoidal Functions and EWMA Model**

In terms of computational effort, the EWMA model does not require nonlinear parameter estimation. Therefore, due to its simplicity and accuracy, the clockwise EWMA has been adopted to model the deterministic component of the temperature data series in this research.

Therefore, the combined deterministic-stochastic method uses the EWMA with $\lambda = 0.45$ and AR(4) to model and predict the deterministic and stochastic components respectively. Table 7.4 gives an example of performance comparison for July of the CIBSE year, between the pure stochastic method and the combined method. It can be seen from this comparison, that the combined method gives smaller errors in terms of the average errors (RMSE and MAE) and the maximum error (MAXAE), while having a small positive bias (ME). The study has also been conducted on the temperature prediction for other months of the CIBSE year and the 1994 weather data. The combined method is simpler, less computationally intensive, and most likely gives smaller prediction errors.

The prediction errors for the CIBSE year and 1994 are presented in Table 7.5 using the combined deterministic-stochastic method. It can be seen that although the maximum errors (MAXAE) are large due to random variations in temperature, the average errors (RMSE and MAE) are acceptable for the two sets of weather data and the predictions are without bias (ME). The small average errors indicate that this method can follow the general trend of ambient temperature variations (this can be further illustrated in Figure 7.7).

| Methods | RMSE (°C) | MAE (°C) | ME (°C) | MAXAE (°C) |
|---|---|---|---|---|
| stochastic | 2.07 | 1.50 | -0.01 | 8.04 |
| combined | 1.88 | 1.41 | 0.13 | 6.62 |

**Table 7.4 Performance Comparison between the Pure Stochastic and Combined Methods**

| Periods | RMSE (°C) | MAE (°C) | ME (°C) | MAXAE (°C) |
|---|---|---|---|---|
| CIBSE year | 2.14 | 1.58 | 0.01 | 10.40 |
| 1994 | 2.46 | 1.81 | -0.02 | 14.25 |

**Table 7.5 Prediction Errors for the CIBSE Year and 1994 from the Combined Deterministic-Stochastic Method**

The performance of the expanded combined method is investigated in two steps. First, the daily average temperature is modelled and the model performance is examined. Second, the performance of the expanded combined method is assessed in terms of its predictions of the daily average temperature, amplitude of variations in temperature and the ambient temperature.

To examine the influence of solar radiation on daily average temperature, $\bar{T}_d$ has been modelled by two methods, the first by a standard AR(2), which models the temperature independently and ignores its correlation to the daily total radiation, the second using an ARX(2) with $n = 2$ and $m = 0$ to include the effect of solar radiation (Equation 7.13). The accuracy of the two methods is compared in Table 7.6 for September 1994.

| Methods | RMSE (°C) | MAE (°C) | ME (°C) | MAXAE (°C) |
|---|---|---|---|---|
| independent | 1.38 | 1.11 | 0.66 | 3.01 |
| correlated | 1.47 | 1.15 | 0.76 | 3.31 |

**Table 7.6 The Influence of Solar Radiation on the Prediction of Daily Average Temperature**

It can be seen that all the errors from the independent model are smaller in September. Due to the highly random behaviour of global radiation, the correlation between daily average temperature and total radiation during each month is uncertain. The correlation for September 1994 is similar to the average value of monthly calculated correlations, $\rho_{xy} = 0.2$. It has also been observed from this study that the error differences between the two methods do not change significantly with the correlation for each month. Therefore, it is concluded that it is not necessary to consider the correlation of daily average temperature to global radiation, and the daily average temperature can be modelled with sufficient accuracy from its past observations.

Therefore, in the expanded combined method, the daily average temperature is calculated by AR(2), and the amplitude of temperature variations is modelled by the same procedure as in the combined deterministic-stochastic method. The results from the expanded method are displayed in Table 7.7, where the forecast errors of daily average temperature $\bar{T}$, amplitude of the temperature variations $\Delta T$ and the ambient temperature $T$ ($T = \bar{T} + \Delta T$) are compared with those from the combined method. Since in the combined method, the daily average temperature $\bar{T}$ and the amplitude $\Delta T$ are not modelled separately, they have been calculated from the predicted temperature $T$.

| | RMSE (°C) | | MAE (°C) | | ME (°C) | | MAXAE (°C) | |
|---|---|---|---|---|---|---|---|---|
| | expanded | combined | expanded | combined | expanded | combined | expanded | combined |
| $\bar{T}_7$ | 1.49 | 1.43 | 1.22 | 1.09 | 0.08 | 0.13 | 3.86 | 4.27 |
| $\Delta T_7$ | 1.36 | 1.22 | 1.07 | 0.96 | 0.01 | 0.00 | 5.23 | 4.37 |
| $T_7$ | 1.94 | 1.88 | 1.50 | 1.41 | 0.08 | 0.13 | 6.30 | 6.62 |
| $\bar{T}_9$ | 1.38 | 1.09 | 1.11 | 0.94 | 0.66 | -0.05 | 3.01 | 2.40 |
| $\Delta T_9$ | 1.25 | 1.16 | 0.98 | 0.88 | 0.02 | 0.00 | 4.42 | 4.06 |
| $T_9$ | 1.94 | 1.79 | 1.41 | 1.24 | 0.67 | -0.05 | 6.07 | 5.41 |

**Table 7.7 Performance Comparison of the Two Combined Methods**

In Table 7.7, the subscripts 7 and 9 have been added to denote the errors for July of the CIBSE year and September of 1994. It can be seen that most errors from the combined method are smaller than those from the expanded method. Although the prediction error MAXAE of the daily average temperature for July is 0.4 °C larger and there is more bias (ME) from the combined method, the average errors RMSE and MAE are both smaller. It also gives a better performance in predicting the amplitude of the temperature variations. The results for September 1994 indicate that all the errors from the combined method are smaller than those from the expanded method. In particular, the mean errors (ME) of the daily average temperature and the ambient temperature from the combined method show no bias, compared with the high positive bias (ME>>0.0 °C) from the expanded method. The comparison between temperature predictions for other periods illustrates that these two methods result in a similar range of errors. However, the combined method is slightly more accurate and has the advantage to be much simpler in structure and operation.

From the investigation on the performance of the pure stochastic method, the combined deterministic-stochastic method and the expanded combined method (Table

7.4 and 7.7), it is concluded that the combined deterministic-stochastic method is competent in accuracy and simplicity for short-term forecasting of temperature, and it is therefore, adopted to model and forecast the ambient temperature in this research.

### General Performance of the Combined Deterministic-Stochastic Method

Figure 7.6 shows the ambient temperature prediction for July of the CIBSE year and Figure 7.8 for September of 1994 using the combined method.

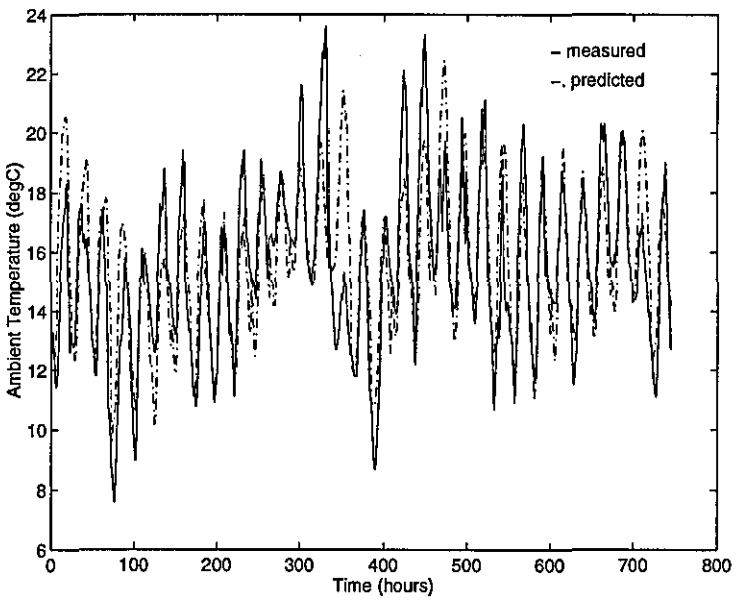


**Figure 7.6, The Predicted Ambient Temperature Profile for July of the CIBSE year**

It can be observed that the model is able to follow the pattern of temperature change, although when a sudden change in weather occurs, the model can take one or two days to re-align with the new pattern. For instance, Figure 7.7 shows the results for $14^{th}$-$17^{th}$ July of the CIBSE year. On the $15^{th}$ July, there is a sudden drop in temperature of approximately 8.3 °C, which inevitably leads to larger prediction errors. However, the model has re-aligned with the new pattern by the next day, giving much smaller prediction errors for the $16^{th}$ and $17^{th}$ July.

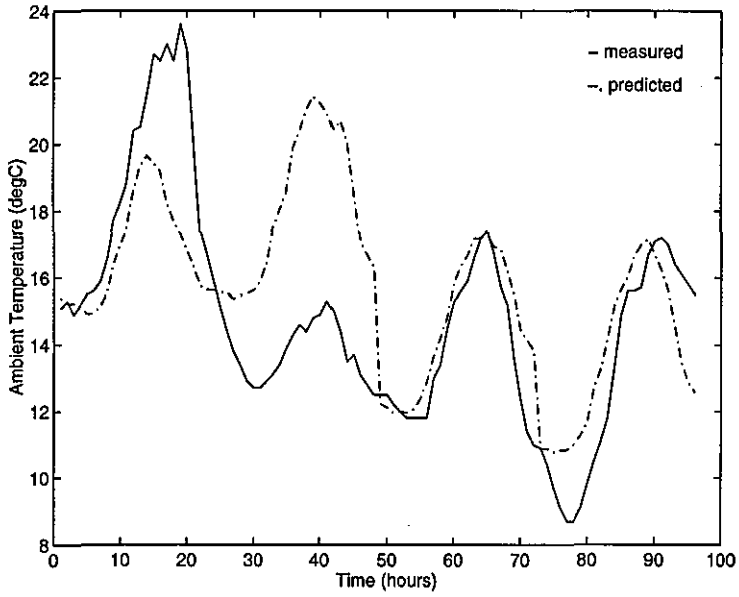


**Figure 7.7, The Predicted Ambient Temperature Profile from 14th to 17th July of the CIBSE year**

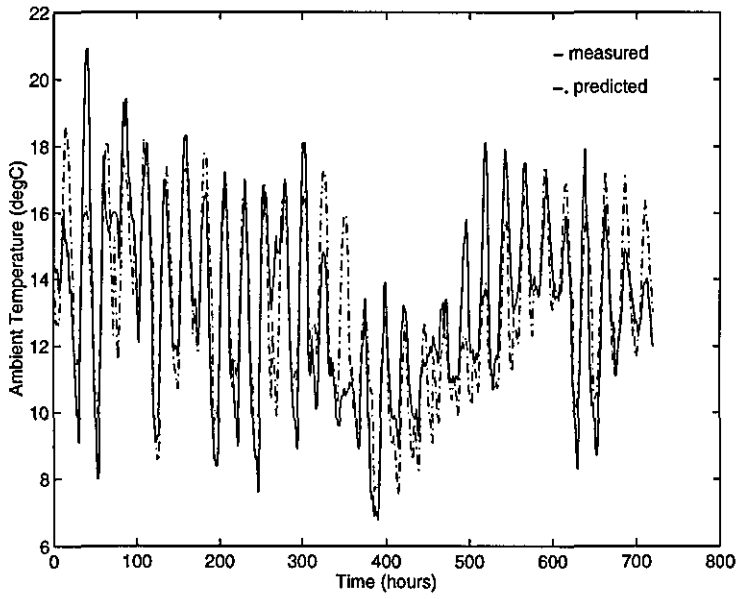


**Figure 7.8, The Predicted Ambient Temperature Profile for September, 1994**

## 7.3 Radiation Prediction

Like the ambient temperature, the solar radiation is also a nonstationary stochastic data series. The hourly sampled radiation data (global, diffuse and direct) exhibit even more random behaviour than the temperature data. The global, diffuse and direct radiation are all modelled in this research, but only the global radiation is taken as the example here to illustrate the prediction model.

### 7.3.1 The Properties of Radiation Time Series

Figure 7.9 displays the nonstationary properties of the global radiation. It is seen that the global radiation has a strong periodicity; the radiation at night is deterministically zero, reaching the peak in the middle of the day. The standard deviations indicate a much higher variation of the hourly global radiation in the middle of day, the highest variation being 218 W/m$^2$, 68.5% of the highest mean radiation of 318 W/m$^2$. This implies a significant change in the hourly radiation throughout an entire year.

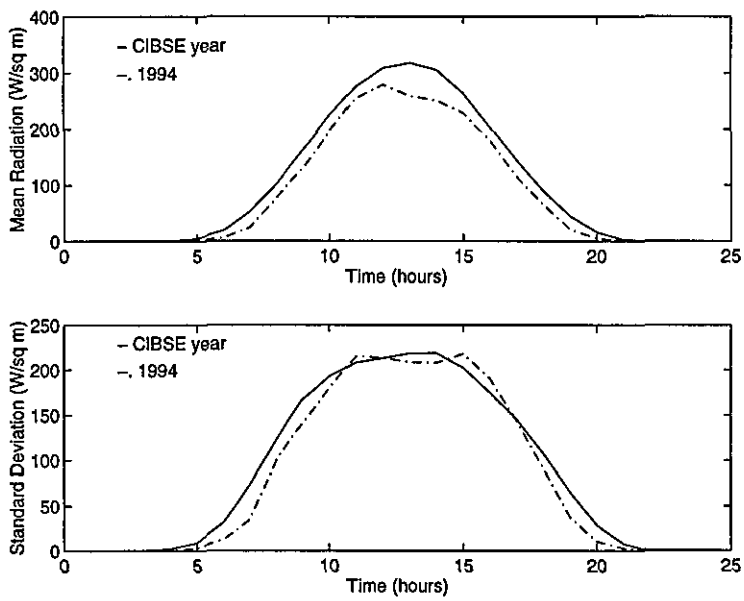


**Figure 7.9, Hourly Mean and Standard Deviation of the Global Radiation**

In order to apply a stochastic model to the radiation data series, the series has been reconstructed to a 17 hour periodicity instead of 24 hour, from 5:00 am to 9:00 pm when there is noticeable incidence of solar radiation on the earth (for the winter period, shorter hours of periodicity may be used).

### 7.3.2 The Radiation Prediction Model

As discussed in Section 7.2.1, the solar radiation can be modelled independently. From the results of the temperature model comparisons (Section 7.2.8), the combined deterministic-stochastic method has been shown to accurately model the nonstationary temperature data series. This method can also be used to predict the solar radiation, since the ambient temperature and solar radiation have similar deterministic and stochastic properties. In the combined radiation method, the radiation data are divided into deterministic and stochastic parts. The stochastic part is modelled using the ARMA time series technique. Two methods may be used to model the deterministic part: the EWMA model and sinusoidal functions.

#### Deterministic Modelling

The clockwise EWMA model is the same as that used for the ambient temperature prediction. In the sinusoidal function method, Equation 7.10 is used to model the deterministic trend and periodicity of the radiation data, with $\omega = \frac{2\pi}{17}$ and $R_1 = r_1 = 0$, $B_j$, $b_j$, $C_j, (j = 1, 2, ..., n)$ being estimated by the nonlinear estimation routine. In this method, the daily average global radiation $\bar{G}_d$ is predicted by an AR(2) model as an independent data series (Section 7.2.6). The amplitude of hourly radiation is then modelled by sinusoidal functions. Such hourly amplitude can be assumed to be constant within a month, mainly depending upon the sun's position in each hour. This differs from the sinusoidal function method for modelling the deterministic element of the ambient temperature, where the parameters are updated daily.

Table 7.8 compares the performance between the EWMA and the sinusoidal function method for July of the CIBSE year. All prediction errors from the EWMA model are much smaller, with nearly no bias (ME) and smaller average errors (RMSE and MAE) and maximum error (MAXAE). The EWMA mode is, therefore, used for modelling the deterministic part of the solar radiation.

| Methods | RMSE ($W/m^2$) | MAE($W/m^2$) | ME($W/m^2$) | MAXAE ($W/m^2$) |
|---|---|---|---|---|
| EWMA | 116.08 | 68.69 | 3.50 | 473.38 |
| sinusoidal | 155.00 | 111.37 | 29.14 | 554.23 |

**Table 7.8 Performance Comparison between EWMA Model and Sinusoidal Function Method for Modelling Solar Radiation**

### Stochastic Modelling

The stochastic part, which is the errors in the deterministic prediction of the radiation data, still appears to be nonstationary, with a much higher mean and standard deviation in the middle of day than during the morning and evening hours. The periodicity of the stochastic part is unstable due to the dramatic variations in amplitude (hourly variations in global radiation indicate a frequent and sharp increase or decrease in some consecutive hours of one day). It has been found that the ARMA model fails to model the stochastic part, since the solar radiation varies randomly with high frequency and large amplitude, as shown in Figure 7.10. As a result, the prediction from the ARMA model appears to be a filtered response to a high frequency disturbance, which is in fact the prediction error from the deterministic model. By including the stochastic part, the error in modelling the global radiation is not significantly reduced than using the deterministic prediction alone.

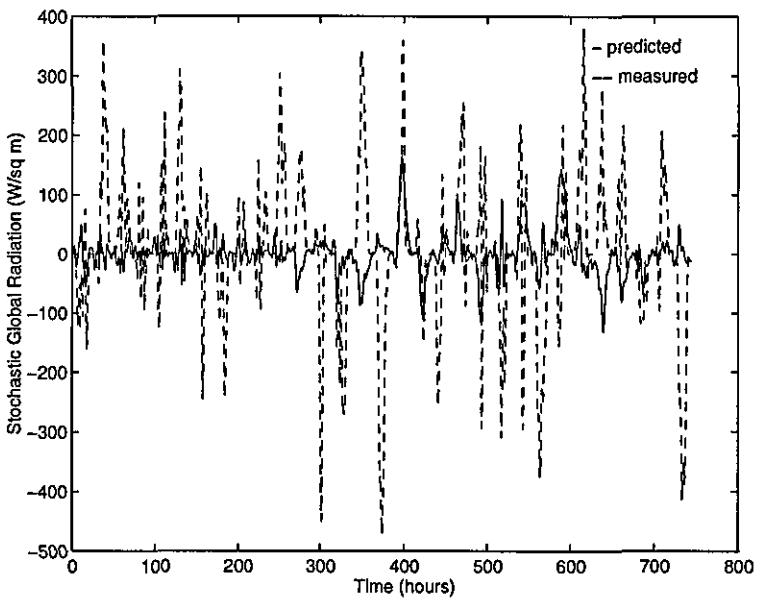


**Figure 7.10, Modelling Stochastic Element of Global Radiation**

Therefore, the purely deterministic, clockwise EWMA model is adopted in this research to model the solar radiation. Figure 7.11 gives an example of one week prediction of the global radiation from the $17^{th}$ to $23^{th}$ September, 1994. It can be seen that the EWMA model gives a reasonable accuracy in forecasting the high stochastic solar radiation.

Hourly observations of solar radiation are not always measured by building control systems, but the daily total global radiation may be obtained from a local weather station or by prediction (Section 7.2.6). In this case, an empirical ratio can be used to transfer the daily sampled data to hourly values (Liu and Jordan, 1960). Duffie and Beckman (1974) demonstrated the use of the ratio of the hourly average radiation to the daily average radiation to estimate the hourly values from daily data. Solar altitude was also used to calculate the radiation in each hour received on the horizontal surfaces (Yoshida and Terai, 1992). If either the diffuse or direct radiation is not available, the interrelationship between the radiations can be calculated (Liu and Jordan, 1960). However, these approaches have not been investigated further here.

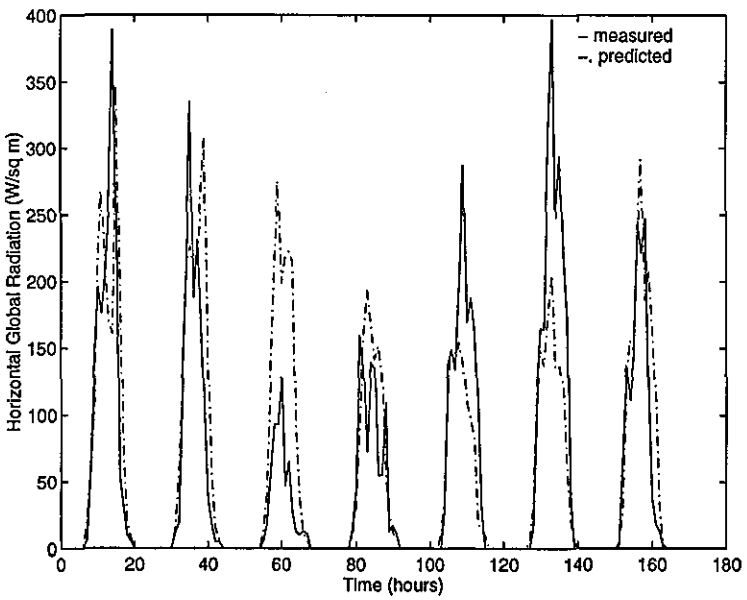


**Figure 7.11, Predicted Profile of Global Radiation from $17^{th}$ to $23^{th}$ September 1994**

## 7.4 Conclusion

Three temperature prediction methods have been investigated for short-term temperature forecast: the pure stochastic method, the combined deterministic-sto chastic method and the expanded method. It has been found that the combined deterministic -stochastic method is the simplest to use and most likely to provide smaller prediction errors. The investigation on the influence of correlation between solar radiation and temperature has indicated that it is not necessary to consider the influence of the daily total solar radiation on the daily average temperature for the short-term temperature forecast. Further, the daily average temperature need not be modelled separately. The combined deterministic-stochastic method can provide an acceptable accuracy in predicting the daily average temperature, amplitude of temperature variations and the ambient temperature. In addition, the investigation on updating the weather prediction within a day has shown that it is not effective in reducing forecasting errors for the daytime temperature and therefore does not improve the optimum scheduling of plant operation for the next day. Consequently, updating the temperature prediction has not been used in this research.

In conclusion, the adaptive algorithm for temperature prediction used in this research consists of a deterministic part which models the deterministic trend, and a stochastic part to account for stochastic variations in the ambient temperature. An EWMA model has been used to account for the deterministic part, and an AR(4) model for the stochastic part of the temperature. Using this method to model the two sets of weather data, the results have indicated that the mean absolute error in predicting the ambient temperature over an entire year is lower than 1.8 °C and the root mean square error lower than 2.5 °C and with no bias. For predicting solar radiation, only the deterministic EWMA model has been used. This algorithm is simple and efficient for use in off-line parameter estimation at the end of every day.

Due to prediction errors in the weather conditions, the performance of the controller developed in this research is inevitably degraded. This will be investigated in Chapter 8.

# Chapter 8

# Performance Analysis of the Optimal Predictive Controller

## Introduction

This chapter investigates the performance of the predictive optimum control strategy in reducing energy cost without violating the thermal comfort in the occupied space. The performance of two optimum control strategies are examined: the setpoint scheduling and the time-stage controller. The effects of the weather prediction errors on the performance of each controller and on cost savings and room comfort during seasonal operations, are investigated and the characteristics of the room thermal conditions for each season analysed. The hollow core ventilated slab building at the University of East Anglia, UK, has been used for this study, together with the real weather data monitored at Garston, Watford, UK, in 1994 (Chapter 6).

The performance of the optimum control strategy applied to different building constructions is also investigated in this chapter. Due to weather prediction errors, the controller performance is inevitably degraded. However, the predicted control strategy can be adapted during the occupancy period to improve the occupant thermal comfort without the need for excessive energy use. Such adaption is also examined in this chapter.

## 8.1 A Comparison of the Optimal Predictive Setpoint Scheduling Control and Time-Stage Control

The setpoint scheduling control allows optimal setpoints for the supply air temperature and flow rate to be determined for each hour of the day. The flexibility provided by this approach means that not only can short, and possibly impractical periods of plant operation occur (Section 6.1), but also that the approach is sensitive to errors in the weather prediction.

The least sensitive period is during the winter when the need for heating dictates a simple control strategy (Section 6.1.4) of full recirculation, with heating at night (Mode 7, Table 3.1) and only the heat recovery device being used during the day (Mode 1, Table 3.1). The transitional season is more sensitive to prediction errors in the ambient conditions since passive cooling and heating dominate the control strategies during these seasons (Section 6.1.3). For instance, the predicted setpoint strategy for the $17^{th}$ of May led to minimum ventilation during occupancy with the supply air setpoint matched to the ambient temperature. However, the predicted ambient temperature was higher than the real ambient temperature and therefore, in order to meet the supply air setpoint, it became necessary to operate the plant. In this case, the plant operation was to use the heat recovery device to increase the supply air temperature and then run the chiller to bring it back to the setpoint (Mode 4, Table 3.1).

The summer operation is also sensitive to prediction errors in the ambient temperature. For instance, the predicted ambient temperature at 3:00 pm on $23^{th}$ June 1994 was 18 °C, and the optimum setpoint was matched to this for free cooling (Mode 2, Table 3.1). However, the actual air temperature was 23.5 °C which required operating the chiller to bring the supply air temperature back to the setpoint (Mode 6, Table 3.1). The relative closeness of the ambient and room temperatures during some periods of summer operation can also lead to prediction errors resulting in a change in the predicted operation of the heat recovery device.

Since the majority of the control variables in the time-stage controller are concerned with the plant operating period, the controller is less sensitive to errors in weather prediction. There are potentially two mechanical heating or cooling stages

in each day, for which the supply air setpoint is a control variable (stages $C_1$ to $C_2$ and $C_3$ to $C_4$ in Figure 6.11). During these stages, the controller can be sensitive to weather prediction errors in much the same way as the setpoint scheduling controller. However, since the setpoints are for mechanical heating or cooling, they are always substantially different from the ambient air temperature and therefore the mode of plant operation is less likely to be effected by the weather prediction errors (the most common effect only being to change the mode of heat recovery device operation).

The more rigid strategy of the time-stage controller may lead to increased occupant discomfort, when for instance, a low predicted ambient temperature leads to a fixed period of free cooling; a subsequently higher real ambient temperature would result in increased occupant discomfort due to insufficient cooling. The more sensitive setpoint scheduling control could be adapted to the real ambient conditions, possibly improving thermal comfort, but at the expense of increased energy consumption (from the plant operation in order to meet the predicted setpoint). The annual operating cost during 1994 was 3.2% higher for the setpoint scheduling control than the time-stage control. The weather prediction errors resulted in very similar levels and periods of discomfort for both control strategies, being typically less than 13% PPD. The exception was in July, when the time-stage control strategy resulted in a maximum of 14% PPD in comparison with 12.9% PPD from the setpoint scheduling strategy.

In conclusion, although the time-stage control is less adaptable to errors in weather prediction, the resulting discomfort has been shown to be similar to that from the more energy expensive setpoint scheduling control. Further, since the time-stage control generally provides more stable and practicable plant operation (Chapter 6), it forms the sole focus of the remains of this chapter.

## 8.2 Annual Performance Analysis for the Time-Stage Control

The analysis of annual performance includes an investigation into the characteristics of the room thermal conditions and the optimum control strategy during each season. The controller performance is also examined for the effect of weather

prediction errors on the performance of the controller, and the performance of the controller in comparison to the conventional control strategy (described in Chapter 2 and Chapter 6). The effects of errors in the weather prediction are evaluated by comparing the room temperatures that result from the conditions when:

- the next day's weather conditions are known (perfect prediction), $T_r$;
- the next day's weather conditions are predicted, $T_{pr}$.

The difference between the two is due to errors in weather prediction, which gives rise to a different control strategy to that when the weather is perfectly predicted. Note that the effects of errors in the modelling of the building and plant have not been addressed (the same models being used to represent the building as are used within the predictive controller), but the sensitivity of the building model to errors in the input parameters has been discussed in Chapter 4, and the influence of building construction on the control strategy is examined in Section 8.3.

Four measures are used to quantify errors. The average errors are quantified by the mean absolute error (MAE) and the root mean square error (RMSE), with RMSE being more sensitive to the extreme errors than MAE. The worst error is given by the maximum absolute error (MAXAE). The bias of the error is indicated by the mean error (ME), with a negative number indicating that a lower value is predicted.

### 8.2.1 Winter Operation

Figure 8.1 illustrates the room temperature profile and standard deviation averaged over the month of February (the solutions for other months throughout the winter period exhibit a similar characteristic). Similarly, Figure 8.2 illustrates the profiles for the average mass temperature of the ventilated slab.

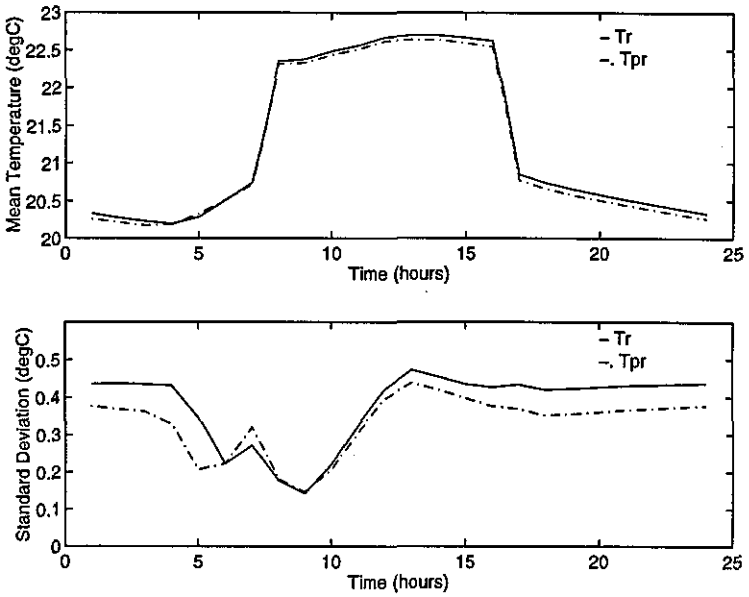


**Figure 8.1, Mean Room Temperature and Standard Deviation Profiles for February**

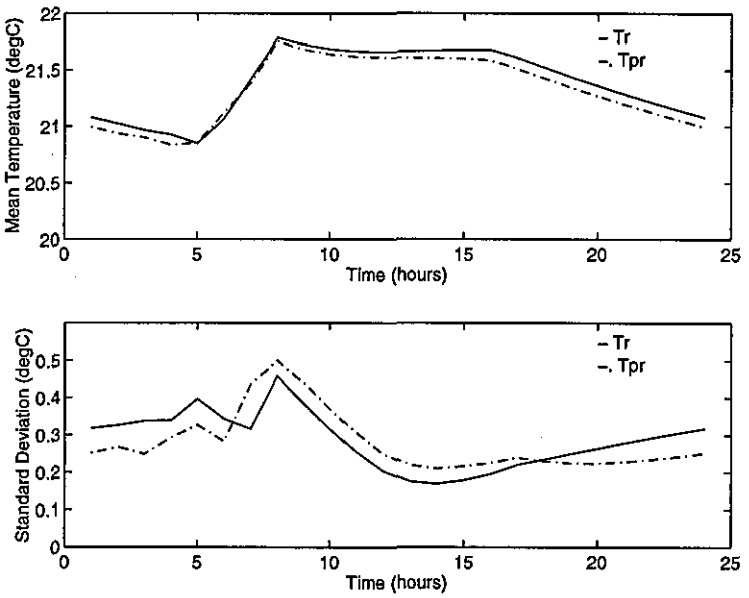


**Figure 8.2, Mean Slab Mass Temperature and Standard Deviation Profiles for February**

These temperature profiles conform to the operational strategy for most of the winter months. Generally, the mass store is preheated to a level that is sufficient to sustain the occupant thermal comfort throughout the occupancy period, during which only minimum ventilation is used with the heat recovery device being in operation. The minimum ventilation is for the occupant fresh air requirement and no additional heating is necessary during this period (the period of high electricity tariff coincides with the start of occupancy, Chapter 6). One important characteristic of the optimization is that in order to minimize energy costs, the building will only just be at the comfort temperature at the start of the occupied period at 8:00 am, with sufficient thermal storage to last the day being controlled by the length of the preheating period. The effectiveness of the optimization in dealing with this critical point in the operating schedule is indicated by the standard deviation in room temperature being lower between 8:00 am and 9:00 am than at any other time of the day. There is also a 99.7% probability that the room temperature will be within 0.6 °C of the comfort limit during this period ($22.3\pm0.6$ °C being in the cool comfort range, PMV $\in [-0.5, 0]$). The room temperature generally increases during occupancy due to internal gains and the reduction in heat loss with higher ambient temperatures. This brings the room temperature to fluctuate well within the comfort band which makes the control less critical and results in higher standard deviations.

Figure 8.2 indicates that the average mass temperature of the thermal store is at its highest at the start of occupancy (8:00 am), since this is the time at which the charging of the thermal load is stopped. The higher standard deviations in mass temperature therefore reflects the variation in ambient conditions and the thermal load that must be offset by energy from the thermal store.

These characteristics in the room thermal conditions under the optimum control strategy indicate that although the level of the thermal store to be charged at night varies with the thermal loads during the occupancy period (this can be indicated by the peak point in the standard deviation of the slab mass temperature), the room thermal conditions are fairly consistent when the occupancy just starts with the room temperature being at the low comfort limit. Therefore, during the normal operating condition in the winter, if the room is preheated to $22.3\pm0.6$ °C at the start of occupancy with sufficient warm mass storage using off-peak electricity at night, the room thermal comfort over the entire occupancy period is most likely to be satisfied. Although it has been observed that this setpoint varies with different

building constructions and heat gains in the occupied space, these characteristics may lead to a simple control scheme under winter operation.

Results in Table 8.1 and Table 8.2 indicate the effects of errors in weather prediction on the room air temperature for February. Table 8.1 shows that during February the mean absolute error in ambient temperature prediction is over 1.6 °C, with a maximum error of 6.3 °C. However, Table 8.2 indicates that errors in ambient temperature prediction of this magnitude have little effect on the control of the room temperature, the mean absolute error here being less than 0.1 °C with the maximum being less than 0.9 °C. This is partly due to the thermal capacity of the building damping fluctuations in the external climate, but also due to the relatively simple plant control strategy during the winter being insensitive to prediction errors. Table 8.3 indicates that errors in ambient condition prediction have led to the comfort constraint of 10.0 % PPD being violated, however, for most occupancy hours, the room thermal comfort is still satisfied. The discomfort under the predictive control in the winter usually occurs at late afternoon, from 3:00 pm to 4:00 pm, when the prediction errors lead to insufficient thermal storage to last the day. This is a result of the accuracy decreasing with the prediction lead time in predicting the ambient conditions (the prediction being conducted at mid-night).

| Period | RMSE (°C) | MAE (°C) | ME (°C) | MAXAE (°C) |
|---|---|---|---|---|
| Occupancy | 2.2 | 1.7 | -0.2 | 6.3 |
| 24 hours | 2.1 | 1.6 | -0.2 | 6.3 |

**Table 8.1, Ambient Temperature Prediction Errors for February**

| Period | RMSE (°C) | MAE (°C) | ME (°C) | MAXAE (°C) |
|---|---|---|---|---|
| Occupancy | 0.2 | 0.1 | -0.1 | 0.8 |
| 24 hours | 0.2 | 0.1 | -0.1 | 0.9 |

**Table 8.2, Room Air Temperature Errors for February**

In comparison to the conventional control strategy, Table 8.3 indicates that the predictive controller reduces energy costs and dramatically improves thermal comfort, although greater energy use is necessary to maintain the thermal comfort.

Both controllers tend to produce slightly cooler than neutral comfort conditions. However, the conventional controller provides insufficient heat input to the system and results in nearly all the occupancy hours being under the cold discomfort with the mean PMV lower than -0.7 and the mean PPD larger than 15%.

The degradation of the predictive control performance can be illustrated in comparison with the perfect control (perfect weather prediction). The predictive control has a 7.6% higher energy cost and 37 hours of the comfort constraint being violated. The performance of the predictive controller is considered to be acceptable during the winter operation and the prediction errors in the ambient conditions impose little influence on the optimal control strategy and the room thermal conditions.

| Type of Controller | Energy Cost (£) | Energy Use (kWh) | Mean PMV | Mean PPD (%) | Maximum PPD (%) | No. of Hours PPD > 10% |
|---|---|---|---|---|---|---|
| Conventional | £46.3 | 332.1 | -0.7 | 15.5 | 21.2 | 248 |
| Predictive | £44.4 | 429.9 | -0.4 | 8.9 | 11.4 | 37 |
| Perfect | £41.2 | 398.4 | -0.4 | 8.6 | 10.0 | 0 |

**Table 8.3, Comparative Performance of the Predictive Controller in February**

### 8.2.2 Transitional Season Operation

The majority of system operation, for UK climatic conditions, is for the transitional seasons between winter and summer. During these periods, active precooling or heating of the thermal store is not normally required, the temperature of the room and thermal store generally being controlled by the operation of the heat recovery device with the ventilation rate being kept at the minimum. Figure 8.3, illustrates the room temperature profiles for April. These profiles are similar to those for winter operation (Figures 8.1), the shape of the profiles being dominated mainly by occupancy patterns. The limited need for active heating or cooling is indicated by the limited range in mass temperature of the thermal store over 24 hours (Figure 8.4).

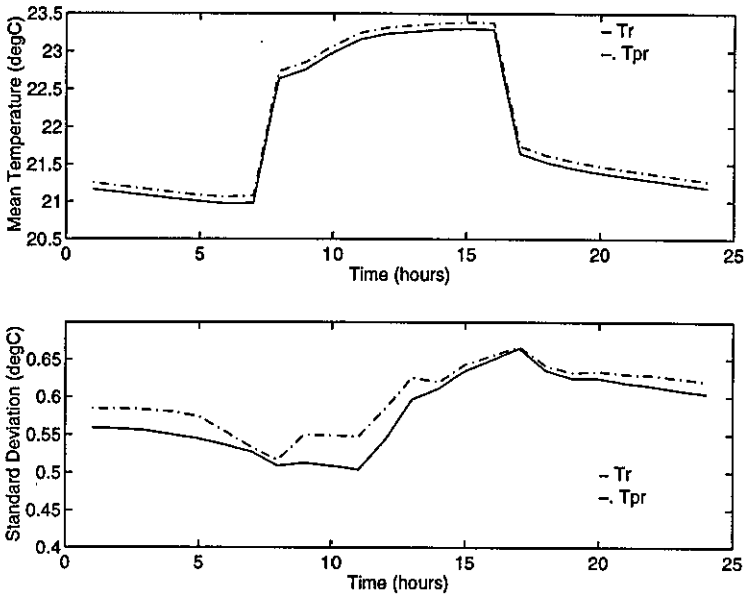


**Figure 8.3, Mean Room Temperature and Standard Deviation Profiles for April**

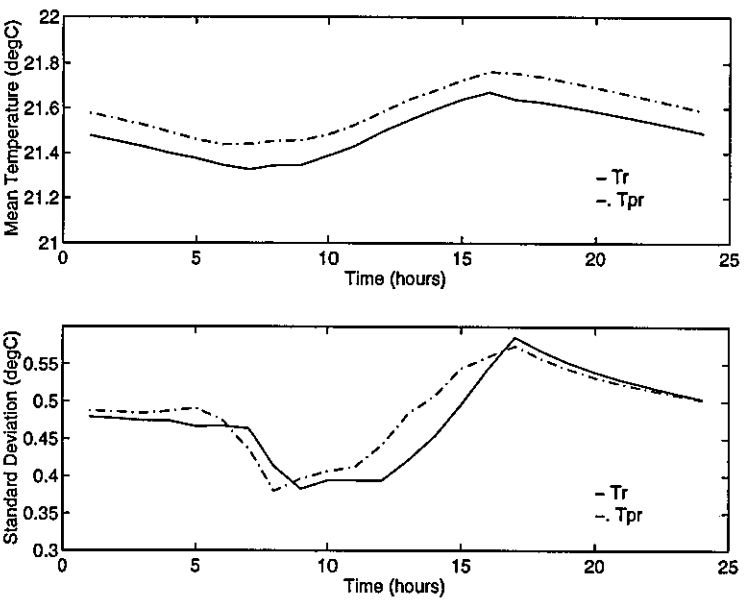


**Figure 8.4, Mean Slab Mass Temperature and Standard Deviation Profiles for April**

Table 8.4 indicates the prediction errors in the ambient temperature for April. As for the winter operation, the effects of these errors on the room temperature are limited by the high thermal capacity of the building (Table 8.5).

| Period | RMSE (°C) | MAE (°C) | ME (°C) | MAXAE (°C) |
|---|---|---|---|---|
| Occupancy | 2.2 | 1.8 | -0.4 | 6.0 |
| 24 hours | 2.1 | 1.6 | -0.3 | 6.5 |

**Table 8.4, Ambient Temperature Prediction Errors for April**

| Period | RMSE (°C) | MAE (°C) | ME (°C) | MAXAE (°C) |
|---|---|---|---|---|
| Occupancy | 0.3 | 0.2 | 0.1 | 0.9 |
| 24 hours | 0.3 | 0.2 | 0.1 | 0.9 |

**Table 8.5, Room Air Temperature Prediction Errors for April**

Table 8.6, indicates that the predictive controller can make major savings in both running cost and energy use over the conventional control strategy, which tends to overcool the building by its rule-based control. The conventional controller has resulted in a much greater level of occupant discomfort with a much higher violated PPD, and more hours of discomfort than the predictive controller.

| Type of Controller | Energy Cost (£) | Energy Use (kWh) | Mean PMV | Mean PPD (%) | Maximum PPD (%) | No. of Hours PPD > 10% |
|---|---|---|---|---|---|---|
| Conventional | £21.2 | 71.5 | -0.4 | 9.1 | 18.1 | 105 |
| Predictive | £5.4 | 39.4 | -0.3 | 6.9 | 10.4 | 2 |
| Perfect | £4.6 | 31.5 | -0.3 | 7.1 | 10.0 | 0 |

**Table 8.6, Comparative Performance of the Predictive Controller in April**

In comparison with the perfect control, although the predictive controller gives slightly higher energy cost, the room comfort is usually satisfied, with only 2 hours of PPD violating 10% and the maximum violated PPD being only 10.4%. Therefore, it can be concluded that the weather prediction errors have little influence on the room thermal conditions, and it is acceptable to use the predictive controller for the transitional seasons.

The optimum control strategy in transitional seasons indicates a simple plant operation strategy with minimum ventilation for the occupancy period and no precooling or preheating period. It may not, therefore, be necessary to schedule the plant operation over 24 hours. The heat recovery device, may be controlled by a local controller during the occupied period according to the thermal requirements in the room.

### 8.2.3 Summer Operation

During the summer operation, the optimum control strategy uses as much night free cooling as possible for relieving the daytime cooling load. For some hot days, the chiller is also operated at night to reduce the temperature of the ventilated slab even more. It is only when an extremely hot day is forecast, that it is necessary to operate the chiller during the occupied period.

Figure 8.5 illustrates the profiles of room temperatures throughout the day averaged for the month of July and Figure 8.6 the corresponding profiles for the average temperature of the ventilated slab.

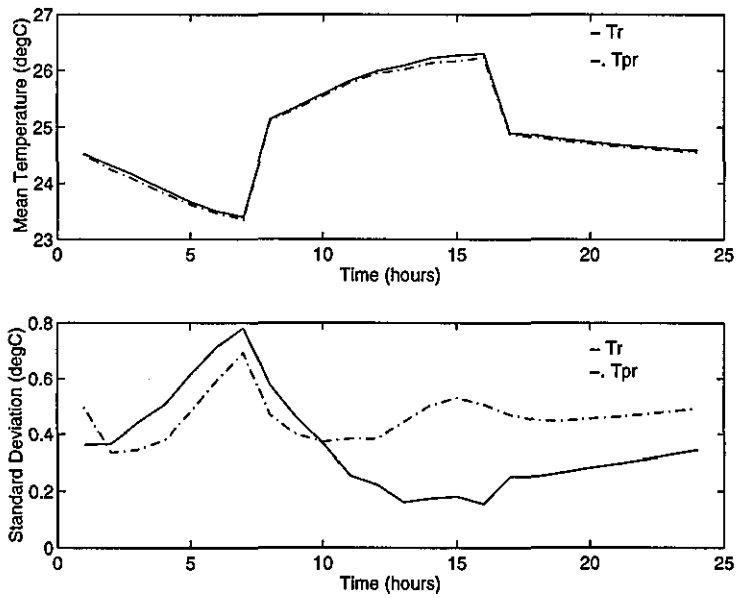


**Figure 8.5, Mean Room Temperature and Standard Deviation Profiles for July**

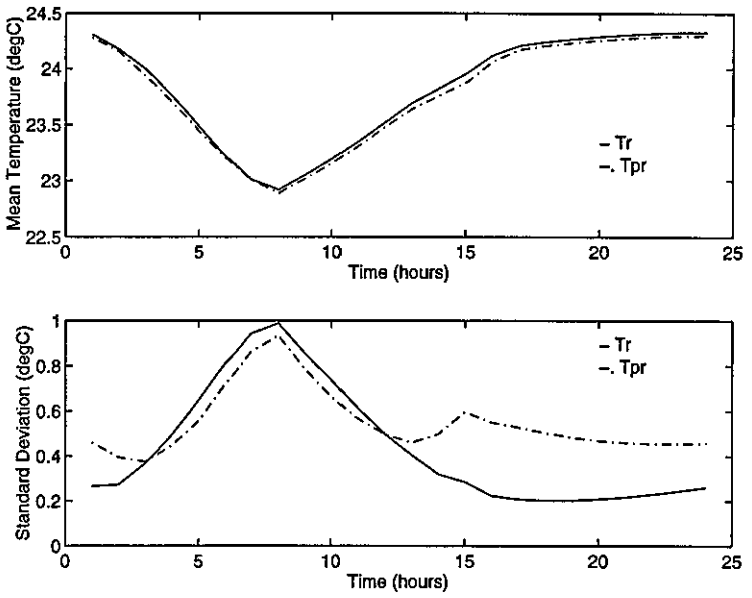


**Figure 8.6, Mean Slab Mass Temperature and Standard Deviation Profiles for July**

The critical period for control is during the late afternoon when the thermal loads tend to reach their peak and the thermal store is most likely to become exhausted. This is in contrast to the period near the start of occupancy (8:00 am), when the room temperature is free to float within the comfort band. Hence, the standard deviation in room temperature is lower during the critical afternoon period than during the start of occupancy. The room is closely controlled to be at the upper limit of the comfort range during the late afternoon (this is illustrated by $T_r$ from the perfect control in Figure 8.5, where the higher standard deviation in $T_{pr}$ during this period is due to weather prediction errors resulting in room temperature beyond the comfort limit for some hours). The temperature of the ventilated slab is at its lowest at the start of occupancy since this is the point at which the high electricity tariff starts and therefore by this time the thermal store must be full charged. The high standard deviation during this period reflects the changing need for cooling with the varying climatic conditions. The slight increase in standard deviation of the mass temperature around 3:00 pm is due to the occasional need for chiller operation during the period of highest cooling load. This occurred for only 8 hours during the entire month, with 39 hours of chiller operation in total.

Table 8.7 indicates the prediction errors in the ambient temperature and Table 8.8 the corresponding errors in room air temperature.

| Period | RMSE (°C) | MAE (°C) | ME (°C) | MAXAE (°C) |
|---|---|---|---|---|
| Occupancy | 3.4 | 2.7 | 0.1 | 9.2 |
| 24 hours | 3.2 | 2.3 | -0.0 | 14.3 |

**Table 8.7, Ambient Temperature Prediction Errors for July**

| Period | RMSE (°C) | MAE (°C) | ME (°C) | MAXAE (°C) |
|---|---|---|---|---|
| Occupancy | 0.5 | 0.4 | -0.1 | 1.8 |
| 24 hours | 0.5 | 0.4 | -0.1 | 2.4 |

**Table 8.8, Room Air Temperature Prediction Errors for July**

As for the winter and transitional season operation, the errors in weather prediction are damped by the mass of the building so that the errors in room temperature are much lower. However, the plant operation is potentially more complicated than in winter and therefore more prone to errors. There is also a greater coupling between the ambient and the room environment in the summer than the winter. During the winter, the approach for saving energy is to keep as much warmth as possible inside the room. This concept is reflected in the optimum strategy that recirculates the preheated room exhaust air through the slab at night and uses the heat recovery device to recover the supply temperature from the warm room exhaust. As a result, the influence of the prediction errors in the weather conditions is reduced by the recirculation of the room air and the use of the heat recovery device. Whereas, during the summer operation, there is a stronger coupling between the ambient and the room temperatures due to the dominant operating modes of night free cooling and supplying fresh air to the ventilated slab at the ambient temperature. There is also a greater influence from the solar gain on the thermal loads. This results in larger room errors than in the winter, relative to the weather prediction errors.

The maximum error in room temperature (MAXAE) during July is a result of a predicted high ambient temperature, which has caused 4 more hours of chiller operation than is necessary on one day during the month.

Table 8.9 compares the performance of the predictive controller with the conventional control strategy. The predictive controller provides closer control of the comfort conditions at a lower cost, but uses slightly more energy. The high cost of

energy in the conventional control is due to the constant use of ventilation only, without operating the chiller (no chiller is included in the conventional system. Chapter 6 has also indicated that for systems that do not include a chiller, the optimum controller results in a better performance than the conventional control strategy). Both controllers have a tendency to give slightly warmer than neutral comfort conditions. The maximum PPD of 14.4% for the predictive controller is due to the weather predictor underestimating the ambient temperatures for the following day, which results in insufficient thermal storage to last the occupancy period.

| Type of Controller | Energy Cost (£) | Energy Use (kWh) | Mean PMV | Mean PPD (%) | Maximum PPD (%) | No. of Hours PPD > 10% |
|---|---|---|---|---|---|---|
| Conventional | £28.7 | 142.1 | 0.1 | 6.7 | 19.9 | 19 |
| Predictive | £24.2 | 158.3 | 0.4 | 8.0 | 14.4 | 45 |
| Perfect | £16.1 | 111.3 | 0.4 | 8.1 | 10.0 | 0 |

**Table 8.9, Comparative Performance of the Predictive Controller in July**

It is seen from Table 8.9 that the number of hours operation above the 10% PPD is higher for the predictive controller than for the conventional controller. However, in the region of 10%, the PPD is sensitive to changes in the room temperature. In this case, the maximum PPD of 14.4% from the predictive controller is due to an increase in room temperature of 0.8 °C only. Further, the majority of the 45 hours of operation are for PPDs that are very close to the 10% constraint limit with only 6 hours of operation above the 12% PPD. This is in contrast to the conventional controller where most of the 19 hours of operation above the 10% PPD limit have much higher values of PPD with a maximum PPD of 19.9% and 16 hours of operation above the 12% PPD.

Due to the weather prediction errors, the predictive controller has resulted in comfort violations and a much higher energy cost than the perfect (weather prediction) controller (with a 50% increase in energy cost and a maximum PPD of 14.4%). Such degradation in the controller performance is primarily due to the optimum control strategy being more sensitive, which is in contrast to the winter operation where a simple strategy is used and the weather prediction errors result in only a slight increase in the operating cost. However, the room errors have indicated that the influence of large ambient prediction errors can be greatly reduced by

the thermal storage system, and the performance of the predictive controller is therefore acceptable.

### 8.2.4 The Characteristics of Room Thermal Conditions and Control Performance in Annual Operation

Figure 8.7 displays the monthly averaged room temperature during the occupancy hours and the monthly averaged slab mass temperature of 24 hours, over the 12 months in 1994. Under the predictive control strategy, the average occupied room temperature is well above 22 °C and below 26 °C, and the average slab mass temperature is between 21 °C and 24 °C over the entire year. The three months of June, July and August exhibit a cooling requirement, with the room and mass temperatures being fairly constant during other months for the winter and transitional period operation. The smoothly distributed average room and mass temperatures indicate that the room thermal conditions are stable and insensitive to the large variations in the ambient conditions. In comparison, the conventional controller results in lower room and mass temperatures over the entire year except for in March when the temperatures are close from both the controllers. The conventional controller also tends to overcool the thermal storage and the room in the transitional seasons, and has insufficient heat input during the winter operation. The local temperature peak in March under the conventional control is a result of the rule-based control for heating input and ventilation, which limits the adaptability of the controller to the ambient conditions.

Figure 8.7 also illustrates the monthly averaged PMV for occupant comfort over 1994. The effectiveness of the predictive control in ensuring the room thermal comfort is indicated by the PMV index being between -0.5 and 0.5 throughout the annual operation. This is in contrast to seven months of cold discomfort (PMV $<$ -0.5) under the conventional control. The effectiveness in reducing energy cost using the predictive control is reflected in the PMV distribution (Figure 8.7), in which during the winter, the room conditions are at the lower limit of the PMV constraint and are at the upper limit during the summer. This result adds to the validity of the whole optimization process.

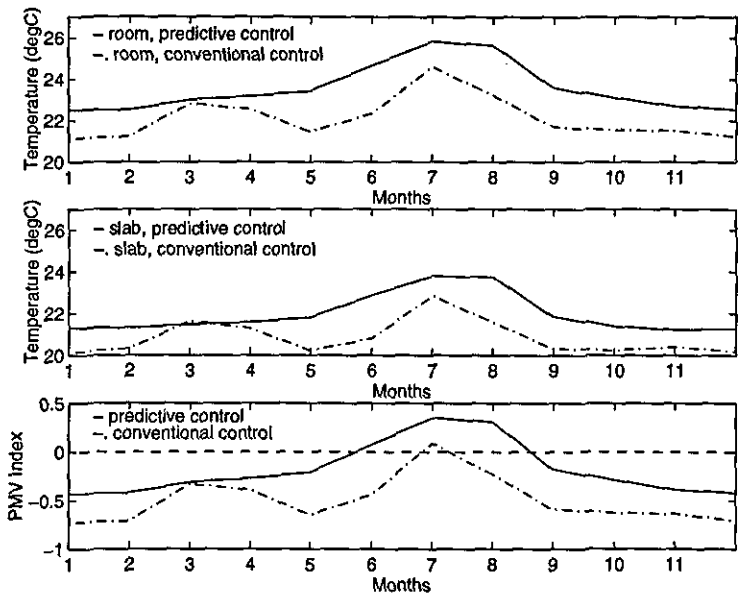


**Figure 8.7, Monthly Occupied Average Room Temperature and PMV Index, and Monthly Average Slab Temperature over 1994**

Table 8.10 shows the percentage of time heating or cooling is required in five bands of the daily average ambient air temperature, each band corresponding to a different thermal load in the room. Mechanical cooling is only required with a 7.4% probability in the temperature band [15°C, 25°C) (the rest 31.6% being from free cooling), while it is always in use when the daily average ambient air temperature is higher than 25°C. The annual daily average ambient air temperature is most likely to be in the band of [0°C, 25°C], for which there is only a 35% probability in total that heating or cooling is required.

| | Temperature Bands | | | | |
|---|---|---|---|---|---|
| | < 0°C | [0°C, 5°C) | [5°C, 15°C) | [15°C, 25°C) | [25°C, 30°C) |
| Percentage of time for heating or cooling | 100% | 85% | 24% | 39% | 100% |

**Table 8.10, Percentage of Time when Heating or Cooling Is Required during Annual Operation**

Figure 8.8 indicates the distributions of annual energy cost and energy use obtained from the predictive controller over 12 months. Substantially higher energy is consumed in the winter and summer months by the mechanical heating and cooling

devices, when the control of occupant comfort is critical. However, due to the high thermal capacity and sufficient insulation of the building, the critical months include only January, February and December for the winter operation and July for the summer operation. March, April and November require heating occasionally, and June and August exhibit a cooling requirement which can be sufficiently satisfied by night precooling without chiller operation.

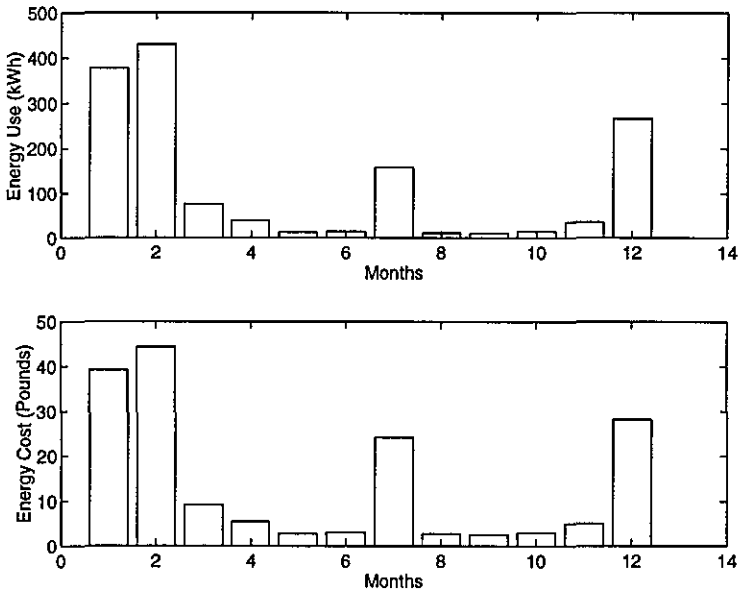


**Figure 8.8, The Distributions of Energy Use and Energy Cost from the Predictive Controller over 1994**

Significant energy and cost savings from the predictive controller can be indicated by comparing its annual performance with those from the conventional controller. The annual energy cost and energy use from the predictive controller are 43.6% and 66.2% respectively of those from the conventional controller. Cost saving is achieved during each season due to the optimum control strategy taking advantage of cheaper off-peak electricity, while the substantially smaller energy use is a result of the operation during the transitional seasons. The energy use in the winter and summer months is slightly higher than that of the conventional controller, since more mechanical heating and cooling is used to ensure occupant comfort.

To summarize, from the analysis of the characteristics of the optimum control strategy during annual operation, the errors in the room thermal conditions under the predictive control are much smaller than the weather prediction errors, while the energy cost and occupant comfort are still controlled to acceptable limits. The

predictive controller is also more effective in reducing energy costs and satisfying occupant thermal comfort than the conventional controller, as a result that the optimization of the plant operation strategy takes advantage of varying ambient conditions and the electricity tariff structure. This is especially true during the summer operation when it is the most critical period for utilizing the thermal storage system to save energy costs. The optimum control strategy is less critical during winter and transitional season operation. The optimum strategy for these seasons suggests that a simplified control strategy could be developed that further reduces the complexity of the control optimization.

## 8.3 The Effect of Building Construction on Controller Performance

The UEA ventilated slab building examined in this research represents a typical heavy weight (high mass), well insulated (low U value) passive building construction. The predictive control applied to this building is effective in saving operating costs without prejudicing the occupant comfort. It has been observed that the effect of weather prediction errors on room thermal conditions is much reduced by the building itself and the relatively insensitive operation strategy from the control optimization.

The effect of the building construction on the performance of the optimum predictive controller is investigated, with other two typical buildings: a light weight, well insulated building (referred to as 'low U value and low mass' in Table 8.13), and a light weight building without insulation (referred to as 'high U value and low mass' in Table 8.13). Since the ceiling and floor structure is standard in the ventilated slab building systems, with one layer of the ventilated slab and a second layer of screed, the variations in the building type investigated in this section apply to the wall construction only. The UEA building wall construction was given in Table 6.1, (indicated by a 'low U value and high mass' in Table 8.13). The construction components of the 'low U value and low mass' building and 'high U value and low mass' building are detailed in Tables 8.11 and 8.12 respectively.

| Walls | Construction |
|---|---|
| External Wall | 19mm render, 100mm mineral fibre, 200mm light weight concrete block, 13mm light weight plaster |
| Internal Walls | 25mm plasterboard, 25mm air gap, 25mm plasterboard |

**Table 8.11, The Construction of 'low U value, low mass' Building**

| Walls | Construction |
|---|---|
| External Wall | 100mm heavy weight concrete block, 25mm air gap, 100mm heavy weight concrete block, 13mm light weight plaster |
| Internal Walls | 25mm plasterboard, 25mm air gap, 25mm plasterboard |

**Table 8.12, The Construction of 'high U value, low mass' Building**

The thermal properties of the three types of wall construction are listed in Table 8.13, where $\Sigma C$ and $\tau_{os}$ are the lumped thermal capacitance and time constant in response to an external thermal disturbance, of the lumped single wall mass node $C_w$ in the thermal network model (Figure 4.8). The last column indicates the time constant of the external wall only (the internal walls being omitted in this calculation), since the change in U value of the building primarily affects the external wall's properties. The influence of the position of the wall layer elements is not investigated here, the insulation layer being located towards the outside of the wall, so as to increase the stability of the wall to ambient disturbances. The two insulated buildings in Table 8.13 follow this concept of arranging the insulation layer.

Comparing the insulated light weight building with the heavy weight building, the wall mass capacitance is reduced by 85.7% while keeping the same U value of the external and internal walls. The time constant is thus significantly reduced, resulting in a quicker response to the ambient disturbances. The third wall type only differs from the second construction in the external wall. The time constant of the external wall is greatly reduced due to the much higher U value of the

external wall, however, the time constant of the lumped wall mass node is slightly lower, due to the same internal wall construction as the second building.

| No. of Types | Building Type | U Value ($W/m^2K$) | $\Sigma C$ (J/K) | $\tau_{os}$ (hours) | $\tau_{os}$ (external) (hours) |
|---|---|---|---|---|---|
| 1 | low U value, high mass | 0.2 (external) 1.4 (internal) | $2.51 \times 10^7$ | 63.3 | 604.6 |
| 2 | low U value, low mass | 0.2 (external) 1.4 (internal) | $3.58 \times 10^6$ | 18.9 | 126.6 |
| 3 | high U value, low mass | 1.8 (external) 1.4 (internal) | $7.59 \times 10^6$ | 17.7 | 29.2 |

**Table 8.13, The Thermal Properties of the Three Types of Building**

The optimal predictive controller has been applied to the two light weight buildings and compared with the performance of the UEA building, during the winter, transitional season and summer operation.

### Winter Operation

In comparison with the heavy weight, well insulated UEA building, the optimum predictive controller produced similar comfort conditions in the light weight well insulated building, but with an increased energy cost (for instance, by 8.2% in February). The profiles of the mean and standard deviation of the room and mass temperatures from the three buildings for February are shown in Figure 8.9 and 8.10 respectively. The characteristics exhibited in the profiles of the insulated light weight building follow those of the insulated heavy weight UEA building, with the mean room temperature increasing slightly quicker during the afternoon. Since the wall is still well insulated, the internal gains cause slightly increasing room temperature in the afternoon but the low mass capacity results in a greater variation in room temperature and therefore higher standard deviation.

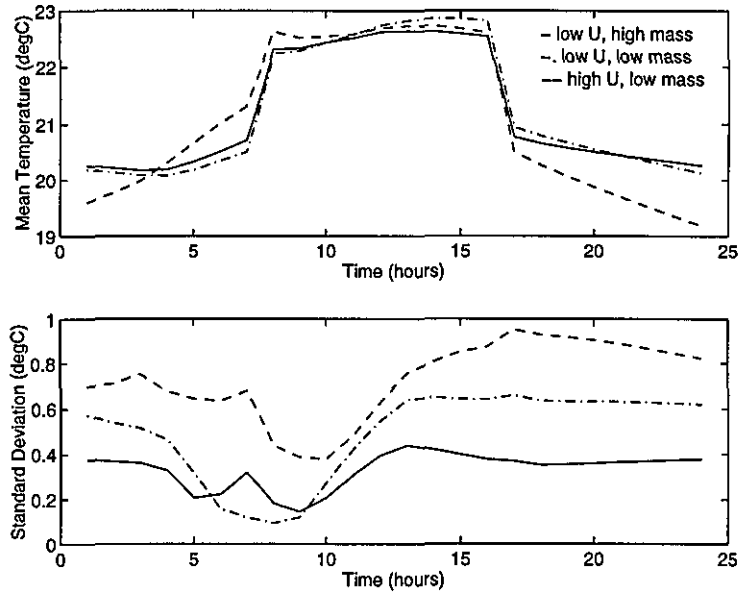


**Figure 8.9, Mean Room Temperature and Standard Deviation Profiles for February from the Three Buildings**

The third type of wall is not well insulated and has a low mass capacity. During winter operation, the performance of the predictive controller is dramatically worse than for the insulated high mass UEA building, with the energy cost for February increasing to £132.7 from £44.4. The maximum comfort violation is also high with a 16.8% PPD, in comparison to a 11.4% PPD for the UEA building. The room mean temperature at 8:00 am was 22.8 °C, 0.5 °C higher than that from the UEA building. This is a result of a higher heat input to the ventilated slab being required and therefore the room temperature is increased by the off-peak heating when the occupancy starts. The mean mass temperature is preheated to the highest level at 8:00 am, when the off-peak electricity period ends. Due to the high rate of heat loss, the rate of discharge of the thermal store is much faster than for either of the two well insulated buildings, which also accounts for the 1.5 °C higher mass temperature at the end of the preheating period. The lack of insulation also leads to greater coupling to the ambient conditions, which results in higher standard deviations in room and mass temperatures (Figures 8.9 and 8.10).

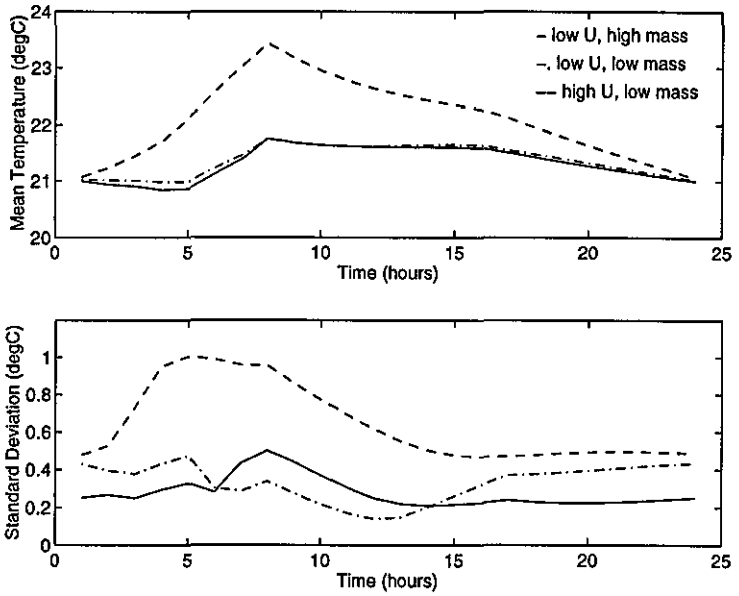


**Figure 8.10, Mean Slab Mass Temperature and Standard Deviation Profiles for February from the Three Buildings**

In conclusion for winter operation, the insulation of the external wall is the most significant factor in the control of the building, especially for the fabric thermal storage system where the storage efficiency will be substantially reduced by the poorly insulated wall, causing the room temperature to fluctuate with the ambient conditions.

### Transitional Season Operation

During the transitional season, the internal room temperature usually floats in the comfort range due to the mild external conditions, and as such the control of the plant operation is not critical. The light weight insulated building resulted in a similar controller performance to the heavy weight building (the mean and standard deviation of room and mass temperatures are similar to Figures 8.3 and 8.4), whereas the control of the uninsulated light weight building was sensitive to the ambient variations, which resulted in some preheating or precooling.

### Summer Operation

During July, the light weight, well insulated building energy cost was 42.2% higher than the heavy weight building. Due to prediction errors in the ambient conditions, the maximum discomfort was also higher at a 16.6% PPD, compared with 14.4%

from the heavy weight building. Figures 8.11 and 8.12 compare the profiles of the mean and standard deviation of the room and slab mass temperatures for the three buildings. The room air and slab mass temperatures at night are cooled to a low level in the insulated low mass building, but rise quickly in the middle of day due to the low mass capacity. However, the profiles for the mean slab mass temperature, and particularly, the standard deviation are similar to the insulated heavy weight building, which indicates the effect of the insulation on decoupling the ambient environment from the inside of the building. This is in contrast to the much high standard deviations for the uninsulated low mass building, where the coupling to the ambient environment causes a greater fluctuation in the room and slab mass temperatures.

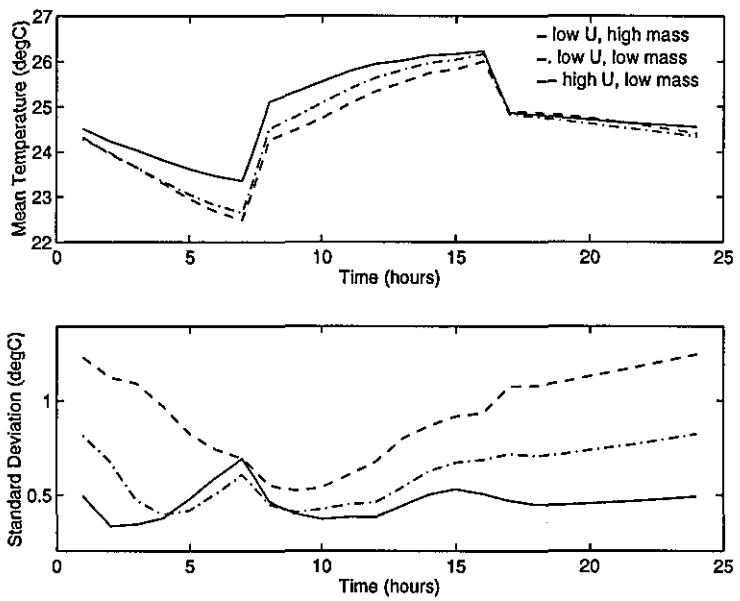


**Figure 8.11, Mean Room Temperature and Standard Deviation Profiles for July from the Three Buildings**

The operating cost for the light weight uninsulated building was 2.4 times as much as that of the heavy weight building, and 1.7 times that of the well insulated low weight building. The discomfort was also high with the PPD approaching 18.8%. Although the hourly mean room and mass temperatures are similar to the insulated low mass building, the standard deviations are higher due to the greater coupling with the ambient conditions. The standard deviation of the slab mass temperature is higher during the precooling period, the peak no longer being at the beginning of the occupancy. Throughout the entire month of July, the fan

was operated for all of the night hours and the chiller was also frequently operated at night and the daytime. Due to the high conductive link with the ambient environment, the energy stored in the slab mass at night is lost to the ambient and the thermal storage is substantially deteriorated.

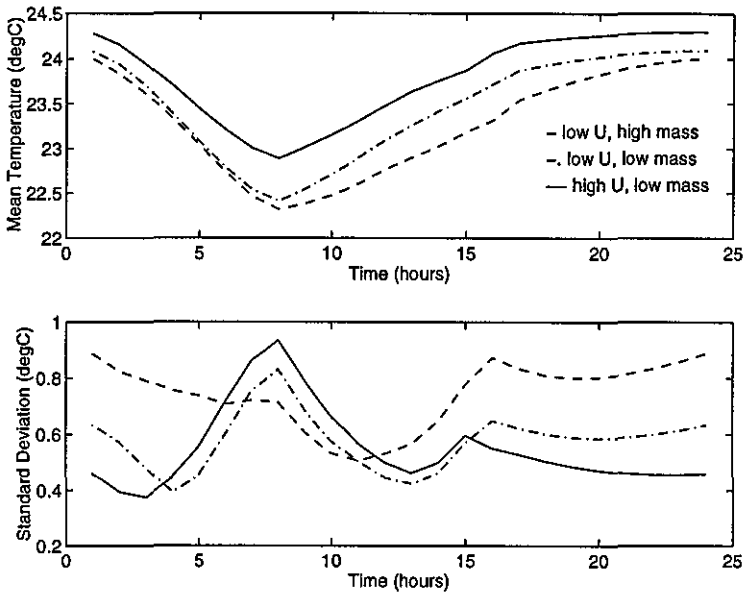


**Figure 8.12, Mean Slab Mass Temperature and Standard Deviation Profiles for July from the Three Buildings**

From this comparison of the performance from the three types of building, the insulation and mass capacity of the building significantly affect the predictive controller performance, of which the insulation is the most critical factor in the winter operation. The level of insulation controls the coupling between the room and ambient environment, so that low levels of insulation result in a greater coupling and less stable room and mass temperatures. The building weight tends to influence the extent to which the ventilated slab is preheated or cooled, with the light weight building requiring more preheating or precooling. A well insulated, heavy weight building, therefore, enables the stable control of the room thermal conditions with an acceptable level of thermal storage.

## 8.4 On-Line Adaption of the Optimal Predictive Control Strategy

The implementation of the optimal predictive controller involves testing the building model, plant models, the applicability of the optimal controller and the weather prediction. The building and plant models are simple and require small amount of data about the building physical measurements, material properties and plant design conditions. The on-line tuning of these models is not investigated in this research and any error due to the modelling of the building and plant is ignored (although the model sensitivity to the input parameters is examined in Chapter 4). However, the predicted control strategy can be adapted with some simple rules to prevent the occupant thermal comfort from exceeding the allowable limit, in case of a large weather prediction error, or a sudden unpredictable change in internal heat gains.

The control adaptor has two functions: the operation of the heat recovery device ('HRD control'), and booster operation for extra heating and cooling. A switchflow unit can also be incorporated into the adaptor to provide a fast response to the thermal loads in the room. Since the aim of the adaptor is primarily to improve thermal comfort, the adaption occurs during the occupied periods.

### Adaptive HRD Control

Other than the resistance to air flow, it is assumed in this research that, the operation of the heat recovery device does not contribute to the air distribution cost. The control of the damper regulates the routing of the air through the device and thus whether heat exchange between the fresh air and the room exhaust air takes place; this however, results in same cost of the fan operation.

The optimal control of the heat recovery device is therefore, purely a result of the temperature requirement in the controlled room. For instance, in the winter, the heat recovery device is always in use to increase the fresh air temperature by the warm room exhaust air. The room is normally controlled in the winter to the low limit of the comfort range. During summer operation, the heat recovery device is frequently not in use when the fresh air temperature is lower than the room air. However, it is in use when the fresh air temperature is higher than the exhaust air

since this will reduce the fresh air supply temperature. The room in the summer is controlled to the upper limit of the comfort range. Hence, when occupant comfort is critical during winter and summer, the heat recovery device is closely controlled by the optimum strategy.

In contrast, the room temperature floats within the comfort range during the transitional seasons, the control of the plant and heat recovery device is therefore not so critical. Since the operation of the heat recovery device has no direct cost penalty in the optimization of the control strategy, the optimum setpoint scheduling control may provide setpoints that result in a random operation of the heat recovery device, as could the time-stage control during the free cooling stages, provided the operation of heat recovery device does not drive the room comfort conditions beyond the limit. However, the operation of the heat recovery device can reduce the room temperature from the middle of the comfort range to the lower limit. Consequently, if the following day is cool, it may be necessary to preheat the slab mass to meet the occupant comfort constraint, where this would not have been necessary if the heat recovery device had not been randomly operated. For instance, in March and April, the inappropriate control of the heat recovery device resulted in preheating operation for 12 hours in total. Similarly, for a warm transitional day, the random operation of the heat recovery device is likely to increase the room temperature to the upper limit of the comfort range, thus causing more hours of night precooling for the following day.

The random operation of the heat recovery device does not occur during the peak summer and winter periods when the operation of the heat recovery device is closely optimized to satisfy the comfort constraint; each day's optimum strategy is also optimal in terms of a longer period of operation. The conflict in implementing the optimum control strategy during the transitional seasons is caused by configuring the optimization problem for a 24 hour planning period. However, in general, the scheduling of one day's control strategy is not influenced by the preceding day's operation (Chapter 6) and extending the planning period to 48 hours would increase the number of variables to be optimized and lead to an increase in prediction errors, due to the longer lead time. Therefore, one day is used in this research as the planning period for optimizing the plant control strategy.

The problems of poor thermal comfort and increased energy use, due to prediction errors and the random operation of the heat recovery device, can be reduced by

on-line control of the heat recovery device. The control rules presented here have been derived from inspection of the system performance and operation, and have been included to indicate the improvement in performance that can be achieved from the close control of the heat recovery device. Further research is required to develop a fully automated procedure for identifying the control rules for any particular building. The control rules applied here for the occupancy period are:

i. if the ambient temperature is more than 15 °C and room temperature is more than 23 °C, the HRD should not be operated;

ii. if the ambient temperature is more than 26 °C and 2 °C higher than the room temperature, the HRD should be operated to reduce the fresh air temperature by the room exhaust air before being supplied to the cooling coil;

iii. if the ambient air temperature is lower than 15 °C, the HRD should be operated to extract the warmth from the room exhaust air.

The first rule ensures that a room which is in the neutral or slightly warm comfort range is not overheated by the use of the heat recovery device. This rule is usually used in the warm transitional season and on early summer days. The second rule is applied to a very hot summer day, and the third rule is for the cool transitional season and winter. If the predicted control strategy results in a heat recovery device operation that is different from these rules, then the rules override the predicted operation. However, this is only true during the occupancy period, since the operation of the heat recovery device is closely controlled by the predicted strategy during other periods, to ensure the optimum preheating or precooling of the ventilated slab.

During March, the application of the adaptive HRD control has resulted in a 23.8% cost saving due to fewer hours of heater operation. The room temperatures are also increased since the HRD control rules eliminate the mode of supplying fresh air at the ambient temperature to the room directly, which tends to reduce the room temperature. The similar improvement has been observed in applying the HRD control to other cool transitional months. During the warm transitional months, such as May and June, the first rule of the adaptive HRD control is frequently applied, which has resulted in the fresh air at the ambient temperature

to be supplied to the room. This has led to lower room temperatures and a 22% reduction in energy cost from the night precooling. Such high energy savings are due to the low total energy cost in the transitional seasons, with a high proportion of the cost being from the heater operation in the cool season and night cooling in the warm transitional season; a small reduction in the number of hours of heater operation and night precooling can substantially reduce the operating cost.

Figure 8.13 compares the room air temperatures in June between the optimal predictive control with and without the adaptive HRD control. The room thermal conditions under the HRD control are more stable, especially during the latter part of the month when the fresh air at the ambient temperature is supplied to the ventilated slab, as the dominant mode of plant operation. Whereas without the HRD control, the optimum control strategy provided by the predictive controller results in the operation of the heat recovery device, leading to higher supply air and room temperatures.

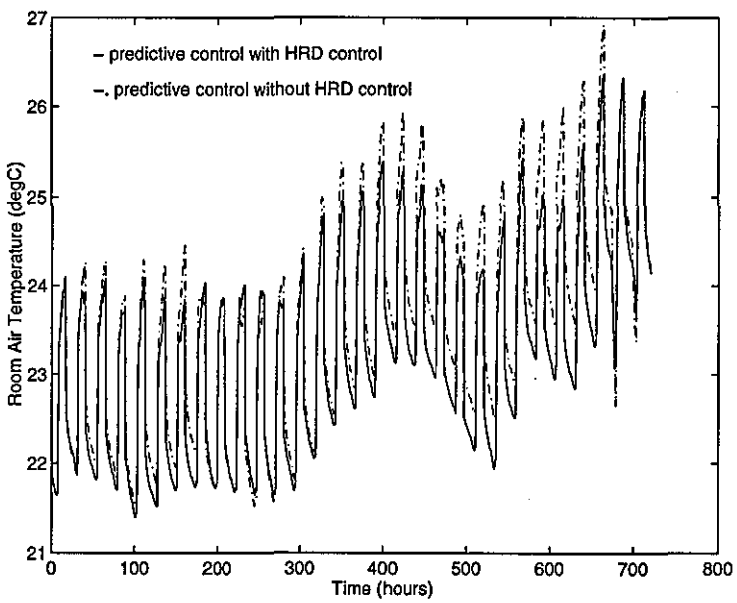


**Figure 8.13, Comparison of Room Temperatures in June with the Use of an Adaptive HRD Control**

The use of the HRD control to override the operation strategy of the heat recovery device during the occupancy hours, can greatly improve the system performance under the implementation of the predictive optimum control strategy, and eliminate the errors associated with a 24 hour planning period.

### Heating and Cooling Booster Control

Due to prediction errors in the ambient conditions, the predictive control of the thermal storage system can lead to room conditions that exceed the comfort limit. The predicted control strategy can be adapted with a boost in heating or cooling to bring the comfort conditions back within the 10% PPD limit. The comfort conditions are usually satisfied in the transitional seasons (Section 8.2), while during the peak winter and summer periods, the prediction errors can lead to the comfort limit being exceeded. The following rules can be used to prevent the violation of the comfort constraint. They have been obtained from inspection of the example system's operation and performance. For any particular building, the setpoints of the supply air temperature from the operation of the heating or cooling booster may be different. The rules, which are applied during the occupied period, are:

i. if the room air temperature is lower than $T_{\text{cold,set}}$, the heater is turned ON to increase the supply air temperature to 35 °C;

ii. if the room air temperature is higher than $T_{\text{hot,set}}$, the chiller is turned ON to reduce the supply air temperature to 12 °C.

Where the setpoints in the winter $T_{\text{cold,set}}$ and in the summer $T_{\text{hot,set}}$ are determined in relation to the room comfort level required and the increase in energy cost from the plant operation. During February, if the comfort limit of 10% PPD is strictly required, the setpoint $T_{\text{cold,set}}$ is set to 22.2 °C. In this case, the plant operating cost is consequently increased by 24.1%, in comparison with the predictive control which has resulted in a maximum PPD of 11.4%. The increased cost is due to 14 hours of heater operation during the occupancy period over the month. The room air temperature is increased by a maximum of 0.8 °C and an average of 0.1 °C.

During July, if the setpoint $T_{\text{hot,set}}$ is set to 26.5 °C, the energy cost due to the use of the booster is increased by 36.2%, but the PPD has been kept below 10.5%. In comparison, the maximum PPD under the predictive control without the booster is 14.4%. The room air temperature is reduced by a maximum of 0.6 °C and an average of 0.1 °C. The significant increase in the energy cost is due to more hours of chiller operation during the occupied hours, the chiller being operated for 27 hours at the daytime and 30 hours at night in July. This is in contrast

to the 6 hours daytime chiller operation and 34 hours at night, provided by the predictive control strategy. Lower setpoints such as 26 °C, result in much higher energy costs and more hours of daytime chiller operation. Therefore, the selection of the setpoint used for the maximum allowable temperature in the room should be based on the cost penalty and the acceptable comfort conditions; the higher the setpoint temperature, the smaller the increase in the plant operating cost, but the more risk of the room overheating and of occupant discomfort. Figure 8.14 shows the room temperatures under the predictive control with and without the adaptive HRD and booster control. The peak room temperatures during occupancy hours are reduced to approximately 26 °C by the use of the adaptor (the setpoint being 26 °C). This reduction greatly increases the operating cost.

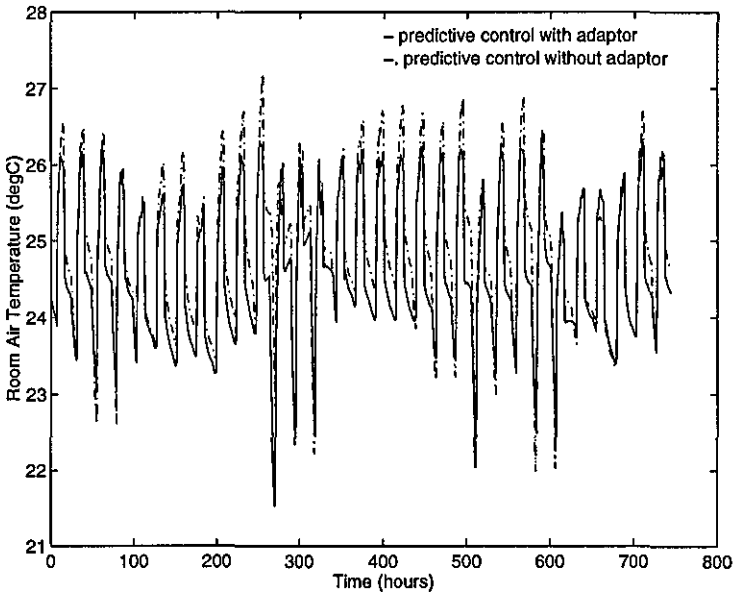


**Figure 8.14, Comparison of Room Temperatures in July with the Use of Adaptive HRD and Booster Control**

Although the effects of building and plant model errors on the predicted control strategy are not investigated in this research (the same models being used to represent the building as are used within the predictive controller), the use of the booster can prevent the room thermal conditions from exceeding an allowable limit as a result of all errors involved in calculating the optimum predicted control strategy and the uncertainty in room heat gains.

### Use of the Switchflow Unit in the Adapted Control

Switchflow operation routes the supply air through only one slab core rather than three cores. By not heating or cooling the entire slab mass storage, the coupling between the ventilation air and the slab mass store is reduced. This should lead to energy savings during the adapted control, when a boost in heating or cooling is required to offset the room thermal loads directly. The influence of the switchflow operation on the room and slab mass temperatures has been investigated in Chapter 4.

The use of switchflow operation during the adapted control in February has resulted in a 6.1% lower energy cost, compared to the adapted control without switchflow operation. The average room air temperature during the occupancy hours is increased by 0.1 °C, with only a small change in the average slab mass temperature over the month.

During July, switchflow operation has reduced the cost by 6.7% and lowered the room air temperature by an average of 0.1 °C. The slab mass temperature is slightly increased by an average of 0.05 °C over the occupancy period, since the switchflow unit uses only one core to supply the chilled air to the room, thus a lower proportion of the mass capacity is involved in the heat exchange with the supply air.

These results demonstrate that the switchflow unit can improve the performance of the predictive controller when integrated in the on-line control adaptor.

From the discussion in this section, it is concluded that when implementing the optimal predictive controller in a hollow core ventilated slab building, the use of an on-line adaptor can improve the system performance and also ensure the occupant comfort in case of large errors in the predicted room thermal conditions.

## 8.5 Conclusion

In comparison to a conventional control strategy during annual operation, the predictive controller has been shown to maintain more consistent thermal comfort conditions than the conventional control strategy. The predictive controller also

reduces energy costs throughout the annual operation, and reduces energy use during the transitional seasons.

Errors in the prediction of the climatic conditions have been shown to be reduced when translated into the temperature of the controlled zone. The reduction is due to the high thermal capacitance of the building and the characteristics of the plant control strategy.

The building construction imposes a large influence on the control performance, where the insulation and mass capacity of the building are the important factors that enable the fabric thermal storage system to achieve an acceptable efficiency and reduce energy costs.

The weather prediction, and optimization of the control strategy is computationally acceptable. The use of an on-line control adaptor can improve system performance and ensure occupant thermal comfort.

# Chapter 9

# Conclusions and Further Work

## 9.1 Conclusions

This thesis has described the development of an optimum predictive controller for hollow core ventilated slab systems. The controller incorporates a model-based optimization of the plant operating schedule and a model for predicting the weather profile for the next day. The controller has been applied to a typical heavy weight well insulated hollow core ventilated slab building. The ability of the controller to utilize the building thermal mass storage in reducing the total operating energy cost and maintaining the room thermal comfort has been investigated.

The design of the controller is described in Chapter 3, where the controller structure, control variables and pertinent components have been identified. The supervisory control variables are the supply air temperature and air flow rate to the ventilated slab for each hour of the 24 hour planning period. The setpoints are simultaneously optimized over the entire planning period so that the setpoint schedule can account for the dynamic nature of the thermal storage. For the setpoints in each hour, the mode of plant operation must be optimized to give the minimum energy consumption while meeting the setpoints. This control structure is robust, computationally efficient, while being flexible in allowing different plant installations to be controlled without affecting the formulation of the optimization of the thermal storage.

The predictive elements of the controller include models for the building and plant, and weather prediction. The building and plant model is the central element of the optimum controller and is described in Chapter 4. The building model must be dynamic, accurate, and robust in allowing the evaluation of different control strategies in the optimization. The plant models are based on well established steady state models. A new model of the hollow core ventilated slab has been integrated with a lumped parameter thermal network zone model. The slab model can simulate the heat exchange between the ventilation air and the slab mass. The zone model can assess the effects of all the major heat disturbances on the room thermal conditions. The integrated slab and zone model parameters can be easily derived, which can allow system control optimization and the investigation of different design solutions. The validation and robustness of the building model have also been described in Chapter 4.

In association with the development of the slab heat exchanger model, an analysis of the measured performance data suggests that the increase in convective heat transfer coefficient around the corners of the air cores is approximately 50 times higher than that for a straight duct. The generality of this value can not be verified completely but appears to be correct for use in the model and agrees with the experimental test data described in this thesis.

The model output has been compared to the measured performance data for two sets of test, the first representing normal operation cycled over several days, and the second for a step input in the supply air temperature to the slab. It was concluded that the model gave an acceptable accuracy for normal operation with a root mean square error in zone air temperature of less than 0.9 °C and 0.5 °C in average slab mass temperature. The errors are generally due to the amplitude rather than a phase shift in the temperature cycle. The step input test gives an insight into the accuracy of the model for the heat exchange between the ventilation air and the slab. The maximum error in air temperature leaving the ventilated slab was 1.1 °C and the root mean square error 0.6 °C, whereas the maximum error for the average temperature of the slab was 0.3 °C, both of which indicate an acceptable level of accuracy.

The weather prediction algorithm is essential to the implementation of the optimal controller. This model is required to predict the ambient dry-bulb temperature and solar radiation for the next 24 hours. An adaptive algorithm has been developed for

weather prediction (Chapter 7). The performance of various prediction methods has been compared, indicating that the short-term temperature prediction can be conducted independently without considering the correlation to the solar radiation. The temperature prediction model includes two elements that can account for the deterministic trends and the stochastic variations of the ambient temperature. A clockwise formulation of the EWMA model is used to evaluate the deterministic daily periodicity of the temperature time series. An ARMA model is used to calculate the stochastic property of the temperature. The ARMA model has an order of 4 autoregressive parameters and no moving average part. Using this combined deterministic-stochastic method to model the two sets of weather data (for the CIBSE weather year and for 1994 at Garston, Watford, UK), the mean absolute error in predicting the ambient temperature for each year was lower than 1.8 °C and the root mean square error lower than 2.5 °C. The model gave no bias in predicting the temperature. For solar radiation, a deterministic model, EWMA model is used to calculate the hourly variations in solar radiation for the next 24 hours. The predictive algorithms for ambient temperature and solar radiation are simple and efficient for use in off-line parameter estimation at the end of every day. For the purpose of the predictive control of building fabric thermal storage systems, it is also found that updating the weather prediction profile within a day does not improve the performance of the controller to provide the optimum plant operating schedule for the next 24 hours. Therefore, updating is not used in this research.

An optimization algorithm should be used to search for the optimum control strategy under the predicted ambient and room thermal conditions, such that the total energy cost is minimized without violating the building occupant thermal comfort. In order to gain confidence in the optimum solution obtained from the optimization, two optimization algorithms have been investigated in solving the control problem (Chapter 3), a Genetic Algorithm (GA) and the Complex method. In Chapter 5, the two optimization algorithms are used to optimize the supply air setpoint schedules over the 24 hour planning period. The perfect knowledge of the next day's weather conditions is assumed to allow a close investigation of the performance of the optimization algorithms in providing an optimum solution. The performance of applying the optimization algorithms in solving the simplified time-stage control problem (detailed description of this controller is given in Chapter 6) is also investigated in Chapter 5.

The performance of the optimization algorithms has been assessed in relation to their ability in finding an optimum solution, the computational overhead, and sensitivity to an initial guess of solution. Although in order to obtain satisfactory performance from the GA search, its parameters must be tuned and its search mechanism configured, the consequently improved performance is evident in the optimum solutions obtained. The results show that the GA is a viable method for investigating the characteristics of the optimum supervisory control of building fabric thermal storage systems. In comparison, the Complex method gives a solution having a higher energy cost than that from the GA search and the schedule of the operating setpoints is clearly sub-optimal. It is also sensitive to the initial guess. The Complex method can not solve the time-stage control problem since it is inefficient in handling integer control variables. Therefore, the GA is selected as the search algorithm in the optimum predictive controller.

Using the Genetic Algorithm as the optimizer, the characteristics of the optimum control strategies have been obtained for the hollow core ventilated slab system under various operating conditions (Chapter 6). This has led to the development of a simplified time-stage controller. The performance of the two optimum controllers, the supply air setpoint scheduling and the time-stage controller, in reducing energy costs and maintaining room thermal comfort has been investigated for various seasonal operations. During the summer, the general characteristics are that the low ambient air temperature and off-peak electric tariff leads to high ventilation rates at night, followed by an initial period during occupancy when the ventilation rate is set to a minimum. The ventilation rate may be increased later in the day to compensate for higher thermal loads. Similarly, where mechanical cooling is required, the chiller will be operated during the off-peak period with supplementary operation during peak periods only when necessary. During the winter, preheating is used to charge the thermal store using higher ventilation and higher supply air temperature at night. When the occupancy starts, only minimum ventilation is used with the heat recovery device in operation. In comparison to a conventional rule-based control strategy, the optimal control strategy provides significant energy cost savings and improved thermal comfort in the occupied space.

The effects of weather prediction errors on the performance of the controller are investigated in Chapter 8. The characteristics of the optimal plant operation and room thermal conditions during each season (for the UK's climate) are also described. Errors in the prediction of the climatic conditions have been shown to be

reduced when translated into the temperature of the controlled zone. The reduction is due to the high thermal capacitance of the building and the characteristics of the plant control strategy. In comparison to a conventional control strategy, the annual operation of the predictive controller has shown that savings can be up to 43.6% in energy cost, and 66.2% in energy use. The cost savings are achieved during each season due to the optimum control strategy making the best use of the building mass storage, free night cooling and cheaper off-peak electricity, while the substantially smaller energy use is a result of the operation during the transitional seasons. It is also indicated that the predictive controller can maintain more consistent thermal comfort conditions than the conventional control strategy.

In order to maximize the storage efficiency of a hollow core ventilated slab building, a well insulated and heavy weight construction are of prime importance, since this minimizes the energy loss from the thermal store to the environment and increases the stability of the room thermal conditions. The on-line adaption of the optimal predictive controller to a hollow core ventilated slab building has also been investigated in Chapter 8. Results show that the use of an on-line adaptor can improve the system performance and also ensure the occupant thermal comfort in case of large errors in the prediction of the ambient and room thermal conditions.

In summary, there are a number of specific conclusions that can be drawn:

- a building model that can accurately model the heat exchange between the ventilation air and the slab mass storage is of prime importance for the evaluation of control strategies of the thermal storage; the model robustness is also essential to allow the optimization of plant operation for all likely operating conditions;
- the Genetic Algorithm requires the tuning of its parameters and configuration of the search mechanism, since the values of parameters may vary with different applications. The GA search has no absolute convergence criterion due to probabilistic nature of the algorithm. The solutions derived from the search have been confirmed by examining the rate of cost reduction and inspection of optimum schedules of control variables;
- the optimum schedule of plant operation is dependent on the schedule of occupancy and electricity tariff structure. Setpoint scheduling control can model all different schedules of occupancy and electricity tariff. The time-

stage control derived in this thesis only applies to the condition that the start of occupancy coincides with the start of on-peak electricity. However, different schedules can be included by modifying the time stages of the controller according to the characteristics derived from the setpoint scheduling control strategies;

- due to the highly stochastic nature of the ambient conditions, the weather prediction errors are inevitably large in some cases. However, the consequent errors in the room thermal conditions are substantially reduced. The building model, weather prediction, and optimization of the control strategy are computationally acceptable, and the controller can produce an optimal control strategy within the limited time period (one hour). Further, the use of an on-line adaptor can ensure the room thermal comfort for all errors in the predictive control of the system;

- the building model used in this thesis assumes a perfect knowledge of the building data and parameters, such as material properties. The on-line implementation of the optimum predictive controller requires an accurate estimation of model parameters to adapt the model to the measured room thermal conditions, which would form part of future work.

## 9.2 Suggestions for Further Work

This thesis has proved the concept of the optimal predictive control of hollow core ventilated slab systems. Further work should address the on-line implementation of the optimum predictive controller. The structure of the building thermal model should be simplified to allow the on-line tuning of the model parameters. The effect of errors in the building model on the optimum control strategy have not been investigated in this thesis. Further work is therefore required to address the on-line tuning of the building model and the need for its simplification. Several other methods can be used for developing an on-line building model, such as neural network models, ARMAX models and a simple physical model.

Neural network techniques have been applied (Gibson, 1997; Ferrano and Wong, 1990), to the prediction of building and plant operation. Most applications of neural network models in the literature are for the prediction of the cooling load

profile for the next 24 hours. Such networks have relatively few input-output variables. However, in this control structure, the thermal response of the building to different control strategies must be modelled, including mass and room temperatures (to allow the calculation of room comfort level). The input to the network would be the driving variables, such as supply air conditions, ambient temperature and solar radiation as well as the room initial thermal states. This would result in a large neural network. The applicability of neural network methods to the building model in this controller should be investigated. ARMAX methods have also been used in the literature (Chen and Athienitis, 1996; Lute and Paassen, 1995). A large dimensional ARMAX model would also be expected in order to account for the building thermal response.

A simple five-parameter *RC* thermal network model could also be used for the on-line tuning building model (Figure 9.1). Four resistances and one capacitance represent the thermal properties of the zone and its response to heat disturbances ($T_{sup}$ is the supply air temperature to the ventilated slab, and the other notations are the same as those in Figure 4.8).

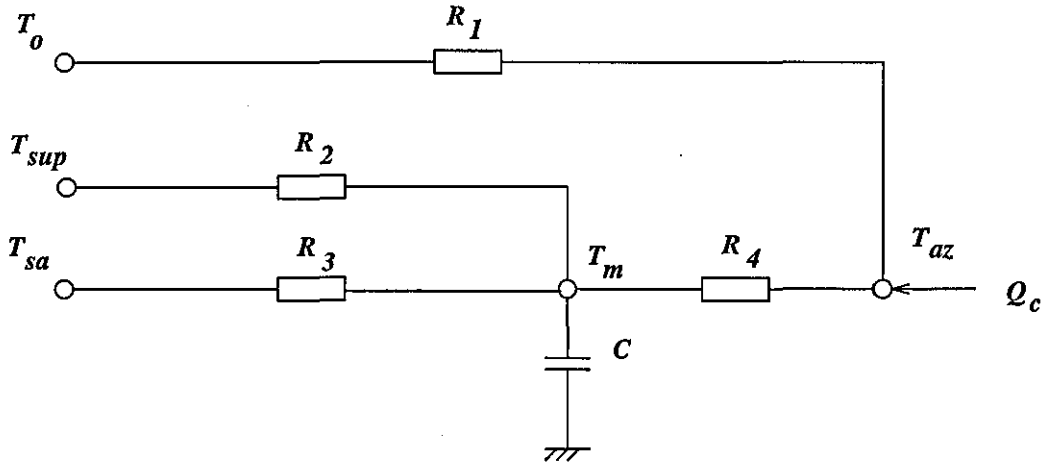


**Figure 9.1, Proposed On-Line Tuning Building Model**

The resistances and capacitance can be identified on-line so as to minimize the error between the measured and modelled temperatures. This model, although more crude than the model of Figure 4.8 in this thesis, has parameters that are easier to tune and adapt to the real response of the building. The model parameters can be estimated by a nonlinear estimation method or on-line recursive estimation. In practice, the tuning could be conducted off-line once a day, just prior to the control optimization. This would enable the model tuning by perhaps a more accurate

nonlinear method. The model parameters could also be updated during a day by recursive on-line estimation to fit to the measured building response, however, this procedure could help for the plant control operation for each hour, may not be of use for the scheduling of night plant operation.

The use of the lower level plant supervisory and local loop controls in reducing the effect of prediction errors should also be examined. The predictive control of plant local control variables can also be optimized for each hour to reduce the errors in local closed loop control. House *et al.* (1991) and Lute and Paassen (1995) demonstrated the energy savings of predictive control compared with conventional ON/OFF and PID control.

The controller described in this thesis relies on the prediction and measurement of the solar radiation. Since solar radiation is not normally measured in buildings (the instrumentation being expensive), the model should be simplified and the hourly solar radiation evaluated from the daily radiation data available from the local weather forecast station.

Although the on-line adaption of the optimum control schedule can be used to meet unforseen disturbances and prediction errors, the internal disturbances such as the occupancy pattern, have been assumed to be known in this research. A means of predicting the internal gains (such as from occupancy and lighting) should be investigated as part of future research.

Moisture in the building and the ambient environment is not modelled in this thesis. For hollow core ventilated slab buildings, the variation in the humidity ratio of the air supplied to the slab is restricted due to the risk of condensation in the slab core. The application of the controller to other large scale building and plant systems, where the building space is precooled at night, may require the use of humidity control. Since the zone temperature setpoint has the most impact on the energy stored in the building mass, humidity may not need to be included as a scheduling control variable, however, during the daytime, at each hour, the predictive optimal control of plant operation must take humidity into account.

The controller developed in this thesis can be applied to other buildings. The building model is a single zone model, with the optimal schedule of plant operating setpoints applied to the single zone. In the case of a large building with multiple zones, the interaction between the thermal requirements in different zones should

be taken into account. Using the control hierarchy employed in this thesis, the primary supervisory control variables that govern the plant operation for each zone should be optimized over 24 hours. The energy input to local reheat coils, air flow rate and discharge air temperature from the air handling unit would be optimized at each hour, the problem being constrained by the high level scheduling control. The performance of the optimal controller for multizone applications should be investigated.

The analysis of building and plant life-cycle cost can also be extended for this optimal controller. Integrating the optimal control strategy into the optimal design of plant storage systems was investigated by Kintner-Meyer and Emery (1995a), and Arkin *et al.* (1997), where the optimal design scheme obtained could take account of the dynamic interaction between the cold storage and the direct cooling plant, and the operational efficiency of the plant equipment was substantially improved. The life-cycle cost of the building fabric thermal storage system should also be investigated in order to obtain an optimum design of plant and building fabric storage. Since the energy stored in the building fabric is difficult to evaluate, some parameters should be identified to represent the size of mass storage that governs the capital cost and operating cost, both being included in the life-cycle cost function. This methodology can offer a complete optimal design and control scheme for the building fabric thermal storage system.

The Genetic Algorithm has proved to be a robust and efficient optimization tool in this controller. Further work on optimal zone thermal conditions can be conducted using the multiobjective Genetic Algorithm to investigate the distribution of thermal comfort within a zone. In this thesis, a single comfort condition in a zone is applied as the constraint in the cost minimization. However, the air distribution in a large space may not be uniform, the PMV values at different locations in the zone are thus different and can be calculated (using a distributed zone thermal model or computational fluid dynamics model). The comfort levels at different locations can form the multiple objectives in the optimization, in addition to the minimization of plant operating cost. The trade-offs between the design criteria and their interactions can be examined closely; the relationship of the PMV values in the zone can be a guide towards the optimum solution of supply air conditions as well as the design of diffusers. Similarly, the optimization procedure presented in this thesis could be converted to a multiobjective procedure by forming the PMV constraints in each hour as multiobjective criteria rather than constraint

functions. The multiobjective optimization principle can also be employed in the optimal control of multizone systems, which can guide the design and control of plant and air handling units serving the zones.

These areas can all be extended from the work based on this thesis. Further work is essential for the full implementation of the optimal control methodology described here. Further research will result in the practical, robust, and efficient control and design of building fabric thermal storage systems.

# References


Abraham, B., and Ledolter, J., 1983. *Statistical Methods for Forecasting*, John Wiley and Sons, Inc.

Allen, G., Kani, M., and Carpenter, S., 1984. "Mechanically Enhanced Passive Solar Thermal Storage", *Proc. SESCI'1984, Calgary*, August, 72-78.

Andresen, I., and Brandemuehl, M.J., 1992. "Heat Storage in Building Thermal Mass: A Parametric Study", *ASHRAE Transactions*, **98(1)**, 910-917.

Arkin, H., Navon, R., and Burg, I., 1997. "HVAC with Thermal Energy Storage: Optimal Design and Optimal Scheduling", *Building Services Engineering Research and Technology*, **18(1)**, 31-38.

Arnold, D., 1993. "Within these Walls", *Building Services Journal*, September, **15(9)**, 41-44.

Arnold, D., 1996. "Mixed-Mode HVAC-An Alternative Philosophy", *ASHRAE Transaction*, **102(1)**, 687-691.

Athienitis, A.K., 1988. "A Predictive Control Algorithm for Massive Buildings", *ASHRAE Transactions*, **94(2)**, 1050-1067.

Augenbroe, G.L.M., and Vedder, H.A., 1985. "Accurate Modelling of Air-Supplied Heat Storage in Hollow Core Slabs", *CLIMA 2000, World Congress on Heating, Ventilation and Air Conditioning*, August, 441-446.

Barnard, N., 1995. "Choosing the Right Fabric", *Building Services Journal*, March, **17(3)**, 31-33.

Bellman, R.E., 1957. *Dynamic Programming*, Princeton University Press, Princeton, New Jersey.

Birrer, W.A, and Ariba, M.A., 1983. "Structural Storage as a Part of a Total System for Energy Efficient Office Buildings: Two Examples", *Solar World Congress Proceedings of the 8th Biennial Congress, Perth*, August, **1**, 397-401.

Box, M.J., 1965. "A New Method of Constrained Optimization and a Comparison with Other Methods", *Computer Journal*, **8(1)**, 42-52.

Braun, J.E., 1988. "Methodologies for the Design and Control of Central Cooling Plant", *Ph.D. Thesis*, University of Wisconsin-Madison.

Braun, J.E., Klein, S.A., Beckman, W.A., and Mitchell, J.W., 1989a. "Methodologies for Optimal Control of Chilled-Water Systems Without Storage", *ASHRAE Transactions*, **95(1)**, 652-662.

Braun, J.E., Klein, S.A., Mitchell, J.W., and Beckman, W.A., 1989b. "Applications of Optimal Control to Chilled-Water Systems Without Storage", *ASHRAE Transactions*, **95(1)**, 663-657.

Braun, J.E., 1990. "Reducing Energy Costs and Peak Electrical Demand Through Optimal Control of Building Thermal Storage", *ASHRAE Transactions*, **96(2)**, 876-888.

BSRIA, 1992. "Dynamic Fabric Energy Storage", *Heating/Piping/Air Conditioning*, January, 91-93.

Bunn, R., 1991. "Termodeck: The Thermal Flywheel", *Building Services Journal*, May, **13(5)**, 41-44.

Bunn, R., 1994. "Slab and Trickle", *Building Services Journal*, February, **16(2)**, 30-32.

Bunn, R., 1995. "Teaching Low Energy", *Building Services Journal*, April, **17(4)**, 19-23.

Cascia, M.A., 1988. "Optimizing Chiller Plant Energy Savings Using Adaptive DDC Algorithms", *ASHRAE Transactions*, **94(2)**, 1937-1946.

Chen, T.Y., and Athienitis, A.K., 1996. "Ambient Temperature and Solar Radiation Prediction for Predictive Control of HVAC Systems and a Methodology for Optimal Building Heating Dynamic Operation", *ASHRAE Transactions*, **102(1)**, 26-36.

Chipperfield, A., and Fleming, P., 1995a. "Gas Turbine Engine Controller Design Using Multiobjective Genetic Algorithms", *Genetic Algorithms in Engineering Systems: Innovations and Applications*, September, 214-219.

Chipperfield, A., and Fleming, P., 1995b. "Genetic Algorithms in Control Systems Engineering", *Genetic Algorithm in Design Optimization*, The Institution of Electrical Engineers and The Institution of Civil Engineers, London.

CIBSE, 1986. *CIBSE Guide Book*, The Chartered Institution of Building Services Engineers, London, UK.

Clarke, J.A., 1985. *Energy Simulation in Building Design*, Adam Hilger Ltd, Bristol and Boston.

Clarke, J.A., Yaneske, P.P., and Pinney, A.A., 1990. "The Harmonisation of Thermal Properties of Building Materials", *Report TN91/6, Building Environmental Performance Analysis Club*, Building Research Establishment, UK.

Conniff, J.P., 1991. "Strategies for Reducing Peak Air-Conditioning Loads by Using Heat Storage in the Building Structure", *ASHRAE Transactions*, **97(1)**, 704-709.

Crabb, J.A., Murdoch, N., and Penman, J.M., 1987. "A Simplified Thermal Response Model", *Building Services Engineering Research and Technology*, **8**, 13-19.

Cumali, Z., 1988. "Global Optimization of HVAC System Operations in Real Time", *ASHRAE Transactions*, **96(2)**, 1729-1744.

Daryanian, B., and Norford, L.K., 1994. "Minimum-Cost Control of HVAC Systems under Real Time Prices", *Control Applications, IEEE Conference*, August, **3**, 1855-1860.

Davies, M.G., 1993. "Definitions of Room Temperature", *Building and Environment*, **28(4)**, 383-398.

Dickinson, S.J. and Brashaw, A., 1995. "Genetic Algorithm Optimization and Scheduling for Building Heating Systems", *Genetic Algorithms in Engineering Systems: Innovations and Applications*, September, 106-111.

Duffie, J.A., and Beckman, W.A., 1974. *Solar Energy Thermal Processes*, John Wiley and Sons, Inc.

El-Keib, A.A., Ma, X., and Ma, H., 1995. "Advancement of Statistical Based Modelling Techniques for Short-Term Load Forecasting", *Electric Power Systems Research*, **35**, 51-58.

Fan, J.Y., and McDonald, J.D., 1993. "A Real-Time Implementation of Short-Term Load Forecasting for Distribution Power Systems", *IEEE Transactions on Power Systems*, **9(2)**, 988-993.

Fanger, P.O., 1970. *Thermal Comfort: Analysis and Applications in Environmental Engineering*, Danish Technical.

Ferrano, F.J., and Wong, K.V., 1990. "Prediction of Thermal Storage Loads Using a Neural Network", *ASHRAE Transactions*, **96(2)**, 723-726.

Forrester, J.R., and Wepfer, W.J., 1984. "Formulation of a Load Prediction Algorithm for a Large Commercial Building", *ASHRAE Transactions*, **90(2B)**, 536-551.

Gibson, G.L., 1997. "A Supervisory Controller for Optimization of Building Central Cooling Systems", *ASHRAE Transactions*, **103(1)**.

Givoni, B., 1976. *Man, Climate and Architecture*, 2nd edition, Applied Science, London.

Givoni, B., 1984. "Options and Applications of Passive Cooling", *Energy and Buildings*, **7**, 297-300.

Goldberg, D.E., 1989. *Genetic Algorithms in Search, Optimization and Machine Learning*, Addison-Wesley publishing Company, Inc.

Goonatilake, S., and Feldman, K., 1994. "Genetic Rule Induction for Financial Decision Making", *Genetic Algorithms in Optimisation, Simulation and Modelling*, IOS Press.

Hartman, T.B., 1988. "Dynamic Control: The Weather Predictor and HVAC Control", *Heating/Piping/Air Conditioning*, May, 97-101.

Hartman, T.B., 1995. "Global Optimization Strategies for High-Performance Controls", *ASHRAE Transactions*, **101(2)**, 679-687.

Hassid, S., 1985. "A Linear Model for Passive Solar Calculations: Evaluation of Performance", *Building and Environment*, **20(1)**, 53-59.

Hawes, D.W., Feldman, D., and Banu, D., 1993. "Latent Heat Storage in Building Materials", *Energy and Buildings*, **20**, 77-86.

Hoffman, M., and Feldman, M., 1981. "Calculation of the Thermal Response of Buildings by the Total Thermal Time Constant Method", *Building and Environment*, **16(2)**, 71-85.

Hokoi, S., and Matsumoto, M., 1988. "An Analysis of Stochastic Properties of the Heating Load in an Intermittently Air-Conditioned Building", *Energy and Buildings*, **11**, 259-266.

Holman, J.P., 1986. *Heat Transfer*, McGraw-Hill, Inc.

Holst, J., Madsen, H., and Thyregod, P., 1987. "A Method for Using Hourly Predictions of Weather Observations in Optimal control of Heat Supply to Buildings", *Proceedings of 3rd International Congress on Building Energy Management, ICBEM*, 380-389.

House, J.M., Smith, T.F., and Arora, J.S., 1991."Optimal Control of a Thermal System", *ASHRAE Transactions*, **97(2)**, 991-1001.

House, J.M., and Smith, T.F., 1995."A System Approach to Optimal Control for HVAC and Building Systems", *ASHRAE Transactions*, **101(2)**, 647-660.

ISO, 1984. "Moderate Thermal Environments - Determination of the PMV and PPD indices and Specification of the Conditions for Thermal Comfort", *ISO 7730.*

Jakob, M., 1945. *Heat Transfer*, **I**, John Wiley and Sons, Inc.

Jekel, T.B., Mitchell, J.W., and Klein, S.A., 1992. "Operational Strategies for Reducing Coil Loads", *ASHRAE Transactions*, **98(1)**, 919-925.

Jiang, Y., and Hong, T., 1993. "Stochastic Analysis of Building Thermal Process", *Building and Environment*, **28(4)**, 509-518.

Kawashima, M., Dorgan, C.E., and Mitchell, J.W., 1995. "Hourly Thermal Load Prediction for the Next 24 Hours by ARIMA, EWMA, LR, and an Artificial Neural Network", *ASHRAE Transactions*, **101(1)**, 186-200.

Keeney, K.R., and Braun, J.E., 1996. "A Simplified Method for Determining Optimal Control Strategies for Thermal Storage in Building Mass", *ASHRAE International Journal of Heating, Ventilation, Air-Conditioning and Refrigerating Research*, **2(1)**, 59-78.

Keeney, K.R., and Braun, J.E., 1997. "Application of Building Precooling to Reduce Peak Cooling Requirements", *ASHRAE Transactions*, **103(1)**.

Kendrick, C.C., 1995. "The Use of Structural Components to Provide Thermal Storage and Night Cooling in a Building at the University of East Anglia", *MSc Thesis*, School of Mechanical Engineering, Cranfield University, UK.

Kintner-Meyer, M., and Emery, A.F., 1995a. "Cost Optimal Analysis and Load Shifting Potentials of Cold Storage Equipment", *ASHRAE Transactions*, **101(2)**, 539-548.

Kintner-Meyer, M., and Emery, A.F., 1995b. "Optimal Control of an HVAC System Using Cold Storage and Building Thermal Capacitance", *Energy and Buildings*, **23(1)**, 19-31.

Klein, S.A., Beckman, W.A., Mitchell, J.W., *et al.*, 1994. "TRNSYS. A transiet system simulation program", Version 14.1. Madison: Solar Energy Laboratory, University of Wisconsin.

Laret, L., 1980. "Use of General Models with a Small Number of Parameters: Theoretical Analysis", *Proceedings of CLIMA 2000*, Budapest, 263-276.

Levenhagen, J.I., and Spethmann, D.H., 1993. *HVAC Controls and Systems*, McGraw-Hill, Inc.

Liu, B.Y.H., and Jordan, R.C., 1960. "The Interrelationship and Characteristic Distribution of Direct, Diffuse and Total Solar Radiation", *Solar Energy*, **4**, 1-19.

Liu, M., Athar, A., Reddy, A.T., Claridge, D.E., Haberl, J.S., and White, E., 1995. "Reducing Building Energy Costs Using Improved Operation Strategies for Constant-Volume Air-Handling Systems", *ASHRAE Transactions*, **101(2)**, 688-700.

Ljung, L., 1987. *System Identification Theory for the User*, Englewood Cliffs, NJ: Prentice-Hall, Inc.

Lomas, K.J., 1991. "Dynamic Thermal Simulation Models of Buildings: New Method for Empirical Validation", *Building Services Engineering Research and Technologies*, **12(1)**, 25-37.

Lomas, K.J., and Eppel, H., 1992. "Sensitivity Analysis Techniques for Building Thermal Simulation Programs", *Energy and Buildings*, **19**, 21-44.

Lombard, C., and Mathews, E.H., 1992. "Efficient, Steady State Solution of a Time Variable RC Network for Building Thermal Analysis", *Building and Environment*, **27(3)**, 279-287.

Lute, P., and Paassen, D.V., 1995. "Optimal Indoor Temperature Control Using a Predictor", *IEEE Control Systems Magazine*, **15(4)**, 4-10.

MacArthur, J.W., Mathur, A., and Zhao, J., 1989. "On-Line Recursive Estimation for Load Profile Prediction", *ASHRAE Transactions*, **95(1)**, 621-628.

Mackle, G., Savis, D.A., and Walters, G.A., 1995. "Application of Genetic Algorithms to Pump Scheduling for Water Supply", *Genetic Algorithms in Engineering Systems: Innovations and Applications*, September, 400-405.

Mathews, E.H., Richards, P.G., and Lombard, C., 1989. "A Tool for Predicting Hourly Air Temperatures and Sensible Energy Loads in Buildings at Sketch Design Stage", *Energy and Buildings*, **14**, 61-80.

Mathews, E.H., Rousseau, P.G., Richards, P.G., and Lombard, C., 1991. "A Procedure to Estimate the Effective Heat Storage Capability of a Building", *Building and Environment*, **26**, 179-188.

Mathews, E.H., Richards, P.G., and Lombard, C., 1994. "A First-Order Thermal Model for Building Design", *Energy and Buildings*, **21**, 123-145.

Matsumoto, M., Hokoi, S., and Takamura, H., 1990/1991. "An Analysis of Stochastic Properties of Room Air Temperature and the Heating Load during the Autumn", *Energy and Buildings*, **15-16**, 875-886.

Meierhans, R.A., 1993. "Slab Cooling and Earth Coupling", *ASHRAE Transactions*, **99(2)**, 511-518.

Morris, F.B., Braun, J.E., and Treado, S.J., 1994. "Experimental and Simulated Performance of Optimal Control of Building Thermal Storage", *ASHRAE Transactions*, **100(1)**, 402-414.

Nizet, J.L., Lecomte, J., and Litt, F.X., 1984. "Optimal Control Applied to Air Conditioning in Buildings", *ASHRAE Transactions*, **90(1B)**, 587-600.

Oestreicher, Y., Bauer, M., and Scartezzini, J.-L., 1996. "Accounting Free Gains in a Non-Residential Building by Means of an Optimal Stochastic Controller", *Energy and Buildings*, **24(3)**, 213-221.

Olson, R.T., and Liebman, J.S., 1990. "Optimization of a Chilled Water Plant Using Sequential quadratic Programming", *Engineering Optimisation*, **15**, 171-191.

Olson, R.T., 1993. "A Dynamic Procedure for the Optimal Sequencing of Plant Equipment, Part I: Algorithm Fundamentals", *Engineering Optimisation*, **21(1)**, 63-78.

Pandit, S.M., and Wu, S.M., 1983. *Time Series and System Analysis with Applications*, New York: John Wiley and Sons.

Pape, F.L.F, Mitchell, J.W., and Beckman, W.A., 1991. "Optimal Control and Fault Detection in Heating, Ventilating, and Air-Conditioning Systems", *ASHRAE Transactions*, **97(1)**, 729-735.

Press, W.H, Teukolsky, S.A., Vetterling, W.T., and Flannery, B.P., 1992. *Numerical Recipes in C*, Second Edition, Cambridge University Press.

Rahman, S., and Hazim, O., 1992. "A Generalized Knowledge-Based Short-Term Load-Forecasting Technique", *IEEE Transactions on Power Systems*, **8(2)**, 508-514.

Rao, S.S., 1984. *Optimization Theory and Application*, Wiley Eastern Limited.

Raychaudhuri, B.C., 1965. "Transient Thermal Response of Enclosures: The Integrated Thermal Time-Constant", *Int. J. Heat and Mass Transfer*, **8**, 1439-1449.

Rink, R.E., 1994. "Optimal Operation of Solar Heat Storage with Off-Peak Energy Price Incentive", *Optimal Control Applications and Methods*, **15(4)**, 251-266.

Rink, R.E., and Li, N., 1995. "Aggregation/Disaggregation Method for Optimal Control of Multizone HVAC Systems", *Energy Conversion and Management*, **36(2)**, 79-86.

Rupanagunta, P., Baughman, M.L., and Jones, J.W., 1995. "Scheduling of Cool Storage Using Non-Linear Programming Techniques", *IEEE Transactions on Power Systems*, **10(3)**, 1279-1285.

Ruud, M.D., Mitchell, J. W., and Klein, S.A., 1990. "Use of Building Thermal Mass to Offset Cooling Loads", *ASHRAE Transactions*, **96(2)**, 820-829.

Schibuola, L., and Romagnoni, P., 1996. "Hourly Weather Data Generation by Simplified Methods for Long Term Energy Analysis in Building Climatisation", *CIBSE/ASHRAE Joint National Conference*, 70-78.

Seem, J.E., and Braun, J.E., 1991. "Adaptive Methods for Real-Time Forecasting of Building Electrical Demand", *ASHRAE Transactions*, **97(1)**, 710-720.

Shavit, G., 1980. "Design and Control Strategies for Energy Storage", *ASHRAE Transactions*, **86(2)**, 631-644.

Simmonds, P., 1993. "Thermal Comfort and Optimal Energy Use", *ASHRAE Transactions*, **99(1)**, 1037-1048.

Snyder, M.E., and Newell, T.A., 1990. "Cooling Cost Minimization Using Building Mass For Thermal Storage", *ASHRAE Transactions*, **96(2)**, 830-838.

Spethmann, D.H., 1989. "Optimal Control for Cool Storage", *ASHRAE Transactions*, **95(1)**, 1189-1192.

Tahat, M.A., Babus'Haq, R.F., and O'Callaghan, P.W., 1993. "Thermal Energy Storage", *Building Services Engineering Research and Technology*, **14(1)**, 1-11.

Tuomaala, P., 1992. "A Literature Review of Building Related Simulation Models", Helsinki University of Technology.

Varšek, A., Urbančič, T., and Filipič, B., 1993. "Genetic Algorithms in Controller Design and Tuning", *IEEE Transactions on Systems, Man, and Cybernetics*, **23(5)**, 1330-1339.

White, F.M., 1994. *Fluid Mechanics*, Third Edition, McGraw-Hill, Inc.

Willis, S., and Wilkins, J., 1993. "Mass Appeal", *Building Services Journal*, January, **15(1)**, 25-27.

Winwood, R., Benstead, R., Edwards, R., and Letherman, K.M., 1994. "Building Fabric Thermal Storage: Use of Computational Fluid Dynamics for Modelling", *Building Services Engineering Research and Technology*, **15(3)**, 171-178.

Winwood, R., Benstead, R., and Edwards, R., 1997a. "Advanced Fabric Energy Storage I: Review", *Building Services Engineering Research and Technology*, **18(1)**, 1-6.

Winwood, R., Benstead, R., and Edwards, R., 1997b. "Advanced Fabric Energy Storage IV: Experimental Monitoring", *Building Services Engineering Research and Technology*, **18(1)**, 25-30.

Wright, J.A., 1995. "Fitness Function for Highly Constrained Problems", Private Communication.

Wright, J.A., 1996. "HVAC Optimisation Studies: Sizing by Genetic Algorithm", *Building Services Engineering Research and Technology*, **17(1)**, 7-14.

Yoshida, H., and Terai, T., 1990/1991. "An ARMA Type Weather Model for Air-Conditioning, Heating and Cooling Load Calculation", *Energy and Buildings*, **15-16**, 625-634.

Yoshida, H., and Terai, T., 1992. "Modelling of Weather Data by Time Series Analysis for Air Conditioning Load Calculations", *ASHRAE Transactions*, **98(1)**, 328-345.

Zheng, G.R., and Zaheer-Uddin, M., 1996. "Optimization of Thermal Processes in a Variable Air Volume HVAC System", *Energy*, **21(5)**, 407-420.

Zmeureanu, R., and Fazio, P., 1988. "Thermal Performance of a Hollow Core Concrete Floor System for Passive Cooling", *Building and Environment*, **23(3)**, 243-252.

# Appendix A

# The Complex Algorithm

The Complex method, proposed by Box (1965), is an adaption of the Simplex direct search method for solving constrained minimization problems. The method works on a sequence of geometric figures each having $K$ vertices ($K \geq n+1$, $n$ is the number of variables). The method progressively rolls over the complex figure towards the constrained optimum; the complex then converges or collapses on the optimum.

The search procedure according to Rao (1984) is illustrated below:

1. Constitute an initial geometric figure. In order to do so, find $K \geq n+1$ points, each of which satisfies all the constraints. $X_1$ is a given initial solution, and the remaining $K-1$ points are generated randomly. $f(X_1)$ is the objective function of $X_1$. Each of the $n$ variables ($i = 1, 2, ..., n$) of the $j^{\text{th}}$ point $x_{i,j}$ ($x_{i,j} \in X_j$) has to be found by random within its bounds $[x_{i,low}, x_{i,high}]$.

$$x_{i,j} = x_{i,low} + r_{i,j}(x_{i,high} - x_{i,low}),\ i = 1, 2, ...n;\ \ j = 1, 2, ...K. \qquad \text{(A.1)}$$

   By this definition, $r_{i,j}$ is a random number lying in (0,1). If the newly generated $X_j$ does not satisfy the constraints, the trial point $X_j$ is moved half way towards the centroid of the remaining, already accepted points.

$$X_j = \frac{1}{2}(X_j + X_o) \qquad \text{(A.2)}$$

Where $X_o$ is the centroid of the already accepted points.

$$X_o = \frac{1}{j-1}\sum_{l=1}^{j-1} X_l \tag{A.3}$$

This process is continued until $K$ points have been found. The initial geometric figure (complex) is formed and the initialization is completed.

2. The objective function is evaluated at each of the $K$ points (vertices). $X_h$ is the solution with the largest function value. A new point $X_r$ is then obtained by reflection,

$$X_r = (1+\alpha)X_o - \alpha X_h \tag{A.4}$$

Where $\alpha \geq 1$, $X_o$ is the centroid of all vertices except $X_h$,

$$X_o = \frac{1}{K-1}\sum_{l=1, l\neq h}^{K} X_l \tag{A.5}$$

3. Test for feasibility of the new point $X_r$. If $X_r$ is feasible, and $f(X_r) < f(X_h)$, $X_h$ is replaced by $X_r$. A new geometric figure (complex) is formed and the search continues with Step 2. If $f(X_r) \geq f(X_h)$, $X_r$ is not in the direction of the minimum. A new $X_r$ is then calculated by reducing $\alpha$ by a factor of 2 until a satisfactory $X_r$ is found or $\alpha$ is smaller than a prescribed small quantity $\epsilon$. If $X_r$ is still not found, the process is discarded and a new search is started with the second largest function value instead of $X_h$.

4. If $X_r$ at any stage is infeasible, it is moved half way towards the centroid until it is feasible.

$$(X_r)_{new} = \frac{1}{2}(X_o + X_r) \tag{A.6}$$

This step can be continued so long as the complex has not collapsed into its centroid.

5. A new complex can always be generated by means of $X_r$ replacing $X_h$. The convergence of the process is tested according to,

   (a) The complex shrinks to a specified small size $\epsilon_1$.

   (b) The standard deviation of the function value becomes sufficiently small, i.e.

$$\frac{1}{K}\sum_{j=1}^{K}[f(X_o') - f(X_j)]^2 \Big]^{\frac{1}{2}} < \epsilon_2$$

   Where $X_o'$ is the centroid of all the $K$ vertices of the current complex, and $\epsilon_2$ is a specified small number.

Two suggestions were made by Rao (1984) for the value of $\alpha$ and the selection of $K$,

I. $\alpha$ is initially 1.3.

II. $K \geq 2n + 1$. Too small a $K$ may result in a complex collapsing across a constraint boundary.

Obviously the Complex method is computationally simple without requiring derivatives of the objective function $f(X)$ and the constraint function $g(X)$. These procedures can be applied to the building optimization directly.

# Appendix B

# The Genetic Algorithm

The three basic genetic operators in the GA search, reproduction, crossover and mutation, all work on a binary coding of problem variables. GAs search from a population of solutions rather than a single solution. A solution within a population is termed an 'individual'. In a given generation, the number of individuals is the population size. The GA presented here is based on Goldberg's (1989) 'Simple Genetic Algorithm' (SGA).

Each of the problem variables is represented by a binary number of $B$ bits. The binary numbers of each variable are concatenated to produce a binary string that then represents an individual solution in the population. To evaluate an individual, each bit of the whole binary scheme is decoded sequentially to a digital number for each variable. The objective function and the feasibility of the solution is represented by a fitness, the better the solution, the higher the fitness.

The procedures in the GA search are described by the following algorithm:

1. Randomly initialize a population of solutions (the first generation $g = 0$). The output from this step is the population set,

$$oldpop = \{Y_{1,0}, Y_{2,0}, ..., Y_{maxpop,0}\}$$

where $maxpop$ is population size. $Y_{i,0}$ is $i^{\text{th}}$ candidate individual of the population in $g = 0$ generation (for each $Y_{i,0} \in oldpop$, $i = 1, 2, ..., maxpop$).

2. Compute the objective function value and fitness value of the population. This is divided into three substeps:

   (a) decode $Y_{i,0} \in oldpop$, $i = 1, 2, ..., maxpop$, to $X_{i,0} \in oldpop$, $i = 1, 2, ..., maxpop$. Where $X$ is the corresponding real variable value of binary string $Y$.

   (b) evaluate the objective function and the solution feasibility for each $X_{i,0} \in oldpop$, $i = 1, 2, ..., maxpop$, through function calls (the building and plant simulation models in this research).

   (c) compute the fitness value of each $X_{i,0} \in oldpop$, $i = 1, 2, ..., maxpop$, by means of the objective function value and feasibility information. If an individual is infeasible, a penalty function is introduced to reduce the fitness associated with the individual.

3. Generate a new population by the following operations. The output from this process is a new population set at generation $g = 1$.

$$newpop = \{Y_{1,1}, Y_{2,1}, ..., Y_{maxpop,1}\}$$

   (a) Reproduction: selecte individuals in the population *oldpop* according to the fitness value associated with them. The basic selection strategy is based on the weight of each individual within the whole population, the higher the weight, the greater its chance of selection. In Equation B.1, $p(Y_{i,0})$ is the weight of the individual $Y_{i,0}$,

$$p(Y_{i,0}) = fit(Y_{i,0}) / \sum_{i=1}^{maxpop} fit(Y_{i,0}),\ i = 1, 2..., maxpop. \qquad \text{(B.1)}$$

   (b) Mutation: if a randomly generated probability is lower than the mutation probability $P_m$, the mutation operator flips the value of the bits $B_{j,i,0}$ which is the $j^{\text{th}}$ bit of the $i^{\text{th}}$ individual in generation $g = 0$. The new $B_{j,i,0}$ is obtained by the following algorithm.

$$\begin{cases} B_{j,i,0} = B_{j,i,0}, \text{ in probability of } (1 - P_m); \\ B_{j,i,0} = \bar{B}_{j,i,0}, \text{ in probability of } (P_m). \end{cases}$$

   Where $\bar{B}_{j,i,0}$ is,

$$\begin{cases} \bar{B}_{j,i,0} = 0, \text{ if } B_{j,i,0} = 1; \\ \bar{B}_{j,i,0} = 1, \text{ if } B_{j,i,0} = 0; \end{cases}$$

(c) Crossover: If a randomly generated probability is lower than the crossover probability $P_c$, the crossover operator randomly selects a crossover position at which it swaps the two parent strings.

$$\begin{cases} Y_{i,1} = Y_{i,0}, \text{ in probability of } (1 - P_c); \\ Y_{i,1} = Y'_{i,0}, \text{ in probability of } (P_c). \end{cases}$$

$$i = 1, 2, ..., maxpop.$$

Where, $Y'_{i,0}$ is one of the new child individual after crossover. If the two parent strings are represented by,

$$Y_{i1,0} = B_{1,i1,0}, B_{2,i1,0}, ..., B_{s,i1,0}, B_{s+1,i1,0}, ..., B_{N,i1,0}$$
$$Y_{i2,0} = B_{1,i2,0}, B_{2,i2,0}, ..., B_{s,i2,0}, B_{s+1,i2,0}, ..., B_{N,i2,0}$$

and the crossover position is at $s\,(1 \leq s \leq N)$, the new $Y_{i1,1}$ and $Y_{i2,1}$, are then obtained from the crossover operation.

$$Y_{i1,1} = B_{1,i1,0}, B_{2,i1,0}, ..., B_{s,i1,0}, B_{s+1,i2,0}, ..., B_{N,i2,0}$$
$$Y_{i2,1} = B_{1,i2,0}, B_{2,i2,0}, ..., B_{s,i2,0}, B_{s+1,i1,0}, ..., B_{N,i1,0}$$

This operation selects two individuals as parent strings and produce two children at the following generation.

(d) Add new individuals $Y_{i,1}$, i=1,2,...,*maxpop*, to the new population set (*newpop*).

4. To obtain the next generation, *oldpop* = *newpop*, and repeat the procedure from Steps 2 to 3 (until convergence). In a genetic algorithm search, there is no hard coded convergence criterion due to probabilistic nature of the algorithm. The algorithm is normally allowed to run for a fixed number of generations, the number of generations required being obtained from inspection of the rate of convergence for a particular problem.

**Formulation of the Fitness Function (Wright, 1995)**

The fitness function converts the minimization of the energy cost objective to a maximization problem, and penalizes the fitness for constraint violations. Objective functions to be minimized can be converted to fitness form by:

$$F_i = G_{max} - G_i \tag{B.2}$$

where: $F_i$ and $G_i$ are the fitness and objective functions of an indivual in the population, and $G_{max}$ is either the maximum objective function value in the current population or the maximum from all populations in the current optimization.

Penalty Function

There are generally two approaches to penalizing the fitness value of infeasible solution points; the first is simple rejection of the solution by setting the fitness to zero, and the second is to penalize the fitness in relation to the degree of infeasibility. The second approach has the advantage that slightly infeasible solutions may be selected for reproduction which can help move an otherwise convergent population along a constraint boundary, and therefore, is the approach that has been adopted in this research. The penalty is applied to each infeasible individual prior to the conversion to fitness form by Equation B.2, ($G_{max}$ may or may not be infeasible, depending on the range of solutions in the population).

The goals of the penalty formulation are to ensure that the best of the feasible solutions are among the fittest individuals, and that highly infeasible solutions are among the least fit individuals. Individuals having minor constraint violations should have a fitness that gives them some chance of being selected for reproduction. These goals are achieved by forming the penalty in two parts, the first part provides a normalized measure of the degree of infeasibility, $C_{norm,i}$; $C_{norm,i} = 0.0$ indicates a feasible individual, and $C_{norm,i} = 1.0$ an individual for which all constraints have been violated to their maximum extent (a range of "violation" being assigned to each constraint function). The second part applies a penalty, $P$, based on the degree of infeasibilty, $C_{norm,i}$, and and a measure of the difference, $\delta$, in objective function values for the "best" and "worst" individuals in the current population:

$$G_i = G_i + \delta(1.0 + P) \tag{B.3}$$

The "best" individual has a feasible solution with the lowest objective function value. The "worst" individual has the highest infeasibility $C_{norm,worst}$, of the

solutions having an objective function value lower than the "best" individual. The penalty, $P$, is of an exponential form:

$$P = \frac{e^{\beta M} - 1}{e^{\beta} - 1}; \quad M \neq 0.0 \tag{B.4}$$

where: $M = \frac{C_{norm,i}}{C_{norm,worst}}$

Equation B.3 results in the objective function value of the worst individual being increased by twice $\delta$, other infeasible solutions being penalized to a lesser degree (both $\delta$ and $P$ being functions of $M$). The exponential penalty gives some control over the severity of the penalty. Positive values of $\beta$ lead to lower penalties for slightly infeasible solutions.

These procedures for the GA search have been implemented and combined with the building and plant simulation models in the optimal controller.

# Appendix C

# Publications To Date

Publications associated with this thesis to date are:

1. Ren, M.J., and Wright, J.A., 1996. "A Ventilated Slab Thermal Storage System Model", accepted for publication in *Building and Environment.*

2. Ren, M.J., and Wright, J.A., 1997. "Optimal Control of Fabric Thermal Storage Systems", *CLIMA 2000 Conference*, Belgium, September.

3. Ren, M.J., and Wright, J.A., 1997. "Predictive Optimal Control of Fabric Thermal Storage Systems", *The Fifth International Conference of IBPSA (International Building Performance Simulation Association)*, Prague, Czech Republic, September.